



**University of
Zurich**^{UZH}

Flood-duration-Frequency (QdF) Analysis in the Aare River Basin based on Simulated Discharge Time Series

GEO 511 Master's Thesis

Author

Joel Rüttsche

14-714-414

Supervised by

PD Dr. Daniel Viviroli

Faculty representative

Prof. Dr. Jan Seibert

30.01.2021

Department of Geography, University of Zurich

Abstract

In this thesis, flood frequency analyses for 18 stations in the Aare River Basin was done using simulated discharge time series with a combined length of 300,000 years. Flood characteristics and the seasonality of floods were investigated using the Flood-duration-Frequency (QdF) method and visualized for each station and season. Uncertainty of QdF curves was presented based on the simultaneous plotting of the 29 quantiles of the individual scenarios (model confidence), as well as with the comparison of the neighboring measuring stations. In addition, the goodness-of-fit of the QdF model was determined using the rRMSE for different return periods. In a next part, the focus was set on extreme floods with return periods of 10'000 years. Here, the development of such floods was analyzed in relation to the precipitation distribution and the influence of snowmelt. The results show that with the help of the simulations reliable and consistent QdF curves can be generated, which agree relatively well with the observed values. The simulated QdF curves show that the magnitude of floods is strongest in summer and weakest in winter. Furthermore, a certain precipitation structure can be recognized for all stations and seasons before and during extreme flood events, with precipitation maxima occurring mainly in a band extending from the east of the Aare basin to the southwest. The influence of snowmelt is classified as small for these extreme flood events.

Table of Contents

List of Tables.....	5
List of Figures.....	6
1. Introduction.....	9
1.1 Motivation.....	9
1.2 Broader Context	10
1.3 Goals, Research Questions & hypotheses.....	10
1.4 Structure.....	11
2. Data	12
2.1 EXAR (Extreme Weather Aare-Rhein)	13
2.1.1 Weather Generator GWEX	14
2.1.2 Hydrological model HBV.....	15
2.1.3 Routing Model RS Minerve.....	15
2.2 Software	15
3. Theory and Methods	16
3.1 Extreme Value Theory	16
3.1.1 Generalized Extreme Value Distribution.....	16
3.2 Block Maxima	17
3.3 Return Period, Return Level & Plotting Position	18
3.4 Parameter Estimation.....	19
3.4.1 Maximum Likelihood Method (MLE).....	19
3.4.2 Method of L-moments	20
3.5 Uncertainty.....	20
3.6 Flood-Duration-Frequency Curves (QdF)	21
3.6.1 Local QdF model.....	21
3.6.2 Converging QdF model.....	22
3.6.3 Validation	24
3.7 Extreme Flood Events ($T = 10'000$).....	25
3.7.1 Precipitation distribution	25
3.7.2 Snowmelt.....	25
4. Results	27
4.1 Group Duration d_1	30
4.1.1 Maigrauge.....	30
4.1.2 Rossens.....	33
4.1.3 Schiffenen.....	36
4.2 Group Duration d_2	39

4.2.1 Aarberg.....	39
4.2.2 Le Châlet.....	42
4.2.3 Niederried.....	45
4.2.4 Wettingen.....	48
4.3 Group Duration d3	51
4.3.1 Beznau	51
4.3.2 Gösgen.....	54
4.3.3 Klingnau	57
4.3.4 Mühleberg	60
4.3.5 Rapperswil.....	63
4.3.6 Ruppoldingen	66
4.3.7 Wichelsee	69
4.3.8 Wildegg.....	72
4.4 Group Duration d6	75
4.4.1 Bannwil.....	75
4.4.2 Flumenthal.....	78
4.4.3 Wynau	81
5. Discussion.....	82
5.1 Duration.....	82
5.2 Seasonality.....	82
5.3 Grouping.....	83
5.4 Adequacy.....	84
5.5 Confidence.....	85
5.6 Observations	86
5.7 Precipitation distribution	87
5.8 Snowmelt.....	87
6. Conclusion	88
7. References.....	90
8. Appendices.....	93
8.1 Appendix A	93
8.2 Appendix B.....	129
9. Personal declaration.....	147

List of Tables

Table 1: Overview over the 18 Stations	13
Table 2: Discharge measuring stations.....	14
Table 3: Delta parameter values and assigned duration.....	25
Table 4: Seasonal and meaned Delta parameter for all stations	27
Table 5: Maigrauge Flood statistics.....	29
Table 6: Rossens Flood statistics	32
Table 7: Schiffenen Flood statistics	35
Table 8: Aarberg Flood statistics	38
Table 9: Le Châlet Flood statistics	41
Table 10: Niederried Flood statistics.....	44
Table 11: Wettingen Flood statistics	47
Table 12: Beznau Flood statistics	50
Table 13: Gösigen Flood statistics	53
Table 14: Klingnau Flood statistics	56
Table 15: Mühleberg Flood statistics	59
Table 16: Ruppenswil Flood statistics	62
Table 17: Ruppoldingen Flood statistics.....	65
Table 18: Wichelsee Flood statistics	68
Table 19: Wildegg Flood statistics	71
Table 20: Bannwil Flood statistics	74
Table 21: Flumenthal Flood statistics.....	77
Table 22: Wynau Flood statistics.....	80

List of Figures

Figure 1: Aare River Basin.....	12
Figure 2: Influence of GEV parameters on PDF	17
Figure 3: Mean and Maximum discharge for durations d1 and d6.....	21
Figure 4: QdF curves for Aarberg scenario 1 in winter.....	22
Figure 5: Influence of Delta parameter on the converging QdF curves	24
Figure 6: QdF curves for Maigrauge	28
Figure 7: Precipitation distributions maps for Maigrauge and duration d1	28
Figure 8: Temperature difference map for Maigrauge in spring and duration d1.....	29
Figure 9: QdF curves for Rossens	31
Figure 10: Precipitation distributions maps for Rossens and duration d1.....	31
Figure 11: Temperature difference map for Rossens in spring and duration d1.....	32
Figure 12: QdF curves for Schiffenen	34
Figure 13: Precipitation distributions maps for Schiffenen and duration d1.....	34
Figure 14: Temperature difference map for Schiffenen in spring and duration d1.....	35
Figure 15: QdF curves for Aarberg	37
Figure 16: Precipitation distributions maps for Aarberg and duration d2.....	37
Figure 17: Temperature difference map for Aarberg in spring and duration d2.....	38
Figure 18: QdF curves for Le Châlet	40
Figure 19: Precipitation distributions maps for Le Châlet and duration d2.....	40
Figure 20: Temperature difference map for Le Châlet in spring and duration d2.....	41
Figure 21: QdF curves for Niederried	43
Figure 22: Precipitation distributions maps for Niederried and duration d2	43
Figure 23: Temperature difference map for Niederried in spring and duration d2.....	44
Figure 24: QdF curves for Wettingen	46
Figure 25: Precipitation distributions maps for Wettingen and duration d2.....	46
Figure 26: Temperature difference map for Wettingen in spring and duration d2.....	47
Figure 27: QdF curves for Beznau	49
Figure 28: Precipitation distributions maps for Beznau and duration d3.....	49
Figure 29: Temperature difference map for Beznau in spring and duration d3	50
Figure 30: QdF curves for Gösgen	52
Figure 31: Precipitation distributions maps for Gösgen and duration d3.....	52
Figure 32: Temperature difference map for Gösgen in spring and duration d3.....	53
Figure 33: QdF curves for Klingnau	55
Figure 34: Precipitation distributions maps for Klingnau and duration d3.....	55
Figure 35: Temperature difference map for Klingnau in spring and duration d3.....	56
Figure 36: QdF curves for Mühleberg	58
Figure 37: Precipitation distributions maps for Mühleberg and duration d3.....	58
Figure 38: Temperature difference map for Mühleberg in spring and duration d3	59
Figure 39: QdF curves for Rapperswil	62
Figure 40: Precipitation distributions maps for Rapperswil and duration d3.....	62
Figure 41: Temperature difference map for Rapperswil in spring and duration d3.....	63
Figure 42: QdF curves for Ruppoldingen.....	64
Figure 43: Precipitation distributions maps for Ruppoldingen and duration d3	64
Figure 44: Temperature difference map for Ruppoldingen in spring and duration d3	65
Figure 45: QdF curves for Wichelsee.....	67
Figure 46: Precipitation distributions maps for Wichelsee and duration d3	67
Figure 47: Temperature difference map for Wichelsee in spring and duration d3	68

Figure 48: QdF curves for Wildegg	70
Figure 49: Precipitation distributions maps for Wildegg and duration d3.....	70
Figure 50: Temperature difference map for Wildegg in spring and duration d3.....	71
Figure 51: QdF curves for Bannwil	73
Figure 52: Precipitation distributions maps for Bannwil and duration d6.....	73
Figure 53: Temperature difference map for Bannwil in spring and duration d6.....	74
Figure 54: QdF curves for Flumenthal.....	76
Figure 55: Precipitation distributions maps for Flumenthal and duration d6	76
Figure 56: Temperature difference map for Flumenthal in spring and duration d6.....	77
Figure 57: QdF curves for Wynau.....	79
Figure 58: Precipitation distributions maps for Wynau and duration d6	79
Figure 59: Temperature difference map for Wynau in spring and duration d6	80
Figure 60: Winter and summer QdF curves for Aarberg and individual flood durations.....	93
Figure 61: Autumn and spring QdF curves for Aarberg and individual flood durations	94
Figure 62: Winter and summer QdF curves for Bannwil and individual flood durations.....	95
Figure 63: Autumn and spring QdF curves for Bannwil and individual flood durations	96
Figure 65: Winter and summer QdF curves for Beznau and individual flood durations.....	97
Figure 65: Autumn and spring QdF curves for Beznau and individual flood durations	98
Figure 66: Winter and summer QdF curves for Flumenthal and individual flood durations	99
Figure 67: Autumn and spring QdF curves for Flumenthal and individual flood durations.....	100
Figure 68: Winter and summer QdF curves for Gösigen and individual flood durations	101
Figure 69: Autumn and spring QdF curves for Gösigen and individual flood durations.....	102
Figure 70: Winter and summer QdF curves for Klingnau and individual flood durations	103
Figure 71: Autumn and spring QdF curves for Klingnau and individual flood durations	104
Figure 72: Winter and summer QdF curves for Le Châlet and individual flood durations.....	105
Figure 73: Autumn and spring QdF curves for Le Châlet and individual flood durations	106
Figure 74: Winter and summer QdF curves for Maigrauge and individual flood durations	107
Figure 75: Autumn and spring QdF curves for Maigrauge and individual flood durations.....	108
Figure 76: Winter and summer QdF curves for Mühleberg and individual flood durations.....	109
Figure 77: Autumn and spring QdF curves for Mühleberg and individual flood durations	110
Figure 78: Winter and summer QdF curves for Niederried and individual flood durations	111
Figure 79: Autumn and spring QdF curves for Niederried and individual flood durations.....	112
Figure 80: Winter and summer QdF curves for Rossens and individual flood durations	113
Figure 81: Autumn and spring QdF curves for Rossens and individual flood durations	114
Figure 82: Winter and summer QdF curves for Ruppenswil and individual flood durations	115
Figure 83: Autumn and spring QdF curves for Ruppenswil and individual flood durations	116
Figure 84: Winter and summer QdF curves for Ruppoldingen and individual flood durations.....	117
Figure 85: Autumn and spring QdF curves for Ruppoldingen and individual flood durations.....	118
Figure 86: Winter and summer QdF curves for Schiffenen and individual flood durations	119
Figure 87: Autumn and spring QdF curves for Schiffenen and individual flood durations.....	120
Figure 88: Winter and summer QdF curves for Wettingen and individual flood durations	121
Figure 89: Autumn and spring QdF curves for Wettingen and individual flood durations.....	122
Figure 90: Winter and summer QdF curves for Wichelsee and individual flood durations.....	123
Figure 91: Autumn and spring QdF curves for Wichelsee and individual flood durations	124
Figure 92: Winter and summer QdF curves for Wildegg and individual flood durations	125
Figure 93: Autumn and spring QdF curves for Wildegg and individual flood durations.....	126
Figure 94: Winter and summer QdF curves for Wynau and individual flood durations.....	127
Figure 95: Autumn and spring QdF curves for Wynau and individual flood durations.....	128

Figure 96: Seasonal converging QdF curves for Aarberg	129
Figure 97: Seasonal converging QdF curves for Bannwil	130
Figure 98: Seasonal converging QdF curves for Beznau.....	131
Figure 99: Seasonal converging QdF curves for Flumenthal	132
Figure 100: Seasonal converging QdF curves for Gösgen	133
Figure 101: Seasonal converging QdF curves for Klingnau	134
Figure 102: Seasonal converging QdF curves for Le Châlet	135
Figure 103: Seasonal converging QdF curves for Maigrauge	136
Figure 104: Seasonal converging QdF curves for Mühleberg.....	137
Figure 105: Seasonal converging QdF curves for Niederried	138
Figure 106: Seasonal converging QdF curves for Rossens	139
Figure 107: Seasonal converging QdF curves for Rapperswil	140
Figure 108: Seasonal converging QdF curves for Ruppoldingen	141
Figure 109: Seasonal converging QdF curves for Schiffenen	142
Figure 110: Seasonal converging QdF curves for Wettingen	143
Figure 111: Seasonal converging QdF curves for Wichelsee.....	144
Figure 112: Seasonal converging QdF curves for Wildegg	145
Figure 113: Seasonal converging QdF curves for Wynau	146

1. Introduction

1.1 Motivation

In August 2005, an extreme flood event happened in Switzerland. This flood was the largest natural event since 1972. It caused up to CHF 3 billion in damage through the destruction of infrastructure and agriculture, overwhelmed local emergency forces, and took 6 lives (Bezzola and Hegg, 2007; Hilker et al., 2008). Shortly after such catastrophic events, many people ask themselves: What is the probability of such a flood and how can the protection against it be improved.

Extreme value analyses (EVT) can help to address these questions. Using extreme value analyses return period (probability of occurrence) and return level (discharge peak and volume) of frequently occurring but also rare floods can be estimated. EVT is widely used in hydrology and climatology, and the results can be applied to reservoir operations, spillway analyses, floodplain managements, hydraulic structure designs, or risk management in general (Javelle et al., 2002a). The foundations for extreme value analysis are measured time series of a variable, for example precipitation or runoff. Oftentimes, these measured time series are too short and/or incomplete. As a result, extreme value analyses are subject to large uncertainties and the risk can ultimately be incorrectly assessed. Particularly extremely rare events can hardly be characterized correctly in terms of their occurrence and magnitude with measured time series.

In this thesis, instead of observed and measured time series, simulated ones are utilized. Simulated time series have the advantage that they can be generated for any length and thus rarer events can be studied more precisely. The time series used in this thesis are provided by EXAR (Extreme Events Aare-Rhein) by various federal agencies of Switzerland. A total of 300 scenarios were simulated, each with a length of 1,000 years and an hourly resolution. These scenarios can be freely combined and result in total length of 300'000 years (289'000 years for the discharge). Due to these long time series one has now the possibility to investigate extremely rare events.

The simulations were generated for 18 dams or power plants, all located in the Aare river basin in Switzerland. Thus, it is extremely important to know accurate flood characteristics for these sites. Consequently, the results of this thesis can be used to improve the assessment of flood risk at these sites and possibly enhance protection against flooding. To analyze floods adequately, flood duration-frequency (QdF) analysis was applied to the simulated runoff time series in this thesis.

Floods in Switzerland can be caused by precipitation and snowmelt. Since these quantities are subject to a strong seasonal cycle, floods also have different intensities in the four seasons. To identify in which season floods can become most severe, the datasets were subdivided seasonally.

Besides the seasonal QdF curves, another focus is on extremely rare floods with return periods of 10'000 years. These floods have a much more extreme intensity than the 2005 event in Switzerland and have never been observed naturally, but could possibly occur in the future. These floods were analyzed with respect to their precipitation distribution and the possible input of snowmelt. The reason why floods with a return period of 10'000 years were chosen is that one does not often have the chance to work with such long time series and hence it is thrilling to study floods that are as extreme as possible.

1.2 Broader Context

Floods can be characterized by several variables: The peak discharge, the specific peak discharge, the flood volume, the mean maximum discharge over a certain duration and many more (Musy et al., 2005). In classical flood frequency analyses, usually only the peak discharge is used to describe floods. Other quantities like the flood volume or the flood duration are disregarded. In this thesis the Flood-duration-Frequency (QdF) analysis is applied. The QdF approach is structured similarly as the IDF curves often used for precipitation in climatology (Bell, 1976; Pilgrim, 1987; Sivapalan and Blöschl, 1998). In comparison to the IDF however the QdF approach is relatively underused in flood frequency analysis. The basis for the QdF approach was done by NERC (1975), Sherwood (1994), Ballocki and Burges (1994), and Galéa and Prudhomme (1997). There are two ways to implement the QdF method. The first one is the peak-volume analysis (Ashkar, 1980), where the flood duration, peak and volume are treated as random variables. The second one is the flood-duration-frequency analysis where the flood duration is fixed as a parameter (Galéa et al., 2000; Meunier, 2001; Javelle et al., 2002a; Javelle et al., 2002b; Galéa et al., 2000; Zaidman et al., 2003). In this thesis the second approach is chosen. Javelle et al. (1999) also developed a converging QdF approach, which is also implemented in this thesis (Javelle et al., 2000; Javelle et al., 2003). Most flood frequency analyses are done for small catchment areas or stations where measurements of runoff or precipitation exist, but also regionalization methods have been developed to extrapolate flood frequency analysis to ungauged basins (Hosking, 1997; Ouarda et al., 2000; Javelle et al., 2002a). The regionalization method, however, was not tackled in this thesis.

1.3 Goals, Research Questions & hypotheses

The main goal of this thesis is to statistically evaluate the simulated discharge data with reliable QdF-curves and to compare them to QdF curves of nearby measuring stations. Another objective is to estimate spatial connections between extreme flood events with return periods of 10'000 years and precipitation as well as to estimate the influence of snowmelt on these events. The research questions are therefore structured as follows:

The Research questions are:

1. How do the discharge quantiles differ for varying durations?
2. What are the seasonal differences of the QdF curves and in which seasons do the strongest floods occur?
3. What are the differences between the QdF curves for the 18 stations?
4. How do observed discharge values and quantiles compare to the simulated values and quantiles?
5. Which stations are susceptible to small duration or large duration floods?
6. How is the precipitation distributed for flood events with 10'000 years return period?
7. What is the influence of snowmelt on flood events with 10'000 years return period?

The hypotheses corresponding to these questions are:

1. The discharge quantiles for shorter durations are steeper than for longer durations, because the maximum mean discharges are smoothed out for longer durations.
2. For same return periods, the corresponding return levels tend to be the smallest for all stations in winter, whereas for the other seasons the QdF curves are more similar and the highest return values are station specific.

3. The different stations have vastly different QdF curves in terms of the magnitude of the maximum mean discharge values, as well as the relevant flood durations. Stations within proximity are more similar than stations far away.
4. QdF curves of simulated stations and QdF curves of observed stations are relatively similar. If the station with simulated data is near an observation station, the simulated QdF curves tend to compare better to the observed quantiles and values than for stations far apart.
5. Stations with large catchment areas are rather susceptible to slow and smoothed floods, whereas stations with a small relevant catchment area are more prone to flash floods.
6. During and before the flood events with 10'000 years return period, the precipitation is focused in the catchment area of the station. In the whole Aare basin, the amount of precipitation during an event with 10'000 years return period is extremely large over several days for all seasons.
7. The influences of spring snowmelt during floods with 10'000 years return period is small. Precipitation is the driving factor for all very extreme flood events.

1.4 Structure

An introduction to the subject was made in Chapter 1. The motivation, the objectives and the research questions were presented, as well as the link to similar topics. Chapter 2 presents the three long, simulated data sets, as well as the observed data sets. Furthermore, the model chain that generates these simulated data sets is described. The softwares used in this work are also briefly introduced. In chapter 3 the methodology and theory of this thesis are presented. All relevant aspects of extreme value theory are described, as well as the methodology used to generate the QdF curves. This chapter also indicates how the QdF curves are validated, how uncertainties are handled, as well as the methods used to describe and analyze floods with 10'000 year return periods. In Chapter 4 the results of all 18 stations are presented and described. In Chapter 5 these results are discussed and compared. Finally, the conclusion where the research questions are answered is presented in chapter 6. In Chapter 7 the references are listed and in chapter 8 additional figures are shown.

Aare River Basin

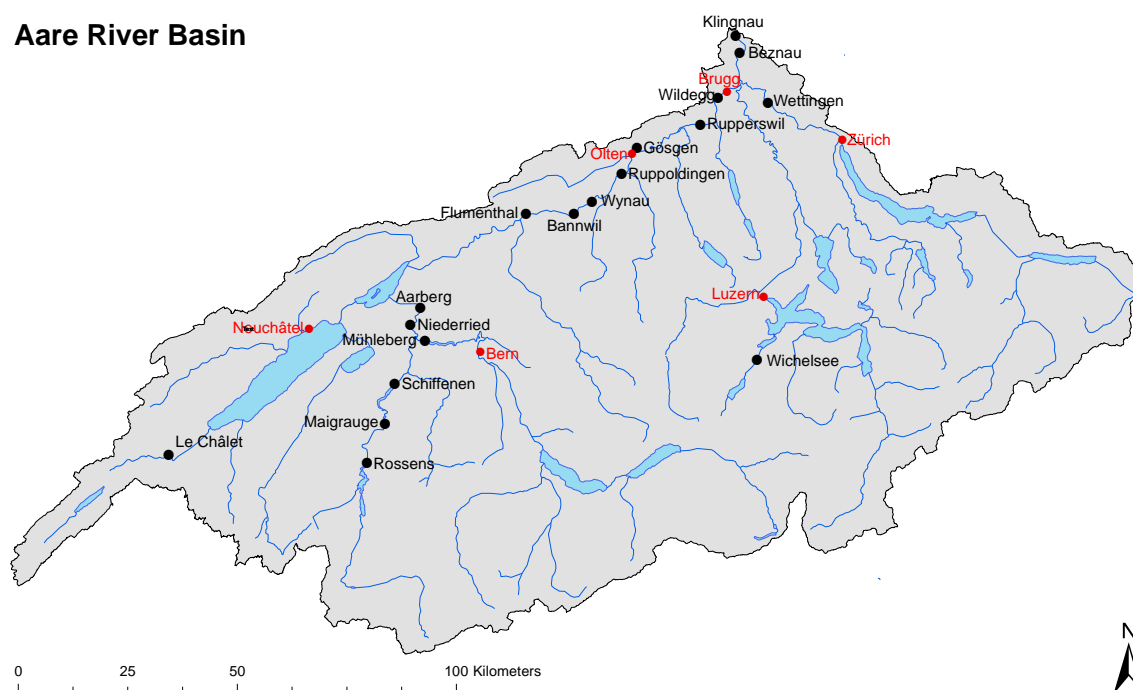


Figure 1: Overview of the Aare river basin and the 18 stations. Stations are marked as black dots, large cities as red dots and lakes and rivers in blue.

2. Data

The bases of this thesis are three huge data sets of precipitation, temperature and discharge timeseries for several stations in the Aare region. These data sets all originate from the project EXAR (Extreme Flood Aare Rhein) in which many federal agencies of Switzerland are involved. The time series are simulations and have an hourly resolution. The discharge data set is given for 18 stations, which are located at dams and nuclear power plants in the Aare region and thus at places where considerable hazard potential exists. The location of the 18 stations is displayed in Figure 1. The temperature and precipitation data sets are averaged for the 79 catchments and 10 large lakes in the Aare basin and therefore cover the entire area under investigation. The units of the datasets are m^3/s , $^{\circ}\text{C}$ and mm for discharge, temperature and precipitation timeseries, respectively. The individual scenarios of the data sets each have a length of 1,000 years, but can be freely combined to obtain a total length of 300,000 years (289,000 years for the runoff data set). The datasets are stationary, and thus don't contain any possible climate change impacts. The stations for which the runoff simulations were generated are briefly described in Table 1 in terms of their catchment area size and on which river they are located.

Additional data sets used are provided by the Swiss Federal Office of Environment (BAFU). These datasets are the historical discharges of measuring stations, which are located in the vicinity of the simulated stations in m^3/s , as well as the generalized background map for the representation of hydrological data (BAFU, 2014) and the subcatchments of Swiss waters bodies with sizes above 2 km^2 (BAFU, 2010). The measuring stations are described in Table 2 and show in which period measurements have taken place and to which station with simulated runoff time series they are compared to. In the following subchapters, the generation process of the simulated runoff temperature and precipitation time series is briefly described.

Table 1: The 18 stations in the Aare river basin with their relevant catchment area and on which river they are located.

Station	Catchment area (km ²)	River
Aare basin	17'709	-
Klingnau	17'687	Aare
Beznau	17'602	Aare
Wildeggen	11'669	Aare
Rupperswil	11'298	Aare
Gösgen	10'820	Aare
Ruppoldingen	10'114	Aare
Wynau	9'867	Aare
Bannwil	9'839	Aare
Flumenthal	9'582	Aare
Aarberg	5'092	Aare
Niederried	5'078	Aare
Mühleberg	3'168	Aare
Wettingen	2'377	Limmat
Schiffenen	1'406	Saane
Maigrange	1'267	Saane
Rossens	952	Saane
Le Châlet	342	Orbe
Wichelsee	308	Sarner Aa

2.1 EXAR (Extreme Weather Aare-Rhein)

In the Swiss project EXAR (Extreme Floods Aare-Rhein), the Federal Office of Environment (FOEN) is working with the Swiss Federal Nuclear Safety Inspectorate (ENSI), the Federal Office of Energy (SFOE), the Federal Office of Civil Protection (FOCP), the Federal Office of Meteorology and Climatology (MeteoSwiss) and many other institutions such as the University of Zurich, the ETH Zurich, the University of Bern and many more to assess the risk of extreme flooding in the Aare/Rhein region. The objective of the project is to review the existing bases for the assessment of extreme flood hazards in the Aare and Rhein region, to identify and close problem areas and gaps, to update the hazard assessment and to consequently improve the flood protection of the infrastructure of the area (Bafu, n.d.). To achieve these goals, a stochastic multisite weather generator GWEX, the hydrological model HBV and the routing model RS Minerve were used to generate precipitation, temperature and runoff time series for the Aare and Rhine regions. Because the creation of the simulations is not part of this thesis, but the results are used, the next three subsections summarize the work done for these simulations based on the not yet published EXAR main report Phase B (Andres et al., 2019).

Table 2: Discharge measuring stations of BAFU, with measuring period and with which simulation station they are paired with.

Measuring Station	Measurement Period	Simulation Station
Aare - Bern, Schönau	1917 - 2019	Mühleberg
Aare - Brugg	1916 - 2019	Rupperswil, Wildegg
Aare - Brügg, Aegerten	1968 - 2019	Flumenthal
Aare - Hagneck	1983 - 2019	Aarberg, Niederried
Aare - Murgenthal	1916 - 2019	Bannwil, Gösgen, Ruppoldingen, Wynau
Aare - Untersiggenthal, Stilli	1934 - 2019	Beznau, Klingnau
Limmat - Baden, Limmatpromenade	1951 - 2019	Wettingen
Orbe - Orbe, Le Chalet	1972 - 2019	Le Châlet
Saane - Laupen	1944 - 2019	Schiffenen
Sarine - Fribourg	1911 - 2019	Maigrauge, Rossens
Sarner Aa - Sarnen	1907 - 2019	Wichelsee

2.1.1 Weather Generator GWEX

A multisite stochastic weather generator GWEX was used in EXAR to generate precipitation and temperature time series (Evin et al., 2018). Weather generators are statistical models, which describe the weather as a stochastic process and that can create synthetic time series of any length based on observed sequences of weather variables (Wilks and Wilby, 1999). This is a tremendous advantage, because the generated time series are based on observed characteristics and are therefore relatively realistic. However, this dependence on past values also brings a disadvantage, because the measured precipitation amounts are only accurate for one measuring point or station. To generate values for an entire region, several stations must be combined and interpolated over the area. Thus, it depends on the interpolation method and may introduce errors or uncertainties (Moreno and Roldan, 1999: 65). Also, the models need long, historical and daily weather series for calibration, which are oftentimes not available (Smith and Hulme, 1998).

In GWEX the occurrence of precipitation and the amount of precipitation are generated separately and independently. The occurrence of precipitation was done by a first-order Markov chain, the precipitations amounts were estimated using an extended generalized Pareto distribution (papastathopoulos and Tawn, 2013). The temperature model in GWEX (Evin et al., 2019) simulates standardized values for each station daily. The temporal and spatial correlation is again mapped with a first-order markov process.

The validation of these time series was performed with a second weather generator SCAMP. Both weather generators can reproduce the temporal and spatial characteristics of the observed precipitation and temperature. Especially for heavy precipitation, which is of utmost importance for the occurrence of floods, GWEX and SCAMP show similar results. However, it must be noted that the heavy precipitation results from extrapolation of observed values measured over the past 85 years and therefore has a large uncertainty.

2.1.2 Hydrological model HBV

The HBV model (Bergström, 1992) version HBV light (Seibert, 1997) was used for the hydrological simulations. HBV is a conceptual hydrological catchment model with precipitation and temperature time series as the basic inputs. The HBV model includes four different routines, the snow, soil moisture, hydrograph deformation and groundwater routines. For each of these routines and subcatchments several parameters have to be estimated, calibrated and validated. The results of the HBV model are continuous and hourly discharge simulations of about 300'000 years for each subcatchment in the Aare basin.

2.1.3 Routing Model RS Minerve

To model the entire Aare basin, the routing model RS Minerve was used to build a hydraulic model. (Garcia Hernandez et al., 2016). Hydraulic models are mostly used to detect critical (discharge) situations, to trigger alarms or to ensure the targeted management of reservoirs. In RS Minerve focus was paid on retention effects that can dampen flood waves, like lakes or dams. Synthetic hydrographs were used to determine areas with standing and flowing retention. Lake regulations are also incorporated in RS Minerve.

The results of the entire model chain from the weather generator GWEX to the hydrological model HBV to the hydraulic model RS Minerve are hourly runoff hydrographs of 289'000 years, because 11'000 years had to be excluded for consistency reasons.

2.2 Software

The huge data sets and statistical analyses were handled/performed using the software Rstudio (R Development Core Team, 2009). Rstudio uses the programming language *R*, which is rooted in the programming language *S*. Rstudio is suitable for statistical analysis because it is straightforward to organize data, perform calculations, and create graphs. Another advantage of *R* is that every user can improve the software's code or create packages. In this thesis, the *extRemes* package was used for the maximum likelihood estimates of the generalized extreme value distributions (Gilleland et al., 2009).

ArcMap was used to create catchment, temperature and precipitation maps. ArcMap is part of ArcGIS owned by ESRI. ArcMap is used to view, analyze, create and edit geospatial data (ESRI, 2011).

3. Theory and Methods

Extreme value theory (EVT) is a sub-field of statistics. The extreme value theory is concerned with the tails of probability distributions, which means with the maximas and minimas. The goal of EVT is to statistically describe these maxima and minima in terms of their probability, their return period and their return level. Another goal of EVT is to estimate the probability, return period and return level beyond the observed maxima and minima by fitting a quantile to the observed maxima and minima. The basics of extreme value theory are time series of the variable which one wants to investigate. Since this thesis is concerned with floods, the discharge maxima (mean maximum discharges) time series are investigated. EVT is more precise and the uncertainty is smaller, the longer the time series are and the more accurately they are measured. Long and accurate time series however are oftentimes not present in reality. The next section provides an overview of the necessary features of EVT. Two main approaches exist in extreme value theory, the block maxima approach and the peak-over-threshold approach. The chosen approach in this thesis is the block maxima approach.

3.1 Extreme Value Theory

Consider a sequence of random variables X_1, X_2, \dots, X_n with length n . The variables satisfy the assumptions of independence and identical distribution i.i.d. and have a cumulative distribution function F . The maximum of this sequence is $M_n = X_{max} = \max(X_1, X_2, \dots, X_n)$. In this thesis, the variable X is the discharge Q in desired resolution (hourly, daily, 2 days, 3 days or 6 days), n the number of observed or simulated values in a season and therefore X_{max} the seasonal discharge maxima.

3.1.1 Generalized Extreme Value Distribution

For sufficiently large n the exponential and normal distributions of the maxima M_n converge to the same asymptotic shape, the generalized extreme value distribution. This convergence is fast for exponential distributions and slower for normal distributions. Because of this convergence to a single a same distribution (-family) the GEV is also defined as max-stable. A distribution is only max-stable if it is a GEV distribution (Coles, S. 2001). This is also called the Extremal Types Theorem (Fisher and Tippet, 1928):

The maximum of many i.i.d. random variables is distributed like the generalized extreme value distribution independently of the parent distribution if there is convergence at all.

The generalized extreme value distribution is defined as follows:

$$G(X_{max}; \mu, \sigma, \xi) = \begin{cases} e^{-(1+\xi \frac{X_{max}-\mu}{\sigma})^{-\frac{1}{\xi}}} & \xi \neq 0 \\ e^{-e^{-\frac{X_{max}-\mu}{\sigma}}} & \xi = 0 \end{cases}$$

1

and defined on:

$$\left\{ X_{max}: 1 + \xi \frac{X_{max} - \mu}{\sigma} > 0 \right\},$$

where $\mu \in R$, $\sigma > 0$ and $\xi \in R$.

The parameters μ, σ, ξ of the generalized extreme value distribution are called location (μ), shape (σ) and scale (ξ).

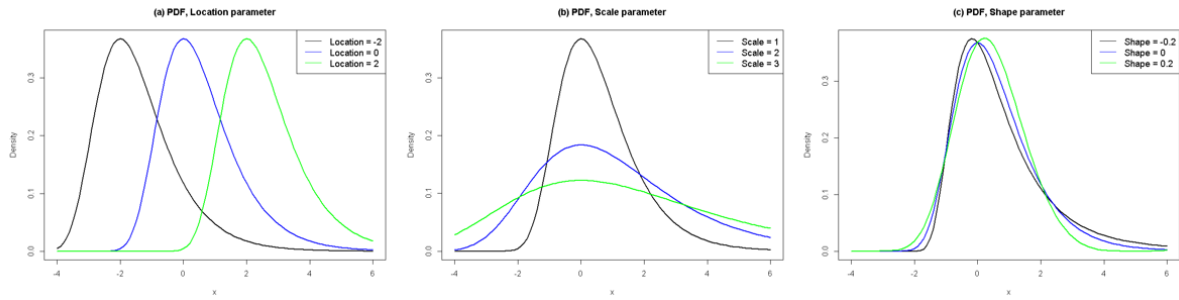


Figure 2: Influence of the three GEV parameters on the probability density function (PDF). In each figure, 2 parameters are held constant, while the remaining one is changed. In (a) the location parameter is changed, in (b) the scale parameter and in (c) the shape parameter.

The influence of the three parameters on the GEV distribution is shown in Figure 2. While one parameter is being changed, the other two parameters are held constant. Thus, each parameter can be examined separately and its influence on the distribution can be determined. The graphs show that the Location parameter marks the position of the density maximum of the distributions (Figure 2a). The Scale parameter changes the spread of the distributions (Figure 2b). In equation 1, as long as M_n is GEV distributed, $\frac{X_{max}-\mu}{\sigma}$ does not depend on the Location and Scale parameter, but only on the Shape parameter. The Shape parameter largely determines the tail behavior of the distribution and can take three different forms, depending on the sign of the parameter. The three types are:

1. $\xi = 0$, Gumbel distributions, with an infinite upper end point and an exponential decay of the tail of the probability density distribution.
2. $\xi > 0$, Fréchet distributions, with an infinite upper end point and a polynomially decay of the tail of the probability density distribution.
3. $\xi < 0$, Weibull distributions, with a finite upper end point and thus the probability is zero for values above the end point.

The Generalized Extreme Value distribution hence consists of the Gumbel, Fréchet and Weibull distributions and is therefore classified as a family of distributions (Fukutome et al., 2018).

3.2 Block Maxima

The Block Maxima approach attempts to describe the probability distribution of maxima of blocks. In the Block Maxima approach, the first step is to divide the dataset into equal chunks of data. In EVT most of the times the datasets are divided into yearly blocks of a variable, in this thesis however into seasonal blocks of discharge. The next step is to determine and extract the maxima of these blocks. Subsequently, by estimating the GEV parameters with the help of a parameter estimation technique, a GEV distribution is fitted to the extracted block maxima and return periods and return levels are calculated.

The selection of an adequate block size is a delicate issue in the block maxima approach. Too small block sizes can cause biases, because the parent distribution might not yet have been able to converge to the GEV distribution, and too large block sizes can lead to large sampling errors, especially if the number of blocks is too small. The desired block size therefore depends on the parent distribution. For exponential distributions, the convergence is fast and thus a smaller block size is needed, for normal distributions, the convergence is slow and a larger block size are preferred.

An alternative to the Block Maxima Approach is the Peak-over-Threshold Approach. In the Peak-over-Threshold Approach exceedances above a certain threshold are extracted and the Generalized Pareto Distribution (GPD), similar to the GEV distribution, is fitted to the exceedances.

3.3 Return Period, Return Level & Plotting Position

If one wants to consider discharges, respectively floods from a statistical point of view, it is necessary to establish general rules concerning these quantities. Such a general rule is called the frequency of non-exceedance, also called cumulative frequency analysis, which determines the probability that the discharge Q will not exceed a certain critical value x_Q . The counterpart to this rule is the frequency of exceedance. It determines the probability that the critical value will be exceeded. The following equation expresses the frequency of non-exceedance (Musy and Higy, 2011):

$$F_Q(x_Q) = P(Q \leq x_Q)$$

2

In equation 2, P expresses the Probability. The return period T (in years) of an event can be inferred from the frequency of non-exceedance or its probability and is defined as:

$$T = 1 - P$$

3

In Extreme Value Theory if an event happens once every y years, this event has a return period of y years. Therefore, the probability that such an event happens is:

$$P = \frac{1}{y}$$

4

Hence if an event exceeds a critical value with a probability of 0.01 the Return Period associated with this event is 100 years. We can see that a discharge with return period T is an event that is exceeded on average every T years.

In order to estimate the return period T from measured data the standard procedure is first to rank the block maxima/peak-over-thresholds in increasing order of magnitude and secondly to use a plotting method to determine the return periods for different events.

The selection of the plotting position is heavily discussed and multiple plotting formulas have been developed. According to Makkonen (2006) the Weibull plotting position is the optimal one, because other formulas tend to overestimate the return period and therefore underestimate the risk. The Weibull plotting position is defined as follows:

$$T = \frac{m}{N + 1}$$

5

N is the number of events and m is the rank of the event, from smallest $m = 1$ to largest $m = N$. In return level plots, the return period is usually displayed logarithmically.

The return level assigned to a return period of y years is the amount of runoff that is exceeded on average at least once every y years. Therefore, the return period belongs to the $(1 - p)^{th}$ quantile of the GEV distribution. For any p ($p \in [0,1]$) a return level can be calculated by inverting the function G in equation 1:

$$G^{-1}(1 - p; \theta) = \begin{cases} \mu - \frac{\sigma}{\xi} (1 - [-\ln(1 - p)]^{-\xi}) & \xi \neq 0 \\ \mu - \sigma \ln[-\ln(1 - p)] & \xi = 0 \end{cases}$$

6

The location and scale parameters μ, σ in equation 6 are linear, whereas the shape parameter ξ is nonlinear. Therefore ξ is much more important than the other parameters and its estimation is much more critical for return levels associated with long return periods. (Coles, 2001; Katz et al., 2005)

3.4 Parameter Estimation

There are several methods available to estimate the shape, scale and location parameters of the GEV distribution. Each has its own positive and negative aspects and the optimal parameter estimation can differ for every dataset. The most important parameter estimation methods are the Maximum Likelihood Method (ML), the method of probability weighted moments or the method of L-moments. In this thesis, the maximum likelihood method was predominantly used, but when the results for a station did not fit sufficiently, the method of L-moments was applied instead.

3.4.1 Maximum Likelihood Method (MLE)

The concept of ML is based on the Likelihood L . The likelihood L is defined as the probability of drawing a data measurement sample m_i of a distribution with specified parameters θ :

$$L = \text{prob}(\{m_i; \theta\}) = \prod_i^n f(m_i; \theta)$$

7

f is the probability density of the distribution, θ the vector of parameters (in the case of GEV $\theta = (\mu, \sigma, \xi)$) and L is the Likelihood function, which is a function of the parameters θ .

The goal of ML is then to find the parameters μ, σ, ξ for which the probability of drawing $\{m_i, i = 1, \dots, N\}$ as a random sample from the GEV would be largest (The set of parameters for which L is maximized). This is called the Maximum Likelihood Estimate (MLE). The Maximum Likelihood Estimate is found numerically and thus computationally demanding but it is robust against outliers. MLE in this thesis are found with the help the extRemes package in R (Gilleland et al., 2009).

3.4.2 Method of L-moments

L-moments are used to describe the shape of a probability density function (pdf). They are related to conventional moments, where the standard deviation, skewness, and kurtosis are calculated. For L-moments, these quantities are referred to as L-scale, L-skew, and L-kurtosis. The first L-moments is defined as follows:

$$\lambda_1 = \int x f(x) dx$$

8

$f(x)$ is the probability density function of the distribution. The second L-Moment can be described by the next equation:

$$\lambda_2 = \frac{1}{2} \int \int_{x>y} (x - y) f(x) f(y) dx dy$$

9

and the third L-moment:

$$\lambda_3 = \frac{1}{3} \int \int \int_{x>y>z} (x - 2y + z) f(x) f(y) f(z) dx dy dz$$

10

Therefore L-moments are functions of the distribution parameters. For the GEV, the parameters μ, σ, ξ have to be set so that the first three sample L-moments are equal to the first three L-moments of the GEV. The method of L-moments is easier to implement than the maximum likelihood method, because it can be solved analytically.

3.5 Uncertainty

Usually in Extreme Value Theory the uncertainty of a GEV is estimated with confidence Intervals. Confidence intervals are statistical intervals that are intended to locate the position of one or more true parameters of a population with a certain probability. The most prominent one is the 95%-confidence interval. The 95%-confidence interval can be explained as the interval whose limits enclose the true parameters 95% of the time and do not enclose it 5% of the time. Confidence intervals can be generated by resampling, with the asymptotic maximum likelihood confidence method or the likelihood-Profile confidence method.

In this thesis, no confidence intervals are used. The rationale for this is due to the length of the used datasets. Since the individual simulated scenarios have a cumulative length of 289,000 years and can be freely combined, a total of 28 runoff time series with a length of 10'000 years each were created (one with 9'000 years length). The uncertainty can now be represented by plotting all of the 29 time series simultaneously. This not only visualizes the uncertainty more effectively, but also averts the uncertainty from the GEV model to the data acquisition of the weather generator.

3.6 Flood-Duration-Frequency Curves (QdF)

In classical flood frequency analysis floods are only characterized by their instantaneous peak value. For a complete understanding of floods however, different volumes and durations have also be taken into account. The Flood-duration-frequency approach in this chapter considers these quantities by expressing the flood duration as a fixed parameter. The QdF and converging QdF approach follows the work of Javelle et al. (2002a).

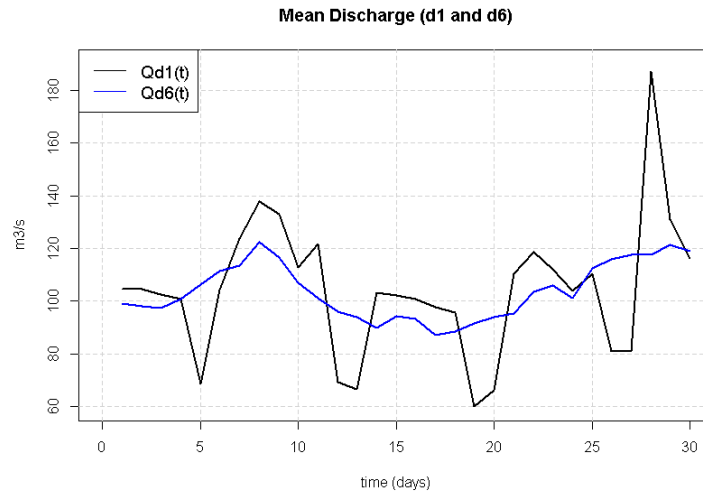


Figure 3: Mean discharge for durations $d_1 = 1$ day and $d_6 = 6$ days. The black line indicates the d_1 discharge time series, the blue line the d_6 time series. The maxima of the two discharge time series are at different locations. For the d_1 time series, the maxima is at 28 days, for the d_6 time series the maxima is at 8 days.

3.6.1 Local QdF model

Floods can be characterized by their (instantaneous) peak value (Q_{max}) based on the discharge time series. The discharge time series, however, can reveal not only instantaneous peak values, but also maximum values of mean discharges ($Q_{max,d_1}, Q_{max,d_2}, \dots, Q_{max,d_N}$) for some durations (d_1, d_2, \dots, d_N). A moving average filter with duration d can be used to obtain the mean maximum discharge values of duration d over the entire instantaneous discharge time series. The result is a new discharge time series with duration length d :

$$Q_d(t) = \frac{1}{d} \int_{t-\frac{d}{2}}^{t+\frac{d}{2}} Q(t) dt$$

11

As in classical Extreme Value Theory it is now possible to extract block maximas or peaks-over-thresholds of the newly generated time series.

Figure 3 shows the influence of the newly created meaned discharge time series ($Q_{d_1}(t), Q_{d_6}(t)$) with durations d_1 and d_6 on their respective maximas. It can be noticed, that the two average discharge time series have maximas at different times. For $Q_{d_1}(t)$ the maxima Q_{max,d_1} is at day 28, and the maxima Q_{max,d_6} for $Q_{d_6}(t)$ is at day 8. Therefore, two different flood events are represented by the meaned discharge time series. The maximum discharge volume $V_{max,d}$ can be calculated by the maxima of the time series and the duration:

$$V_{max,d} = Q_{max,d} * d$$

12

21

For the flood event at day 28 the maximum discharge Volume 131 m³/s and for the event at day 8, 732 m³/s. Even though Q_{max,d_1} is much higher than Q_{max,d_6} , V_{max,d_1} is of much smaller magnitude than V_{max,d_6} .

As in classical Extreme Value Theory the next step is to fit a distribution to the newly generated time series with different durations, and flood quantiles $Q_{max,d}(T)$ can be estimated. In the example in figure 4, the QdF method is carried out for annual maxima in the winter season for Aarberg. The parameters of the GEV distribution are estimated with the method of L-moments.

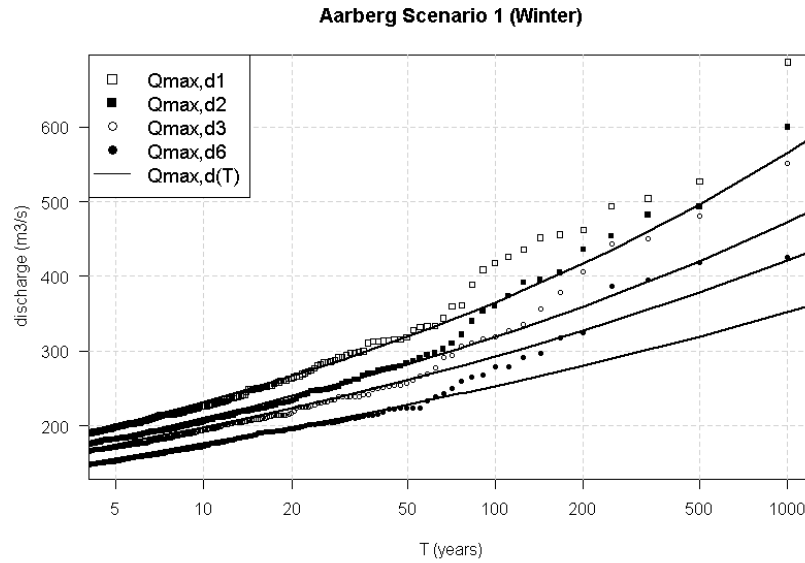


Figure 4: QdF curves for the Aarberg scenario 1 in winter. Filled black circles indicate the discharge maxima for the duration d6, empty circles the maxima for the duration d3, filled squares the maxima for the duration d2, empty squares the maxima for duration d1 and the black lines represent the corresponding quantiles.

3.6.2 Converging QdF model

The quantiles $Q_{max,d}(T)$ shown in Figure 4 depend only on the duration d . However it can be advantageous to design quantiles as a function of both d and T . These new quantiles $Q_{max}(d, T)$ are based on two hypotheses (Javelle et al., 2002a):

1. The evolution of $Q_{max}(d, T)$ for a given return period can be described by a hyperbolic form.
2. The distributions are related to themselves along a horizontal line (When d tends to infinity, the hyperbolas align with a horizontal line $Y = K$ defined by a critical value K)

Considering these two hypotheses, the QdF model takes the form:

$$Q_{max}(d, T) = \frac{Q_{max}(d = 0, T) - K}{1 + d/\Delta} + K$$

13

and can be simplified for $K = 0$ (Javelle et al., 2001):

$$Q_{max}(d, T) = \frac{Q_{max}(d = 0, T)}{1 + d/\Delta}$$

14

$Q_{max}(d = 0, T)$ denotes the distribution of instantaneous peak discharge maxima and the parameter Δ describes the shape of the hyperbolas. Δ characterizes flood dynamics for different stations or basins and is therefore also referred to as characteristic flood duration. For example, high Δ values indicate slow floods and small values indicate quicker floods, as indicated by Figure 5 for Flumenthal ($\Delta = 40$) and Schiffenen ($\Delta = 8$).

As for the quantiles $Q_{max,d}(T)$ the parameters of the GEV distribution must be estimated for the $Q_{max}(d, T)$ quantiles, but additionally the Δ parameter as well. To estimate Δ equation 14 is used. First, every value of maximum mean discharge $Q_{max,d}(j)$ is scaled:

$$q_{max,d_i}(j) = Q_{max,d}(j) \left[1 + \frac{d_i}{\delta} \right]$$

15

The scaled values $q_{max,d_i}(j)$ are then calculated over the different durations d_i and meaned:

$$\bar{q}_{max,d}(j) = \frac{1}{N} \sum_{i=1}^N q_{max,d_i}(j)$$

16

The parameter Δ can then be approximated as the optimized value δ , which minimizes the dispersion of the following equation:

$$\Delta = \delta^{opt} = \min \left\{ \frac{1}{NV} \frac{1}{N} \sum_{j=1}^{NV} \sum_{i=1}^N \left[\frac{q_{max,d_i}(j) - \bar{q}_{max,d}(j)}{\bar{q}_{max,d}(j)} \right]^2 \right\}$$

17

N is the number of durations and NV is the number of maximum mean discharge values.

The estimation of the location, scale and shape parameters is then done by Maximum Likelihood Estimation or Method of L-moments, using the mean time scaled values $\bar{q}_d(j)$. After that, equation 14 can be utilized to create quantiles for every for any duration d .

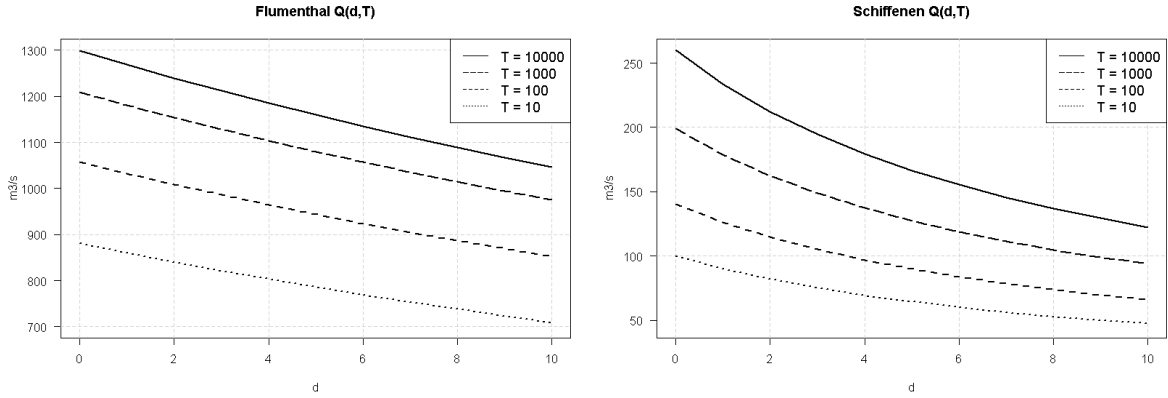


Figure 5: Influence of the Delta parameter Δ on the converging QdF curves for Flumenthal (left) and Schiffenen (right). The lines indicate different return periods. For Flumenthal the Delta parameter is high, for Schiffenen the Delta parameter is low.

3.6.3 Validation

There are many possibilities to validate or test the goodness-of-fit of a GEV model. In this thesis, the relative root mean squared error (rRMSE) is chosen. rRMSE is a simpler method that calculates the error percentage of the model in comparison to the observations. In this thesis however, the observations are replaced with the simulated mean maximum discharge values. The rRMSE is chosen because it is simple and because not only can the error be calculated for the model in total, but also for individual return periods. The rRMSE takes the bias and the variance into account:

$$rRMSE(T) = \left[\frac{1}{29} \sum_{S=1}^{29} \left(\frac{X_{max,d}(T) - Q_{max,d}(T)}{X_{max,d}(T)} \right)_{scenario S}^2 \right]^{0.5}$$

18

$X_{max,d}(T)$ is the simulated mean maximum discharge for return period T and $Q_{max,d}(T)$ the fitted Quantiles of the mean maximum discharge for return period T . In this work, the return period was calculated for $T = 10$, $T = 100$, $T = 1'000$ and $T = 10'000$ and for duration d_1 .

The rRMSE calculates the accuracy of the model in percent, but does not give a score if the model fit is adequate. The evaluation of the model on the basis of the rRMSE is therefore subjective. Since floods with extreme return periods of 10'000 years are under investigation in this thesis, relatively large errors can still be acceptable. For example in Javelle et al. (2002a), an error of 13% is considered appropriate for the 100 year return period. Therefore, for the 10'000 year return period error below 30% should be just acceptable.

3.7 Extreme Flood Events (T = 10'000)

Using the QdF curves, it was made easy to determine extreme flood events with return period of 10'000 years. To investigate these flood events with respect to precipitation distribution and snowmelt, the simulated precipitation and temperature time series are considered. Because the simulated precipitation and temperature time series are not point or station measurements like the simulated discharge time series, the associated 89 subcatchments must first be created in ArcMap.

In this thesis, not single flood events were analyzed, but several at the same time. The events originate from the 29 combined scenarios which add up to 10'000 years. Since one of the 29 scenarios has a combined length of only 9000 years, the flood event with a return period of 9000 years is considered there. Thus 116 flood events were investigated per station (29 per season). Flood events with different durations were generated by the QdF curves, but only one duration per station was considered in this chapter. The decision which duration is most important for each station was made pragmatically based on the Δ parameter of the converging QdF curves. As mentioned in chapter 3.6.2, the Δ parameter is also called the characteristic duration and reflects whether the station is more likely to be affected by slow floods or flash floods. According to the Δ parameter each station was divided into a group with characteristic flood duration, as shown in Table 3.

Table 3: Delta parameter values and their assigned durations d (days)

Δ	Duration d (days)
0-10	1
10-20	2
20-30	3
>30	6

3.7.1 Precipitation distribution

To analyze the precipitation distribution before and during an event with return periods of 10'000 years, such floods had to be localized. This was made easy with the help of the QdF curves. After localizing the event, the corresponding Precipitation values for every catchment can be extracted from the precipitation time series. This step was repeated for each combined scenario, for every season and for each station. The precipitation was then summed up for 6 days before the event and the one day during the event. Afterwards the precipitation amounts were assigned to their corresponding subbasin and classified according to Jenks Natural Breaks. Jenks Natural Breaks divides the data into natural categories. The breaks are set in such a way that the variance within a category is minimized and the variance with respect to other categories is maximized (Jenks and Caspall, 1971). The results are choropleth maps, which show spatial tendencies in precipitation during and before all extreme flood events with return periods of 10'000 years at a station and for a season and thus where precipitation is largest and lowest in the Aare River Basin.

3.7.2 Snowmelt

The Influence of snowmelt on extreme floods is harder to estimate than the influence of precipitation, because precipitation causes a rather direct response in discharge, whereas for snowmelt, certain conditions must be present. The conditions are that there must be large amounts of snow present, which for the most part only exist in winter or in spring, as well as temperatures large enough to melt a substantial amount of snow. These conditions should only match for the spring season and therefore only spring is taken into consideration in this subchapter. Again, the first step is as for the precipitation distribution to localize flood events with return periods of 10'000

years. Based on the assumption that there is sufficient snow, snowmelt can only have a significant impact on the flood if temperatures are above 0°C and an increase in temperature can be detected prior to the event. The reasoning behind this is that large amounts of snow must melt in order to have a significant impact on flooding. The energy for the melting process comes from a rise in temperature over a short period of time. The temperature difference was again displayed graphically in the results, and the categories are again made with Jenks Natural Breaks.

However, if there exists a noticeable increase in temperature, that does not necessarily mean that snowmelt is having an impact on the flood event, but rather that there exists the potential for a lot of snow to melt. But based on the available data we don't know for sure if snow is present before the flood event. In order to estimate whether and how large the influence of snowmelt is, the runoff coefficient C is calculated from the discharge Q and precipitation P for every season:

$$Q = P * C$$

19

The dimensionless proportion C is usually calculated for the surface runoff of an area and reflects soil type, gradient, permeability and land use of an area. In this thesis, the runoff coefficient C is being alienated to compare the precipitation total of the whole Aare region with the discharge of the station. Obviously not all precipitation is participating in the flood event, but it gives an overview of the percentage of precipitation involved. The runoff coefficient of the spring season of a station is then compared to the runoff coefficient of the other seasons. If the spring runoff coefficient is considerably higher than the runoff coefficient of the other seasons and if and only if there is a substantial increase in temperature visible, there is a high probability that the snowmelt has an impact on the flood event, because the missing precipitation is being compensated by the water input from snowmelt.

4. Results

In this chapter, the results of the 18 stations are presented. The Delta parameter Δ was used to divide the stations into 4 groups with different assigned and specific durations. The stations were then examined with focus on these durations. The assigned duration for each station and season can be seen in Table 4. The converging QdF curves for each station and season are listed in Appendix B.

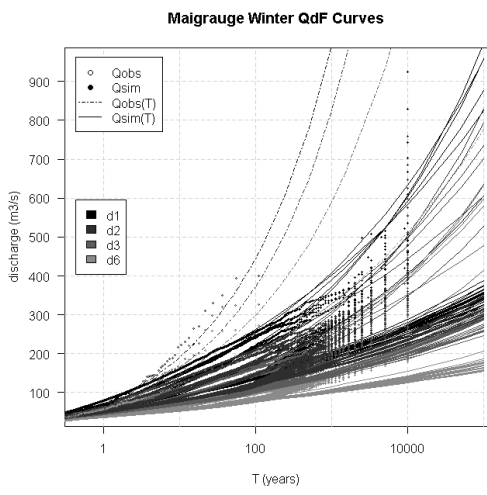
For each station 4 QdF curves (1 per season), 4 precipitation choropleth maps (1 per season), 1 temperature difference choropleth map (spring season) and a Table with flood statistics for the flood events with 10'000 years return period and rRMSE values were created.

The QdF curves show the 29 simulated mean maximum discharge values (filled dots) and simulated quantiles (thick lines) of the combined scenarios, as well as the observed mean maximum discharge values (unfilled dots) and observed quantiles (dotted lines) for a nearby measuring station for the 4 different durations d1, d2, d3 and d6 (shades of grey). Since the QdF curves are sometimes a bit cluttered, because a total of 4 different durations with 29 scenarios each are shown, the QdF curves for individual durations are included in Appendix A. The x-axes of the QdF curves represent the return period in years and are logarithmic; the y-axes show the corresponding mean maximum discharge return levels in m³/s.

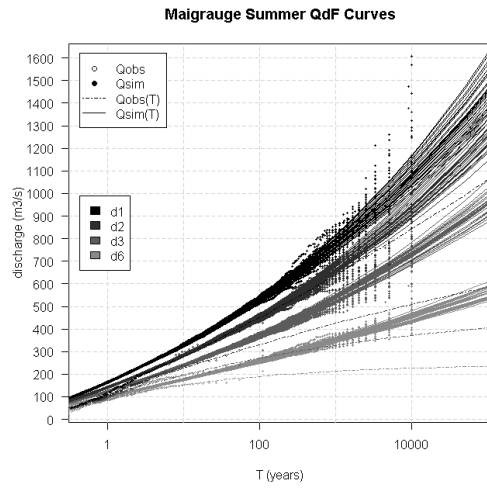
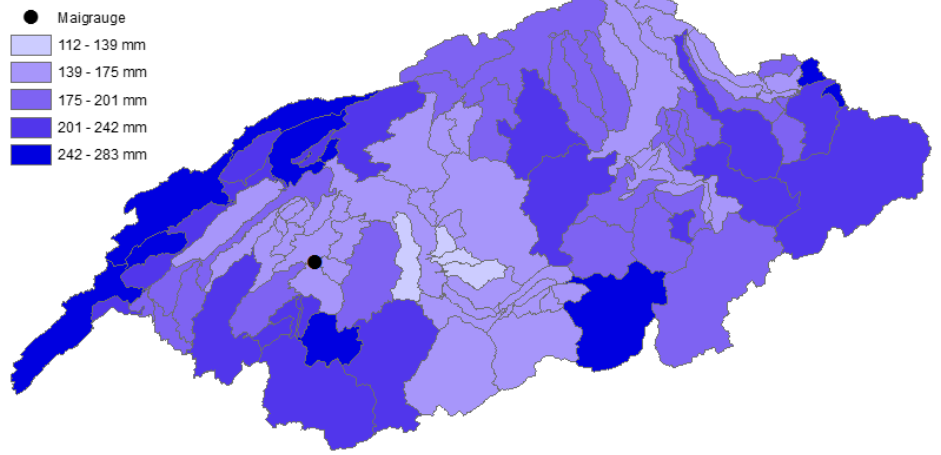
In the precipitation choropleth maps the precipitation is summed up over 7 days and averaged for all scenarios in mm (shades of blue), in the temperature choropleth map, the temperature difference in °C between the day of the event and 7 days before the event is presented (shades of red). In all the maps, the station is represented as a dot and the nearby measuring station as a triangle.

Table 4: Seasonal and meaned delta parameter Δ values for all stations as well as the assigned characteristic flood duration d in days.

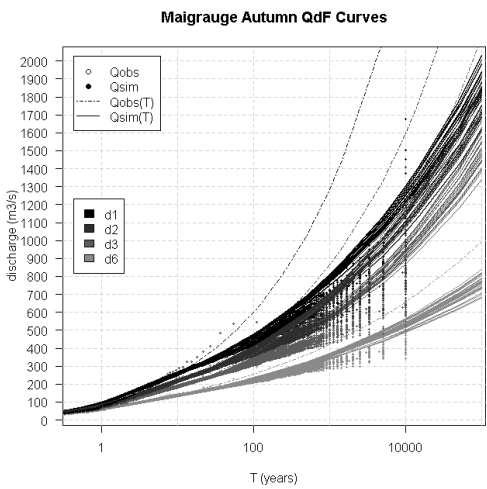
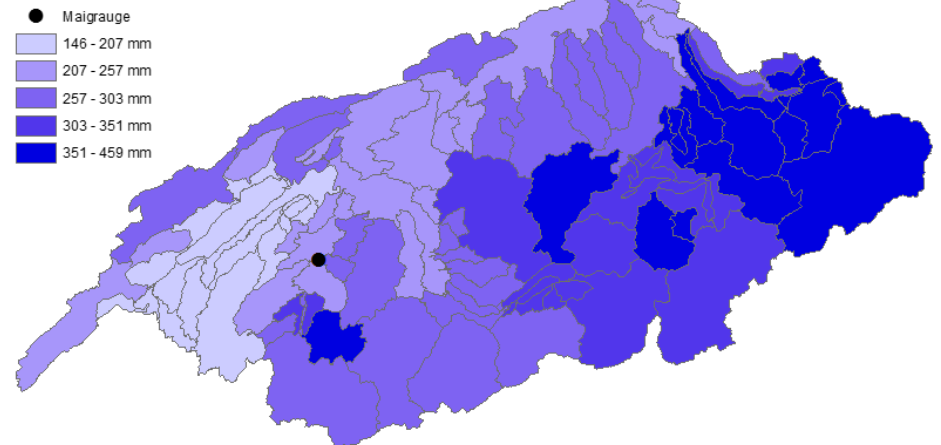
Station	Δ - Winter	Δ - Spring	Δ - Summer	Δ - Autumn	Δ - Mean	Assigned Duration (days)
Aarberg	19.5	19	16.1	17	17.9	2
Bannwil	21.7	41	35.2	27.4	31.3	6
Beznau	18.5	28.9	27	24.8	24.8	3
Flumenthal	22.3	42	36.1	28.1	32.1	6
Gösgen	19.6	37.1	32.6	25.5	28.7	3
Klingnau	18.4	28.6	27	25	24.8	3
Le Châlet	13	21.4	7.9	7.4	12.4	2
Maigrauge	8.6	9.9	6.3	7.2	8	1
Mühleberg	21	32.6	29	27.5	27.5	3
Niederried	19.6	19	16.1	17	18	2
Rossens	8	11.1	6.4	6.4	7.9	1
Rupperswil	18.9	35.3	31.3	24.5	27.5	3
Ruppoldingen	20.8	37.9	33.8	26.4	29.7	3
Schiffenen	8.4	9.9	6.3	7.2	8	1
Wettingen	15.6	22.3	21.6	19.6	19.7	2
Wichelsee	22.7	20	20	26.8	22.3	3
Wildeggen	18.5	34.2	30.9	24.4	27	3
Wynau	21.6	40.7	35.1	27.3	31.2	6



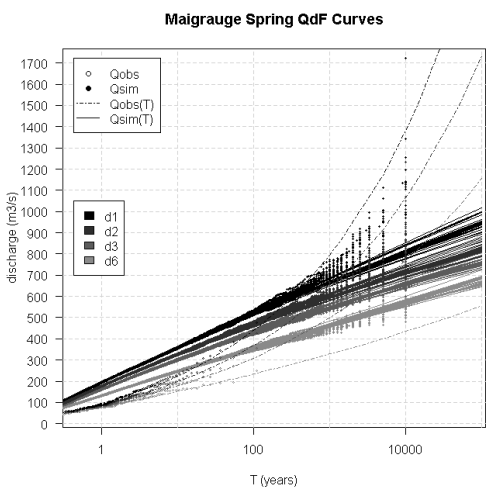
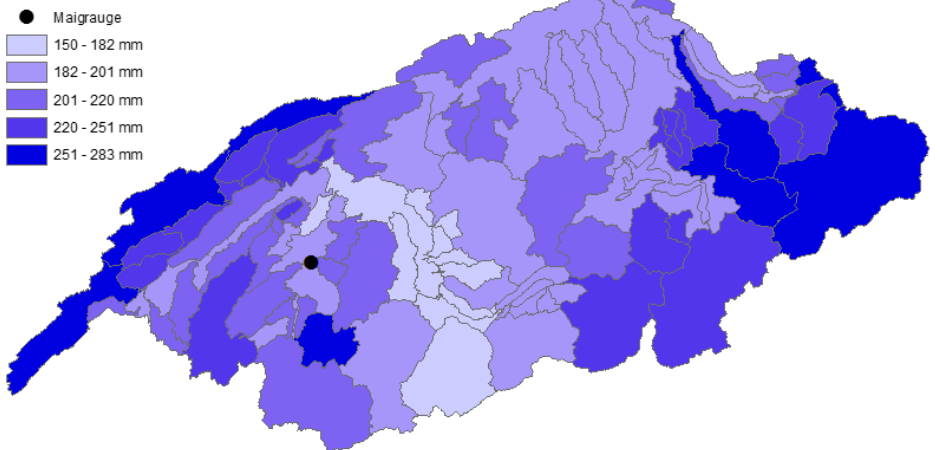
Maigrauge Winter Precipitation



Maigrauge Summer Precipitation



Maigrauge Autumn Precipitation



Maigrauge Spring Precipitation

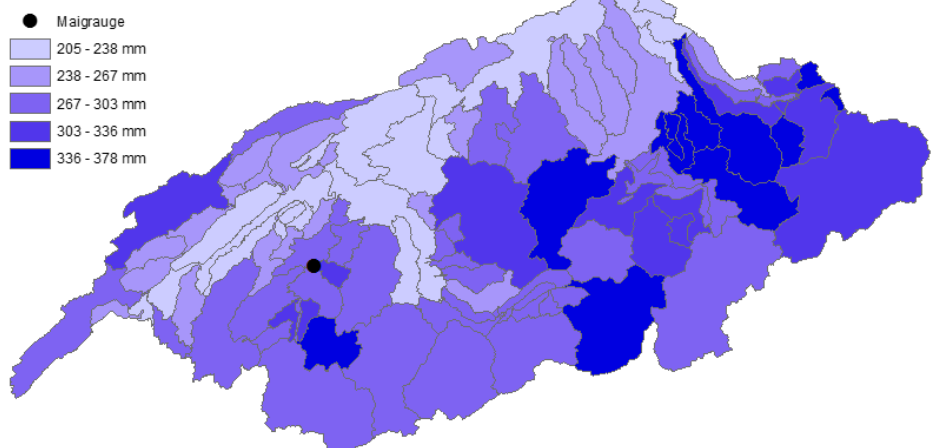


Figure 7: QdF curves for Maigrauge. From top to bottom: winter, summer, autumn, spring.

Figure 6: Precipitation distribution maps for Maigrauge and duration d1. From top to bottom: winter, summer, autumn, spring.

Table 5: Seasonal mean maximum discharge sum, mean, minimum value, maximum value and range for the 10'000 year return period floods and duration $d1$ in m^3/s , seasonal runoff coefficient C for the 10'000 year return period and duration $d1$ and seasonal rRMSE values for duration $d1$ and return periods $T=10$, $T=100$, $T=1'000$ and $T=10'000$ in %.

Maigrauge	Winter	Spring	Summer	Autumn
Q_{sum} ($d1$, $T = 10'000$) (m^3/s)	14828	28935	34418	30183
Q_{mean} ($d1$, $T = 10'000$) (m^3/s)	511	998	1187	1041
Q_{min} ($d1$, $T = 10'000$) (m^3/s)	350	750	941	728
Q_{max} ($d1$, $T = 10'000$) (m^3/s)	924	1721	1609	1676
Q_{range} ($d1$, $T = 10'000$) (m^3/s)	574	971	668	948
C ($d1$, $T = 10'000$)	0.08	0.1	0.12	0.15
rRMSE ($d1$, $T = 10$) (%)	1.5	0.6	1.2	4.5
rRMSE ($d1$, $T = 100$) (%)	1.9	1.5	1.1	8.3
rRMSE ($d1$, $T = 1'000$) (%)	22.6	6.6	3.9	15.1
rRMSE ($d1$, $T = 10'000$) (%)	45.7	23	12.8	31.5

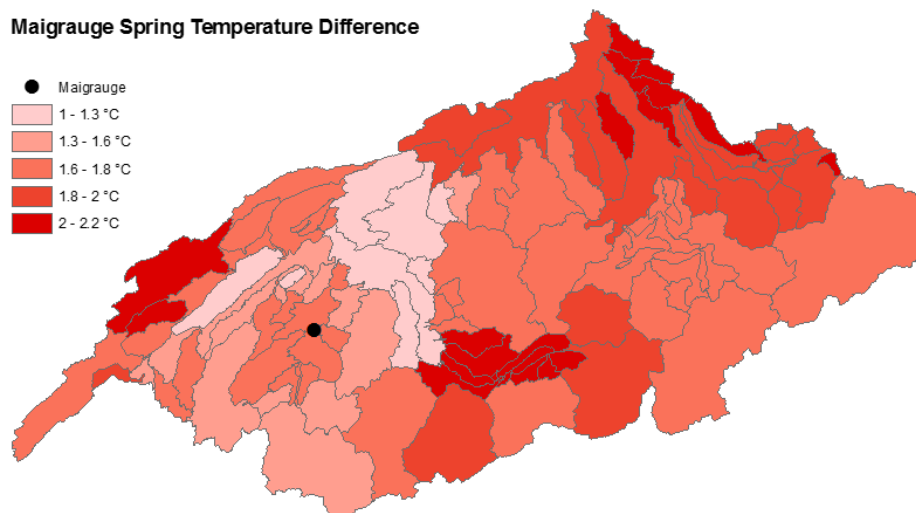


Figure 8: Temperature difference map for Maigrauge in spring and duration $d1$.

4.1 Group Duration d1

4.1.1 Maigrauge

The simulated QdF curves of Maigrauge in Figure 6 can adequately describe the simulated mean maximum discharges in spring, summer and autumn until a return period of approximately $T = 1'000$ years. For larger return periods ($T > 1'000$ years), the spring quantiles tend to underestimate the return level by 50-100 m^3/s , whereas the autumn ones tend to overestimate it with similar magnitude. In winter, something strange occurs. In some scenarios, the maximum mean discharge of certain scenarios is disproportionately large over all return periods compared to the other scenarios (50-200 m^3/s at $T = 100$ years). This leads to an extreme spreading of the quantiles. The fitted probability distributions are Fréchet in winter, summer and autumn and Weibull in spring. In Table 5, the rRMSE shows a fairly good result in summer (12.8%) and spring (23%), a moderate result in autumn (31.5%) and a large error for the 10'000 year return period in winter (45.7%). Largest 10'000-years return period floods with respect to the mean can be observed in summer (1187 m^3/s), followed by spring (998 m^3/s), autumn (1041 m^3/s) and winter (511 m^3/s). However, the largest singular values are observed in spring (1721 m^3/s) and autumn (1676 m^3/s). The corresponding measuring station to Maigrauge is Fribourg, with an approximate distance of 500 meters.

The observed discharge maxima agree with the simulated ones in summer and autumn. In spring the observed maximum mean discharge seems to be slightly smaller than the simulated one ($\sim 50 m^3/s$). In winter, return values are much higher for return periods between 10 and 100 years in the observed case ($\sim 50-200 m^3/s$). The fitted probability distributions are quite similar in winter and summer, but the observed quantiles are much steeper. In the observed case the fitted probability distributions are of Fréchet and Weibull nature for spring and summer respectively, in the simulations, the assumption are Weibull distributions for spring and Fréchet distributions for summer.

In the precipitation map for Maigrauge in Figure 7 the precipitation is high for all subbasins in the Aare region (122-459 mm) and there are clear structures visible in the precipitation distributions for flood events with return periods of 10'000 years and duration d1. The precipitation distributions tend to be similar for autumn and winter, as well as summer and spring. In summer and spring there is a clear gradient in precipitation noticeable between southeast and northwest. The precipitation maxima are predominantly found in a band ranging from east to southwest, minima in the north and the west. In autumn and winter the precipitation structure is more or less divided into west, central and east. Maxima are most of time located in basins at the western and eastern border of the Aare region, whereas minima are identified in the central part. Directly at the station Maigrauge the precipitation is comparatively low in winter, summer and autumn and relatively high for spring. In general the precipitation amounts are high in spring (378 mm) and summer (459 mm), and lowest in winter (283 mm) and autumn (283 mm).

The temperature map for spring and duration d1 in Figure 8 shows an overall increase in temperature before the events (1-2.2°C). This increase is largest in the north, south and western part of the Aare basin and lowest in the western central parts. The spring runoff coefficient C (0.1) in Table 5 is lower than the summer (0.12) and autumn ones (0.15), but higher than the winter one (0.08).

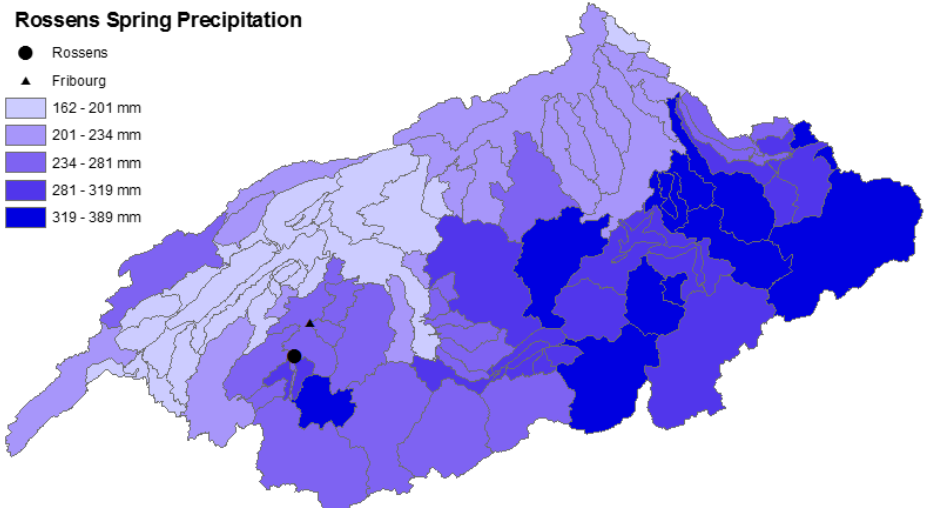
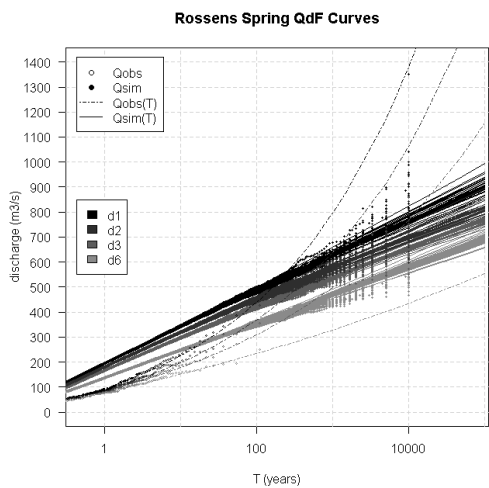
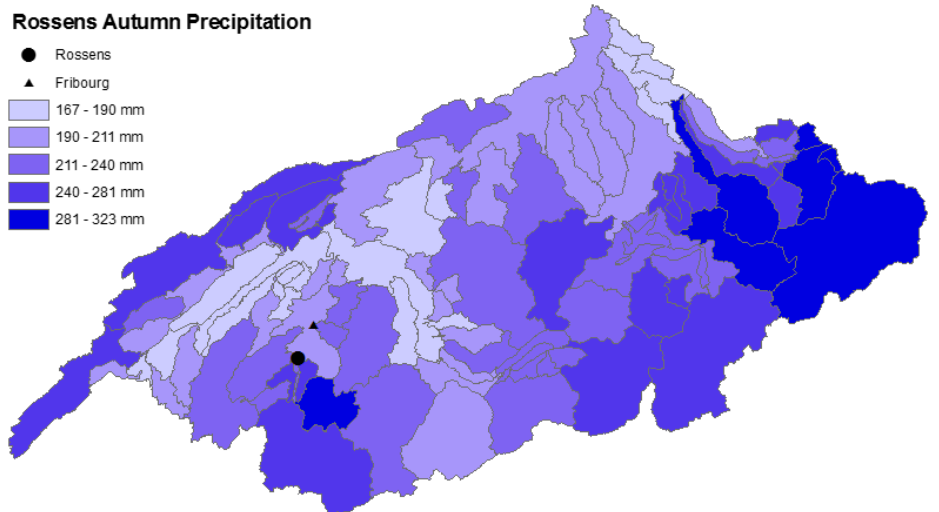
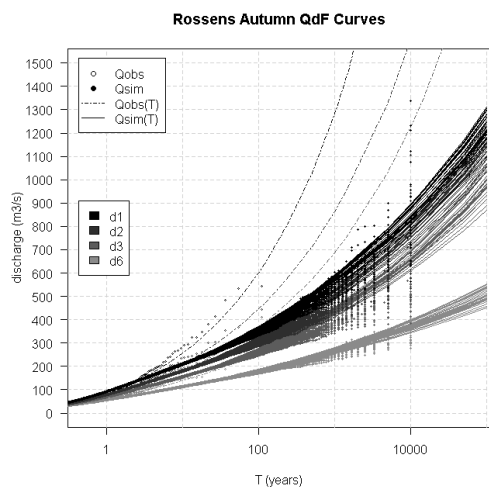
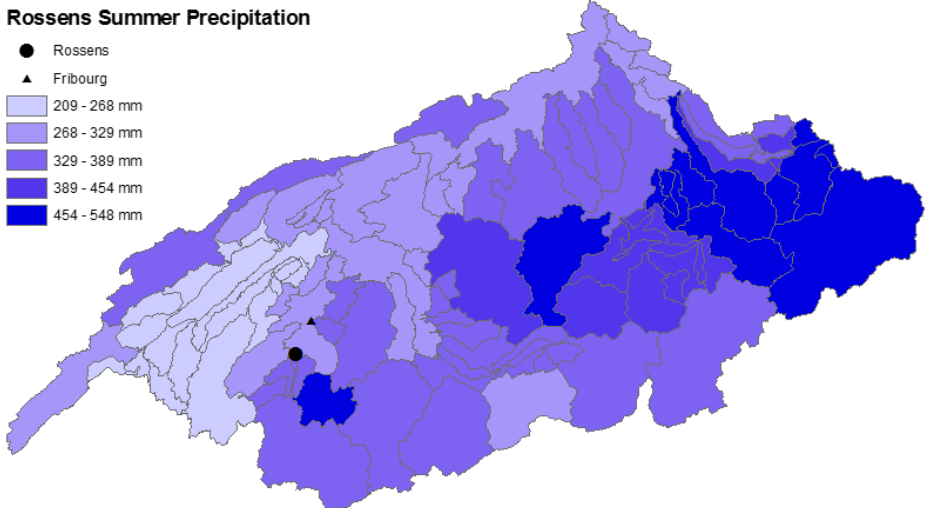
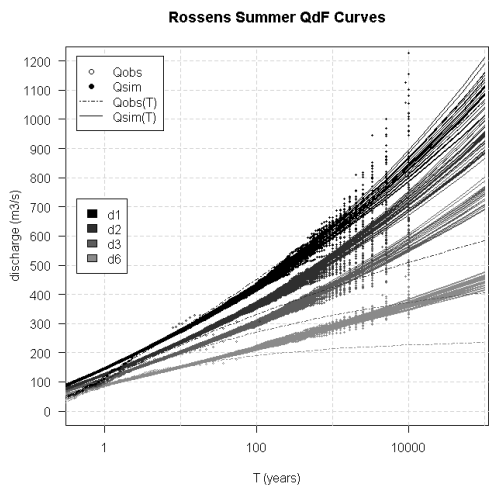
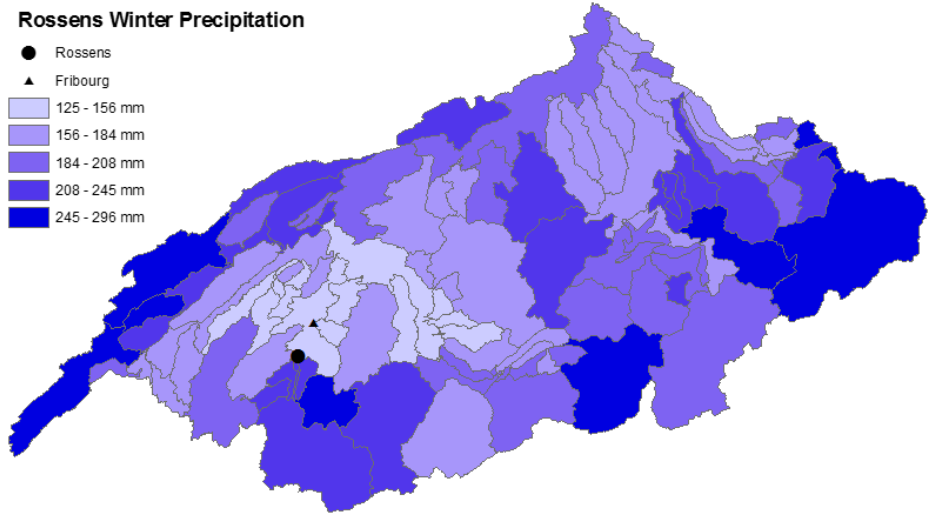
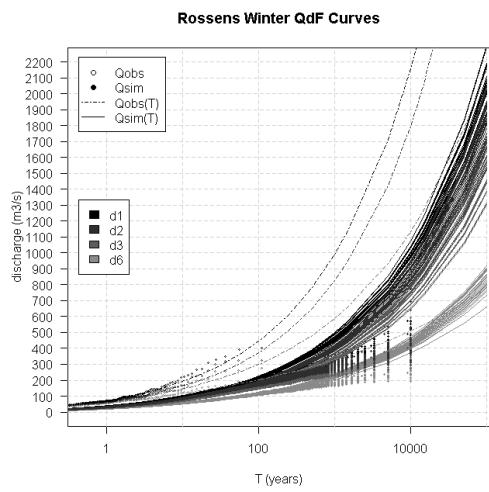


Figure 9: QdF curves for Rossens. From top to bottom: winter, summer, autumn, spring.

Figure 10: Precipitation distribution maps for Rossens and duration d1. From top to bottom: winter, summer, autumn, spring.

Table 6: Seasonal mean maximum discharge sum, mean, minimum value, maximum value and range for the 10'000 year return period floods and duration d1 in m³/s, seasonal runoff coefficient C for 10'000 year return periods and duration d1 and seasonal rRMSE values for duration d1 and return periods T=10, T=100, T=1'000 and T=10'000 in %.

Rossens	Winter	Spring	Summer	Autumn
$Q_{max,sum} (d1, T = 10'000)$ (m ³ /s)	14608	23652	26836	24645
$Q_{mean}(d1, T = 10'000)$ (m ³ /s)	504	816	925	850
$Q_{min}(d1, T = 10'000)$ (m ³ /s)	389	641	689	564
$Q_{max}(d1, T = 10'000)$ (m ³ /s)	894	1350	1226	1337
$Q_{range}(T = 10'000)$ (m ³ /s)	505	709	537	773
$C(d1, T = 10'000)$	0.08	0.08	0.08	0.11
rRMSE (d1, T = 10) (%)	4.8	1.3	1	1.9
rRMSE (d1, T = 100) (%)	9.7	0.9	1.5	5.6
rRMSE (d1, T = 1'000) (%)	5	2.9	3.1	7.8
rRMSE (d1, T = 10'000) (%)	107	14.8	13.2	20

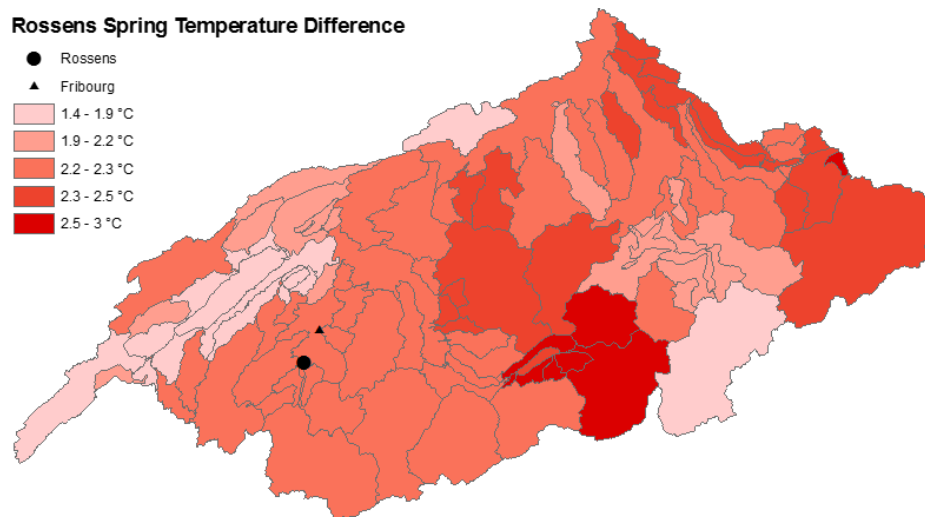


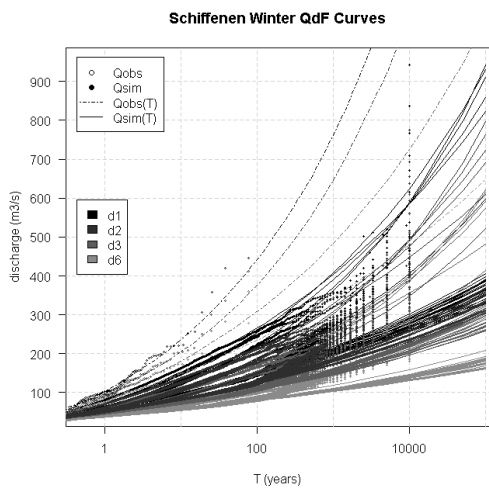
Figure 11: Temperature difference map for Rossens in spring and duration d1.

4.1.2 Rossens

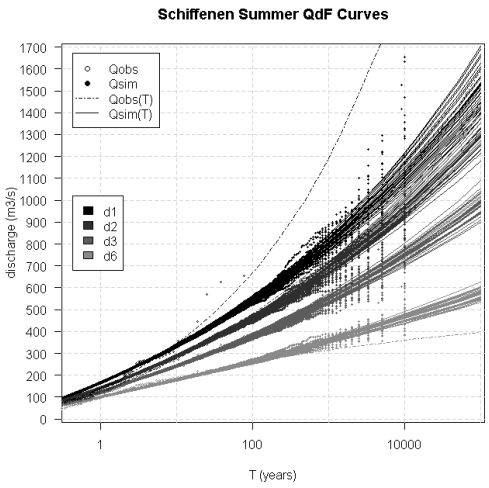
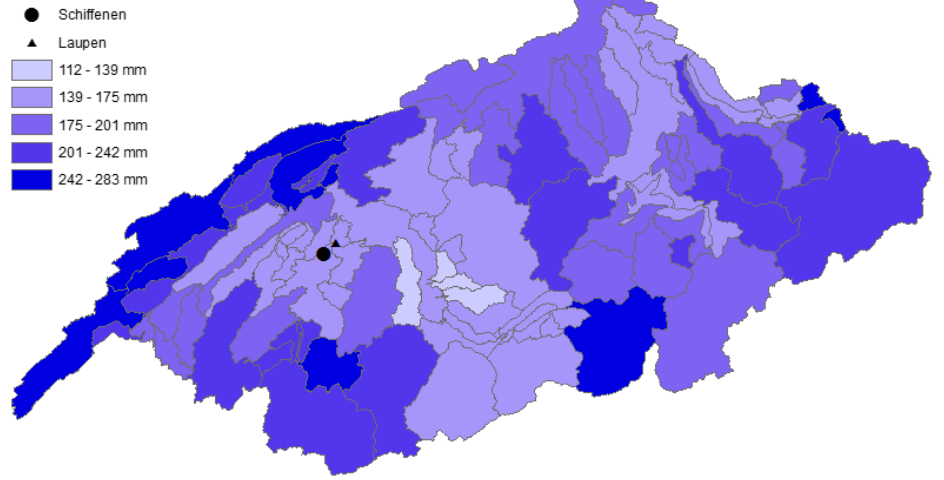
The QdF curves of Rossens are presented in Figure 9. The simulated quantiles can describe the maximum mean discharge for all seasons at low return periods ($T < 100$ years), as well as for high return periods in summer and spring. In autumn, the quantiles tend to overestimate the mean maximum discharge return levels slightly ($\sim 50 \text{ m}^3/\text{s}$). This is also the case in winter, but here the maximum mean discharge is greatly overestimated for extreme return periods ($> 400 \text{ m}^3/\text{s}$ at $T = 10'000$ years). In winter, summer and autumn, the fitted distributions are Fréchet, in spring the Gumbel distributions. The rRMSE in Table 6 is relatively low for spring (1.3-14.8%), summer (1-13.2%) and autumn (1.9-20%) for all return periods, with the exception in winter where the rRMSE is huge for the 10'000-year return period (107%). The 10'000 year return period discharges are highest in summer with respect to the mean ($925 \text{ m}^3/\text{s}$), and highest in spring ($1350 \text{ m}^3/\text{s}$) and autumn ($1337 \text{ m}^3/\text{s}$) with respect to the maximal value. The lowest values appear in winter. Rossens station is compared to the station in Fribourg, with an approximate distance of 10 kilometers. The observed discharge maxima correspond well with the simulated ones in winter, summer and autumn. In the spring season, the observed values are generally lower than the simulated maximum mean discharge values ($\sim 50\text{-}100 \text{ m}^3/\text{s}$). In summer and spring, different distributions were assumed, In winter and autumn the same ones, but the observed quantiles are much steeper.

The Rossens precipitations maps for floods with return periods of 10'000 years and duration $d1$ in Figure 10 show high precipitation for all subcatchments in the Aare region (125-548 mm) and a clear and similar structure for summer, spring and autumn. Highest precipitation is found in the southern and eastern parts of the Aare basin and lower precipitation in the north and the west. One small exception can be recognized in autumn, where a pronounced maxima is located at the western Aare margin. In winter the structure is not as clear as in the remaining seasons, but the precipitation minima are predominantly located in the central region of the Aare basin and maxima around the borders. In all seasons there is relatively high precipitation located at Rossens or at least south of Rossens. The precipitation amounts are generally largest in summer (548 mm), followed by spring (389 mm), and autumn (323 mm), and lowest in winter (296 mm).

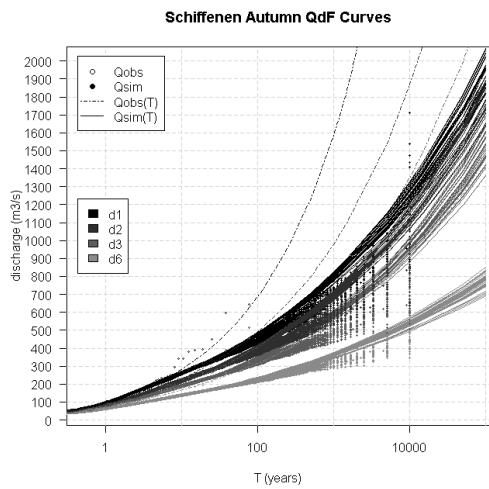
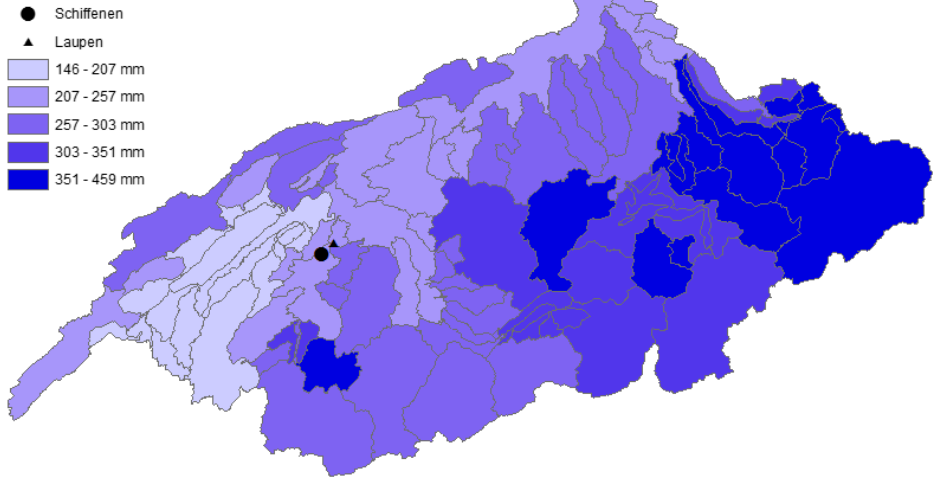
The spring temperature map for duration $d1$ in Figure 11 shows a relatively high increase in temperature in the whole Aare region before the flood events ($1.4\text{-}3^\circ\text{C}$). The temperature increase is smallest in the west and in the southeast, and biggest in the central and southern central part. The spring runoff coefficient C (0.08) in Table 6 is equal to the winter and summer one, but lower than the autumn runoff coefficient (0.11).



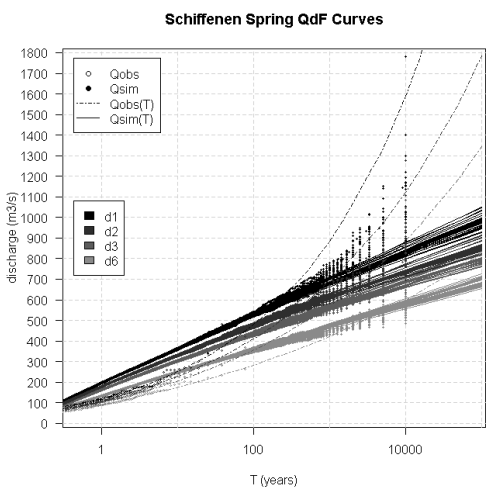
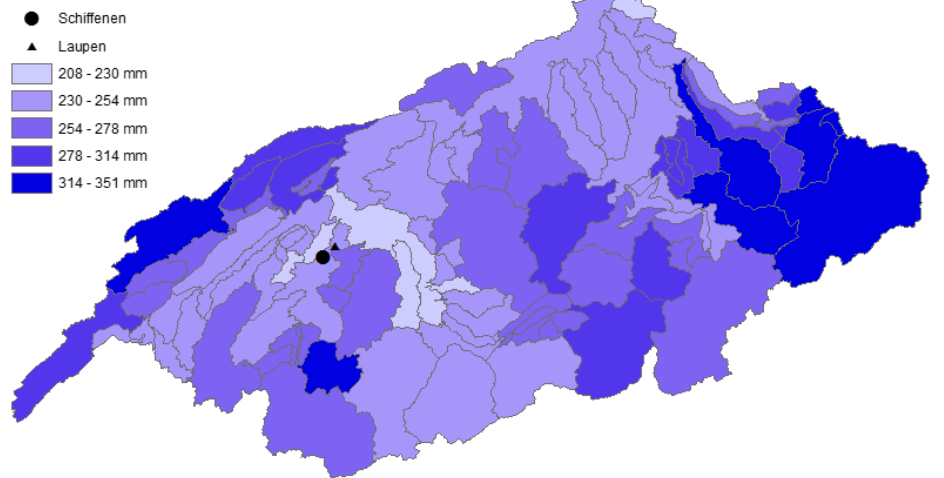
Schiffenen Winter Precipitation



Schiffenen Summer Precipitation



Schiffenen Autumn Precipitation



Schiffenen Spring Precipitation

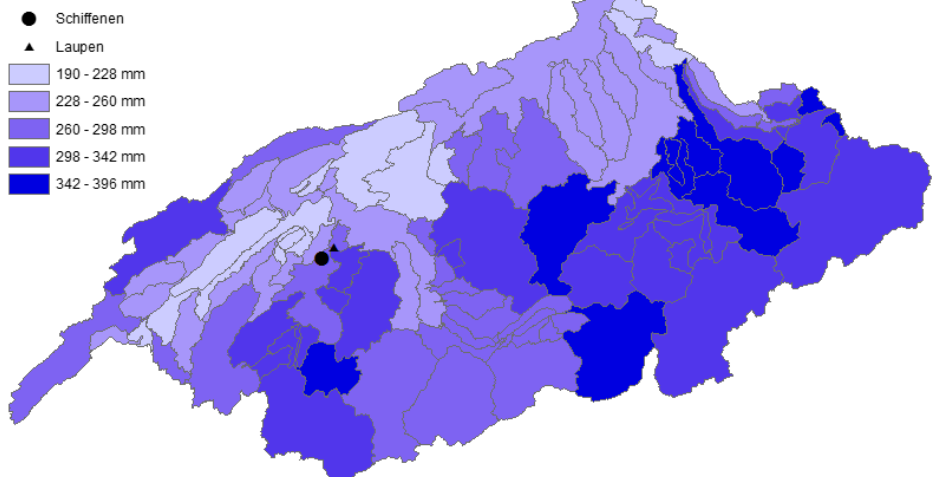


Figure 12: QdF curves for Schiffenen. From top to bottom: winter, summer, autumn, spring.

Figure 13: Precipitation distribution maps for Schiffenen and duration d1. From top to bottom: winter, summer, autumn, spring.

Table 7: Seasonal mean maximum discharge sum, mean, minimum value, maximum value and range for the 10'000 year return period floods and duration $d1$ in m^3/s , seasonal runoff coefficient C for the 10'000 year return period and duration $d1$ and seasonal rRMSE values for duration $d1$ and return periods $T=10$, $T=100$, $T=1'000$ and $T=10'000$ in %.

Schiffenen	Winter	Spring	Summer	Autumn
Q_{sum} ($d1, T = 10'000$) (m^3/s)	15003	29877	35393	30753
Q_{mean} ($d1, T = 10'000$) (m^3/s)	517	1030	1220	1060
Q_{min} ($d1, T = 10'000$) (m^3/s)	351	775	966	744
Q_{max} ($d1, T = 10'000$) (m^3/s)	943	1779	1654	1712
Q_{range} ($d1, T = 10'000$) (m^3/s)	592	1004	688	968
C ($d1, T = 10'000$)	0.08	0.1	0.13	0.13
rRMSE ($d1, T = 10$) (%)	1.3	0.5	1.2	4.5
rRMSE ($d1, T = 100$) (%)	1.7	1.1	1.1	8
rRMSE ($d1, T = 1'000$) (%)	20.2	6.4	3.9	14.8
rRMSE ($d1, T = 10'000$) (%)	42.8	23	12.4	31.3

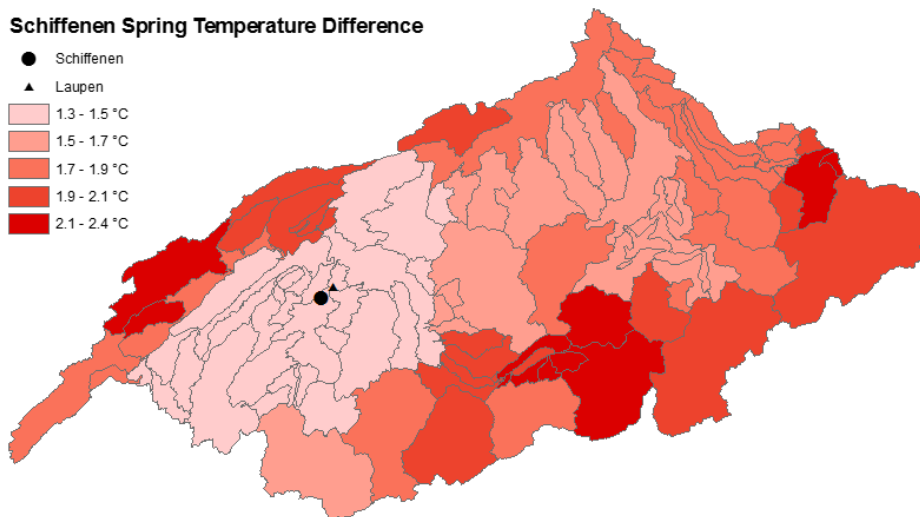


Figure 14: Temperature difference map for Schiffenen in spring and duration $d1$.

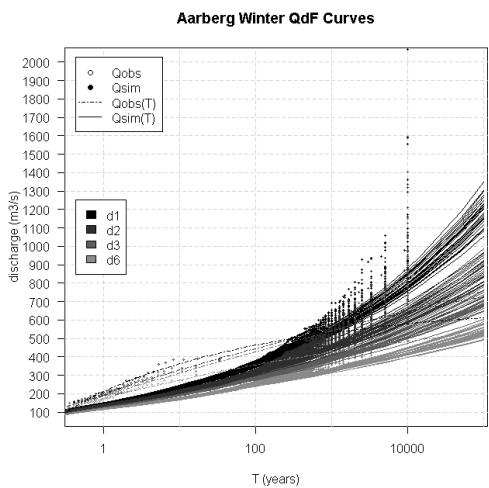
4.1.3 Schiffenen

The simulated quantiles for Schiffenen in Figure 12 can adequately describe the simulated maximum mean discharge data for small return periods ($T < 100$). In autumn and winter, for large return periods ($T = 10'000$), the quantiles tend to overestimate the return level ($\sim 100-200 \text{ m}^3/\text{s}$). In summer and spring, the quantiles also fit relatively well for large return periods. The fitted probability distributions are of Fréchet nature in winter, summer and autumn and of Gumbel or weak Weibull nature in spring. For some winter scenarios the maximum mean discharge values are disproportionately high in comparison to the majority of the remaining scenarios ($50-200 \text{ m}^3/\text{s}$ at $T = 100$ years). This results in an emphasized spread of the quantiles. The rRMSE in Table 7 indicates the best model fit for the 10'000-year return period in summer (12.4%), followed by spring (23%), autumn (31.3%) and the worst fit in winter (42.8%). Largest floods occur in summer, considering the mean of the maximum mean discharge values ($1220 \text{ m}^3/\text{s}$). Single flood events however can be higher in spring ($1779 \text{ m}^3/\text{s}$) or autumn ($1712 \text{ m}^3/\text{s}$), which is why spring and autumn have the highest ranges of mean maximum discharge values (1004 and $968 \text{ m}^3/\text{s}$). In winter the weakest floods occur.

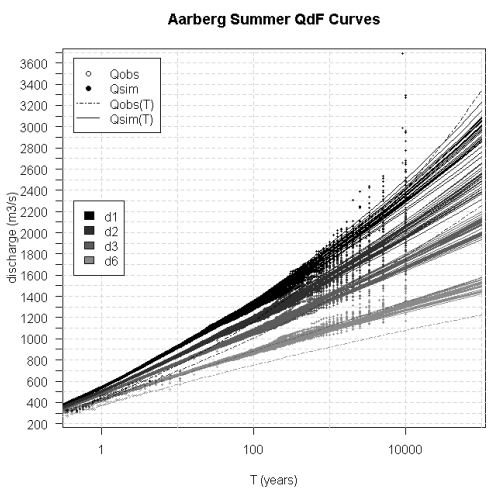
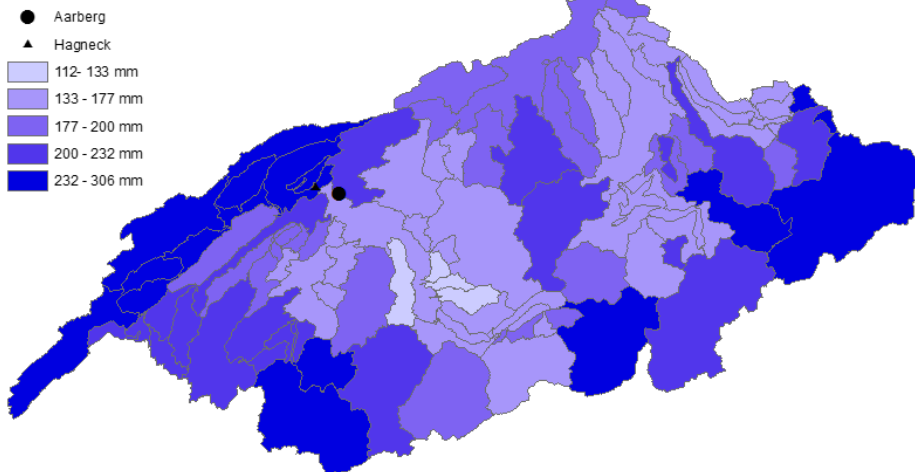
The nearby measuring station of Schiffenen is Laupen with a distance of 4 kilometers. For equal return periods, the observed and simulated maximum mean discharge have similar magnitudes in summer and autumn. In winter the observed discharges are higher ($\sim 100 \text{ m}^3/\text{s}$ at $T = 10$), in spring they are slightly smaller than the simulated values ($\sim 50-100 \text{ m}^3/\text{s}$ at $T = 1$). The observed and simulated quantiles have similar shapes for winter, summer and autumn, because similar Fréchet distributions are assumed. In spring the simulated and observed quantiles originate from different distributions (Gumbel/Weibull in the simulations vs. Fréchet in the observations).

The precipitation maps for Schiffenen and duration d1 in Figure 13 show a very similar precipitation distribution for spring and summer. The precipitation maxima are located in a band ranging from the eastern edge to southwestern edge of the Aare region. In autumn a similar pattern can be detected, but less pronounced than in spring and summer. Here maxima are also identified at the northwestern border basins. In winter, maxima are predominantly found in the western border subcatchments of the Aare basin. In all seasons, there is lower or moderate precipitation directly at Schiffenen, but large precipitation in southeastern direction. In general, precipitation is high in all subbasins (112-396 mm). The strongest season is summer (459 mm), followed by spring (396 mm), autumn (351 mm) and winter (283 mm).

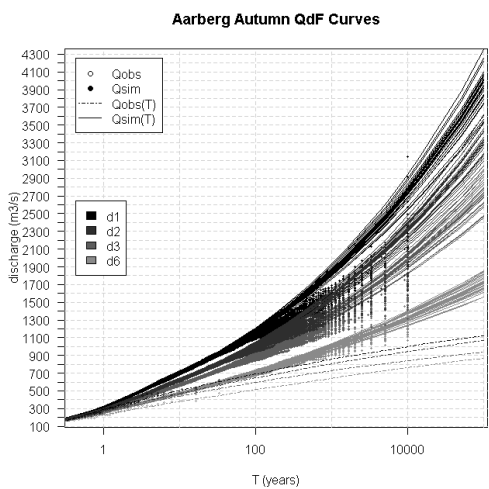
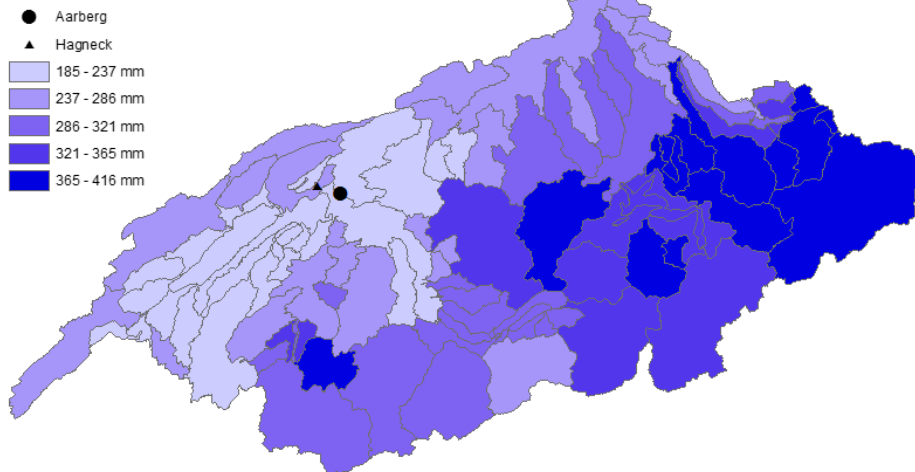
The spring temperature map for duration d1 in Figure 14 indicates a relatively strong increase in temperature before the flood events in all subbasins ($1.3-2.4 \text{ }^\circ\text{C}$). The largest temperature increases are found in the western and southern border basins, lowest temperature increases in a large region around Schiffenen. The spring runoff coefficient C in Table 7 is low (0.1) compared to the autumn and summer ones (0.13).



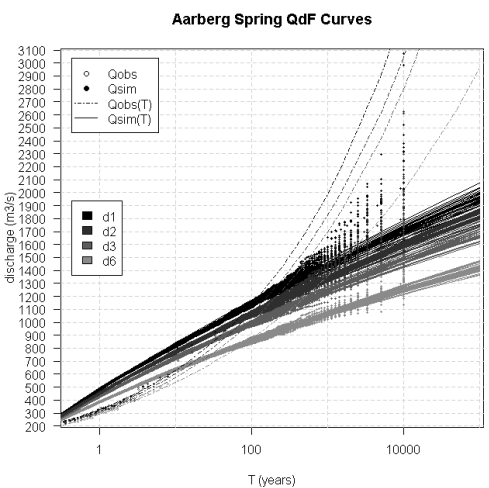
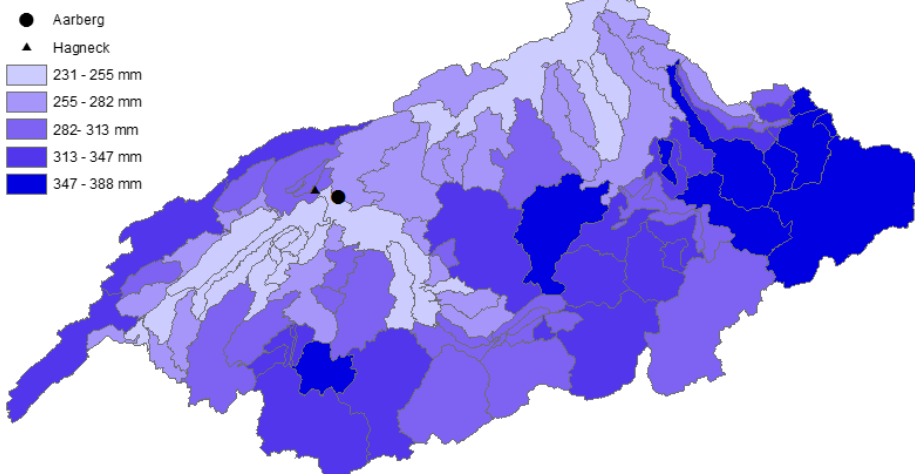
Aarberg Winter Precipitation



Aarberg Summer Precipitation



Aarberg Autumn Precipitation



Aarberg Spring Precipitation

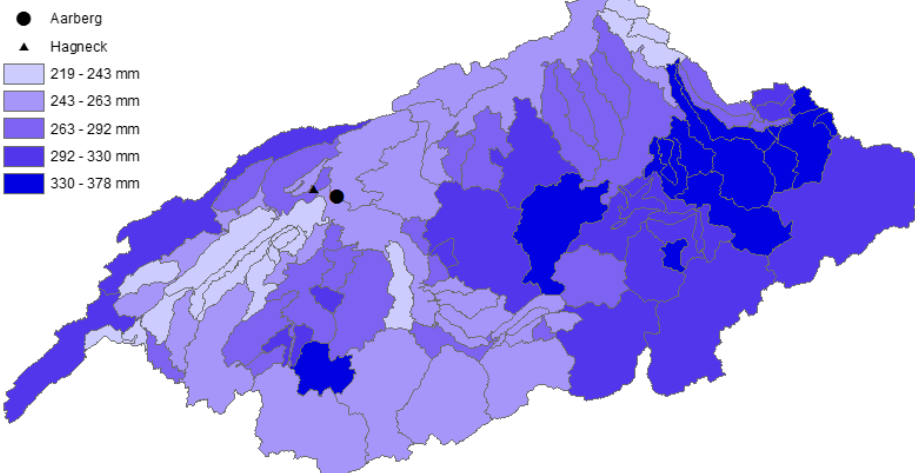


Figure 15: QdF curves for Aarberg. From top to bottom: winter, summer, autumn, spring.

Figure 16: Precipitation distribution maps for Aarberg and duration d2. From top to bottom: winter, summer, autumn, spring.

Table 8: Seasonal mean maximum discharge sum, mean, minimum value, maximum value and range for the 10'000 year return period floods and duration d2 in m³/s, seasonal runoff coefficient C for the 10'000 year return periods and duration d2 and seasonal rRMSE values for duration d1 and return periods T=10, T=100, T=1'000 and T=10'000 in %.

Aarberg	Winter	Spring	Summer	Autumn
Q_{sum} (d2, T = 10'000) (m ³ /s)	27724	53414	62716	54606
Q_{mean} (d2, T = 10'000) (m ³ /s)	956	1842	2163	1883
Q_{min} (d2, T = 10'000) (m ³ /s)	711	1552	1747	1500
Q_{max} (d2, T = 10'000) (m ³ /s)	1587	2625	2990	2745
Q_{range} (d2, T = 10'000) (m ³ /s)	876	1073	1243	1245
C (d2, T = 10'000)	0.14	0.18	0.2	0.19
rRMSE (d1, T = 10) (%)	0.7	0.4	1.8	3.3
rRMSE (d1, T = 100) (%)	5.2	0.9	2.2	5.4
rRMSE (d1, T = 1'000) (%)	18.4	5.6	3.9	17.7
rRMSE (d1, T = 10'000) (%)	37.9	22.4	11.9	30.5

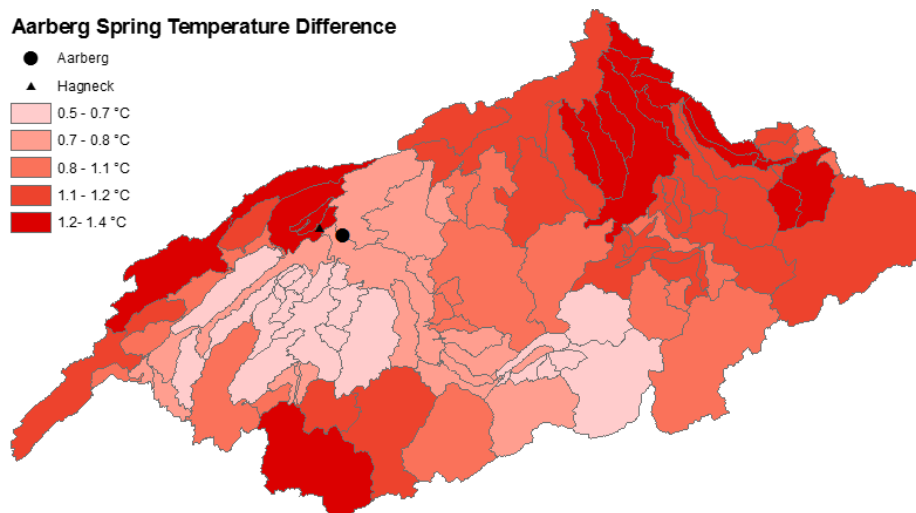


Figure 17: Temperature difference map for Aarberg in spring and duration d2.

4.2 Group Duration d2

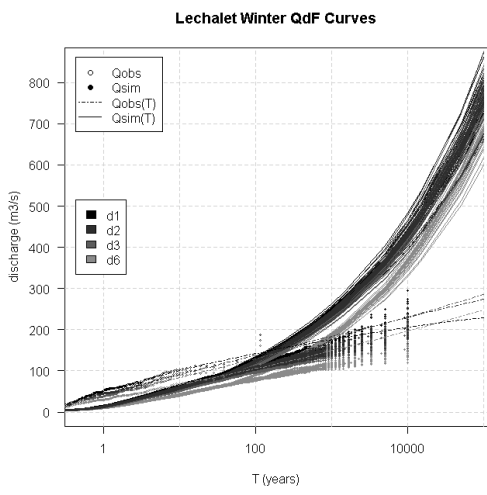
4.2.1 Aarberg

In the QdF curves for Aarberg in Figure 18, the quantiles can represent the simulated maximum mean discharge values well, up until the 100 year return period. For higher return periods the quantiles tend to underestimate the return level in spring, winter and summer and overestimate it in autumn. For Summer the d3, d2 and d1 quantiles belong to Fréchet distributions, whereas the d6 quantiles rather originate from Weibull or Gumbel distributions. For winter and autumn, all quantiles belong to the Fréchet distributions. In Spring, the assumed distributions are the Weibull ones. According to the rRMSE in Table 8, model errors are largest in Winter (0.7-37.9%), followed by Autumn (3.3-30.5%) and Spring (0.4-22.4%) and are best for Summer (1.8-11.9%). According to the QdF curves and the Table 8, events with 10'000 years return period are largest in summer in terms of both the mean (956 m³/s) and the maximal value (2626 m³/s), followed by autumn and spring and by far the smallest in winter. The largest range between the associated flood mean maximum discharge values can be found in autumn and summer.

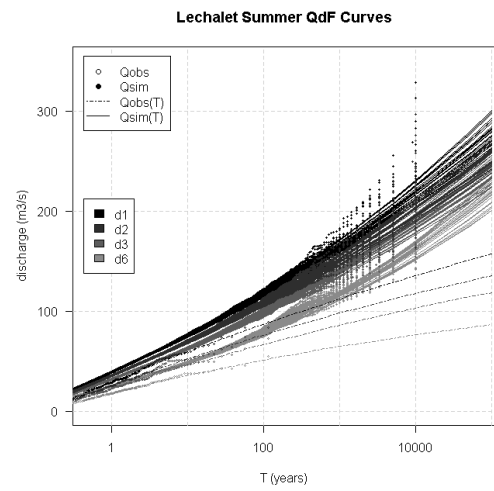
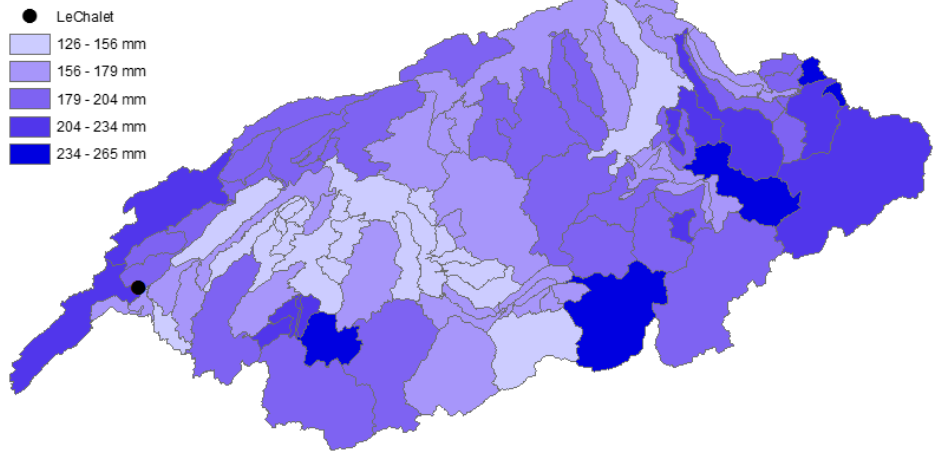
The closest measuring station from Aarberg is Hagneck, with an approximate distance of 7 km. The comparison between observed and simulated maximum mean discharge values is relatively good for all seasons, especially in summer and autumn. In winter the simulated values are smaller than the observed maximum mean discharges (100-200 m³/s at T = 10), in spring they tend to be larger (100-200 m³/s at T = 1). Comparing the observed and simulated quantiles, it is noticeable that for winter, autumn and spring opposite distributions are fitted. The distributions in winter and autumn of the observed case are Weibull distributions and in spring the Fréchet distributions. In summer the distributions are similar.

The choropleth maps for Aarberg and duration d2 in Figure 16 indicate high precipitation amounts for all subbasins in the Aare catchment (112-416 mm). The precipitation distribution shows a similar structure in summer, autumn and spring. Precipitation maxima are generally found in the eastern and southwestern parts of the Aare basin. In autumn the southwestern maxima are less pronounced and most precipitation is predominantly located in the east. In winter, no clear structure can be identified, but most precipitation falls in the eastern, southern and western margins of the Aare catchment. At the station Aarberg precipitation minima are found in all seasons. In general, largest precipitation amounts occur in summer (416 mm), followed by autumn (388 mm) and spring (378 mm) and smallest ones in winter (306 mm).

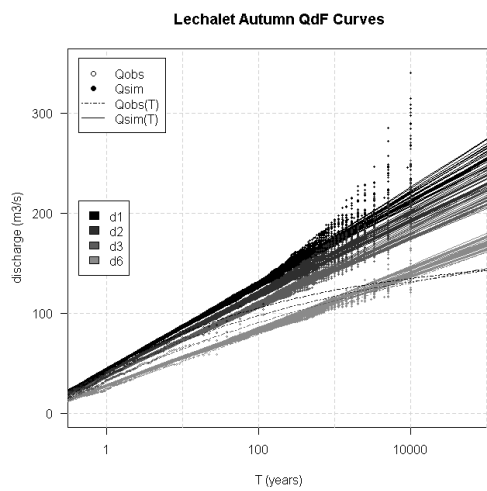
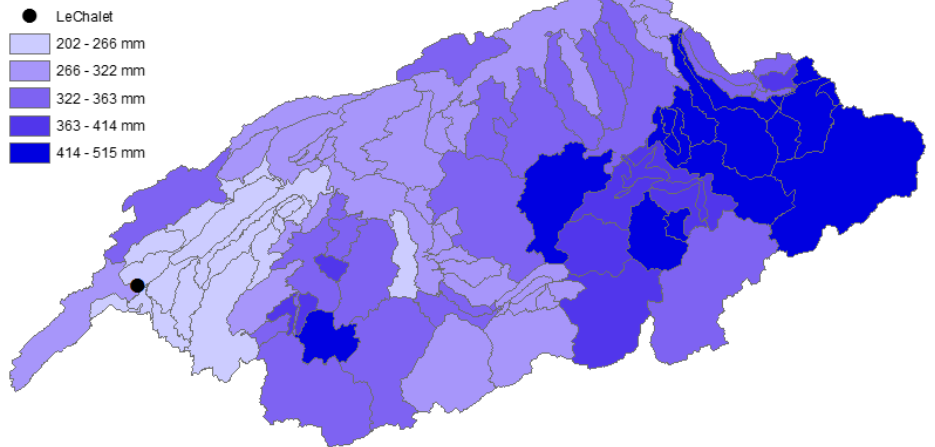
The spring temperature map in Figure 17 indicates a small increase in temperature before the flood events for all subbasins in the Aare region (0.5-1.4°C). Largest temperature increases are located in the western, southwestern and northeastern part of the Aare region. The spring runoff coefficient C (0.18) in Table 8 is higher than the winter runoff coefficient (0.14), but lower than the summer (0.2) and autumn one (0.19).



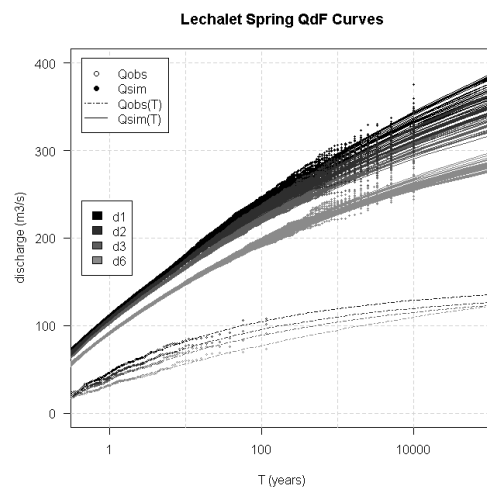
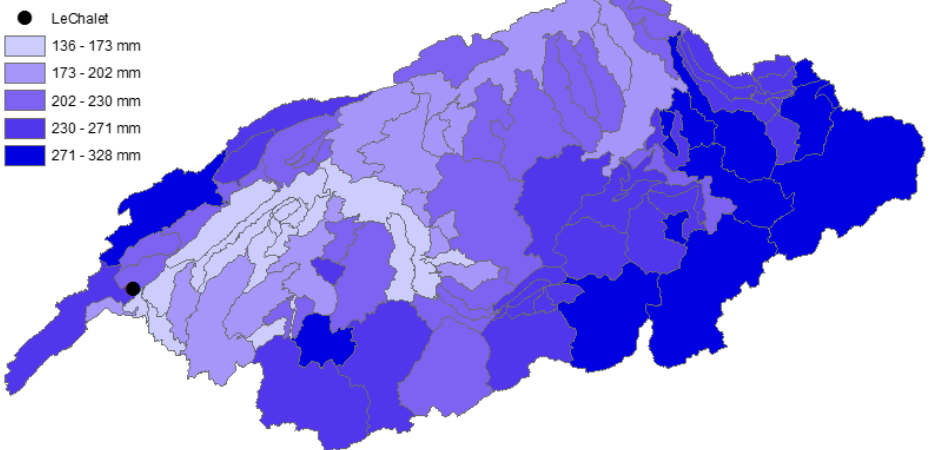
Le Chalet Winter Precipitation



Le Chalet Summer Precipitation



Le Chalet Autumn Precipitation



Le Chalet Spring Precipitation

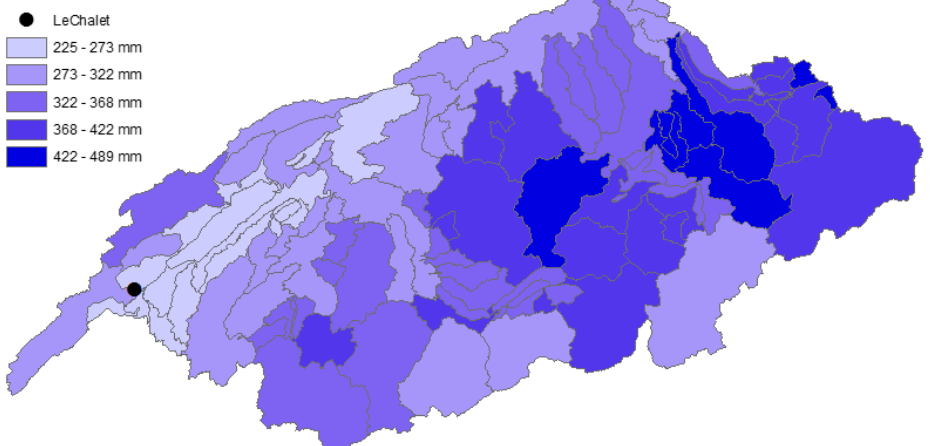


Figure 18: QdF curves for Le Châlet. From top to bottom: winter, summer, autumn, spring.

Figure 19: Precipitation distribution maps for Le Châlet and duration d2. From top to bottom: winter, summer, autumn, spring.

Table 9: Seasonal mean maximum discharge sum, mean, minimum value, maximum value and range for the 10'000 year return period floods and duration d2 in m³/s, seasonal runoff coefficient C for the 10'000 year return periods and duration d2 and seasonal rRMSE values for duration d1 and return periods T=10, T=100, T=1'000 and T=10'000 in %.

Le Châlet	Winter	Spring	Summer	Autumn
Q_{sum} (d2, T = 10'000) (m ³ /s)	6072	8885	6236	6640
Q_{mean} (d2, T = 10'000) (m ³ /s)	209	306	215	229
Q_{min} (d2, T = 10'000) (m ³ /s)	177	298	163	195
Q_{max} (d2, T = 10'000) (m ³ /s)	263	345	296	301
Q_{range} (T = 10'000) (m ³ /s)	86	47	133	106
C (d2, T = 10'000)	0.037	0.02	0.02	0.03
rRMSE (d1, T = 10) (%)	1.7	0.7	1.1	0.8
rRMSE (d1, T = 100) (%)	117.3	1.4	1.3	1.2
rRMSE (d1, T = 1'000) (%)	439.2	1.9	3.5	5.2
rRMSE (d1, T = 10'000) (%)	1210.9	5.3	13	19.1

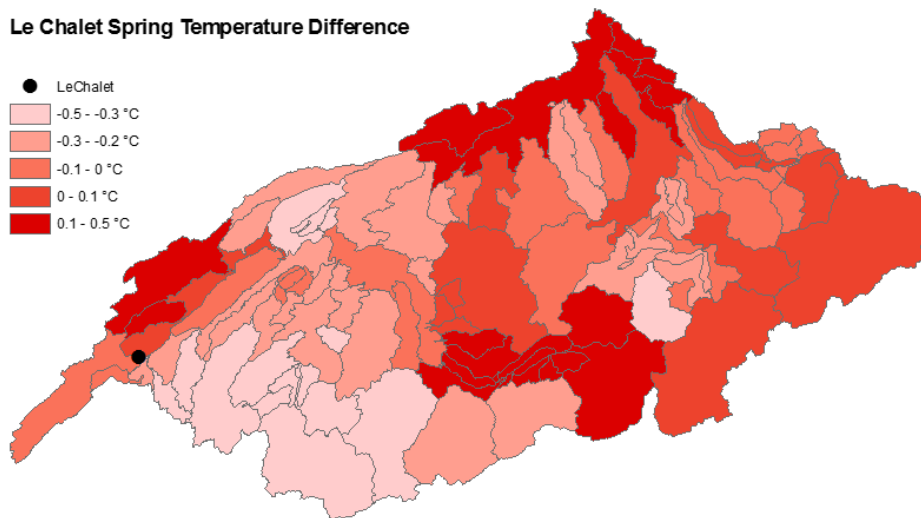


Figure 20: Temperature difference map for Le Châlet in spring and duration d2.

4.2.2 Le Châlet

The simulated QdF curves of Le Châlet in Figure 18 can adequately describe the data for the spring, summer and autumn season for most of the return periods ($T < 1'000$). Only at larger return periods the summer and autumn quantiles tend to underestimate the return levels slightly. In winter only return periods smaller than 100 years can be described accurately by the quantiles. For larger return periods, the quantiles tend to overestimate the return levels by a huge margin ($\sim 100\text{-}200 \text{ m}^3/\text{s}$ at $T = 10'000$). The associated distributions are Fréchet in summer and winter, Weibull in spring and Weibull or Gumbel in autumn. According to the rRMSE in Table 9, the GEV models score well in spring (0.7-5.3%), summer (1.1-13%) and autumn (0.8-19.1%) and unacceptable in winter for extreme return periods (1.7-1210.9%). The maximum mean discharge is highest in spring with respect to the mean ($306 \text{ m}^3/\text{s}$) and maximum value ($345 \text{ m}^3/\text{s}$), followed by autumn ($229 \text{ m}^3/\text{s}$, $301 \text{ m}^3/\text{s}$), summer ($215 \text{ m}^3/\text{s}$, $296 \text{ m}^3/\text{s}$) and winter ($209 \text{ m}^3/\text{s}$, $263 \text{ m}^3/\text{s}$). The simulated QdF curves of Schiffenen are compared to the ones of the measuring station Orbe, located at the same place. In summer and autumn the observed maximum mean discharge values agree with the simulated ones. In winter, the observed values are slightly higher at low return periods ($\sim 50 \text{ m}^3/\text{s}$ at $T = 100$) and in spring considerably lower for all return periods ($\sim 50 \text{ m}^3/\text{s}$ at $T = 1$). In terms of the quantile similarities, different GEV distributions are assumed in winter, summer and autumn, in spring the same ones.

The precipitations maps for Le Châlet and duration d_2 in Figure 19 show a relatively similar structure for all seasons. Precipitation maxima are predominantly found in the eastern part of the Aare basin, as well as in the southwestern part. In autumn and winter additional maxima occur in the western border of the Aare catchment. Directly at Le Châlet, precipitation is relatively low in summer and spring, but considerably high in winter and autumn. The precipitation amount is generally high for all subcatchments (126-515 mm) and largest in summer (515 mm), spring (489 mm) and lowest in autumn (328 mm) and winter (265 mm).

The spring temperature difference map for Le Châlet and duration d_2 in Figure 20 shows temperature increases as well as decreases before the flood events ($-0.5 - 0.5^\circ\text{C}$). Maximum temperature increases are located at the southern, northern and western border basins, maximum decrease in the southwestern part of the Aare basin. The spring runoff coefficient C (0.02) in Table 9 is the smallest compared to the other seasons.

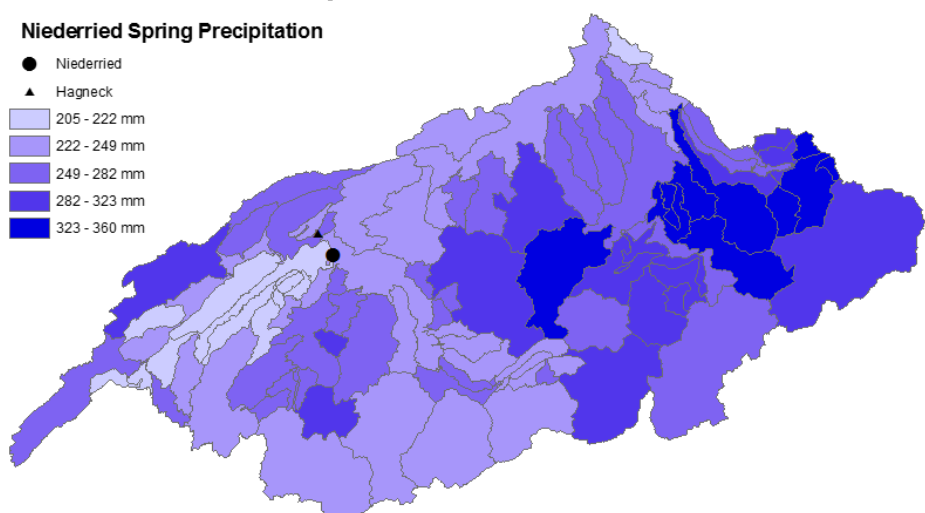
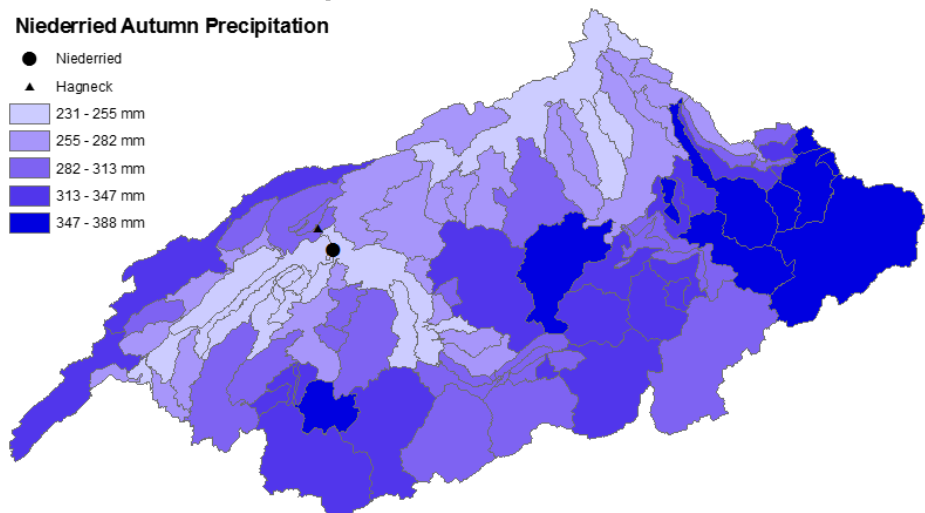
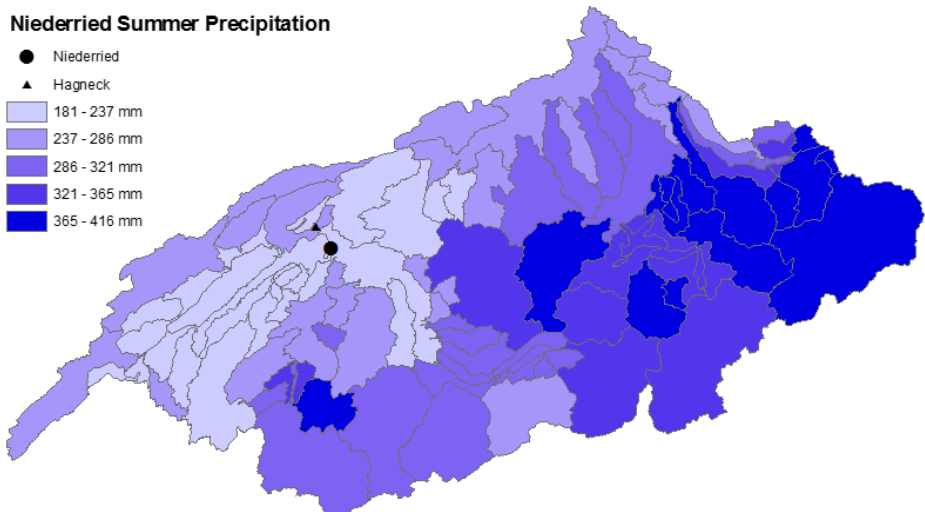
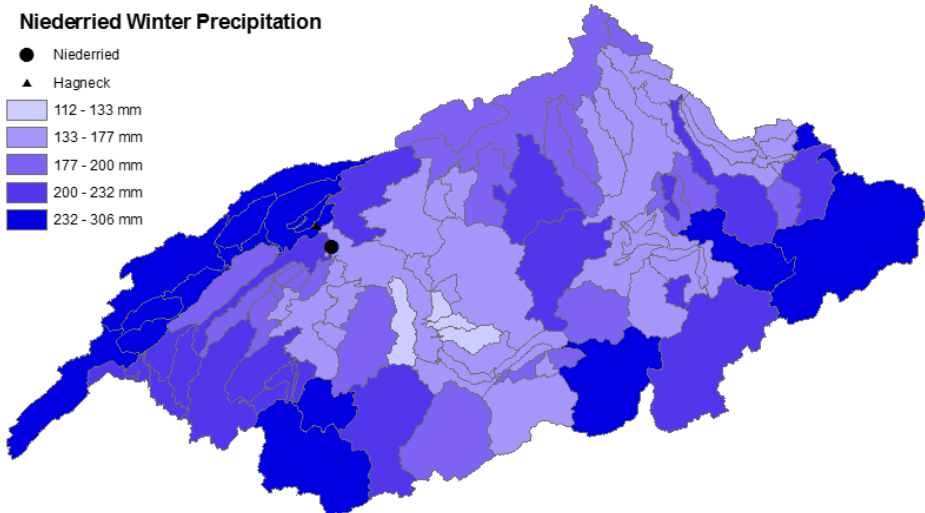
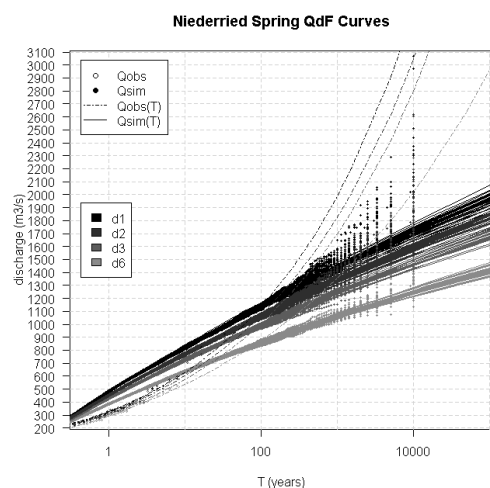
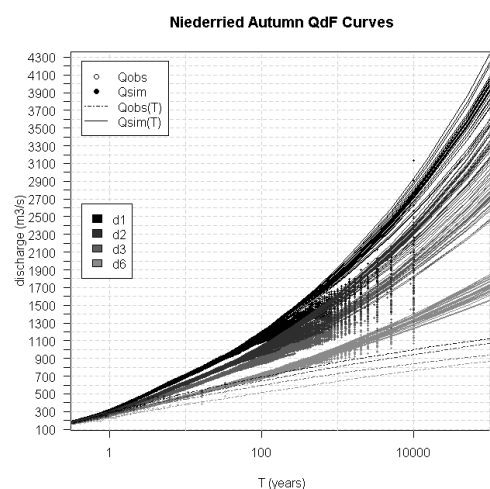
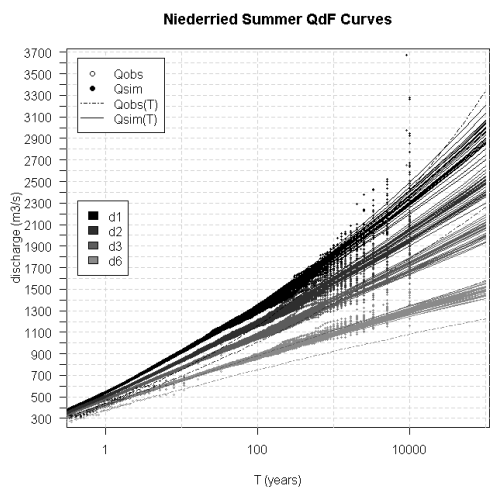
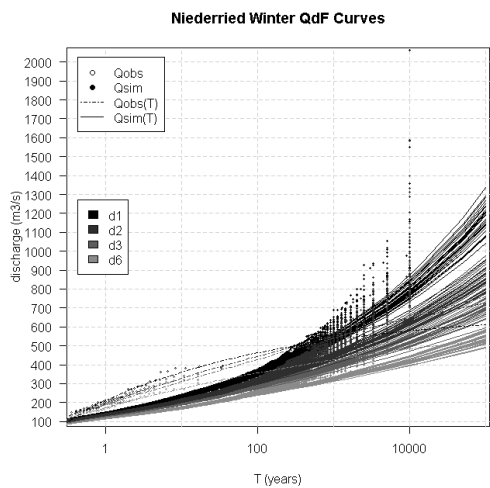


Figure 21: QdF curves for Niederried. From top to bottom: winter, summer, autumn, spring.

Figure 22: Precipitation distribution maps for Niederried and duration d2. From top to bottom: winter, summer, autumn, spring.

Table 10: Seasonal mean maximum discharge sum, mean, minimum value, maximum value and range for the 10'000 year return period floods and duration d2 in m³/s, seasonal runoff coefficient C for the 10'000 year return periods and duration d2 and seasonal rRMSE values for duration d1 and return periods T=10, T=100, T=1'000 and T=10'000 in %.

Niederried	Winter	Spring	Summer	Autumn
Q_{sum} (d2, T = 10'000) (m ³ /s)	27656	53275	62511	54461
Q_{mean} (d2, T = 10'000) (m ³ /s)	954	1837	2156	1878
Q_{min} (d2, T = 10'000) (m ³ /s)	709	1548	1742	1446
Q_{max} (d2, T = 10'000) (m ³ /s)	1581	2617	2976	2737
Q_{range} (d2, T = 10'000) (m ³ /s)	872	1069	1234	1291
C (d2, T = 10'000)	0.08	0.08	0.08	0.11
rRMSE (d1, T = 10)	0.7	0.4	1.8	2.8
rRMSE (d1, T = 100)	5.2	0.9	2.2	13.8
rRMSE (d1, T = 1'000)	18.9	5.6	3.8	39
rRMSE (d1, T = 10'000)	38.3	22.3	11.9	68.7

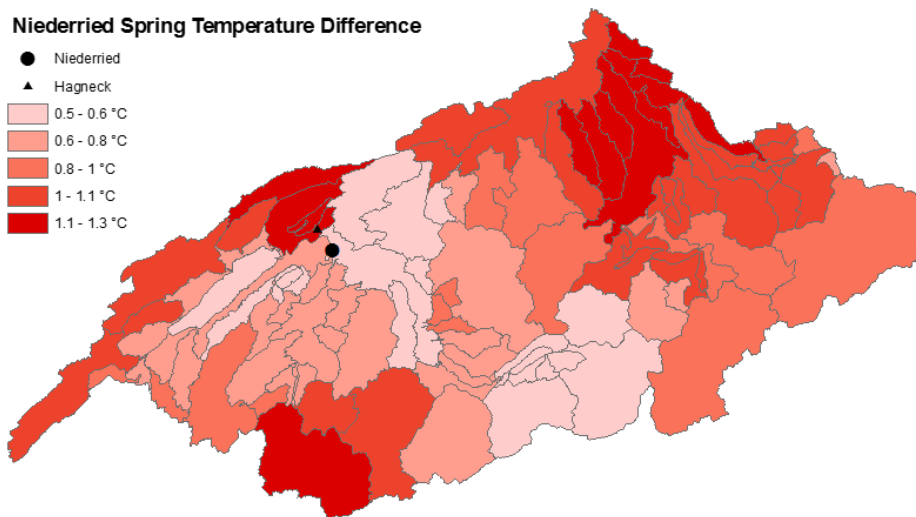


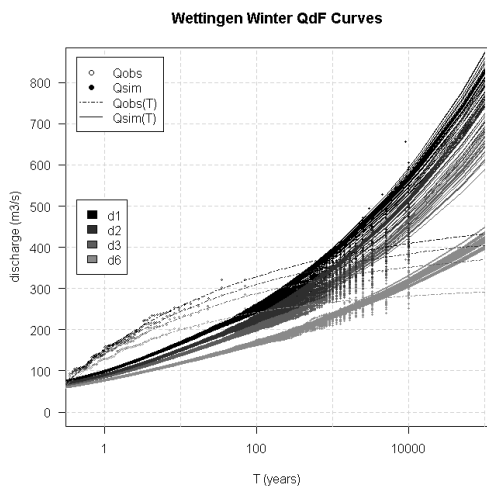
Figure 23: Temperature difference map for Niederried in spring and duration d2.

4.2.3 Niederried

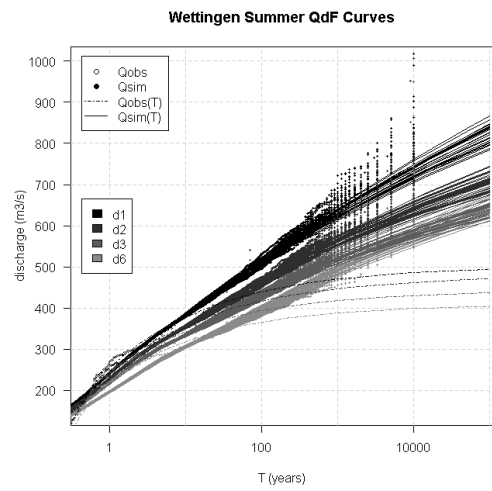
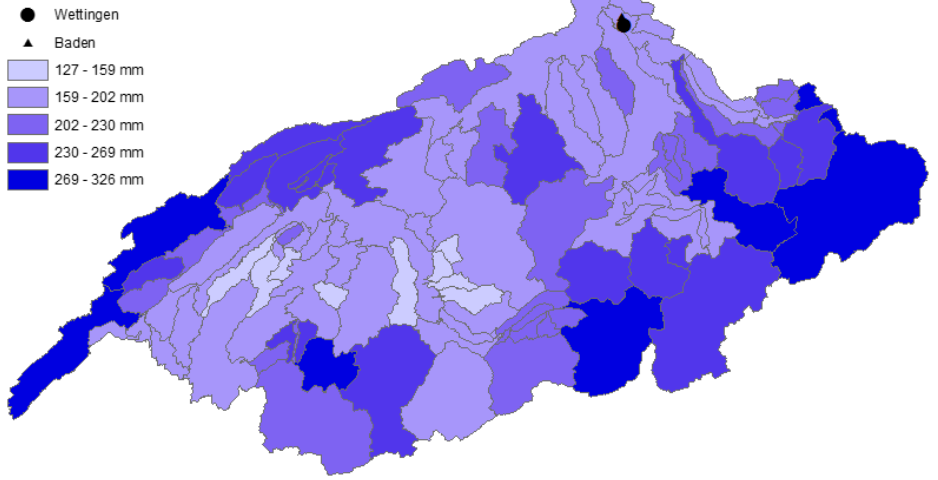
In Figure 21 the QdF curves for Niederried and duration d_2 are shown. In all seasons, the fitted quantiles can adequately describe the simulated mean maximum discharge for return periods up to 100 years. For larger return periods, maximum mean discharges are underestimated in winter ($\sim 100 \text{ m}^3/\text{s}$ at $T = 1'000$) and spring ($\sim 100\text{-}200 \text{ m}^3/\text{s}$ at $T = 1'000$), and tend to be slightly overestimated in autumn. In summer, large return periods can also be well estimated by the quantiles, with the exception of a few outliers. In winter and autumn Fréchet distributions are fitted to the simulated mean maximum discharge data, in spring Weibull distributions and in summer Fréchet or Gumbel distributions. The error score rRMSE in Table 10 indicates the best model fit in summer (1.8-11.9%), second best in spring (0.4-22.3%), a moderate fit in winter (0.7-38.3%) and a poor one in autumn (2.8-68.7%). The largest floods with 10'000-year return period can be observed in summer with respect to the averaged mean maximum discharge values ($2156 \text{ m}^3/\text{s}$), as well as the largest mean maximum discharge value ($2976 \text{ m}^3/\text{s}$). According to the mean, the next biggest floods are in autumn ($1878 \text{ m}^3/\text{s}$) and spring ($1837 \text{ m}^3/\text{s}$) and smallest ones in winter ($954 \text{ m}^3/\text{s}$). The simulated values and quantiles of Niederried are compared to the Hagneck station. The two stations are 7.5 km apart. The observed and simulated values match well in summer and autumn, in spring however the observed maximum mean discharges are smaller than the simulated ones ($\sim 100\text{-}200 \text{ m}^3/\text{s}$ at $T = 1$), whereas in winter the observed ones are larger ($\sim 200 \text{ m}^3/\text{s}$ at $T = 10$). The quantiles match in summer, but differ in the other seasons. In the simulations Fréchet distributions are assumed, in contrast to the Weibull ones in the observations.

In Figure 22 the precipitation distribution maps for flood events with 10'000-years return period for Niederried and duration d_2 are shown. The maps show similar patterns in summer and autumn. In both seasons, precipitation maxima are identified in a band ranging from to eastern to the southwestern part of the Aare basin. In spring the structure is similar, but the southwestern maxima decrease. In winter no clear structure is identified, but in general there are maxima at the western, southwestern, southeastern and eastern borders of the Aare catchment. Precipitation minima are generally found in the western, central and northern subbasins. In all seasons there are comparatively low amounts of precipitation found at Niederried, but further south of the station larger amounts can be found quickly. In general the precipitation amount is high in all subbasins in all seasons (112-450 mm), the largest amounts however occur in summer (415 mm) and autumn (388 mm), followed by spring (360 mm) and winter (305 mm)

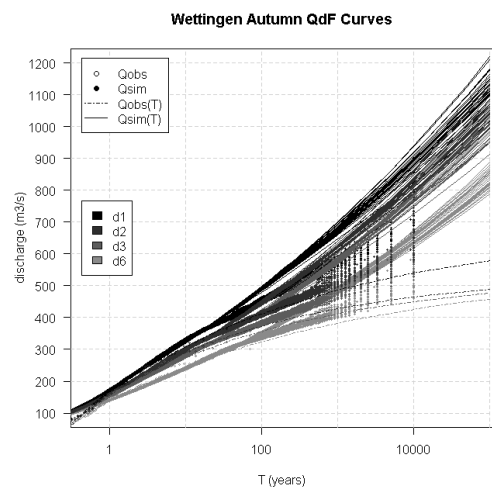
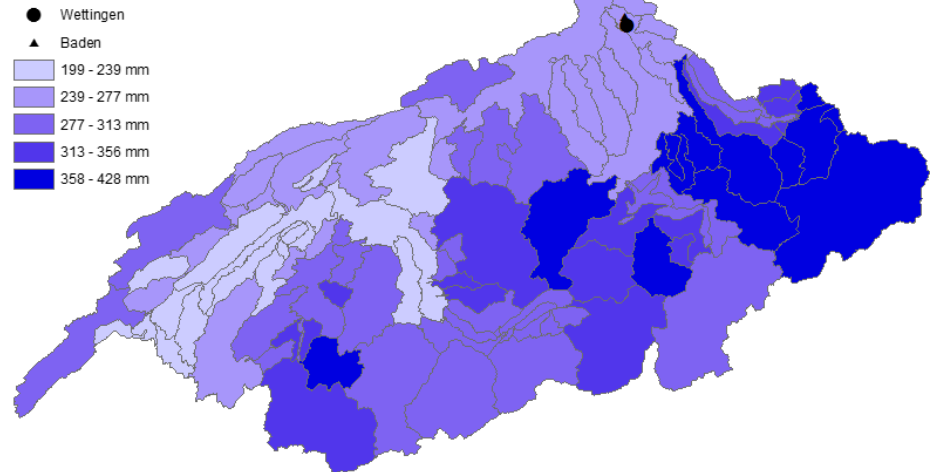
The spring temperature map in Figure 23 shows a small increase in temperature in all the subbasins ($0.5\text{-}1.3^\circ\text{C}$). Largest increases can be found in the southwestern and northeastern part of the Aare region, as well as northwest of Niederried. Smallest increases are identified in the central areas, in easterly direction of Niederried and in the southern parts. The spring runoff coefficient C in Table 10 is the same as the summer and winter ones (0.08), but smaller than the autumn runoff coefficient (0.11).



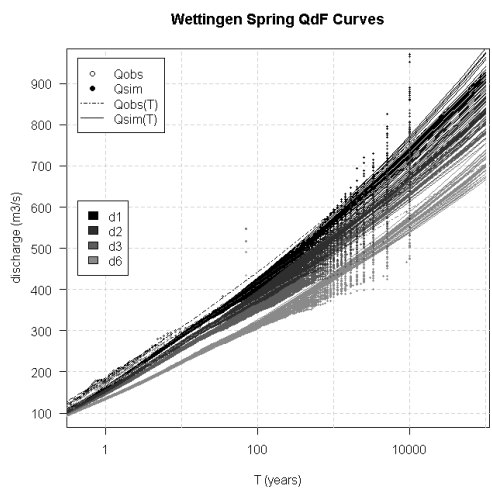
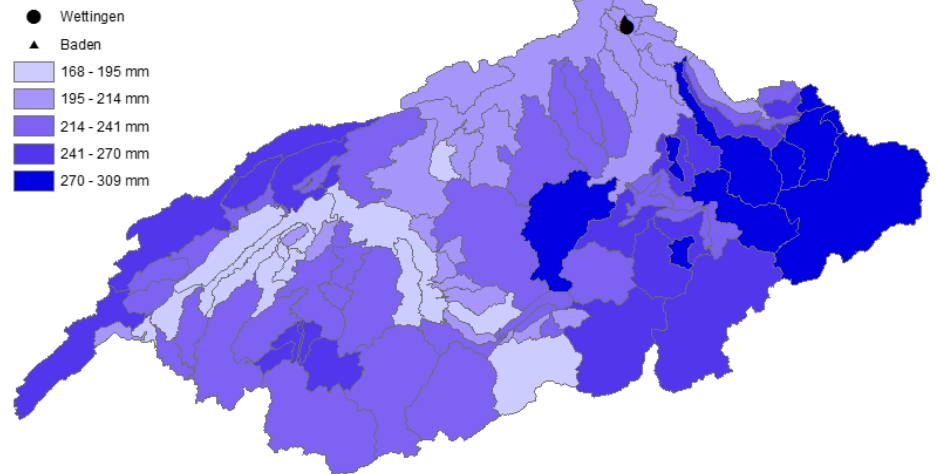
Wettingen Winter Precipitation



Wettingen Summer Precipitation



Wettingen Autumn Precipitation



Wettingen Spring Precipitation

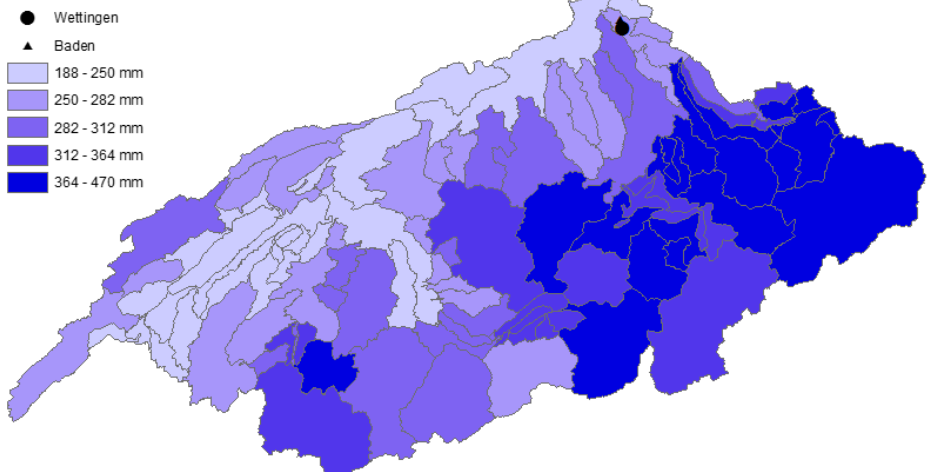


Figure 24: QdF curves for Wettingen. From top to bottom: winter, summer, autumn, spring.

Figure 25: Precipitation distribution maps for Wettingen and duration d2. From top to bottom: winter, summer, autumn, spring.

Table 11: Seasonal mean maximum discharge sum, mean, minimum value, maximum value and range for the 10'000 year return period floods and duration d2 in m³/s, seasonal runoff coefficient C for the 10'000 year return periods and duration d2 and seasonal rRMSE values for duration d1 and return periods T=10, T=100, T=1'000 and T=10'000 in %.

Wettingen	Winter	Spring	Summer	Autumn
Q_{sum} (d2, T = 10'000) (m ³ /s)	13145	20445	21870	18710
Q_{mean} (d2, T = 10'000) (m ³ /s)	453	705	754	645
Q_{min} (d2, T = 10'000) (m ³ /s)	370	572	649	575
Q_{max} (d2, T = 10'000) (m ³ /s)	569	966	1006	772
Q_{range} (d2, T = 10'000) (m ³ /s)	199	394	357	197
C (d2, T = 10'000)	0.06	0.06	0.06	0.07
rRMSE (d1, T = 10) (%)	2.3	2.1	0.3	3.2
rRMSE (d1, T = 100) (%)	5.6	4.3	1.3	8.8
rRMSE (d1, T = 1'000) (%)	16.2	7.8	5	17.7
rRMSE (d1, T = 10'000) (%)	26	11.2	12.9	23

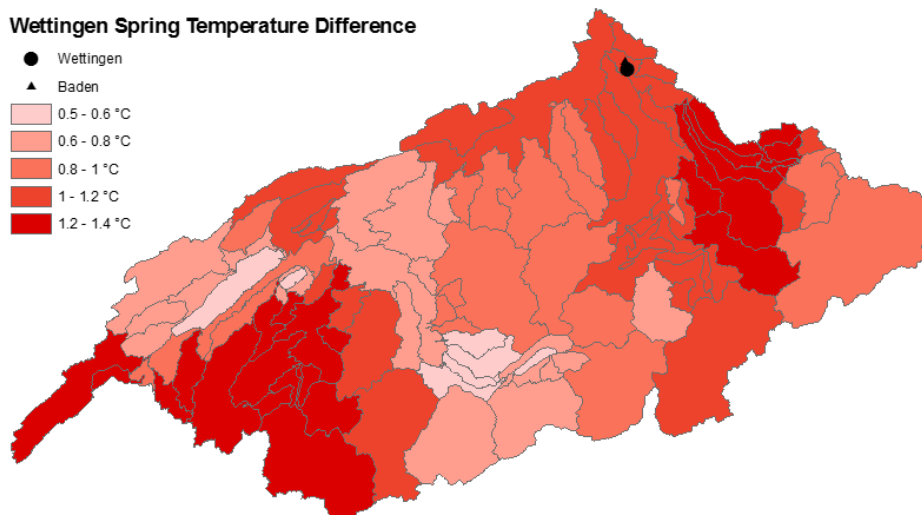


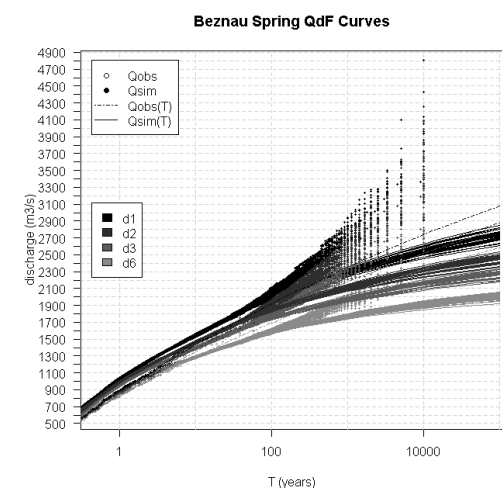
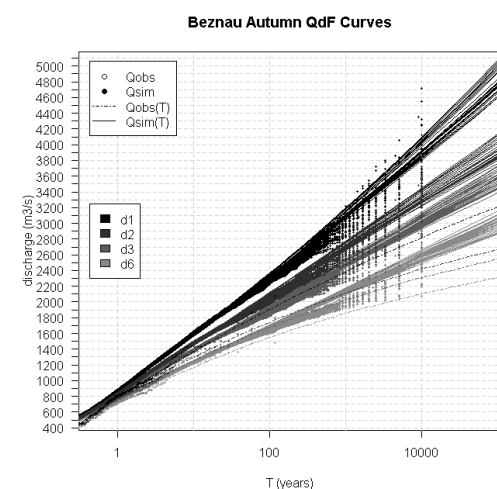
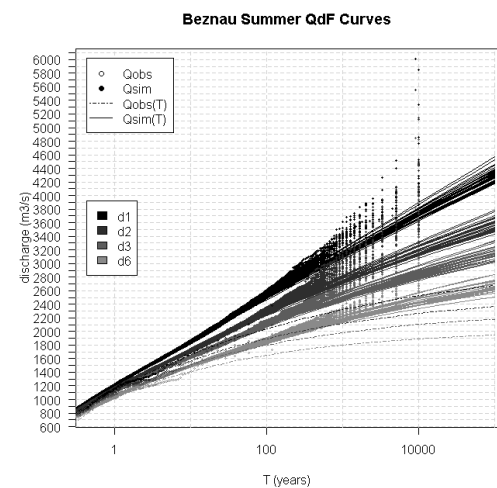
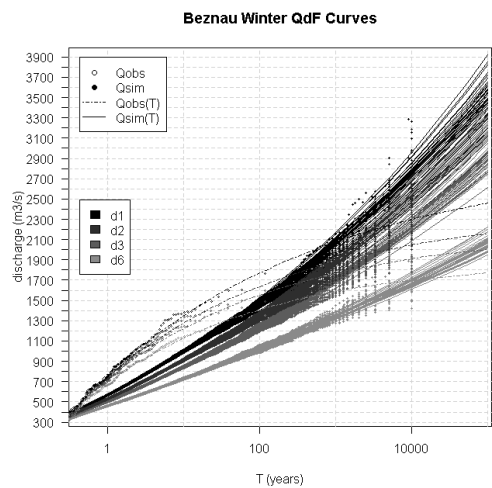
Figure 26: Temperature difference map for Wettingen in spring and duration d2.

4.2.4 Wettingen

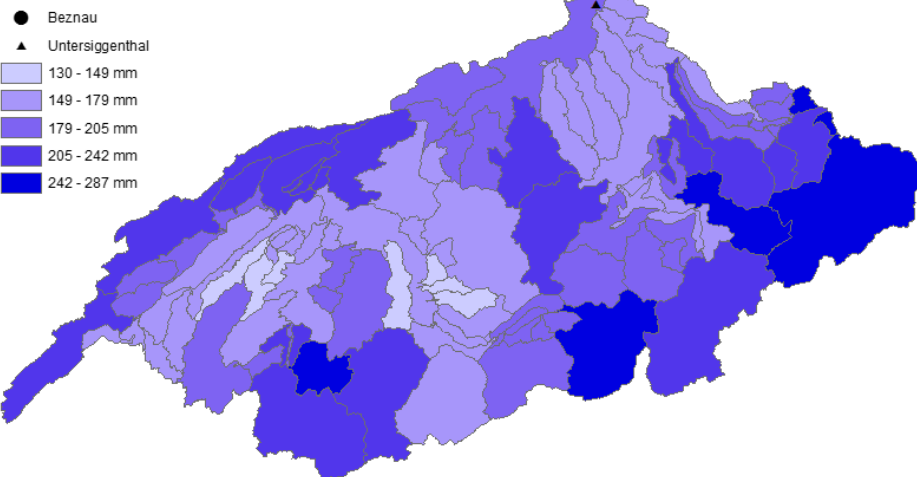
The QdF curves for Wettingen and duration d2 in Figure 24 indicate a good quantile fit for small return periods in all seasons ($T < 100$). In winter, spring and autumn the quantiles tend to overestimate the mean maximum discharge return level at higher return periods ($\sim 50\text{-}100 \text{ m}^3/\text{s}$ at $T = 1'000$), whereas in summer, an underestimation is detected ($\sim 50\text{-}100 \text{ m}^3/\text{s}$ at $T = 1'000$). The winter, autumn and spring quantiles belong to Fréchet distributions, the summer ones to the Weibull family. The quality of the fitted GEV models can be inspected in Table 11 and is low for all seasons and return periods. For the 10'000-year return level, the GEV models perform the best in spring (11.2%) and summer (12.9%) followed by autumn (23%) and winter (26%). In summer floods with return periods of 10'000 years have the highest mean maximum discharge values in terms of the mean ($754 \text{ m}^3/\text{s}$) and the maximal value ($1006 \text{ m}^3/\text{s}$). Second highest meaned values are in spring ($705 \text{ m}^3/\text{s}$), followed by autumn ($645 \text{ m}^3/\text{s}$) and smallest ones in winter ($453 \text{ m}^3/\text{s}$). Wettingen is compared to the station Baden, with an approximate distance of 2 kilometers. The observed maximum mean discharge at Baden match the simulated discharges in Wettingen for summer, autumn and spring very well. In winter, the observed discharges seem to be much higher for relatively small return periods in comparison to the simulated ones ($\sim 50\text{-}100 \text{ m}^3/\text{s}$ at $T = 1$). The quantiles also match well in spring, summer and autumn, even though in autumn the shape parameters have different signs. In winter the quantiles don't match adequately, because different GEV distributions are assumed.

In the Wettingen precipitation maps for duration d2 and return period of 10'000 years, the precipitation is similarly distributed in summer and spring. The precipitation maxima are located in a band ranging from the eastern regions of the Aare basin to the southwestern parts. The precipitation in autumn also shows a relatively similar structure, but the band of precipitation maximum is cut in the central south. Here a new pronounced precipitation maximum can be localized in the northwestern border basins. In winter the precipitation maxima do not show a clear structure. Maxima can be found in the western, eastern, southwestern and southeastern border subcatchments. In all seasons only a comparatively moderate precipitation amount is found at Wettingen. In general, the precipitation amount is high for all subbasins (127-428 mm) and largest precipitation amounts are found in summer (428 mm) and spring (470 mm) and lowest ones in autumn (309 mm) and winter (325 mm).

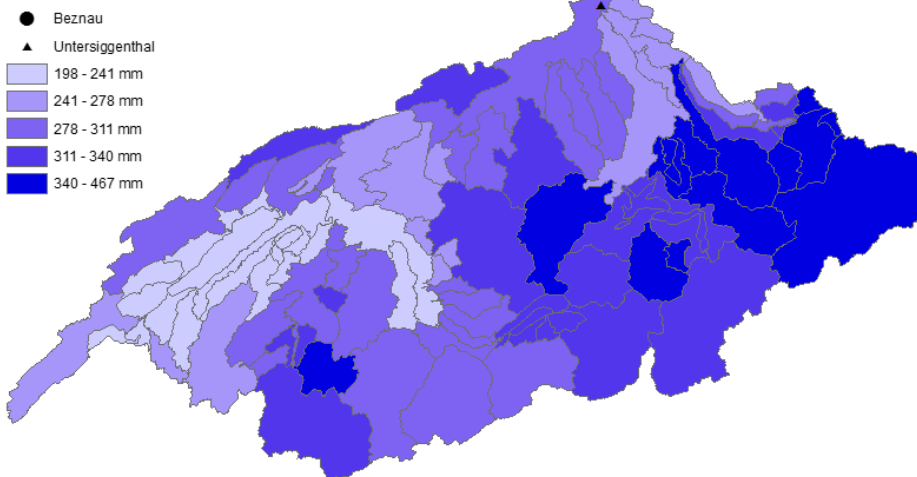
The spring temperature map in Figure 26 shows a general, but small increase in temperature in all the subcatchments ($0.5\text{-}1.4^\circ\text{C}$). The biggest temperature increases are found in the southwest and the east. The runoff coefficient C in Table 11 has the same magnitude in all seasons (0.06 / 0.07).



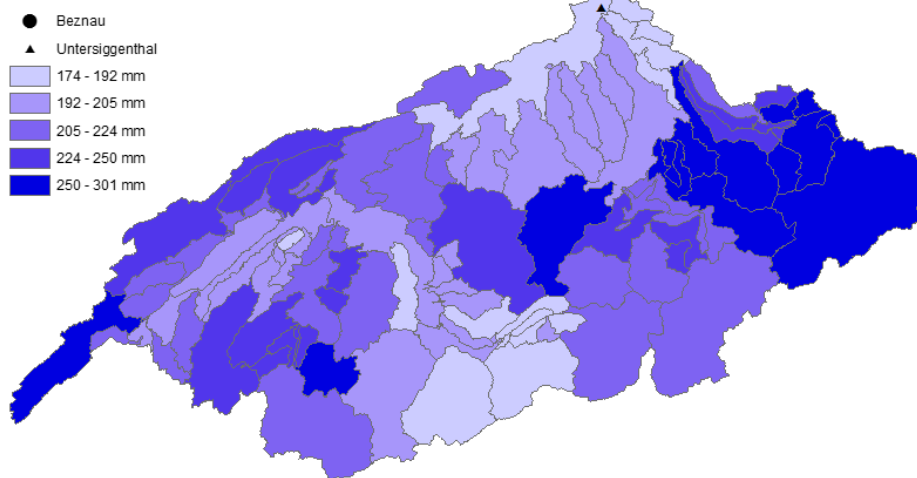
Beznau Winter Precipitation



Beznau Summer Precipitation



Beznau Autumn Precipitation



Beznau Spring Precipitation

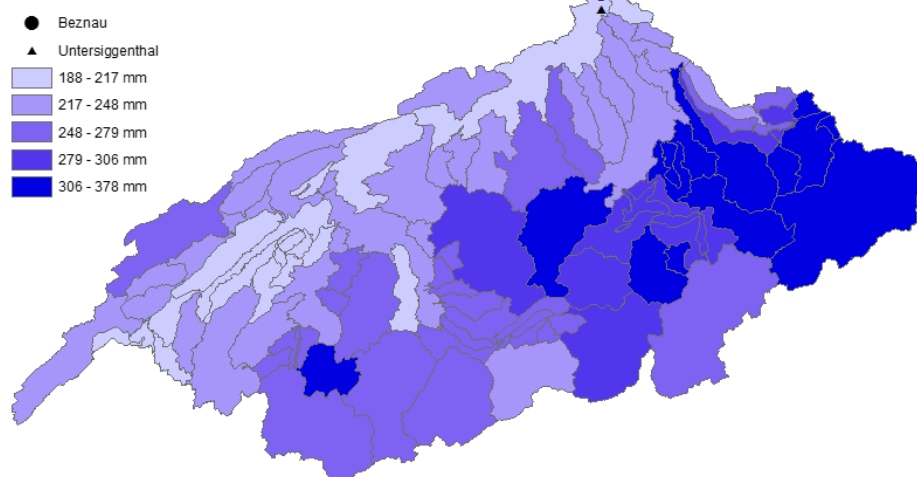


Figure 27: QdF curves for Beznau. From top to bottom: winter, summer, autumn, spring.

Figure 28: Precipitation distribution maps for Beznau and duration d3. From top to bottom: winter, summer, autumn, spring.

Table 12: Seasonal mean maximum discharge sum, mean, minimum value, maximum value and range for the 10'000 year return period floods and duration d3 in m³/s, seasonal runoff coefficient C for the 10'000 year return periods and duration d3 and seasonal rRMSE values for duration d1 and return periods T=10, T=100, T=1'000 and T=10'000 in %.

Beznau	Winter	Spring	Summer	Autumn
Q_{sum} (d3, T = 10'000) (m ³ /s)	63911	87074	103573	89038
Q_{mean} (d3, T = 10'000) (m ³ /s)	2204	3003	3578	3070
Q_{min} (d3, T = 10'000) (m ³ /s)	1779	2648	2893	2675
Q_{max} (d3, T = 10'000) (m ³ /s)	2803	3824	4841	3837
Q_{range} (d3, T = 10'000) (m ³ /s)	1030	1176	1948	1162
C (d3, T = 10'000)	0.34	0.33	0.34	0.43
rRMSE (d1, T = 10) (%)	1.8	1.9	0.4	2
rRMSE (d1, T = 100) (%)	3.3	1.1	2	4.9
rRMSE (d1, T = 1'000) (%)	8.8	10.5	7.5	9.8
rRMSE (d1, T = 10'000) (%)	14.8	24.5	14	14.2

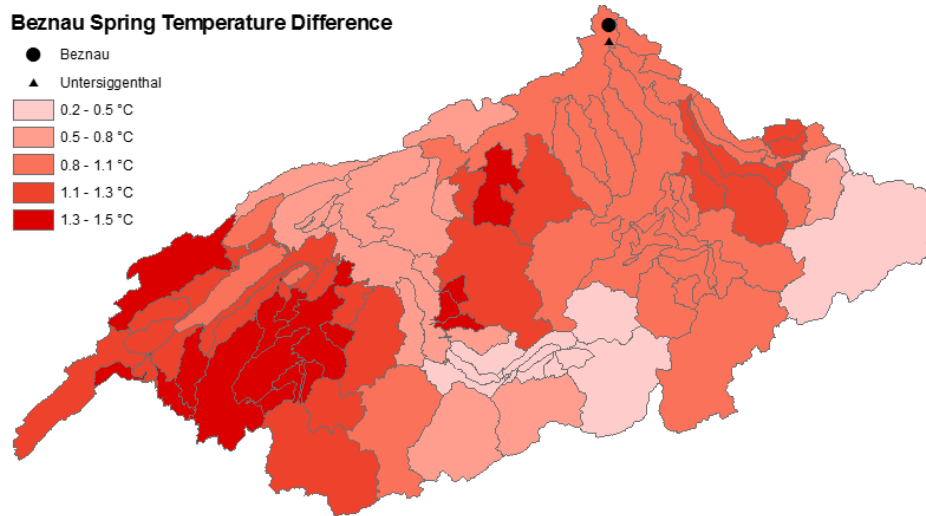


Figure 29: Temperature difference map for Beznau in spring and duration d3.

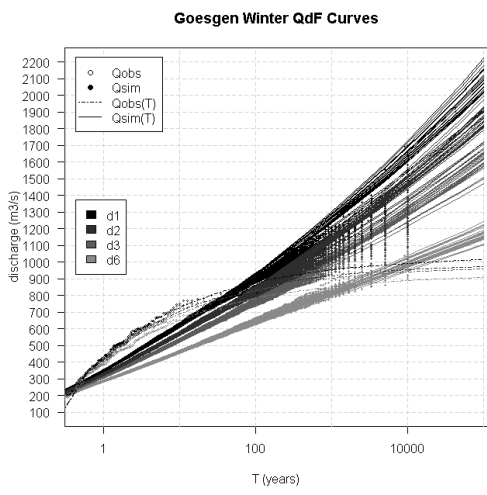
4.3 Group Duration d3

4.3.1 Beznau

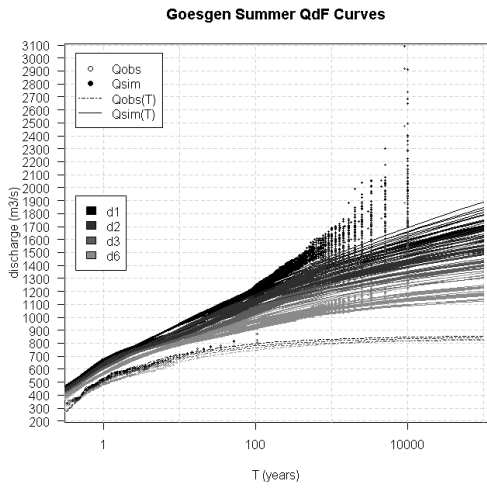
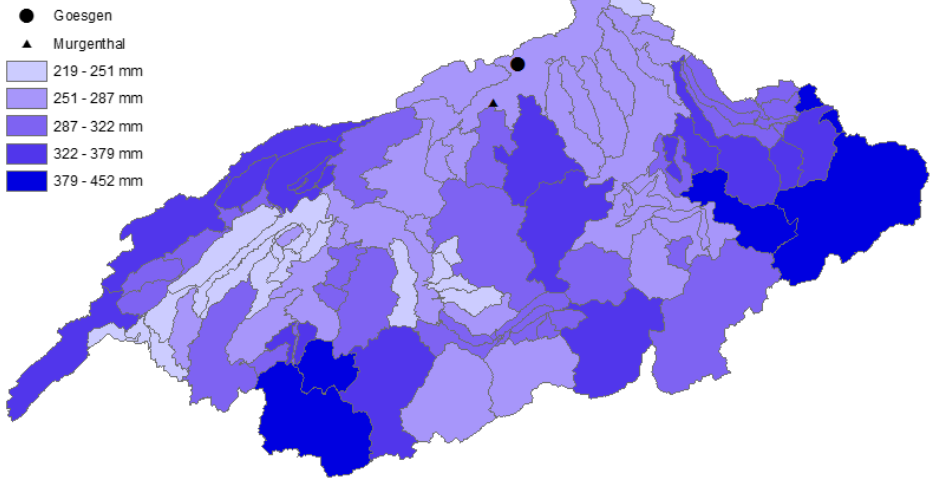
The QdF curves for Beznau and duration d3 in Figure 27 can adequately describe the simulated maximum mean discharge for all seasons at low return periods ($T < 100$). In autumn the quantiles generally overestimate the return level at extreme return periods, in spring and summer an underestimation is visible. In winter, the quantiles can also describe the simulated mean maximum discharge well at higher return levels. In summer and spring the quantiles belong to Weibull distributions, in winter to Fréchet distributions and in autumn to Gumbel or Weibull distributions. The rRMSE in Table 12 indicate low errors for all return periods in winter (1.8-14.8%), summer (0.4-14%) and autumn (2-14.2%) and moderate errors in spring (1.9 – 24.5%). Largest floods are found in summer in terms of the mean (3578 m³/s) and maximum value (4841 m³/s), smallest ones in winter. In spring and autumn floods with 10'000 years return periods have a similar magnitude according to the mean and maximal value. The nearby measuring station is Untersiggenthal, approximately 4.5 km away. Observed and simulated mean maximum discharge values correspond well in summer, spring and autumn, even though the observed values are slightly smaller. In winter however, the observed maximum mean discharges are quite higher for small return periods (~200 m³/s at $T = 1$). The observed and simulated quantiles in summer, autumn and spring compare well and belong to similar Weibull distributions. In winter the quantiles are different, in the observed case Weibull distributions are identified, in the simulated one Fréchet distributions.

The precipitation maps for Beznau and duration d3 in Figure 28 show similar precipitation patterns for summer and spring. Maxima are predominantly found in a band ranging from the east of the Aare basin to the southwest. Minima are located in the northern and western/northwestern parts of the Aare catchment. In winter maxima are found at the western/northwestern, southwestern, southeastern and eastern border subcatchments. In autumn precipitation maxima are identified in the east and southwest, as well as, in the center of the Aare region. In general large amounts of precipitation can be observed in all subbasins (130-467 mm), with most precipitation in summer (467 mm), followed by spring (378 mm), autumn (301 mm) and winter (287 mm).

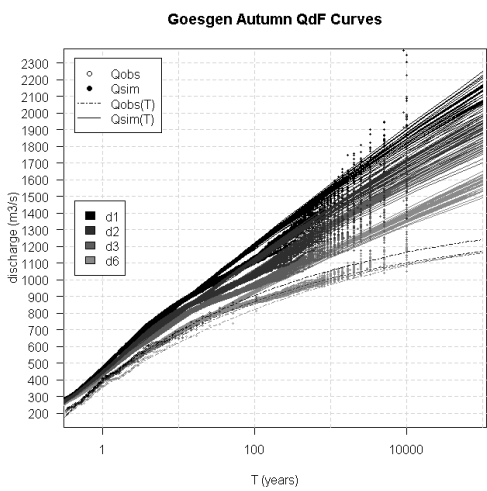
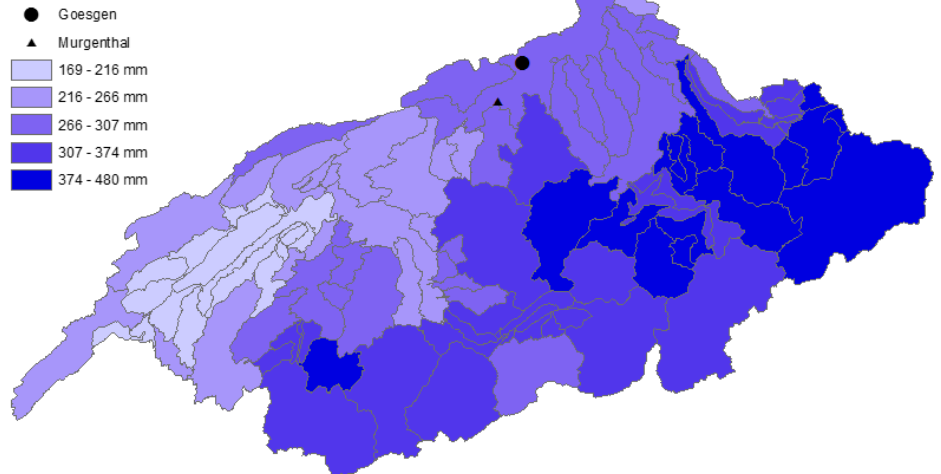
In Figure 29 a small increase in temperature is detected in all subcatchments (0.2-1.5°C). Maximum temperature increases are found in the west of the Aare basin and minima in the eastern and southern subbasins. The spring runoff coefficient C (0.33) in Table 12 has a similar magnitude than the winter (0.34) and summer (0.34) ones, but is smaller than the autumn runoff coefficient (0.43).



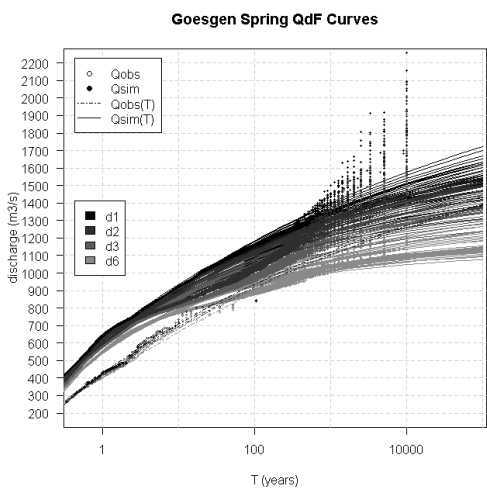
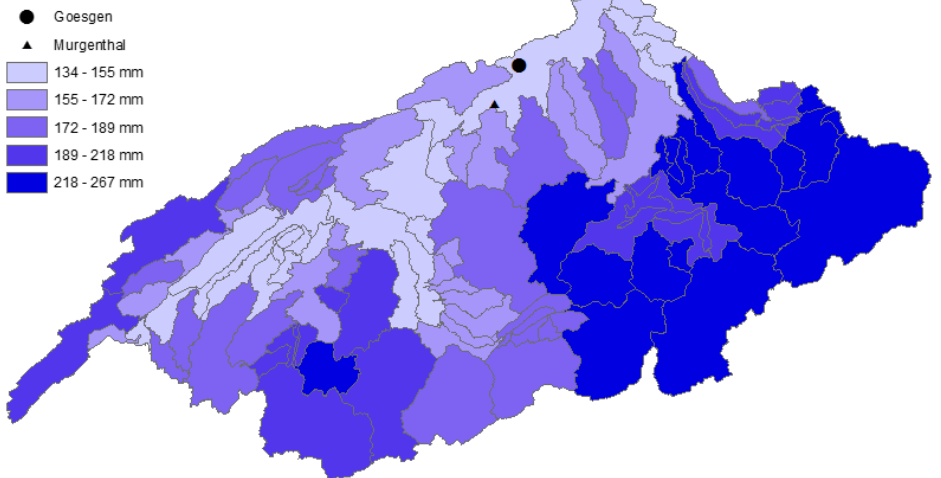
Goesgen Winter Precipitation



Goesgen Summer Precipitation



Goesgen Autumn Precipitation



Goesgen Spring Precipitation

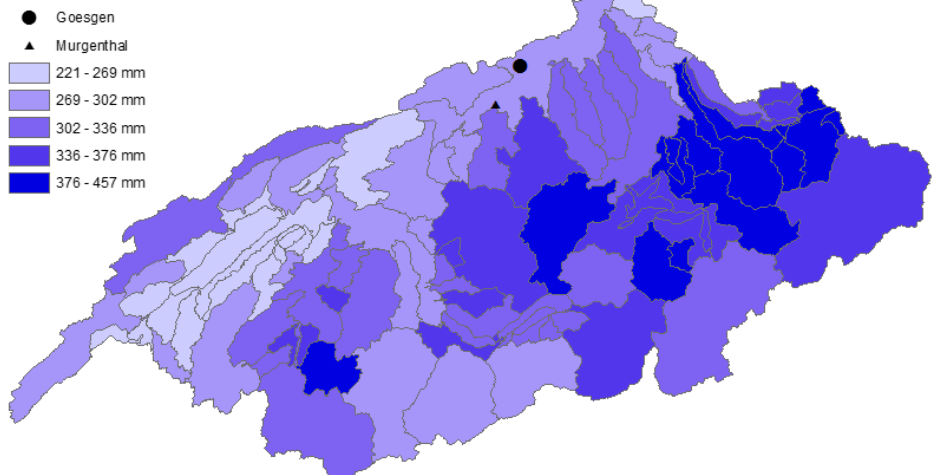


Figure 30: QdF curves for Gösgen. From top to bottom: winter, summer, autumn, spring.

Figure 31: Precipitation distribution maps for Gösgen and duration d3. From top to bottom: winter, summer, autumn, spring.

Table 13: Seasonal mean maximum discharge sum, mean, minimum value, maximum value and range for the 10'000 year return period floods and duration d3 in m³/s, seasonal runoff coefficient C for the 10'000 year return periods and duration d3 and seasonal rRMSE values for duration d1 and return periods T=10, T=100, T=1'000 and T=10'000 in %.

Gösgen	Winter	Spring	Summer	Autumn
Q_{sum} (d3, T = 10'000) (m ³ /s)	35477	44442	51114	43991
Q_{mean} (d3, T = 10'000) (m ³ /s)	1223	1532	1763	1517
Q_{min} (d3, T = 10'000) (m ³ /s)	1016	1309	1338	1239
Q_{max} (d3, T = 10'000) (m ³ /s)	1474	1908	2473	1985
Q_{range} (d3, T = 10'000) (m ³ /s)	458	599	1135	746
C (d3, T = 10'000)	0.1	0.11	0.13	0.21
rRMSE (d1, T = 10) (%)	2	6.6	4.9	2
rRMSE (d1, T = 100) (%)	2.8	7.3	2.4	7.2
rRMSE (d1, T = 1'000) (%)	9.9	5.4	12.4	5.2
rRMSE (d1, T = 10'000) (%)	17.5	22.4	26.6	9.2

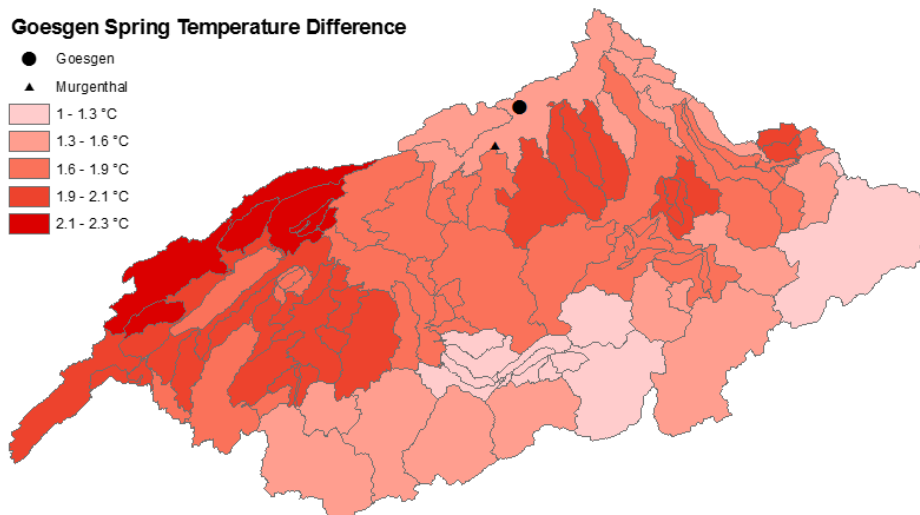


Figure 32: Temperature difference map for Gösgen in spring and duration d3.

4.3.2 Gösgen

The QdF curves of Gösgen in Figure 30 can adequately describe the simulated mean maximum discharge in all seasons for small return periods ($T < 100$). In winter and autumn, the quantiles tend to overestimate the return level at larger return periods ($T > 100$), whereas in summer and spring the quantiles tend to underestimate the return level at these return periods. The summer, autumn and spring quantiles belong to Weibull distributions, in winter to Fréchet or Gumbel distributions. In autumn, summer and spring sections can be identified, where the increase in return level with increasing return periods is considerably reduced in comparison to the next higher/lower return periods. These sections are approximately located between 3 and 300 years return period. The section is less pronounced in autumn than in summer or spring. During these sections the quantiles tend to overestimate the return level, converge with the data at higher return periods ($T = 1'000$) and consequently for more extreme return periods ($T = 10'000$), the return level gets underestimated. This is reflected in the rRMSE in Table 13. The rRMSE in autumn and spring indicate a larger error at the 100 year return period (7.3%, 7.2%) than at the 1'000 year return period (5.4%, 5.2%). In general however, the model scores best in autumn for the 10'000-year return period (9.2%), followed by winter (17.5%), spring (22.4%) and summer (26.6%). Largest floods with 10'000 years return periods and duration d_3 can be observed in summer with respect to the mean (1763 m³/s), the range (1135 m³/s) and the maximum value (2473 m³/s), similar ones in spring and autumn and smallest ones in winter.

The simulated mean maximum discharge and quantiles of Gösgen are compared to the ones of the Murgenthal measuring station. The two stations are 13 km apart. The observed maximum mean discharge is lower in spring, summer and autumn (~50-300 m³/s at $T = 1$) and higher in winter (~100 m³/s at $T = 1$) compared to the simulated values. The quantiles however are relatively similar in autumn, summer and spring, because in all cases Weibull distributions are assumed. The observed quantiles in winter belong to Weibull distributions, the simulated ones to Gumbel/Fréchet distributions.

The Gösgen precipitation maps for flood events with return periods of 10'000 years and duration d_3 in Figure 31 show similar precipitation patterns in spring and summer. Precipitation maxima are predominantly found in the eastern part of the Aare basin as well as in the southwestern part. In autumn the precipitation has a similar structure, but with northward shift. Comparatively low precipitation amounts are found directly at Gösgen in all seasons.

In general, large amounts of precipitation can be observed in all subbasins (169-480 mm) with lowest precipitation in autumn (267 mm), compared to spring (457 mm), summer (480 mm) and winter (452 mm), where the precipitation amounts have similar magnitudes.

The spring temperature map in Figure 32 shows a moderate temperature increase in all subbasins (1 -2.3°C). The biggest increases are found in subcatchments located in the northwestern borders of the Aare region, minimas in the south and east. The spring runoff coefficient C (0.11) is similar to the winter one (0.1), but smaller compared to the summer (0.13) and autumn runoff coefficients (9.2).

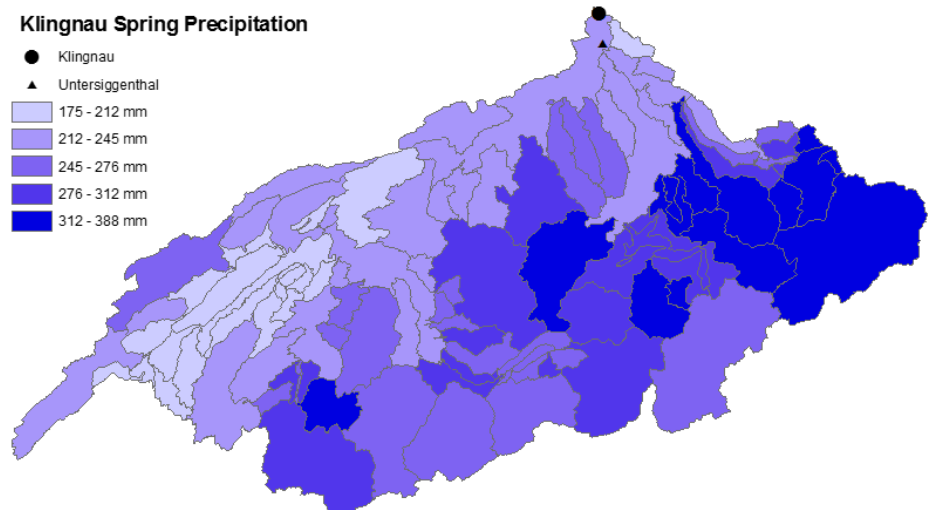
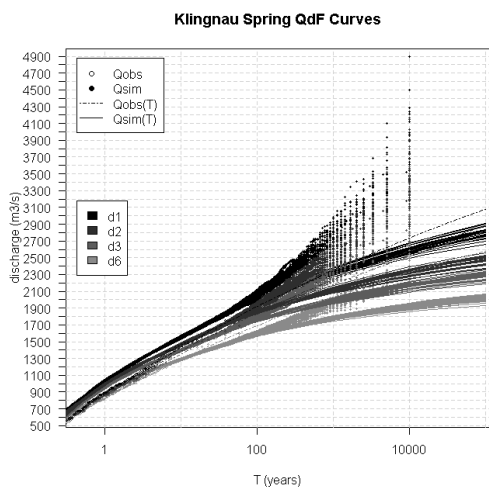
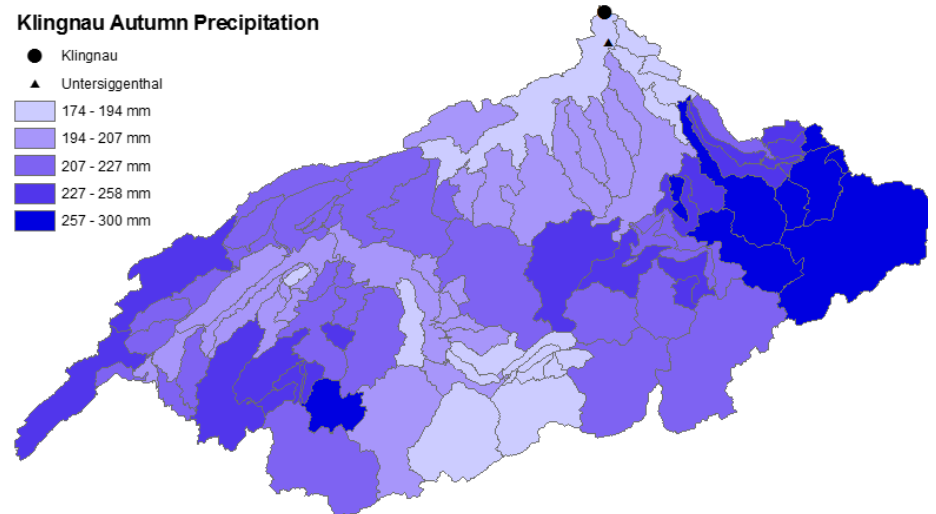
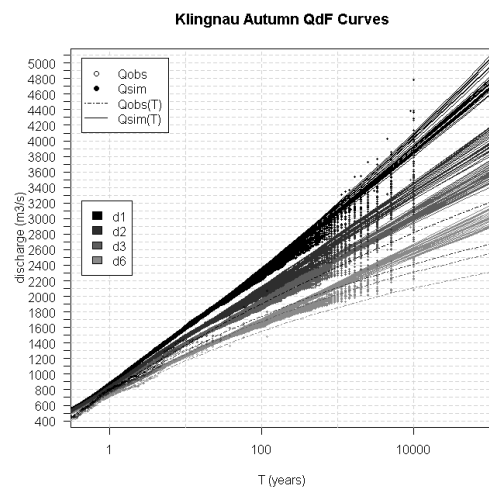
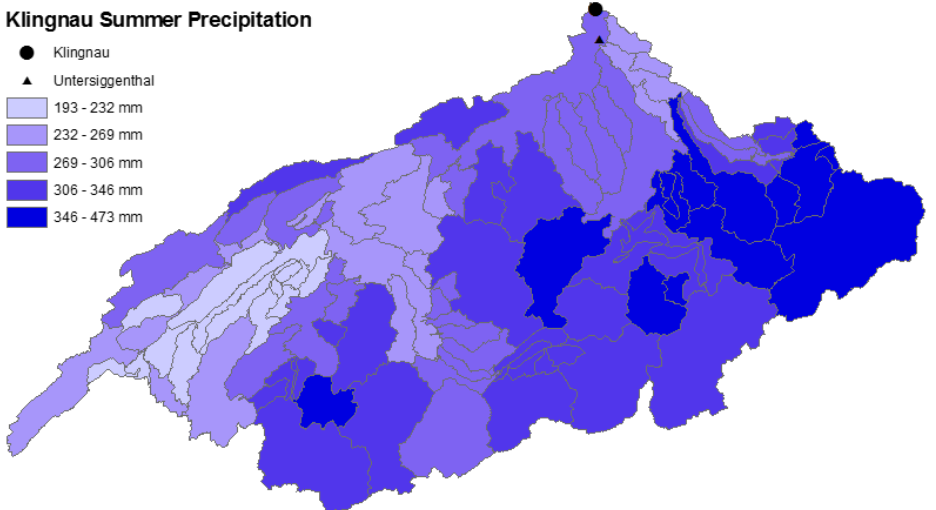
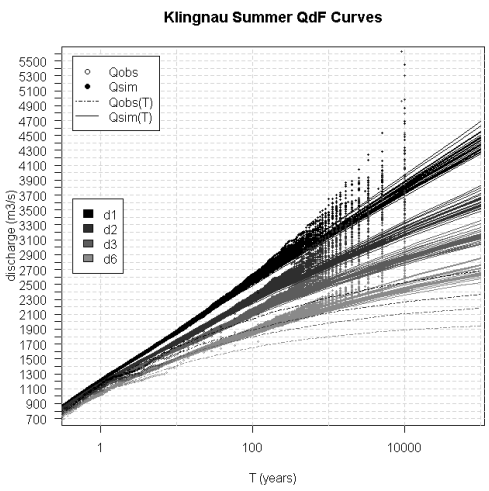
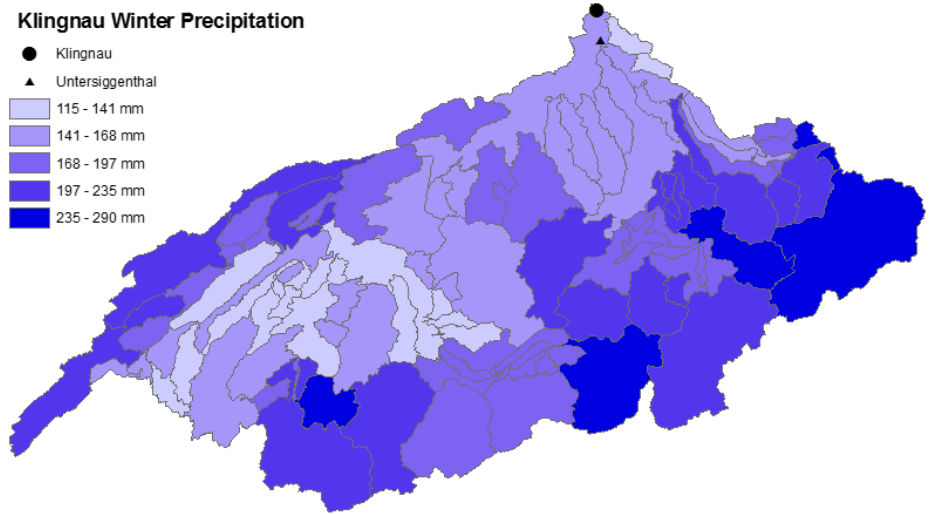
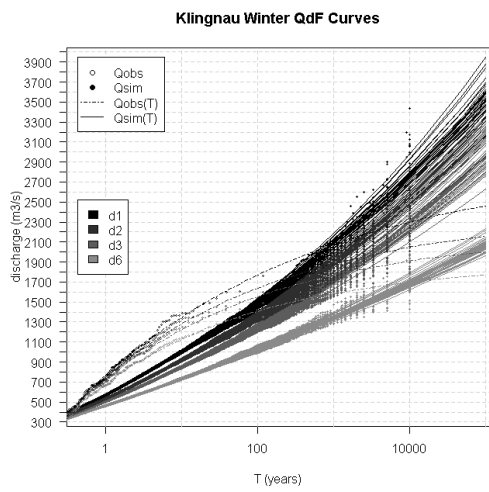


Figure 33: QdF curves for Klingnau. From top to bottom: winter, summer, autumn, spring.

Figure 34: Precipitation distribution maps for Klingnau and duration d3. From top to bottom: winter, summer, autumn, spring.

Table 14: Seasonal mean maximum discharge sum, mean, minimum value, maximum value and range for the 10'000 year return period floods and duration d3 in m³/s, seasonal runoff coefficient C for the 10'000 year return periods and duration d3 and seasonal rRMSE values for duration d1 and return periods T=10, T=100, T=1'000 and T=10'000 in %.

Klingnau	Winter	Spring	Summer	Autumn
Q_{sum} (d3, T = 10'000) (m ³ /s)	64394	87325	104204	89439
Q_{mean} (d3, T = 10'000) (m ³ /s)	2220	3011	3593	3084
Q_{min} (d3, T = 10'000) (m ³ /s)	1789	2676	2898	2705
Q_{max} (d3, T = 10'000) (m ³ /s)	2827	3829	4959	3821
Q_{range} (d3, T = 10'000) (m ³ /s)	1038	1153	2061	1116
C (d3, T = 10'000)	0.32	0.28	0.29	0.37
rRMSE (d1, T = 10) (%)	1.8	1.8	0.3	2
rRMSE (d1, T = 100) (%)	3.2	1.1	1.9	4.7
rRMSE (d1, T = 1'000) (%)	8.6	10.6	6.6	9.3
rRMSE (d1, T = 10'000) (%)	14.4	24.6	13.3	16.4

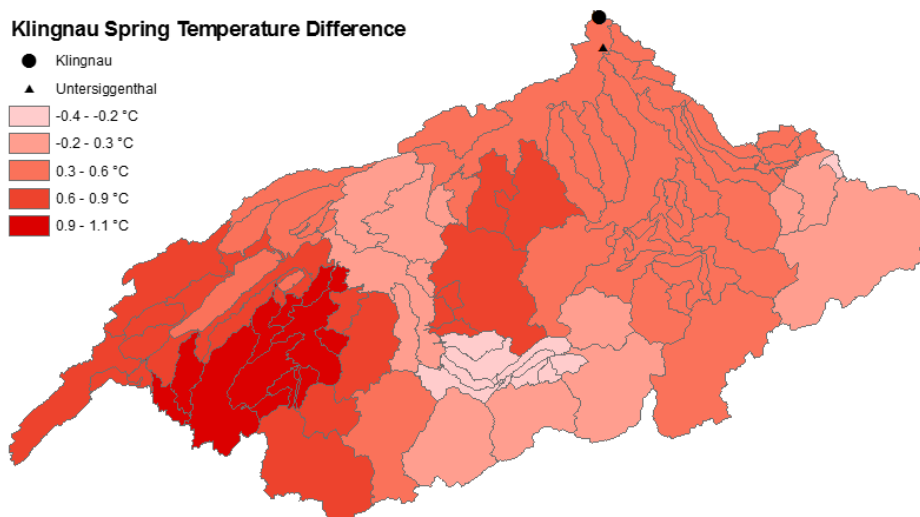


Figure 35: Temperature difference map for Klingnau in spring and duration d3.

4.3.3 Klingnau

The quantiles of the QdF curves of Klingnau in Figure 33 can adequately describe the simulated maximum mean discharge for small return periods in all seasons ($T < 100$). In summer and spring the quantiles tend to underestimate the return level for large return periods, whereas in autumn a slight underestimation can be observed. In spring, summer and autumn Weibull distributions are assumed, in Winter Fréchet distributions. The rRMSE values in Table 14 indicate low errors for all return periods in winter (1.8-14.4%), spring (0.3-13.3%) and autumn (2-16.4%). In summer the error is a bit higher, but still adequate (1.8-24.6%). The largest floods with return periods of 10'000 years are found in summer with respect to the mean (3593 m³/s) and maximum value (4959 m³/s) and smallest ones in winter. Autumn and spring have values of similar magnitude. Klingnau is compared to the Untersiggenthal station. The distance between the two stations is approximately 8.5 kilometers. The observed values tend to be slightly smaller for equal return periods in autumn, spring and summer, whereas in winter they are higher (~200 m³/s at $T = 1$). The quantiles show a similar pattern in autumn, spring and summer, they share similar Weibull distributions. In winter, Weibull distributions are assumed for Untersiggenthal and Fréchet distributions for Klingnau.

The Klingnau precipitation maps for floods with return periods of 10'000 years and duration d_3 in Figure 34 show similar patterns in winter, summer and spring. Precipitation maxima are predominantly found in a band ranging from the east to the southwest of the Aare basin. In autumn maxima are found in the east and the southwest as well, but no band is detected, because low precipitation amounts are found in the south. In all seasons, the precipitation at Klingnau is either a minimum or comparatively low. The precipitation amount in general is high in all subbasins (115-473 mm). Highest precipitation amounts are found in summer (473 mm), followed by spring (388 mm) and are smallest in autumn (300 mm) and winter (290 mm).

According to the spring temperature map in Figure 35, small temperature increases, as well as decreases are identified before the flood events (-0.4-1.1°C). Highest Temperature increases are found in the southwestern part, highest decreases in the southern and eastern parts. The spring runoff coefficient C in Table 14 is the smallest one (0.28) in comparison with the runoff coefficient of the other seasons.

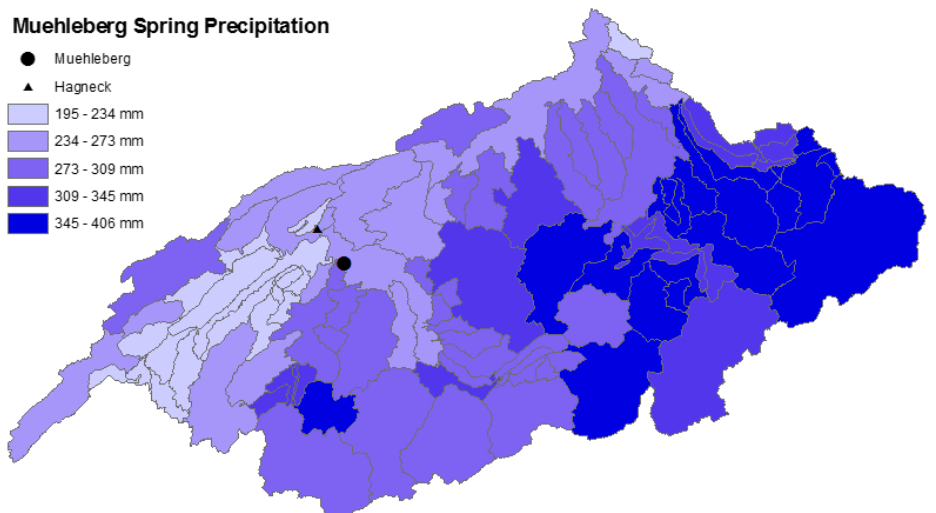
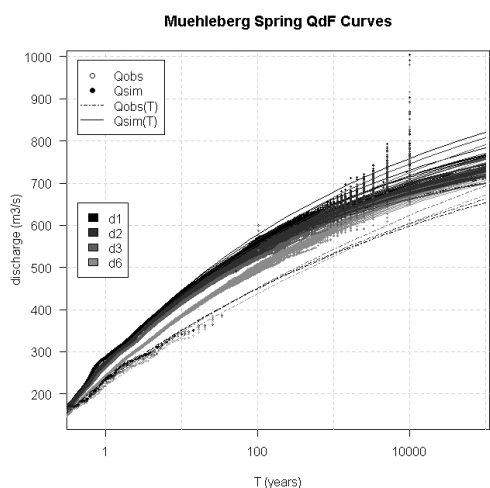
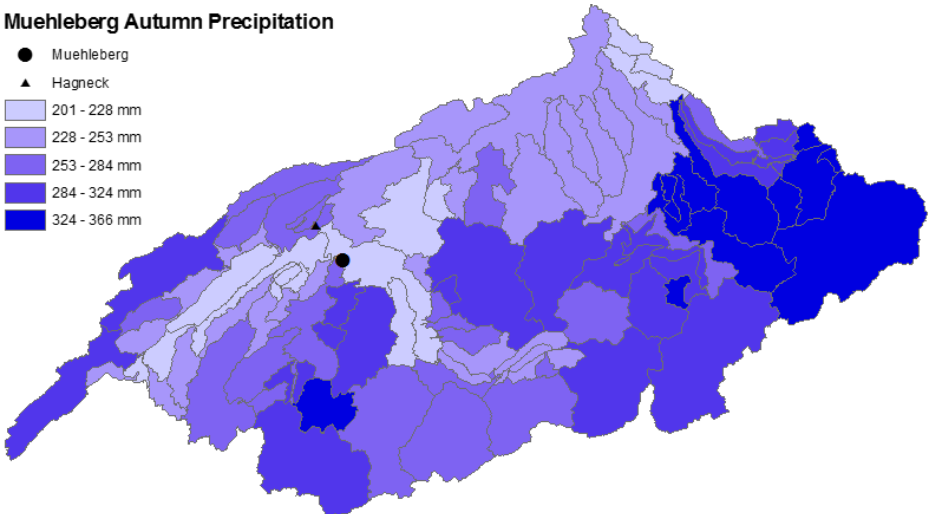
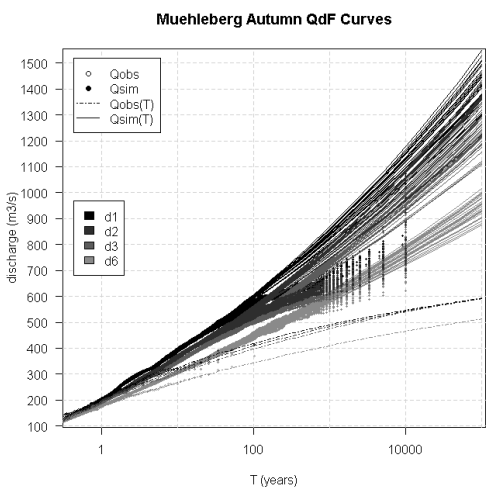
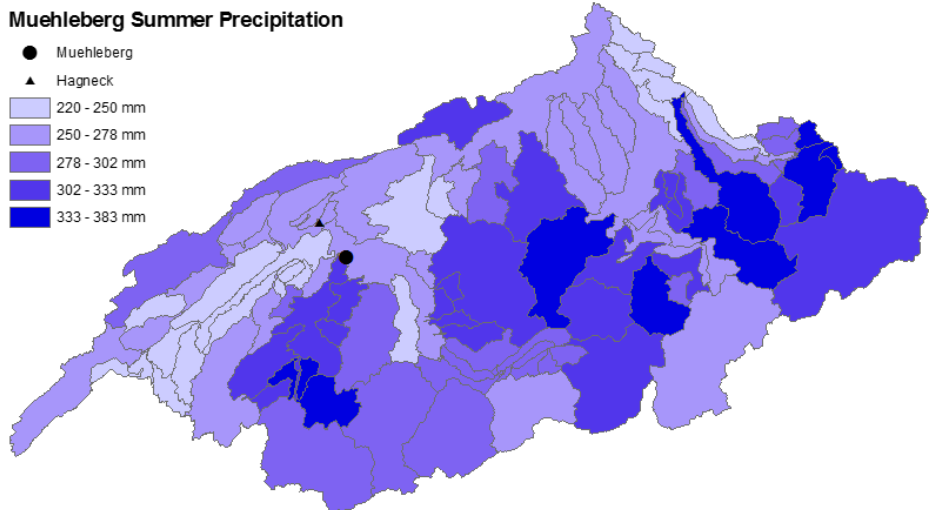
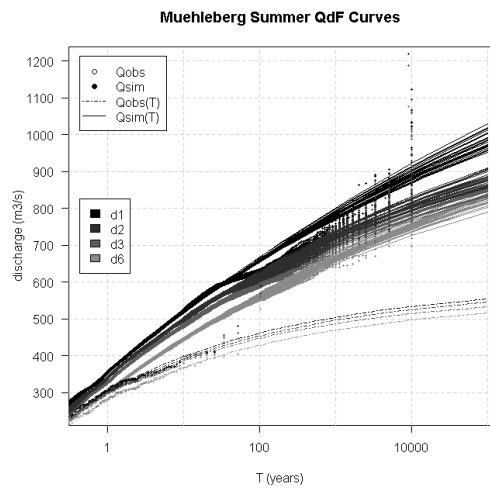
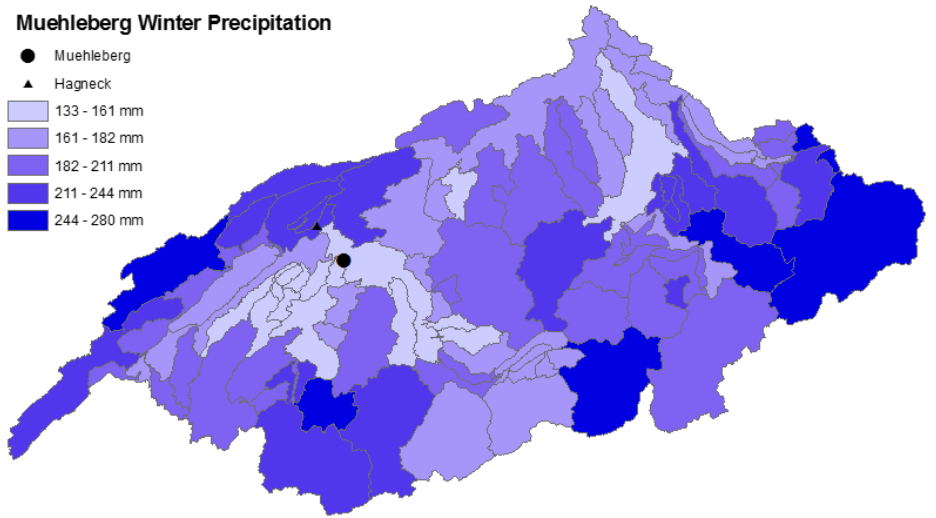
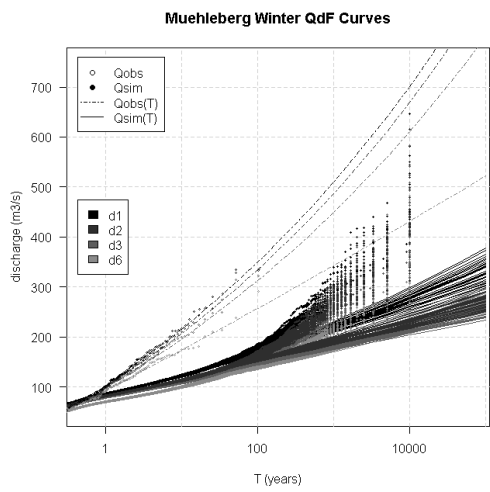


Figure 36: QdF curves for Muehleberg. From top to bottom: winter, summer, autumn, spring.

Figure 37: Precipitation distribution maps for Muehleberg and duration d3. From top to bottom: winter, summer, autumn, spring.

Table 15: Seasonal mean maximum discharge sum, mean, minimum value, maximum value and range for the 10'000 year return period floods and duration d3 in m³/s, seasonal runoff coefficient C for the 10'000 year return periods and duration d3 and seasonal rRMSE values for duration d1 and return periods T=10, T=100, T=1'000 and T=10'000 in %.

Mühleberg	Winter	Spring	Summer	Autumn
Q_{sum} (d3, T = 10'000) (m ³ /s)	11983	21109	25481	23342
Q_{mean} (d3, T = 10'000) (m ³ /s)	413	728	879	805
Q_{min} (d3, T = 10'000) (m ³ /s)	255	657	762	673
Q_{max} (d3, T = 10'000) (m ³ /s)	286	980	1188	1012
Q_{range} (d3, T = 10'000) (m ³ /s)	31	323	426	339
C (d3, T = 10'000) (%)	0.06	0.06	0.07	0.08
rRMSE (d1, T = 10) (%)	2.3	0.4	1.6	2.5
rRMSE (d1, T = 100) (%)	5.3	1.3	3.3	4.2
rRMSE (d1, T = 1'000) (%)	27.9	2.4	2.5	25
rRMSE (d1, T = 10'000) (%)	43.4	11.7	9.3	36

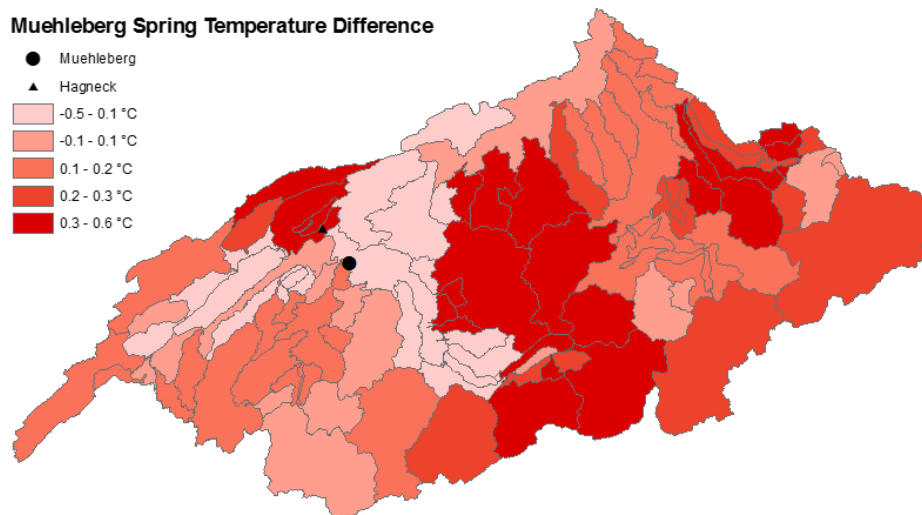


Figure 38: Temperature difference map for Mühleberg in spring and duration d3.

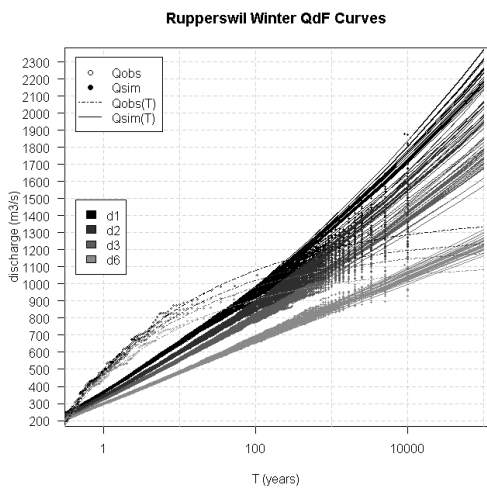
4.3.4 Mühleberg

The QdF curves for Mühleberg are presented in Figure 36. In all seasons, the quantiles can describe the simulated mean maximum discharge adequately up until a return period of around 100 years. At more extreme return periods, the summer and autumn quantiles overestimate the return level, whereas in winter and spring, the quantiles tend to underestimate the mean maximum discharge. The winter and autumn quantiles belong to Fréchet distributions, the summer and spring ones to Weibull distributions. The rRMSE values in Table 15 indicate adequate model results for summer (1.6-9.3%), spring (0.4-11.7%) for all return periods and moderate to poor results for winter (2.3-43.4%) and autumn (2.5-36%) for large return periods. The biggest floods with return periods of 10'000 years are identified in summer with respect to the mean (879 m³/s), followed by autumn (805 m³/s), spring (728 m³/s) and winter (413 m³/s).

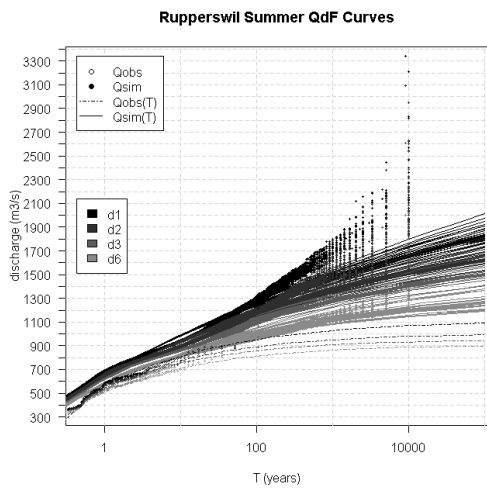
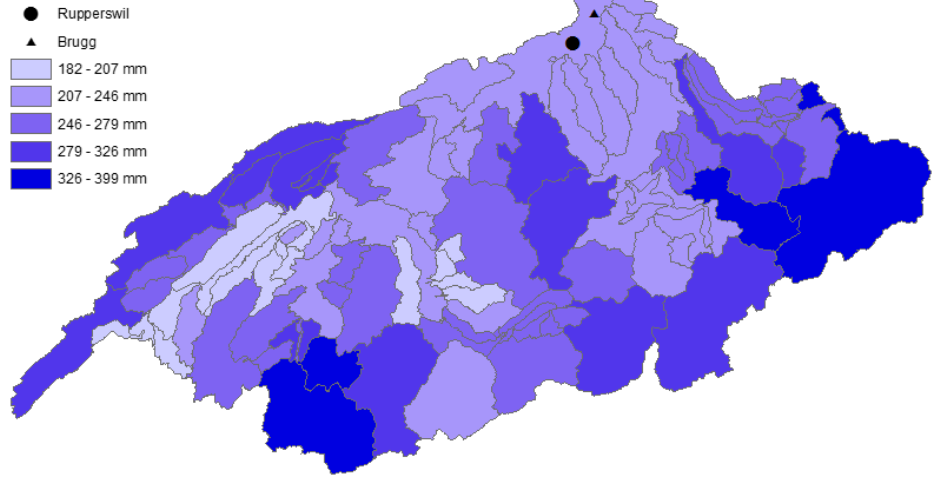
The QdF curves of Mühleberg are compared to the curves of Schönau. The distance between the two stations is approximately 6 kilometers. In all seasons the simulated and observed mean maximum discharge values tend to agree for return periods lower than 1 year. For increasing return periods the simulated values are higher in summer, winter and spring but much smaller in winter. The simulated and observed quantiles compare well in spring. In autumn different distributions are assumed and in winter the return levels for same return periods have a vastly different magnitude.

The precipitation maps for Mühleberg and duration d3 in Figure 37 show similar structures in autumn and spring. Precipitation maxima are found in the eastern, southeastern and southwestern parts of the Aare catchment. In summer these maxima show a slight shift in northward direction. In winter no clear precipitation structure can be recognized. Precipitation maxima in winter are found in basins located at the eastern, southeastern southwestern and western (northwestern) border of the Aare basin. In winter, Mühleberg is located in a precipitation minimum, whereas in spring, summer and autumn there is moderate or high precipitation at the station or directly south of it. In general, all subbasins experience lots of precipitation (133 -406 mm). Lowest precipitation amount are identified in winter (280 mm), largest in spring (406 mm), followed by summer (383 mm) and autumn (366 mm).

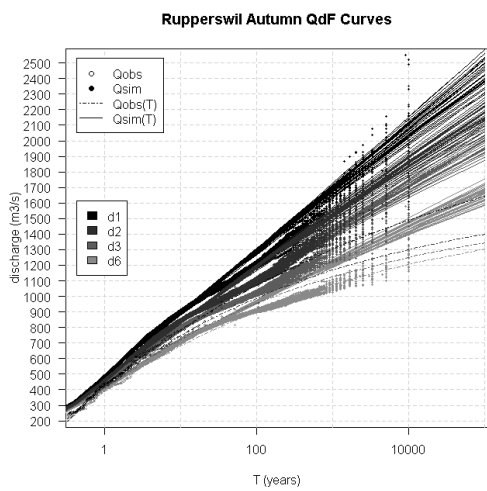
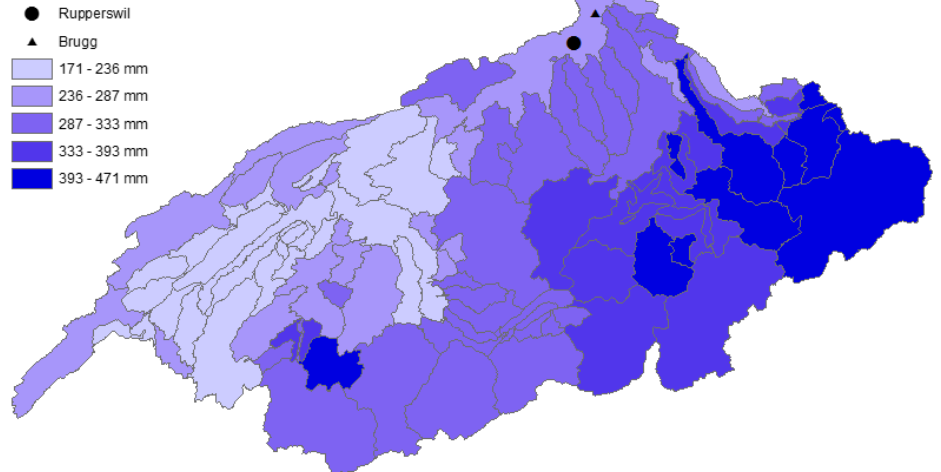
In the spring temperature map in Figure 38 very small temperature increases and decreases are visible (-0.5-0.6 °C). Largest temperature increases are located in the southern and central regions, largest decreases just eastern of Mühleberg and in the western parts of the Aare basin. The spring runoff coefficient C (0.06) in Table 15 is similar to the winter runoff coefficient and slightly smaller than the summer (0.07) and autumn (0.08) ones.



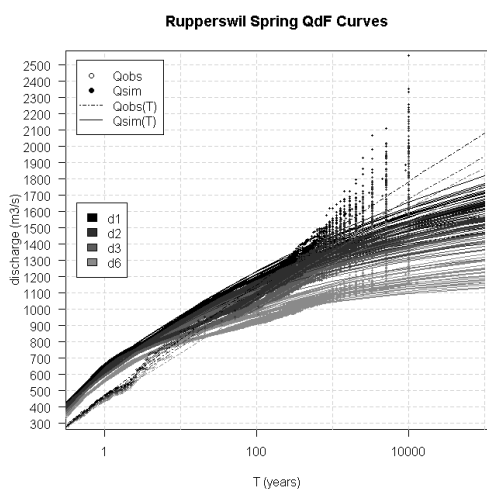
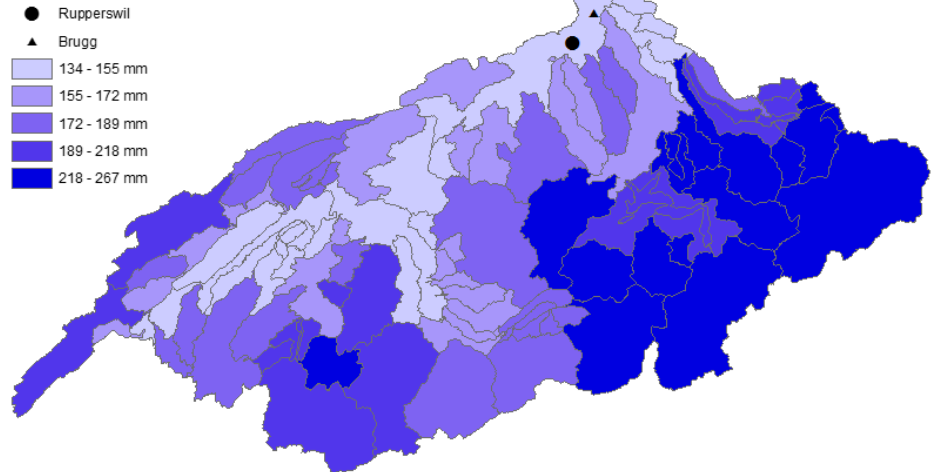
Rupperswil Winter Precipitation



Rupperswil Summer Precipitation



Rupperswil Autumn Precipitation



Rupperswil Spring Precipitation

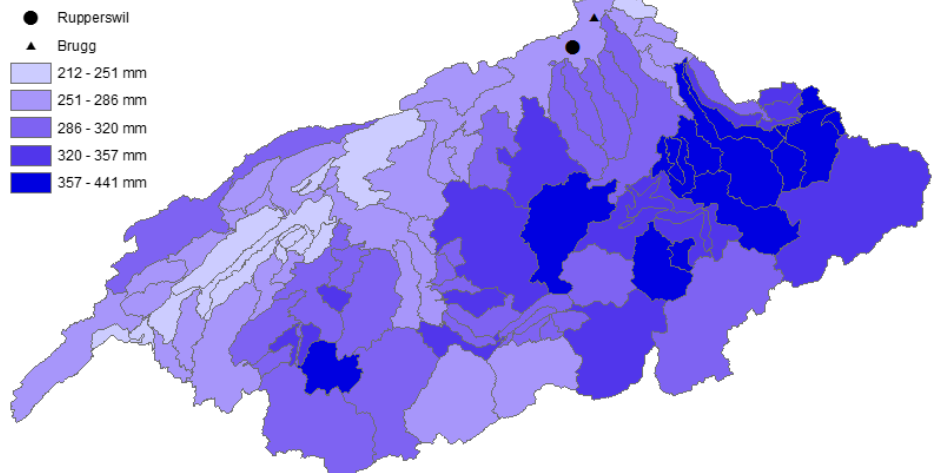


Figure 39: QdF curves for Rupperswil. From top to bottom: winter, summer, autumn, spring.

Figure 40: Precipitation distribution maps for Rupperswil and duration d3. From top to bottom: winter, summer, autumn, spring.

Table 16: Seasonal mean maximum discharge sum, mean, minimum value, maximum value and range for the 10'000 year return period floods and duration d3 in m³/s, seasonal runoff coefficient C for the 10'000 year return periods and duration d3 and seasonal rRMSE values for duration d1 and return periods T=10, T=100, T=1'000 and T=10'000 in %.

Rupperswil	Winter	Spring	Summer	Autumn
Q_{sum} (d3, T = 10'000) (m ³ /s)	38211	47643	54651	47646
Q_{mean} (d3, T = 10'000) (m ³ /s)	1318	1643	1885	1637
Q_{min} (d3, T = 10'000) (m ³ /s)	1088	1383	1435	1328
Q_{max} (d3, T = 10'000) (m ³ /s)	1586	2005	2608	2126
Q_{range} (d3, T = 10'000) (m ³ /s)	498	622	1173	798
C (d3, T = 10'000)	0.13	0.12	0.15	0.22
rRMSE (d1, T = 10) (%)	2	5.6	4.2	1.9
rRMSE (d1, T = 100) (%)	3.1	5.7	2.8	7
rRMSE (d1, T = 1'000) (%)	9.4	7.2	12.6	6.8
rRMSE (d1, T = 10'000) (%)	16.9	23.9	26.7	9.6

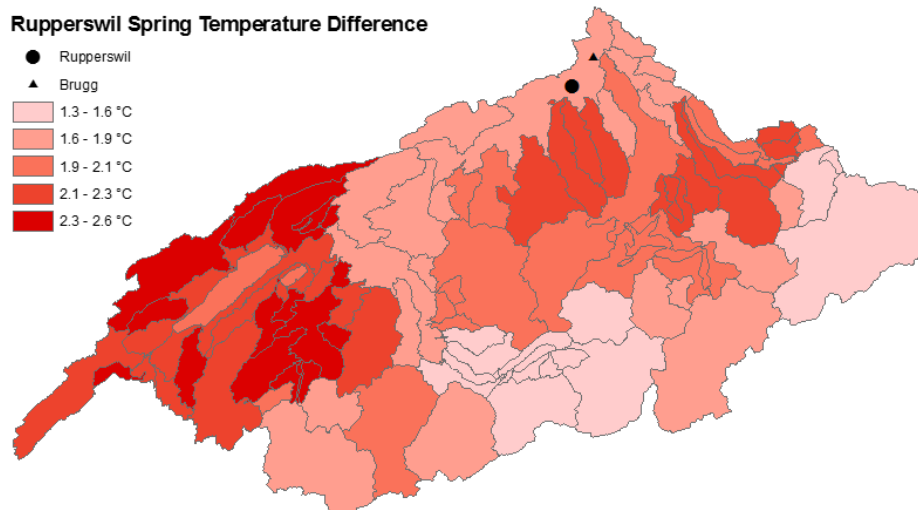


Figure 41: Temperature difference map for Rupperswil in spring and duration d3.

4.3.5 Ruppertsuil

The QdF curves of Ruppertsuil are presented in Figure 42. The fitted quantiles can describe the simulated mean maximum discharge very well for all return periods in winter. In autumn, summer and spring sections can be identified, where the increase of return level with increasing return periods is considerably reduced in comparison to the next higher/lower return periods. These sections are approximately located between 10 and 100 years return period for autumn and spring. The simulated quantiles therefore tend to overestimate the return level at return periods between 10 and 100 years and consequently underestimate the return values between return periods of 1000 and 10'000 years. In summer the section starts at earlier return periods, and likewise the over and underestimation. The winter, summer and autumn quantiles belong to the Weibull distribution, the winter quantiles are either Fréchet for the duration d1, d2 and d3 or Gumbel distributions for the duration d6. The rRMSE in Table 17 indicates good model fits in autumn (1.9-9.6%) and winter (2-16.9%) and moderate ones in summer (4.2-26.7%) and spring (5.6-23.9%). Largest flood events with 10'000 years return periods can be observed in summer in terms of the mean (1185 m³/s) and maximum value (2608 m³/s) and smallest ones in winter. In spring the mean (1643 m³/s) is slightly higher than in autumn (1637 m³/s), but the largest identified flood has an increased magnitude in autumn (2126 m³/s) than in spring (2005 m³/s).

Ruppertsuil is compared to the measuring station Brugg. The two stations are 10 km apart. The observed mean maximum discharges are slightly lower in summer, autumn and spring (~100-150 m³/s at T = 1), but larger in winter for equal return periods (~150 m³/s at T = 1). The simulated and observed quantiles compare fairly well in summer, autumn and spring because similar Weibull distributions are assumed. In winter, Weibull distributions are assumed in the observations and Fréchet/Gumbel distributions in the simulations.

The Ruppertsuil precipitation distribution maps for floods with return periods of 10'000 years and duration d3 in Figure 43 show a clear precipitation structure in summer, autumn and spring. Precipitation maxima are found in the eastern, southeastern as well as the southwestern parts of the Aare basin. In spring, the precipitation maxima in the east have a slight northward shift compared to the autumn and summer ones. In winter, the eastern maxima are less pronounced compared to the other seasons, but instead the southeastern one is slightly increased. New maxima also appear at subbasins at the western/northwestern border of the Aare region. At Ruppertsuil comparatively small to moderate precipitation amounts are found in all seasons. In general, the precipitation amount is large for all subcatchments (134-471 mm). Highest precipitation amounts are identified in summer (471 mm) and spring (441 mm) and smallest ones in winter (399 mm) and autumn (267 mm).

The spring temperature map in Figure 41 indicates a considerable temperature increase for most subcatchments (1.3-2.5°C). Largest temperature increases are found in the west, lowest ones in the south and east. The spring runoff coefficient *C* in Table 16 has the lowest magnitude compared to the other seasons.

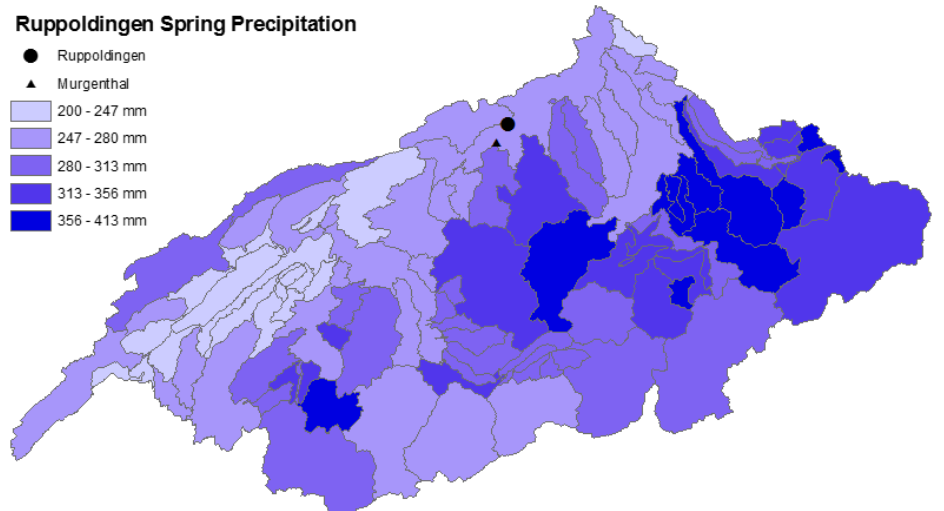
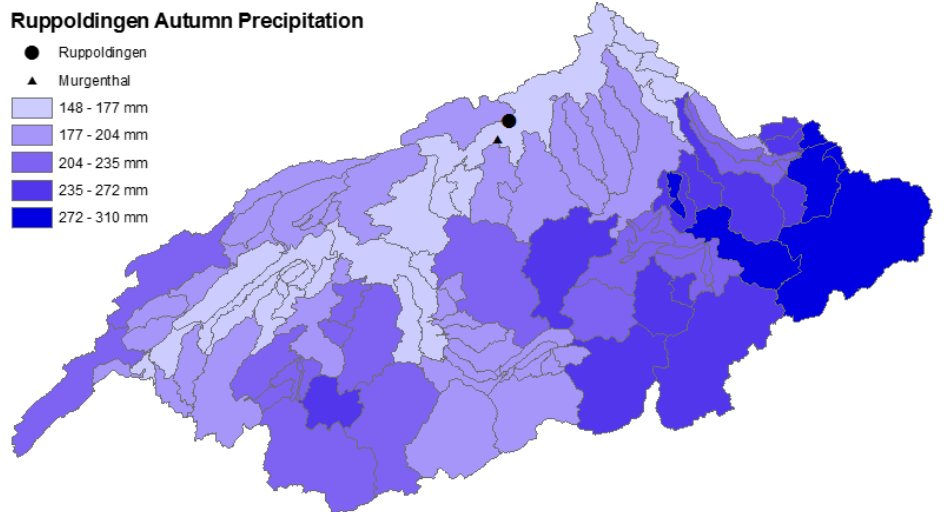
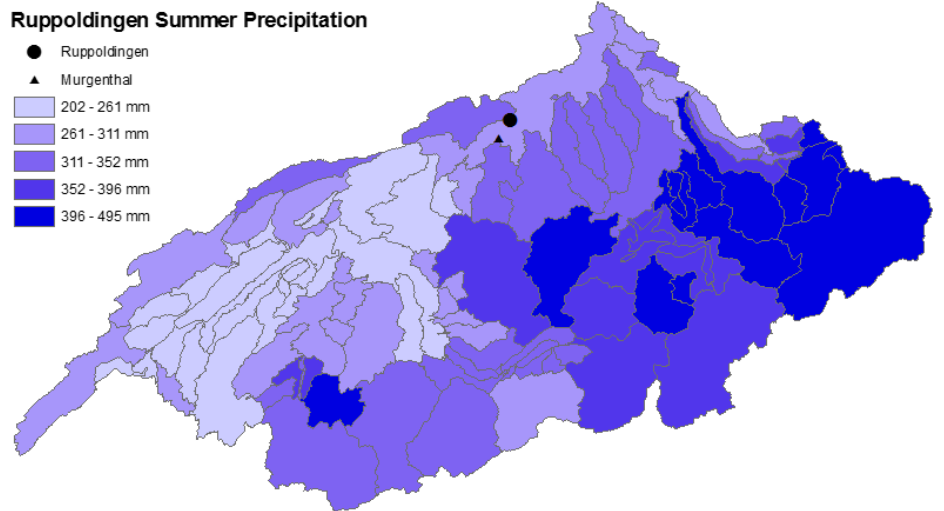
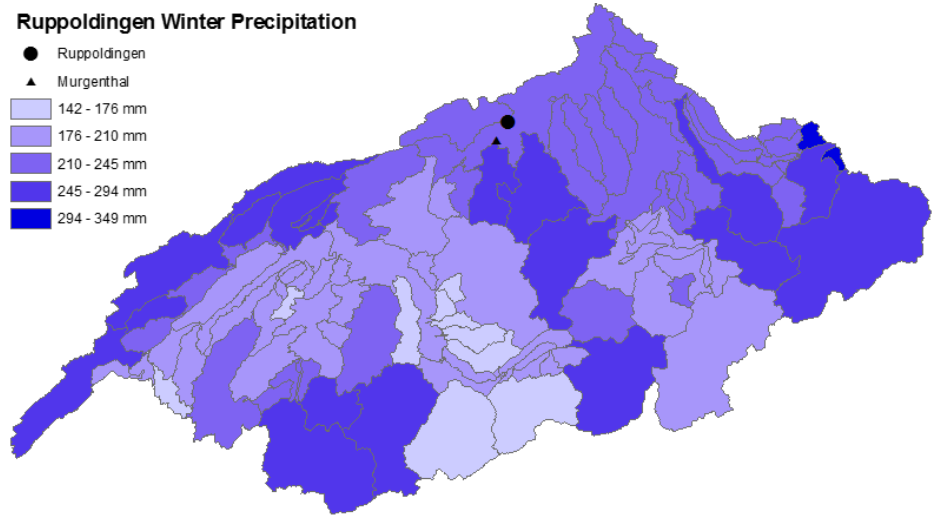
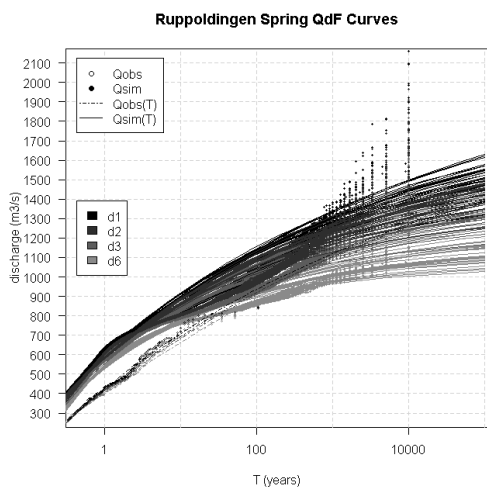
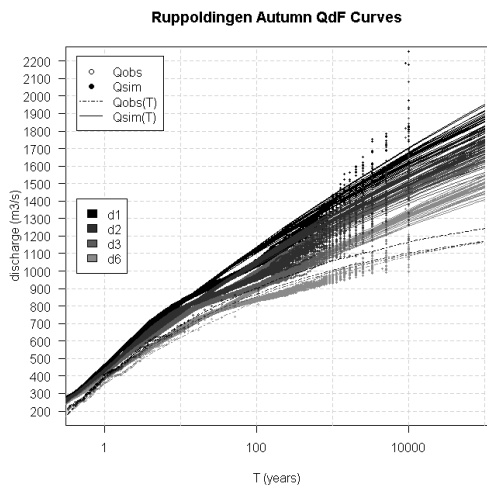
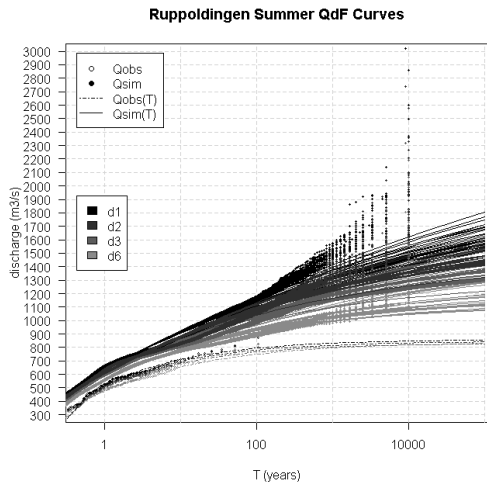
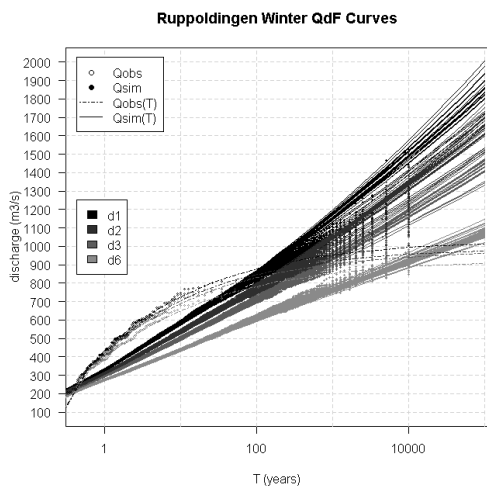


Figure 42: QdF curves for Ruppoldingen. From top to bottom: winter, summer, autumn, spring.

Figure 43: Precipitation distribution maps for Ruppoldingen and duration d1. From top to bottom: winter, summer, autumn, spring.

Table 17: Seasonal mean maximum discharge sum, mean, minimum value, maximum value and range for the 10'000 year return period floods and duration $d3$ in m^3/s , seasonal runoff coefficient C for the 10'000 year return periods and duration $d3$ and seasonal rRMSE values for duration $d1$ and return periods $T=10$, $T=100$, $T=1'000$ and $T=10'000$ in %.

Ruppoldingen	Winter	Spring	Summer	Autumn
Q_{sum} ($d3$, $T = 10'000$) (m^3/s)	32963	41689	47966	40434
Q_{mean} ($d3$, $T = 10'000$) (m^3/s)	1137	1438	1654	1394
Q_{min} ($d3$, $T = 10'000$) (m^3/s)	941	1213	1249	1053
Q_{max} ($d3$, $T = 10'000$) (m^3/s)	1469	1816	2317	1872
Q_{range} ($d3$, $T = 10'000$) (m^3/s)	528	603	1068	819
C ($d3$, $T = 10'000$)	0.13	0.11	0.12	0.17
rRMSE ($d1$, $T = 10$) (%)	2	8.1	5.8	2.1
rRMSE ($d1$, $T = 100$) (%)	2.3	9.6	1.8	7.6
rRMSE ($d1$, $T = 1'000$) (%)	9.4	3.8	11.5	4
rRMSE ($d1$, $T = 10'000$) (%)	17.4	20.2	26.6	9.9

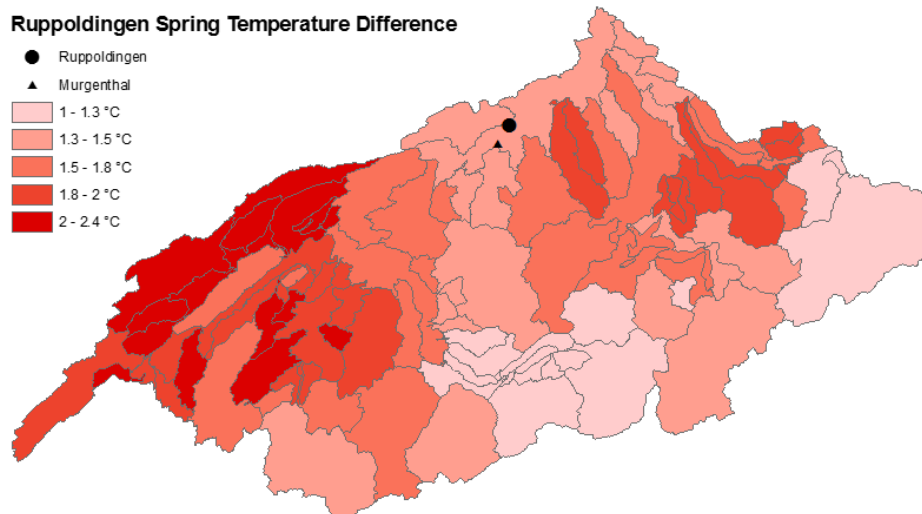


Figure 44: Temperature difference map for Ruppoldingen in spring and duration $d3$.

4.3.6 Ruppoldingen

The QdF curves of Ruppoldingen in Figure 42 agree fairly well with the simulated mean maximum discharge for small return periods in all seasons ($T < 100$). In winter, this agreement tends to extend even up to return periods of 10'000 years. In autumn, summer and spring sections can be identified, where the increase of return level with increasing return periods is considerably reduced in comparison to the next higher/lower return periods. These sections are approximately located between 3 and 30 years return period in summer and spring and between 10 and 300 years return period for autumn. The simulated quantiles tend to overestimate the simulated mean maximum discharge during these sections and ultimately start to underestimate the return level for even more extreme return periods. The spring, autumn and summer quantiles belong to the Weibull distribution family, the winter quantiles to the Fréchet, close to Gumbel distributions. The rRMSE in Table 17 indicates a good model fit in autumn (9.9%), and moderate ones in winter (17.4%), summer (26.6%) and spring (20.2%) for the 10'000 year return period.

Quantiles and mean maximum discharge values of Ruppoldingen are compared to the ones of the measuring station Murgenthal. The distance between the two stations is approximately 6 kilometers. The observed mean maximum discharge at Murgenthal seems to be smaller in summer, spring and autumn compared to the simulated values of Ruppoldingen for same return periods (~ 100 - $200 \text{ m}^3/\text{s}$ at $T = 1$). In winter, the observed values however tend to be larger than the simulated ones ($\sim 100 \text{ m}^3/\text{s}$ at $T = 1$). The observed and simulated quantiles agree well in autumn, summer and spring, because similar Weibull distributions are assumed, whereas in winter opposite distributions are considered.

The precipitation maps of Ruppoldingen for duration d3 show a similar precipitation distribution for summer, autumn and spring. Precipitation maxima are predominantly found in the eastern part of the Aare basin with an additional maximum in the southwest. In spring the eastern maxima seem to have a slight northward shift compared to summer and autumn ones. In winter no clear structure is evident. Maxima are scattered over the whole Aare basin. In all seasons, the precipitation amount at Ruppoldingen is comparatively low. In general high precipitation amounts are present in all subcatchments (142-495 mm). Highest precipitation amounts are identified in summer (495 mm), followed by spring (413 mm) and smallest in winter (349 mm) and autumn (310 mm).

The spring temperature map in Figure 44 indicates moderate to high temperature increase in all subcatchments before the flood events (1-2.4°C). Maximum temperature increases are found in the western part, lowest amounts in the eastern and southern parts of the Aare basin. The spring runoff coefficient in Table 17 has the lowest magnitude compared to the other seasons.

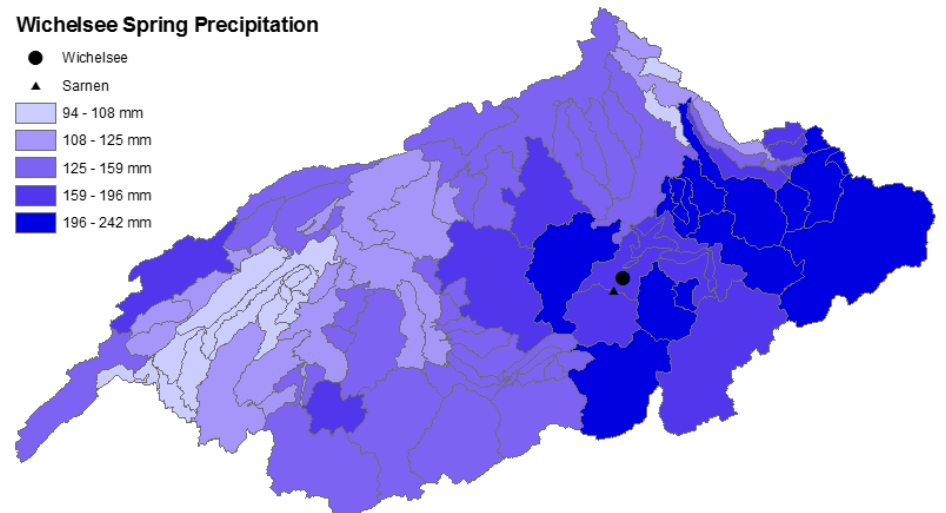
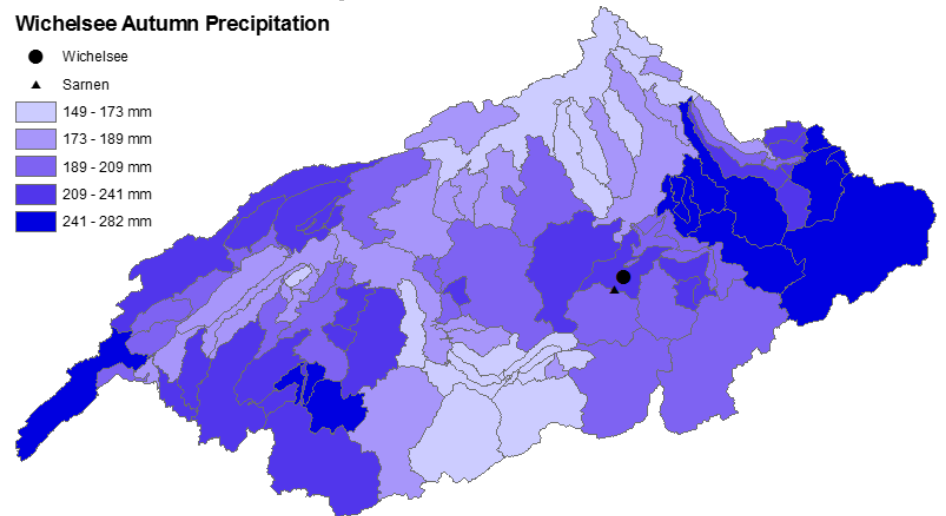
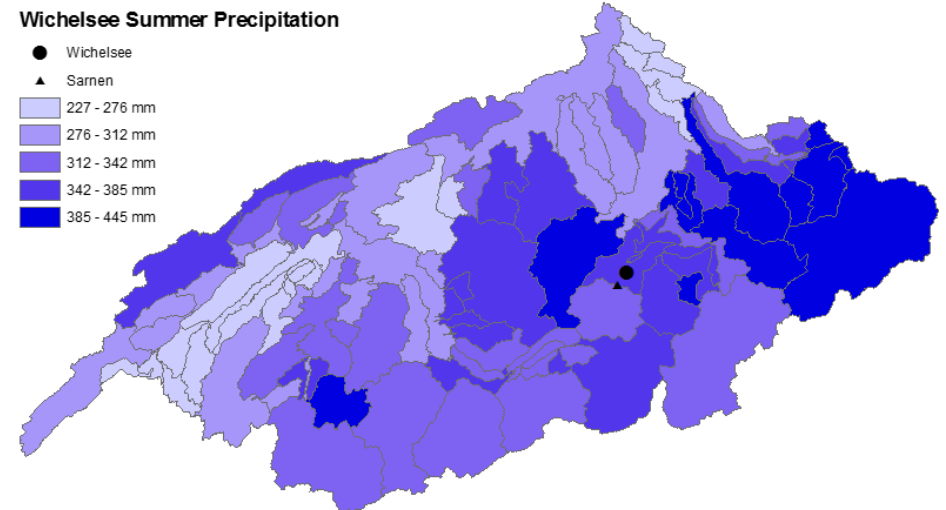
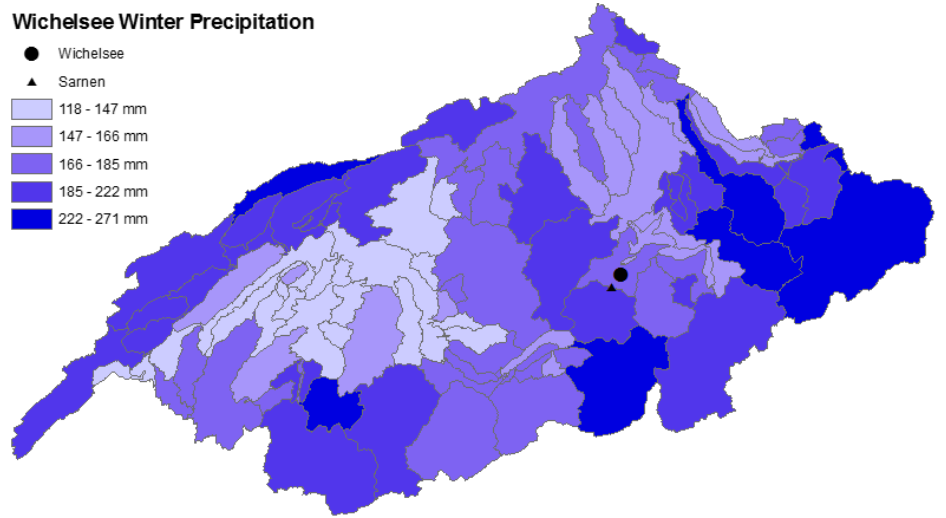
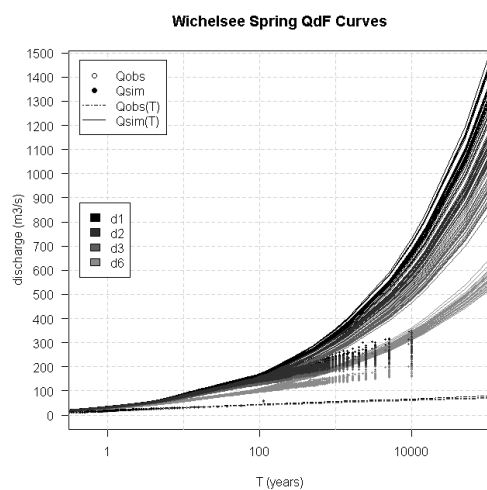
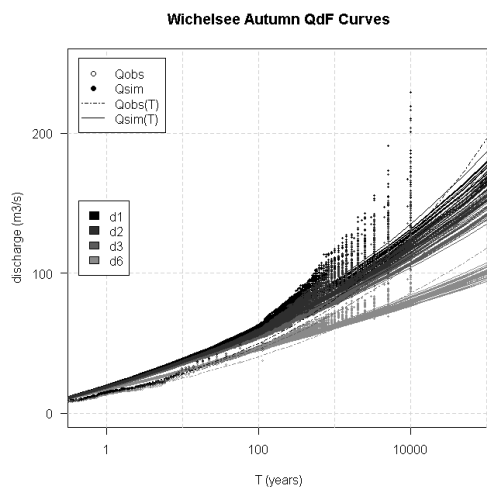
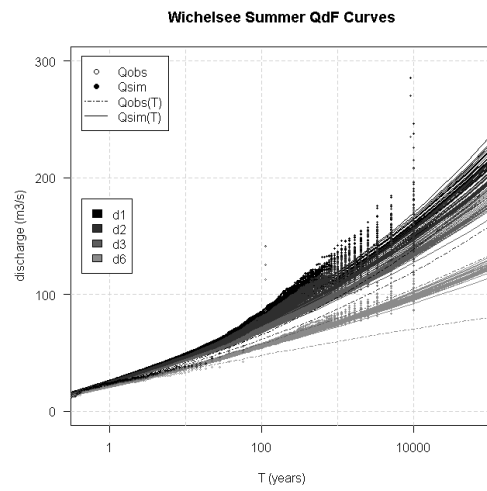
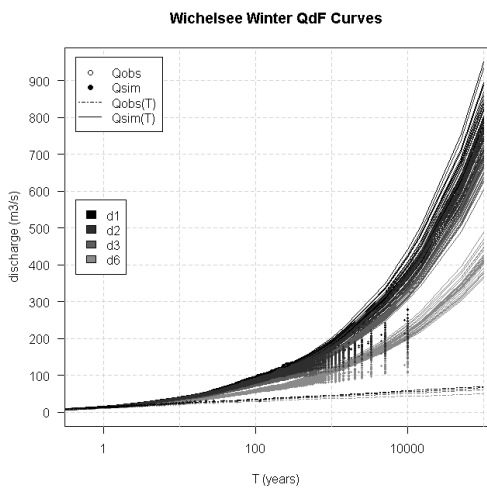


Figure 45: QdF curves for Wichelsee. From top to bottom: winter, summer, autumn, spring.

Figure 46: Precipitation distribution maps for Wichelsee and duration d3. From top to bottom: winter, summer, autumn, spring.

Table 18: Seasonal mean maximum discharge sum, mean, minimum value, maximum value and range for the 10'000 year return period floods and duration d3 in m³/s, seasonal runoff coefficient C for the 10'000 year return periods and duration d3 and seasonal rRMSE values for duration d1 and return periods T=10, T=100, T=1'000 and T=10'000 in %.

Wichelsee	Winter	Spring	Summer	Autumn
Q_{sum} (d3, T = 10'000) (m ³ /s)	5444	7191	4318	3884
Q_{mean} (d3, T = 10'000) (m ³ /s)	188	248	149	134
Q_{min} (d3, T = 10'000) (m ³ /s)	147	203	117	103
Q_{max} (d3, T = 10'000) (m ³ /s)	232	305	235	179
Q_{range} (d3, T = 10'000) (m ³ /s)	85	102	118	76
C (d3, T = 10'000)	0.03	0.05	0.01	0.02
rRMSE (d1, T = 10) (%)	1.8	8	7	1
rRMSE (d1, T = 100) (%)	5.6	5.2	4.5	2.6
rRMSE (d1, T = 1'000) (%)	46	48.1	11.5	14.2
rRMSE (d1, T = 10'000) (%)	135.6	126.4	13.5	24.5

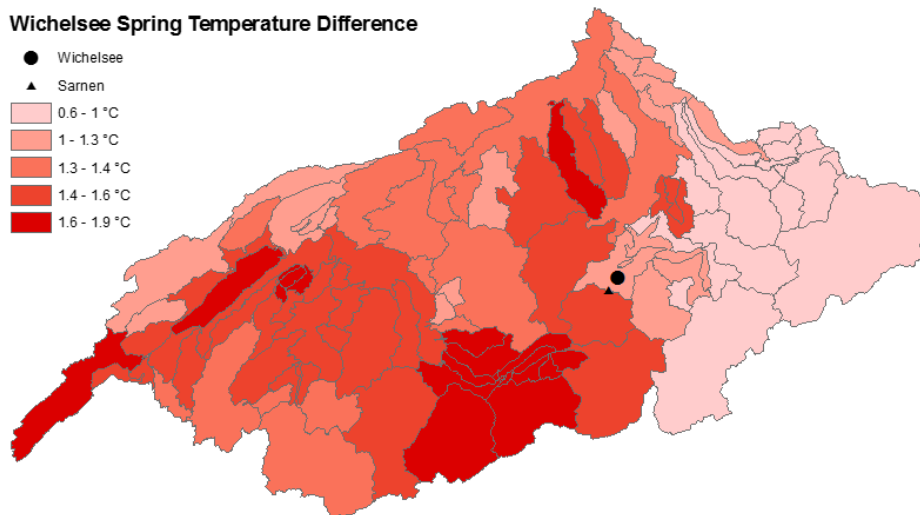


Figure 47: Temperature difference map for Wichelsee in spring and duration d3.

4.3.7 Wichelsee

The QdF curves for Wichelsee in Figure 45 can adequately represent the simulated mean maximum discharge until the 100-year return period. For more extreme return periods, the quantiles tend to underestimate the return level in summer and autumn ($< 50 \text{ m}^3/\text{s}$ at $T = 1'000$) and start to overestimate the return levels in spring and winter by a huge margin ($\sim 200\text{-}300 \text{ m}^3/\text{s}$ at $T = 10'000$). All quantiles belong to the Fréchet distributions. The rRMSE values in Table 18 reflect the quantile over and underestimation and are not adequate for winter (135.6%) and spring (126.4%) at the 10'000-year return period. The summer (13.5%) and autumn (24.5%) rRMSE are very low in comparison. The largest floods with 10'000 years return period occur in spring with respect to the mean ($248 \text{ m}^3/\text{s}$) and maximal value ($305 \text{ m}^3/\text{s}$), followed by winter ($188 \text{ m}^3/\text{s}$, $232 \text{ m}^3/\text{s}$) summer ($149 \text{ m}^3/\text{s}$, $235 \text{ m}^3/\text{s}$) and autumn ($134 \text{ m}^3/\text{s}$, $179 \text{ m}^3/\text{s}$). The quantiles and simulated mean maximum discharges of Wichelsee are compared to the ones of the Sarnen station. The two stations are 4.5 kilometers apart. The simulated and observed values tend to agree very well for all seasons, as well as the quantiles in summer and autumn. The spring and winter quantiles however show large differences in the underlying distribution and the magnitude of the return levels.

The Wichelsee precipitation maps for duration d3 are shown in Figure 46. The precipitation structure shows a relatively similar pattern for all seasons. Maxima are found in the eastern part of Aare region, in the southeastern part, as well as in the northwestern subbasins, located at the border. In all seasons the precipitation amount around Wichelsee is very large. In general all subcatchments receive in comparison to the other stations less precipitation (94-445 mm). Most precipitation is observed in summer (445 mm) and relatively similar amounts in autumn (283 mm), spring (242 mm) and winter (271 mm).

The spring temperature difference map in Figure 47 indicates a moderate increase in temperature in all the subbasins ($0.6\text{-}1.9^\circ\text{C}$). The biggest temperature increases are found southwest of Wichelsee, the smallest increases east of Wichelsee. The spring runoff coefficient C (0.05) in Table 18 is large compared to the coefficients of the other seasons (0.01-0.03)

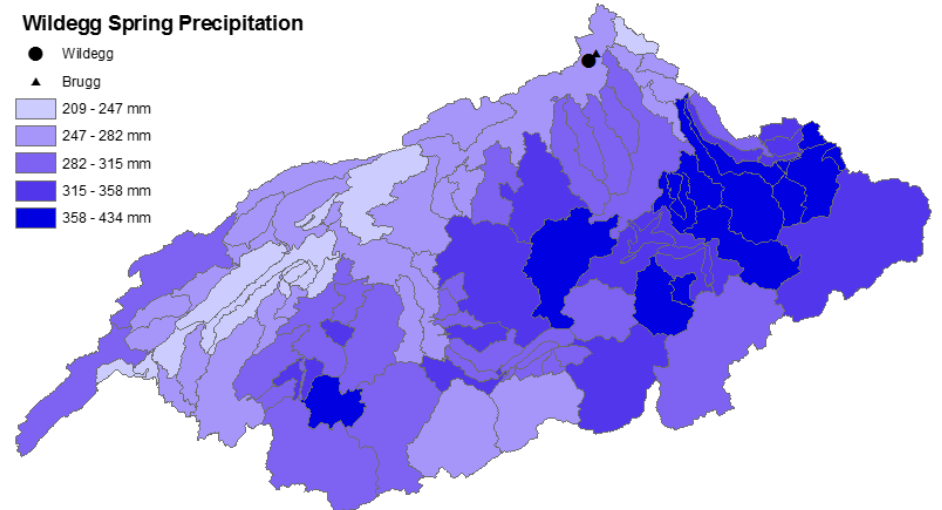
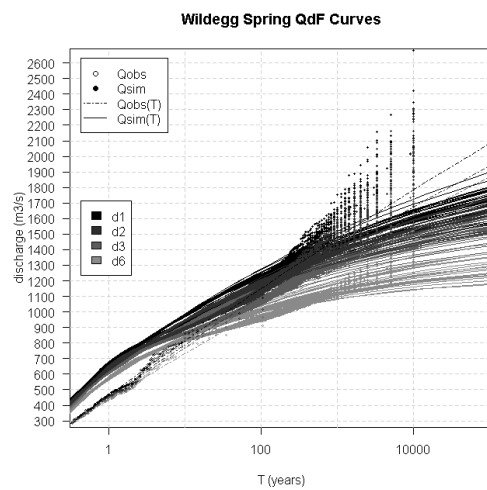
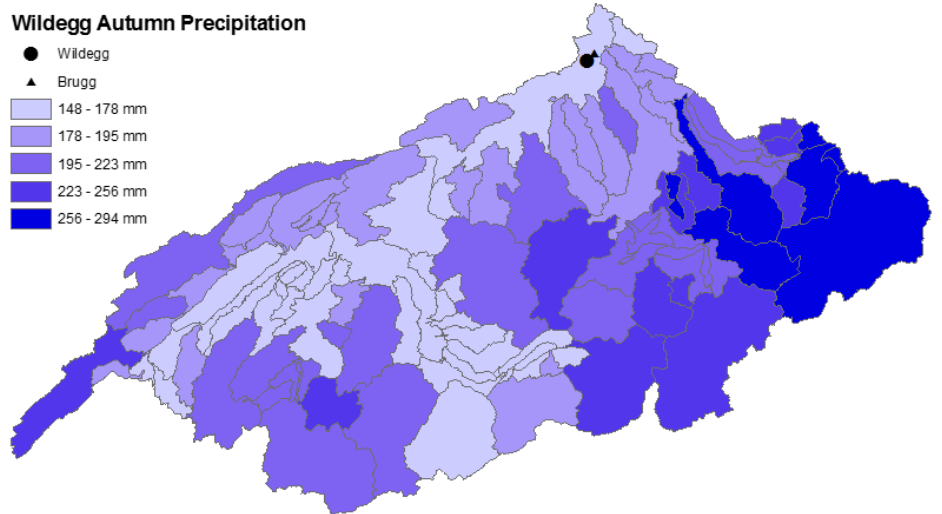
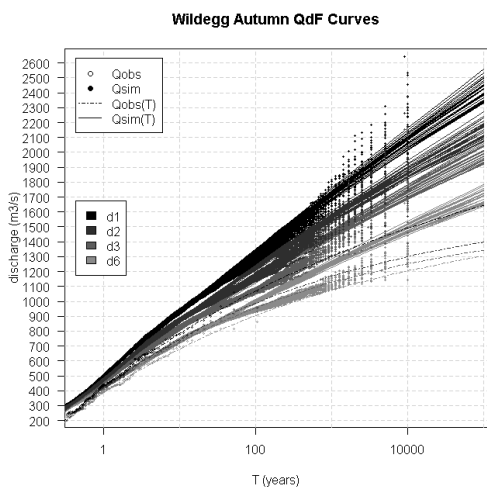
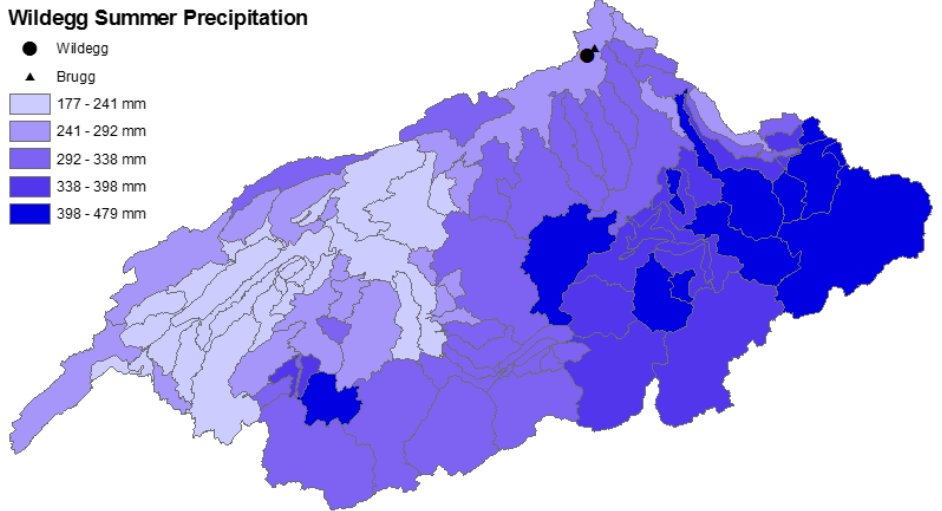
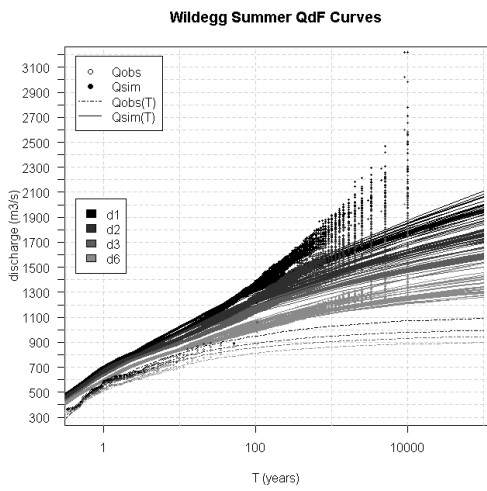
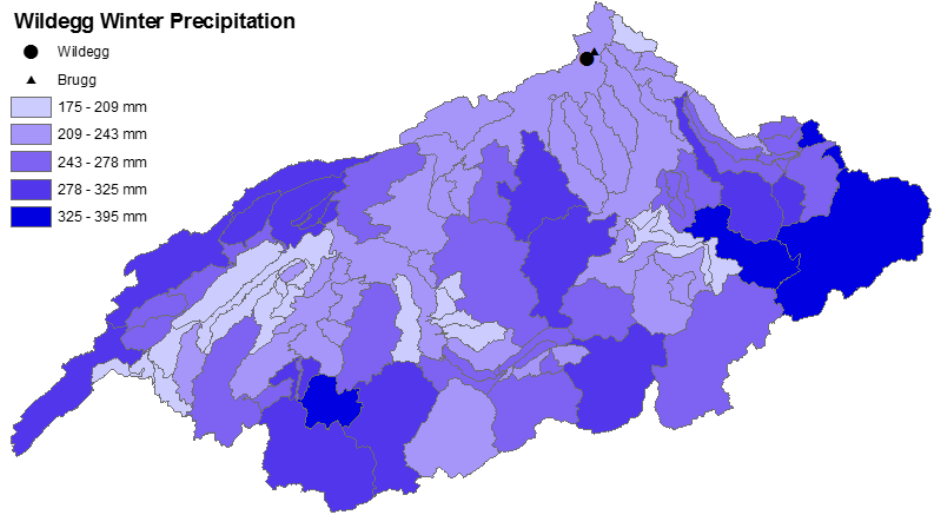
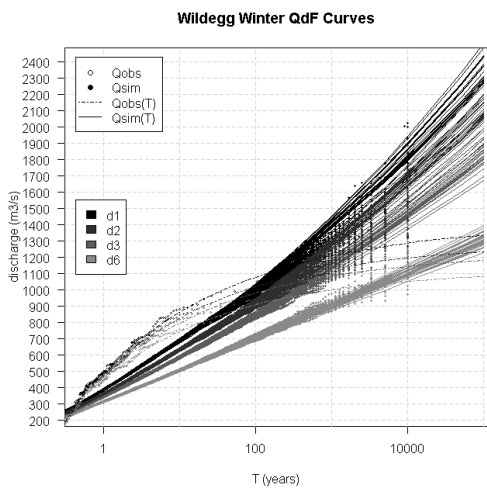


Figure 48: QdF curves for Wildegg. From top to bottom: winter, summer, autumn, spring.

Figure 49: Precipitation distribution maps for Wildegg and duration d3. From top to bottom: winter, summer, autumn, spring.

Table 19: Seasonal mean maximum discharge sum, mean, minimum value, maximum value and range for the 10'000 year return period floods and duration d3 in m³/s, seasonal runoff coefficient C for the 10'000 year return periods and duration d3 and seasonal rRMSE values for duration d1 and return periods T=10, T=100, T=1'000 and T=10'000 in %.

Wildegg	Winter	Spring	Summer	Autumn
Q_{sum} (d3, T = 10'000) (m ³ /s)	40887	50306	56892	50353
Q_{mean} (d3, T = 10'000) (m ³ /s)	1410	1735	1962	1736
Q_{min} (d3, T = 10'000) (m ³ /s)	1172	1466	1517	1389
Q_{max} (d3, T = 10'000) (m ³ /s)	1705	2035	2599	2153
Q_{range} (d3, T = 10'000) (m ³ /s)	533	569	1082	764
C (d3, T = 10'000)	0.14	0.14	0.15	0.22
rRMSE (d1, T = 10) (%)	2	4.6	3.2	1.9
rRMSE (d1, T = 100) (%)	3	4	3.2	6.6
rRMSE (d1, T = 1'000) (%)	8.3	9.1	13.1	8
rRMSE (d1, T = 10'000) (%)	14.7	24.1	24.1	10.6

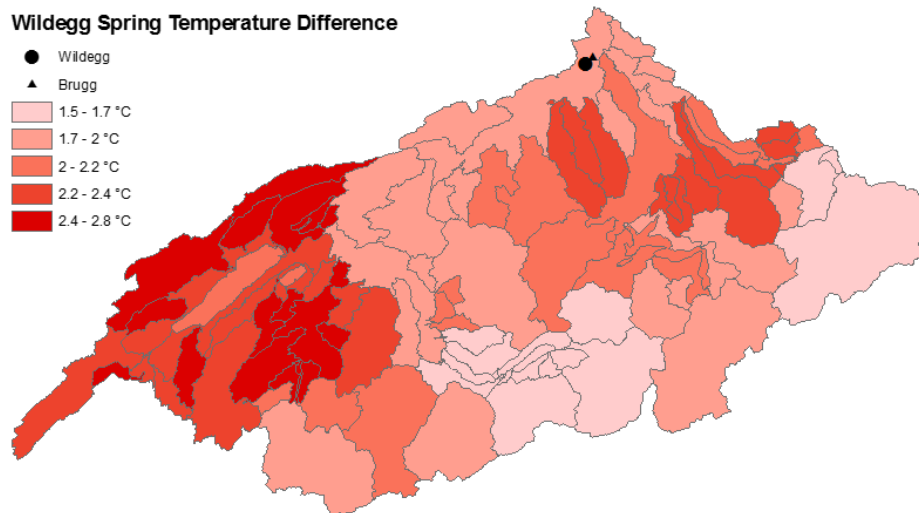


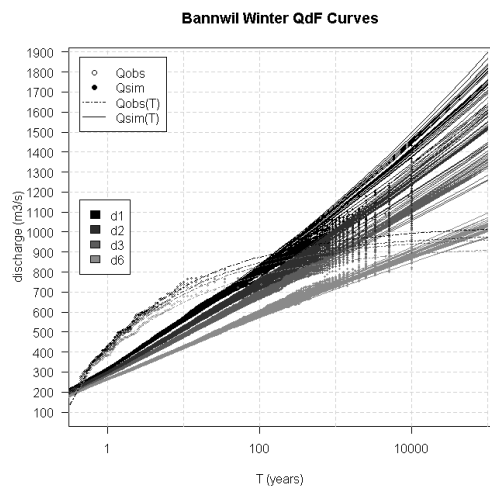
Figure 50: Temperature difference map for Wildegg in spring and duration d6.

4.3.8 Wildegg

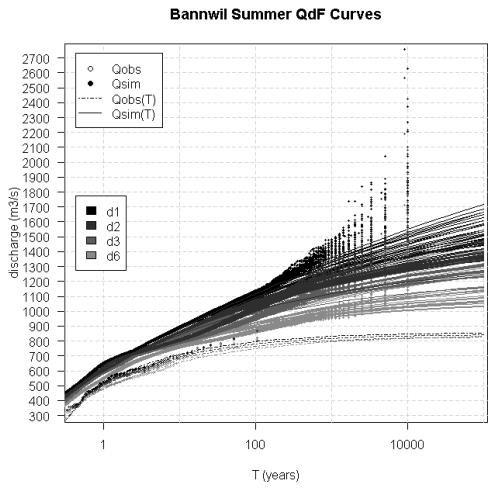
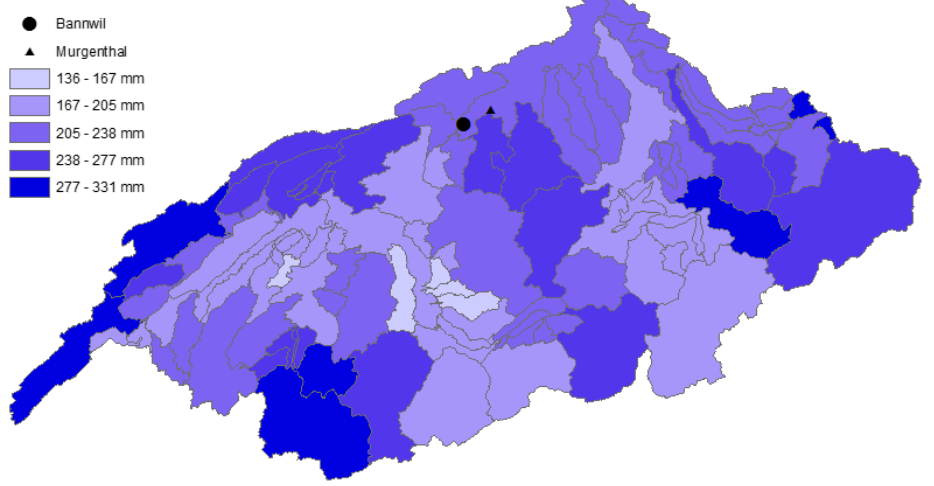
The QdF curves for Wildegg are displayed in Figure 48. The fitted winter quantiles can describe the simulated mean maximum discharge very well for all return periods. In autumn the quantiles tend to overestimate the return levels at return periods of approximately 100 years. In spring and summer there are again sections identified, where the increase in return level slows down. The sections are approximately located between 3 and 30 years for both seasons. Again the quantiles overestimate the return level during these sections and start to underestimate the return level at more extreme return periods. The winter quantiles belong to the Fréchet distributions, the summer, autumn and spring quantiles to the Weibull distributions. The rRMSE in Table 19 indicates good model results for autumn (10.6%) and winter (14.7%) and moderate ones for spring (24.1%) and summer (24.1%) at the 10'000-year return period. Largest floods with 10'000 years return period occur in summer in terms of the mean (1962 m³/s), maximal value (2599 m³/s), and range (1082 m³/s). The smallest floods occur in winter. The mean in spring and autumn have a similar magnitude (1736 m³/s), but in autumn the maximal value (2153 m³/s) is higher than in spring (2035 m³/s). The simulated QdF curves of Wildegg are compared to the ones of the Brugg measuring station. Brugg is approximately 2.5 kilometers away from Wildegg. The observed maximum mean discharge values are lower in summer, autumn and spring than the simulated values (~100-200 m³/s at T = 1). In winter, the opposite is the case and the observed values seem to be much larger for same return periods (~100-200 m³/s at T = 1).

The Wildegg precipitation maps for floods with return period of 10'000 years and duration d3 are shown in Figure 49. In all seasons, precipitation amounts are high in all subcatchments (148-479 mm). The precipitation distribution shows a rather similar pattern for all seasons. Maxima are predominantly found in the eastern and southwestern parts of the Aare region. Only in winter the structure is slightly more diverse, with new maxima in the northwest. Precipitation amount at Wildegg is low in autumn and moderate in summer, winter and spring. In general, most precipitation occurs in summer (479 mm), followed by spring (434 mm) and winter (395 mm) and is smallest in autumn (294 mm).

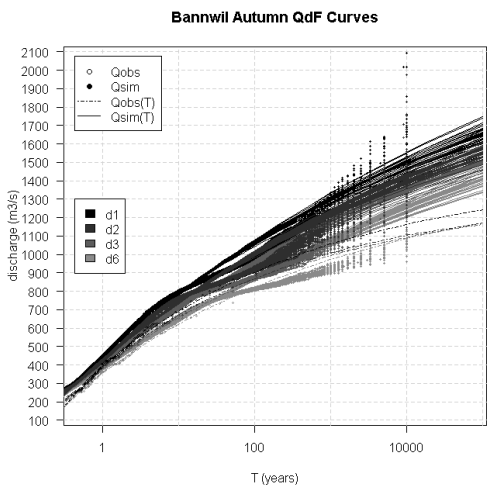
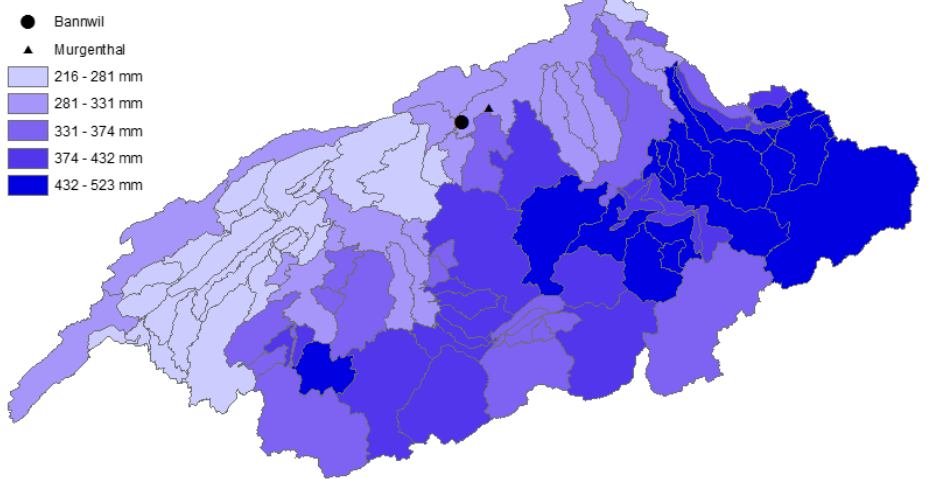
The temperature map in Figure 50 indicates relatively large temperature increases in all the subcatchments (1.5-2.8°C). Highest temperature increases are found in the west, lowest ones in the east and south. The spring runoff coefficient C (0.14) in Table 19 is of similar magnitude as the ones in summer (0.14) and winter (0.15), but smaller than the runoff coefficient in autumn (0.22).



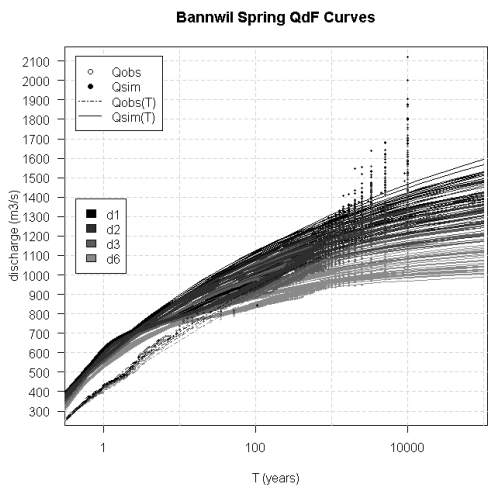
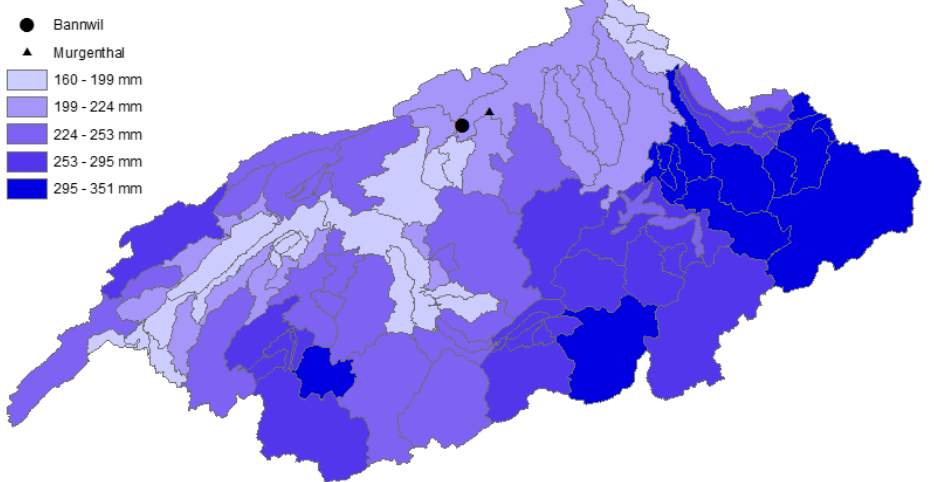
Bannwil Winter Precipitation



Bannwil Summer Precipitation



Bannwil Autumn Precipitation



Bannwil Spring Precipitation

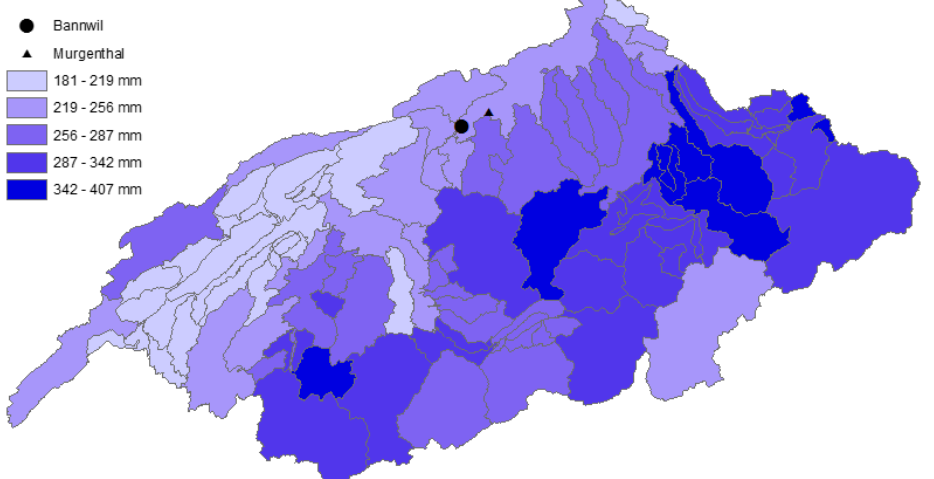


Figure 51: QdF curves for Bannwil. From top to bottom: winter, summer, autumn, spring.

Figure 52: Precipitation distribution maps for Bannwil and duration d6. From top to bottom: winter, summer, autumn, spring.

Table 20: Seasonal mean maximum discharge sum, mean, minimum value, maximum value and range for the 10'000 year return period floods and duration d6 in m³/s, seasonal runoff coefficient C for the 10'000 year return periods and duration d6 and seasonal rRMSE values for duration d1 and return periods T=10, T=100, T=1'000 and T=10'000 in %.

Bannwil	Winter	Spring	Summer	Autumn
Q_{sum} (d6, T = 10'000) (m ³ /s)	26223	32165	36137	31976
Q_{mean} (d6, T = 10'000) (m ³ /s)	904	1109	1246	1102
Q_{min} (d6, T = 10'000) (m ³ /s)	817	1003	1046	959
Q_{max} (d6, T = 10'000) (m ³ /s)	1013	1510	1713	1426
Q_{range} (d6, T = 10'000) (m ³ /s)	196	507	667	467
C (d6, T = 10'000)	0.1	0.08	0.07	0.1
rRMSE (d1, T = 10) (%)	2	8.2	6.5	2.2
rRMSE (d1, T = 100) (%)	2	10.3	1.4	7.8
rRMSE (d1, T = 1'000) (%)	9.7	3.6	10.2	3.1
rRMSE (d1, T = 10'000) (%)	16.8	18.6	25.4	10.8

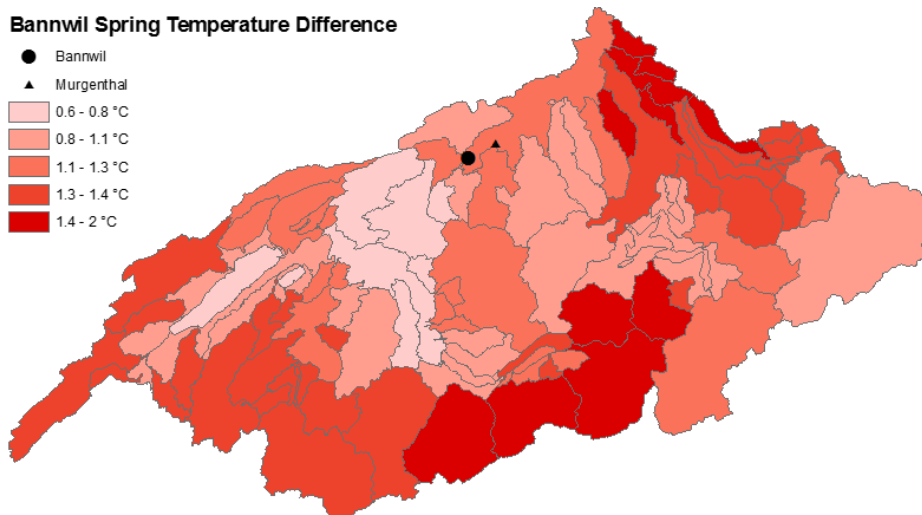


Figure 53: Temperature difference map for Bannwil in spring and duration d6.

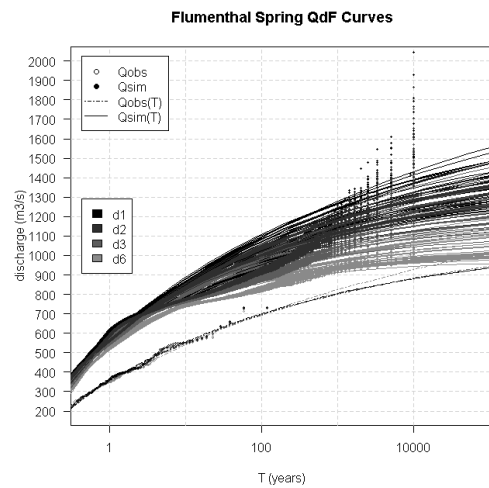
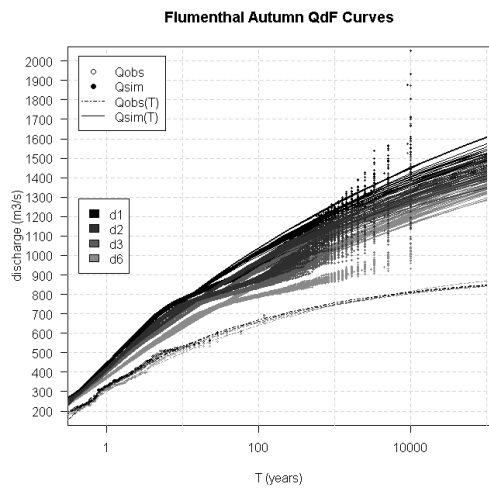
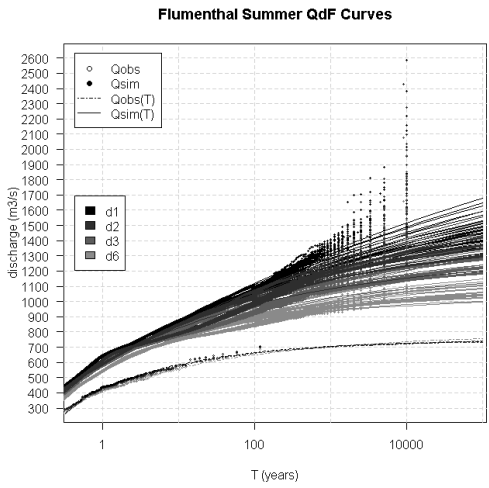
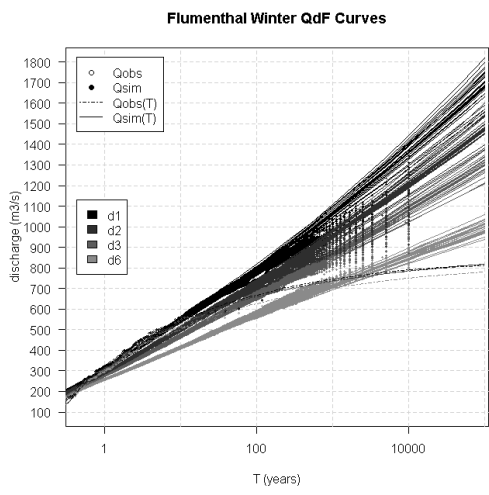
4.4 Group Duration d6

4.4.1 Bannwil

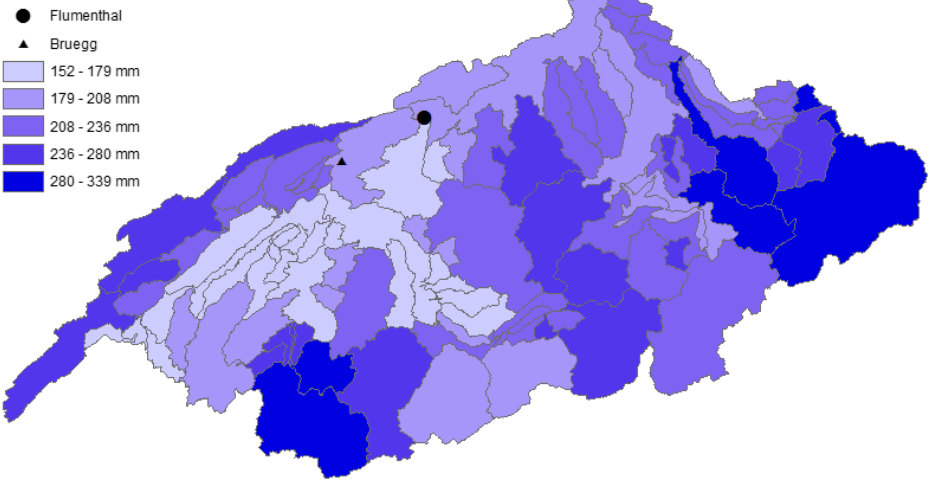
The QdF curves for Bannwil are shown in Figure 51. The winter quantiles can adequately describe the simulated mean maximum discharge for all return periods. In autumn, summer and spring sections with reduced increase in return levels are again identified. The sections are approximately located at return periods between 3 and 100 years. Again overestimation takes place during these sections and consequently an underestimation at more extreme return periods. The summer, autumn and spring quantiles belong to the Weibull distributions, the winter ones to Fréchet or Gumbel distributions. The rRMSE values in Table 20 show good model fits in winter (2-16.6%), spring (8.2-18.6%) and autumn (2.2-10.8%) for all return periods and moderate results in summer at the 10'000-year return period (25.4%). Bannwil is compared to the nearby measuring station Murgenthal. The distance between the two stations is approximately 8.5 kilometers. The observed maximum mean discharge values are generally smaller in summer, autumn and spring, compared to the simulated values (~100-200 m³/s at T = 1) In winter the opposite is the case. The simulated values are lower for equal return periods (~100-200 m³/s at T = 1). The simulated and observed quantiles match relatively well in summer, autumn and spring because similar Weibull distributions are assumed. In winter however Weibull distributions are adopted in contrast to the Fréchet or Gumbel distributions for the simulated quantiles.

The Bannwil precipitation distribution maps in Figure 52 for the return period of 10'000 years and duration d6 show similar precipitation patterns in summer, autumn and spring. The precipitation maxima are located in a band ranging from the east of the Aare basin to the southwest. In winter the precipitation structure is more diverse. Highest precipitation amounts are found in the eastern, western and southwestern subcatchments on the border of the Aare basin. In all seasons, Bannwil is located within low to moderate precipitation amounts. However, large amounts of precipitation can generally be detected in all subbasins in all seasons (136-523 mm). Highest precipitation amounts are identified in summer (523mm), followed by spring (407 mm), autumn (351 mm) and are smallest in winter (331 mm).

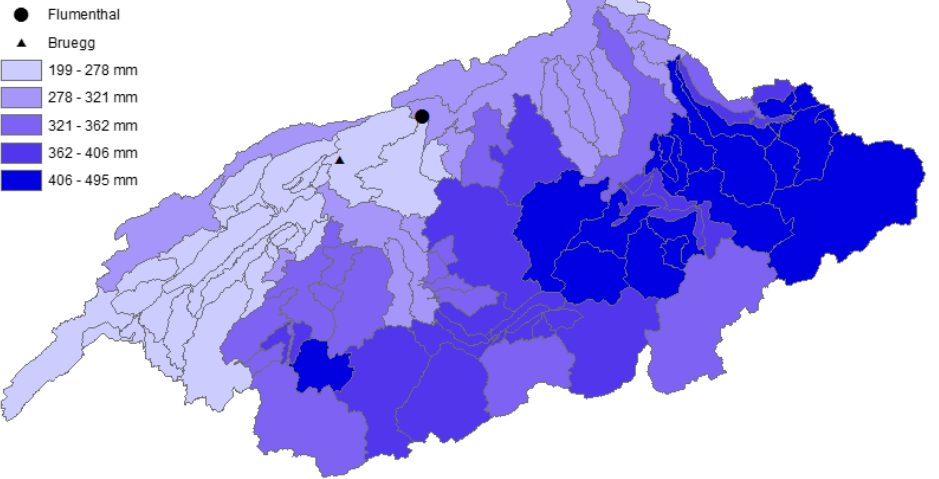
In the temperature map of Bannwil in Figure 53 moderate temperature increases are identified in all subcatchments (0.6-2°C). Largest temperature increases are located in the south and the northeast, lowest increases directly southwest of Bannwil. The spring runoff coefficient C (0.08) in Table 20 is lower than the winter (0.1) and autumn one (0.1).



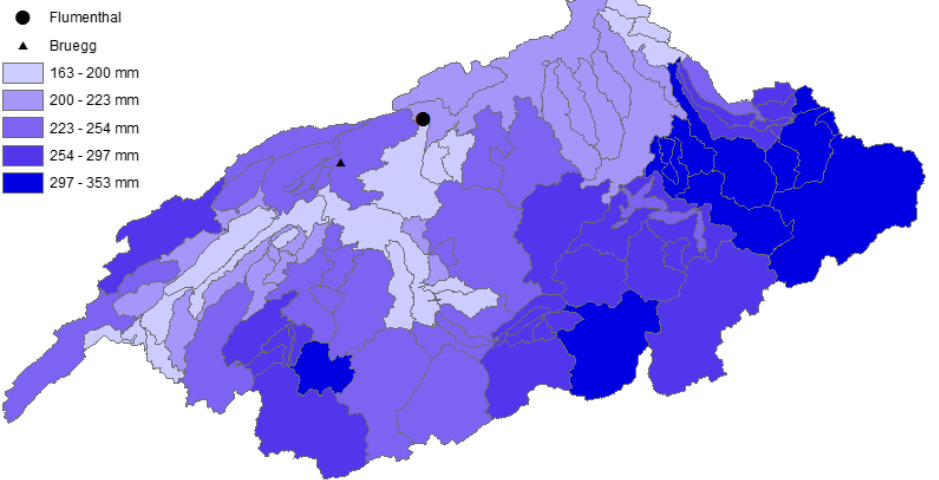
Flumenthal Winter Precipitation



Flumenthal Summer Precipitation



Flumenthal Autumn Precipitation



Flumenthal Spring Precipitation

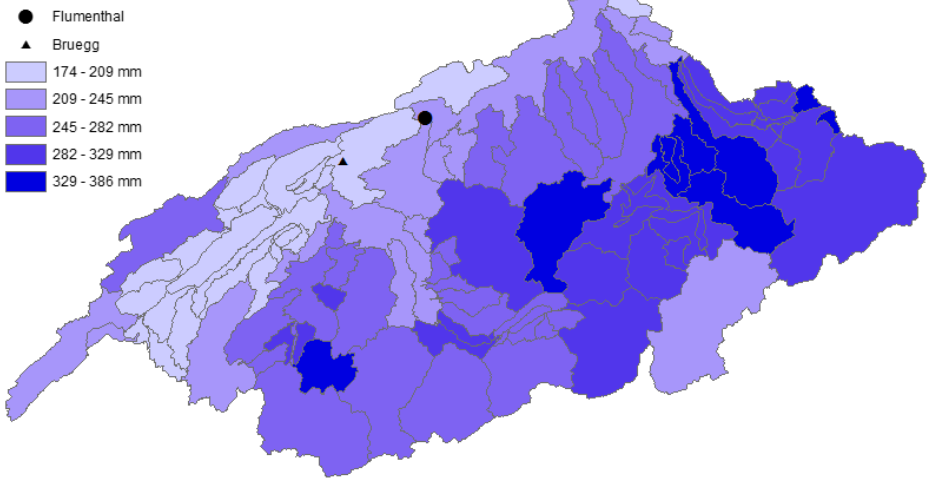


Figure 54: QdF curves for Flumenthal. From top to bottom: winter, summer, autumn, spring.

Figure 55: Precipitation distribution maps for Flumenthal and duration d6. From top to bottom: winter, summer, autumn, spring.

Table 21: Seasonal mean maximum discharge sum, mean, minimum value, maximum value and range for the 10'000 year return period floods and duration d6 in m³/s, seasonal runoff coefficient C for the 10'000 year return periods and duration d6 and seasonal rRMSE values for duration d1 and return periods T=10, T=100, T=1'000 and T=10'000 in %.

Flumenthal	Winter	Spring	Summer	Autumn
Q_{sum} (d6, T = 10'000) (m ³ /s)	25380	31062	34937	30773
Q_{mean} (d6, T = 10'000) (m ³ /s)	875	1071	1205	1061
Q_{min} (d6, T = 10'000) (m ³ /s)	797	968	1015	930
Q_{max} (d6, T = 10'000) (m ³ /s)	993	1491	1657	1379
Q_{range} (d6, T = 10'000) (m ³ /s)	196	523	642	449
C (d6, T = 10'000)	0.1	0.08	0.07	0.1
rRMSE (d1, T = 10) (%)	2.1	8.2	6.9	2.3
rRMSE (d1, T = 100) (%)	2.1	10.7	1.6	8.4
rRMSE (d1, T = 1'000) (%)	9.7	4.6	9	2.4
rRMSE (d1, T = 10'000) (%)	17.2	17.1	24.8	12.2

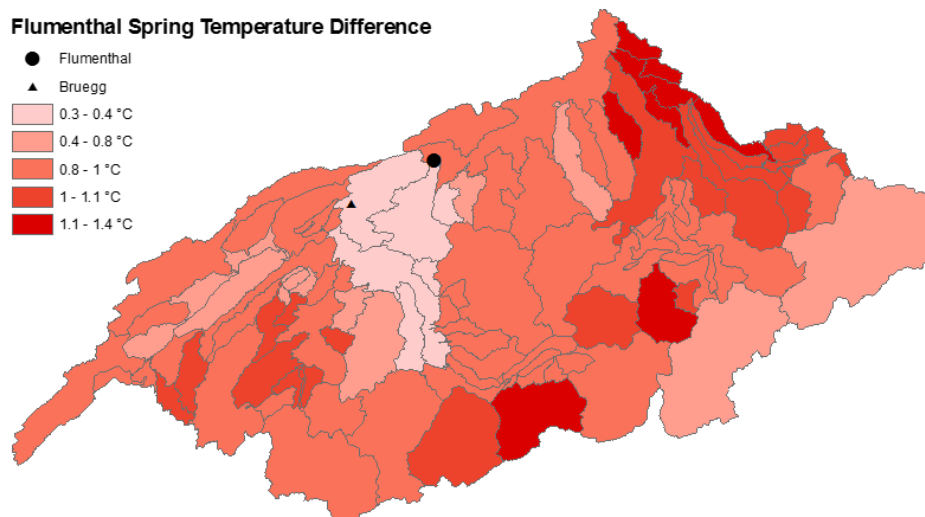


Figure 56: Temperature difference map for Flumenthal in spring and duration d6.

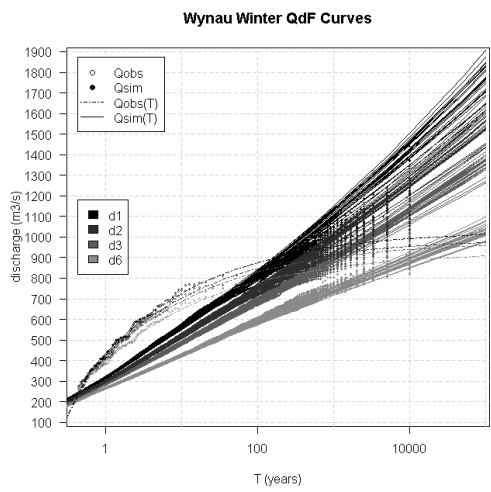
4.4.2 Flumenthal

The QdF curves of Flumenthal in Figure 54 show the same problem as for various stations before. In autumn, summer and spring sections with reduced increase in return level for increasing return periods are identified. The sections are again approximately located between return periods of 3 and 100 years. The consequence is the same. The quantiles tend to underestimate the return level during these sections and consequently underestimate the return level at extreme return periods. In winter the case is different and the quantiles can adequately describe the simulated mean maximum discharge for all return periods. In summer, autumn and spring Weibull distributions are assumed, in winter Fréchet or Gumbel distributions. The rRMSE in table 21 shows best model results in autumn (12.2%), equally good results in winter (17.2%) and spring (17.1%), and moderate results in summer (24.8%) for the 10'000 year return period. Largest floods with return period of 10'000 years are found in summer with respect to the mean (1205 m³/s), followed by spring (1071 m³/s), autumn (1061 m³/s) and winter (875 m³/s).

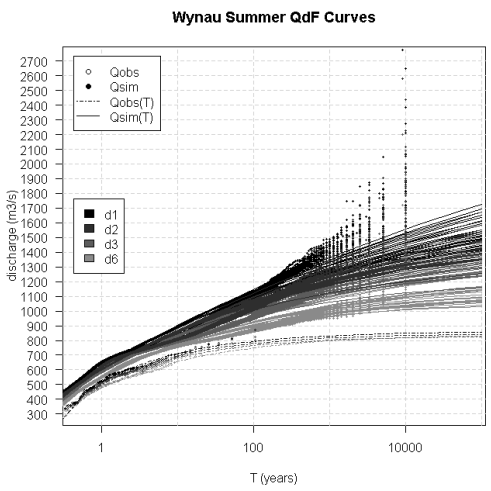
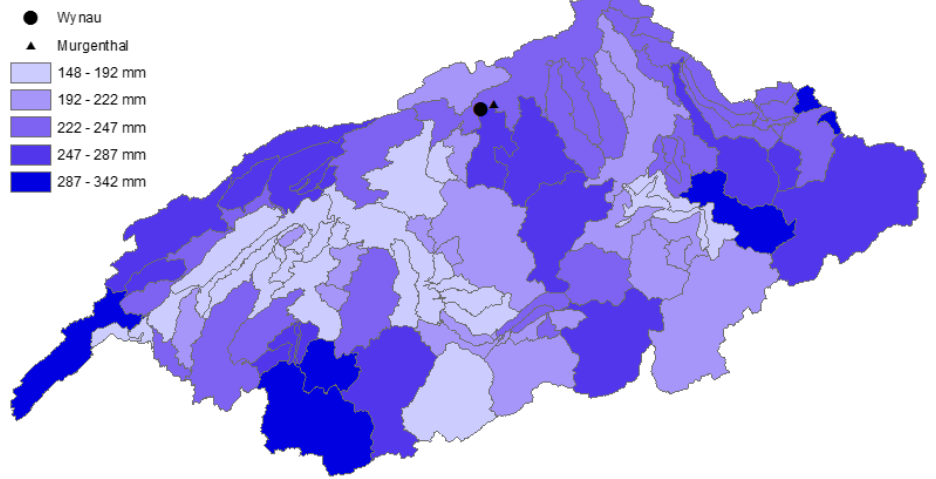
Flumenthal is compared to the measuring station Brügg. The two stations are very far apart with a distance of 26 kilometers. In winter the simulated and observed mean maximum discharge values compare very well, in autumn, summer and spring the observed ones are considerably lower (~100-200 m³/s at T = 1). The simulated and observed quantiles however have a better fit in summer, autumn and spring than in winter, because similar Weibull distributions are assumed, whereas in winter different distributions are adopted.

The Flumenthal precipitation maps for the 10'000-year floods and duration d6 in Figure 55 show similar precipitation distributions in summer, spring and winter. The precipitation maxima are predominantly located in a band ranging from the eastern part of the Aare basin to the southwestern part. This band is still recognizable in winter, but less pronounced. Here, new maxima occur in the western/northwestern subcatchments at the border of the Aare region. In all seasons, Flumenthal is generally located in low or moderate precipitation. However, during/before all floods the precipitation amount is large for all subbasins (152-495mm). The strongest season in terms of precipitation amount is summer (495 mm), followed by spring (388 mm), autumn (353 mm) and winter (339 mm).

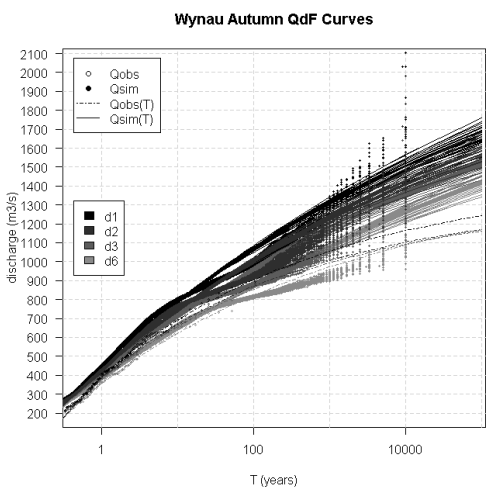
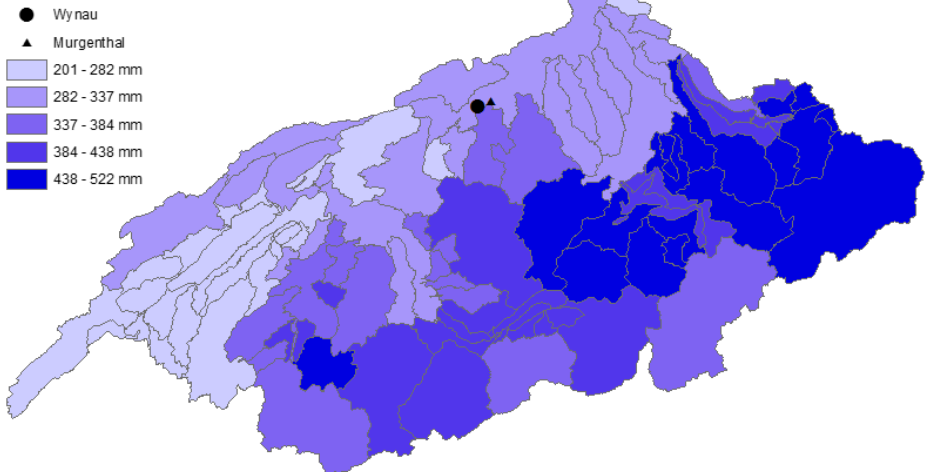
The spring temperature map in Figure 56 shows a small increase in temperature in all subcatchments (0.3-1.4°C). Temperature increase maxima are located in the subcatchments at the northeastern and southern borders of the Aare river basin, minima directly southeast of Flumenthal. The spring runoff coefficient *C* (0.08) has a low magnitude compared to autumn (0.1) and winter (0.1).



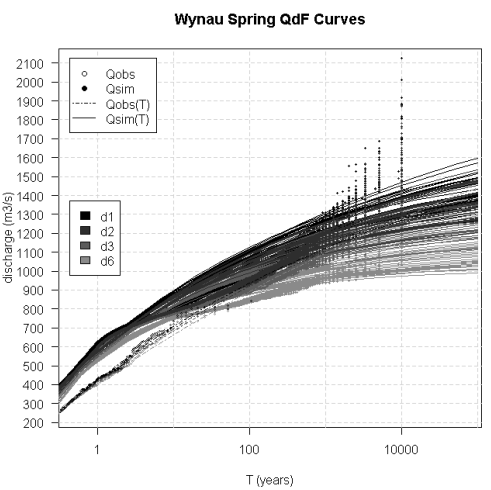
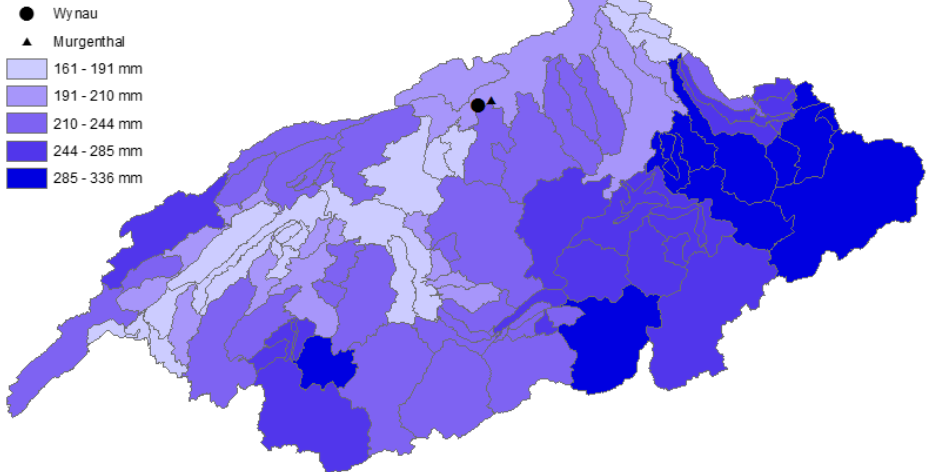
Wynau Winter Precipitation



Wynau Summer Precipitation



Wynau Autumn Precipitation



Wynau Spring Precipitation

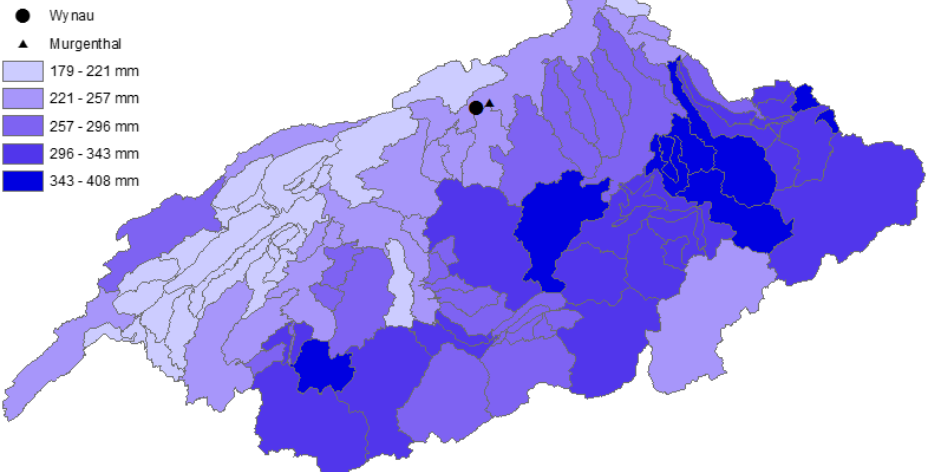


Figure 57: QdF curves for Wynau. From top to bottom: winter, summer, autumn, spring.

Figure 58: Precipitation distribution maps for Wynau and duration d6. From top to bottom: winter, summer, autumn, spring.

Table 22: Seasonal mean maximum discharge sum, mean, minimum value, maximum value and range for the 10'000 year return period floods and duration d6 in m³/s, seasonal runoff coefficient C for the 10'000 year return periods and duration d6 and seasonal rRMSE values for duration d1 and return periods T=10, T=100, T=1'000 and T=10'000 in %.

Wynau	Winter	Spring	Summer	Autumn
Q_{sum} (d6, T = 10'000) (m ³ /s)	26323	32268	36254	32095
Q_{mean} (d6, T = 10'000) (m ³ /s)	908	1113	1250	1107
Q_{min} (d6, T = 10'000) (m ³ /s)	820	1007	1048	962
Q_{max} (d6, T = 10'000) (m ³ /s)	1017	1513	1719	1431
Q_{range} (d6, T = 10'000) (m ³ /s)	197	506	671	469
C (d6, T = 10'000)	0.1	0.08	0.07	0.11
rRMSE (d1, T = 10) (%)	2	8	6.4	2.1
rRMSE (d1, T = 100) (%)	2	10	1.4	7.7
rRMSE (d1, T = 1'000) (%)	10	3.5	10.4	3.3
rRMSE (d1, T = 10'000) (%)	16.9	18.9	25.5	10.6

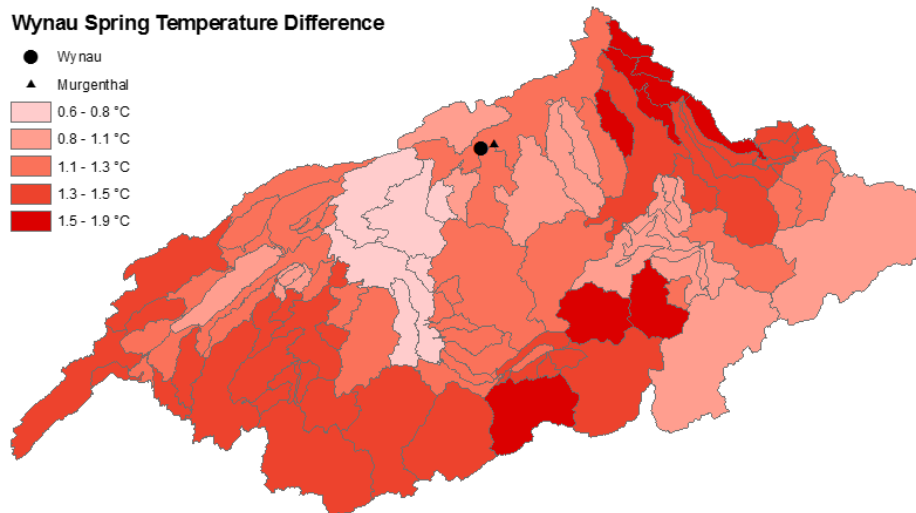


Figure 59: Temperature difference map for Wynau in spring and duration d6.

4.4.3 Wynau

The simulated QdF curves of Wynau in Figure 57 show basically the exact same situation as for Flumenthal and Bannwil. In winter the quantiles can describe the simulated mean maximum discharge adequately, in summer, autumn and winter sections with reduced increase in return level for increasing return periods are identified. The location of the sections are again between 3 and 100 years and influence the fit of the simulated quantiles by overestimating the return level during these sections and by underestimating the return level for more extreme return periods. The summer, spring and autumn quantiles belong to the Weibull distribution, the winter quantiles to the Fréchet/Gumbel distribution. The rRMSE in Table 22 indicates best model results in autumn (10.6%), followed by winter (16.9%) and spring (18.9%) and moderate results in summer (25.5%) for the 10'000-year return period. Largest floods with return period of 10'000 years are found in summer with respect to the mean (1250 m³/s), followed by spring (1113 m³/s), autumn (1107 m³/s) and winter (908 m³/s). Spring is second, because the maximal value (1513 m³/s) is larger than in autumn (1431 m³/s).

Wynau is compared to the measuring station Murgenthal. The distance between the two stations is approximately 3 kilometers. In spring, autumn and summer, the observed mean maximum discharge values are lower than the simulated ones (~100-200 m³/s at T = 1). In winter, the opposite is the case. Here the observed values are of higher magnitude for same return periods than the simulated ones (~100-200 m³/s at T = 1). The spring, summer and autumn quantiles match well, because similar Weibull distributions are adopted, the winter quantiles match poor, because different distributions are assumed.

The Wynau precipitation maps for floods with return period of 10'000 years and duration d6 in Figure 58 show very similar precipitation patterns in summer, autumn and spring. Precipitation maxima are predominantly found in a band ranging from the east of the Aare basin to the southwest. The winter precipitation distribution is more diverse. Maxima are located in the eastern, southwestern and western subcatchments at the border of the Aare basin. In winter relatively large amounts of precipitation can be observed at Wynau, in summer, autumn and spring moderate amounts. In General, large amounts of precipitation can be noted in all subcatchments (148-522 mm). Precipitation amounts have the highest magnitude in summer (522 mm), followed by spring (408 mm), autumn (335 mm) and winter (342 mm).

The temperature map in Figure 59 shows a small to moderate increase in temperature in all subcatchments (0.6-1.9°C). Temperature increase maxima are found in the southern and northeastern parts of the Aare basin, southeast of Wynau. The spring runoff coefficient *C* (0.08) in Table 22 is lower than the coefficient in winter (0.1) and autumn (0.11).

5. Discussion

In this chapter the results are discussed, compared and pattern are highlighted in terms of the duration in subchapter 5.1, seasonality in subchapter 5.2 and the grouping process in subchapter 5.3. Next the adequacy and uncertainties of the QdF models are discussed and the comparisons between observed and simulated values discussed. In the last part the precipitation distribution and influence of snowmelt are stated.

5.1 Duration

For all stations and seasons a similar pattern can be detected when analyzing the mean maximum discharge and QdF quantiles for different durations. At low return periods ($T < 100$), the return levels for all durations are basically the same. With increasing return periods however, the mean maximum discharge values, as well as the quantiles with different flood durations start to spread out. The quantiles have an increased return level for smaller flood durations. At extreme return periods, the difference in maximum mean discharge is consequently quite big. For increasing durations, the discharge time series get more and more smoothed out and thus outliers and extreme discharge values are less pronounced for higher durations. The consequence is, that the quantiles for larger flood durations are less steep. However, the total volume of floods with larger flood durations is greater than for small durations because the mean maximum discharge can be multiplied by the duration to calculate the total flood volume. Since outliers and extreme values are getting smoothed out for higher durations, the uncertainty of the QdF models decreases and accuracy and confidence of the model increases. This is reflected in the spread of the quantiles of the 29 scenarios. For longer durations the quantiles are closer together, than the quantiles of shorter durations.

The different durations usually have the same underlying probability distributions. However, for some stations the distributions may be different. One example can be seen in the QdF curves for Niederried in summer. There, for some (all) scenarios Fréchet distributions are assumed for duration d1, but for duration d6 Weibull distributions are applied. However, the shape parameters of these probability distributions are only weakly positive or negative, so there is little change in the results of the QdF curves for the return level, at least for return periods less than 10,000 years.

5.2 Seasonality

Not surprisingly, the discharge behavior of Switzerland is strongly influenced by seasonality. Considering all stations investigated, the flood magnitudes are strongest in summer. This can be clearly determined from the QdF curves and by the averaged and maximal value of mean maximum discharge of the stations. The only two exceptions are the stations Le Châlet and Wichelsee. At each of these stations, summer discharges are roughly similar in magnitude to those of the remaining seasons, although spring produces the most noticeable floods. The two stations are, in comparison to the remaining stations, remotely located and their relevant catchment area is very small. These stations with small catchments are more influenced by local characteristics of precipitation and snowmelt.

The next highest floods are recorded in spring and autumn. Here it can be discussed in which of these seasons the discharges tend to be the highest, because the mean is quite similar for most of the stations. However, if one had to decide on a season, based solely on the simulated mean maximum discharges, it would be spring, since for floods with 10'000 years return period the highest recorded

values are slightly larger than those in autumn, seen over all stations. For the stations Le Châlet and Wichelsee the mean maximum discharges in spring are even larger than those in summer.

However, looking at the observed mean maximum discharges of the neighboring gauging stations, it can be seen that the mean maximum discharge in spring is often larger in the simulations than in the observations, for stations with small and large catchments. In autumn, the same can be seen for stations with large catchments, but less pronounced than in spring. Therefore, it is quite possible that the mean maximum spring runoff is slightly overestimated in the simulations. Taking this into account, floods in autumn could be larger than in spring.

Seasonal patterns can also be detected in the QdF curves with respect to the underlying probability distribution. In summer, stations with smaller catchment areas (d1 and d2 group) mainly Fréchet distributions are assumed, stations with larger catchment areas (d3 and d6 group) Weibull distributions are applied. In autumn, a similar pattern as in summer can be observed with respect to the probability distributions. However, there are some exceptions, such as Mühleberg (d3), where Fréchet distributions are assumed, or Le Châlet, where a combination of Weibull and Gumbel distributions are considered. In spring the predominant probability distribution are the Weibull distributions. Again a few outliers are present.

The probability distributions are important because it allows cautious extrapolation to even more extreme return periods. Since the Weibull distribution has a finite upper end point, no values can be larger than this end point. In spring many stations are Weibull distributed. Therefore, no return levels can be above that certain value even for very extreme return periods. In contrast, in autumn many stations are Fréchet distributed. The Fréchet distribution has no upper end point, so in theory the return levels become infinitely large with increasing return periods. Thus, it can be cautiously concluded that the potential for even more extreme floods is greater in autumn than in spring.

Across all stations, flood magnitudes are weakest in winter, the only exception being the Wichelsee station, where the winter mean maximum discharges can exceed those of summer and autumn.

The conclusion is that for the entire Aare catchment, floods are strongest in summer, followed by autumn and spring, and weakest in winter. However, variations in the seasonal mean maximum discharge can occur at individual small stations/areas.

5.3 Grouping

The grouping process of the stations was completed using the Delta parameter Δ of the converging QdF curves. The grouping process refers to which stations respond strongest to certain flood durations. In the group of duration d1, floods with short durations (flash floods) are therefore of particular importance, in comparison to the d6 group, where rather long lasting and smooth floods are significant. However, the grouping process also succeeded by classifying stations with similar flood volumes/peaks. In the groups with duration d1, the mean maximum discharges are generally smaller than the discharges of the d6 group. There are some exceptions, for example Beznau and Klingnau, which are in the d3 group, even though the largest discharge volumes can be observed at these stations. Other exceptions are the stations Le Châlet, which is in the d2 group and Wichelsee, in the d3 groups. Both have comparatively low maximum mean discharge values and therefore should rather be classified in a smaller group.

Grouping by characteristic duration has another advantage. Stations in the same group have similar QdF curves and probability distributions. The relevant GEV distributions as well as the parameters

within a group have very similar magnitude and sign. Again there are some exceptions like the stations Wichelsee or Le Châlet.

In addition to that, the grouping process had the consequence that spatially close stations tend to be in the same group. For example in the d1 group, the stations Rossens, Schiffenen and Maigrauge are all located at the Saane River and in close proximity.

The conclusion that can be drawn from the grouping process is that the stations in the Aare catchment can be successfully divided into homogeneous groups with similar discharge and flood characteristics. From this it can be concluded that for stations or areas in the Aare basin where no discharge measurements are available, flood characteristics and QdF curves can be estimated from neighboring stations or areas with discharge measurements. Thus, it is possible to generate coherent QdF curves for the entire Aare basin using regionalization methods.

5.4 Adequacy

According to the rRMSE The QdF models perform very well for the 10, 100 and 1'000 year return periods for almost all stations. Only at the 10'000 year return periods the rRMSE can become substantial. The only exception is the station Le Châlet in winter. Here the rRMSE is already 117.3% at the 100-year return period and exceeds 1000% at the 10'000-year return level. In contrast to that, the spring, summer, and autumn rRMSE for Le Châlet are very small at 5.3%, 13%, and 19.1%, respectively.

The rRMSE shows large differences with respect to seasonality. Tentatively, the QdF models can fit the simulated maximum mean discharge well in summer, spring, and autumn. Exceptions are the stations Wichelsee in spring, as well as Niederried in autumn, where the rRMSE for the 10'000 year return period exceeds 100%.

The adequacy of the QdF models is worst in winter. The stations Maigrauge, Rossens, Schiffenen, Aarberg, Le Châlet, Niederried and Wichelsee, all have a high error percentage for the 10'000 year return period. For two stations, Wichelsee and Rossens, the error exceeds 100% for the 10'000 year return period and for Le Châlet the error is even bigger than 1'000%. For these rRMSE values, the QdF models are obviously not acceptable anymore. The mentioned stations above all have a small relevant catchment area. Thus it can be concluded, that the QdF performance is worse at stations with small catchment area, at least in the winter season.

In general, some conclusions can be drawn with the help of the rRMSE values. As already mentioned, the biggest accuracy issues of the QdF models occur in winter, plus the poorest scores are found at stations with small catchments (and thus in groups with smaller durations d). At stations with larger catchments, the rRMSE values tend to be smaller and the models thus fit better. In these catchments, however, a different problem arises. In spring, summer and autumn, the rRMSE values for the 100-year return periods can be larger than those for the return period of 1'000 years. Normally this should not be the case, because the error should be reduced for smaller return periods.

This phenomenon is apparent at the stations Gösgen, Rapperswil, Ruppoldingen, Bannwil, Flumenthal and Wynau and also reduced at Mühleberg. The cause of this problem can be visualized using the QdF curves for single durations in Addendum 1. Normally, the mean maximum discharge values increase relatively steadily or uniformly with increasing return periods. At these stations, however, there exists a section, where the increase in return level is reduced considerably. These sections are located approximately between the 3 and 30 years return period in summer, between 3 and 100 years in spring and between 3 and 30 years in autumn for the duration d1. For higher

durations these sections shift towards larger return periods. Since the fitted quantiles of the GEV models cannot describe these sections accurately, the return level during these sections is overestimated and thus the rRMSE gets relatively large at return periods of approximately 100 years. After these sections the mean maximum discharge values increase again with the same rate as before the sections and the fitted quantiles converge with the data at an approximate return period of 1'000 years. Consequently, the rRMSE is relatively accurate at return periods of 1'000 years and most of the time considerably smaller than for the 100-year return period. Another consequence results from these sections. For the 10'000-year return period, the return levels get underestimated by a substantial amount. This is due to the fact, that the probability distributions and thus the GEV parameters are influenced by these sections. Consequently the GEV distribution is of Weibull nature, even though for large return periods, a Fréchet or Gumbel distribution would be more appropriate. If one wants to get reliable QdF curves for extreme return periods, diminishing these sections prior to the model application might be advantageous if even possible.

5.5 Confidence

The confidence of the QdF models is illustrated by the simultaneous plotting of the 29 quantiles. Based on the QdF curves of all stations and all seasons, it can be stated that the confidence of the GEV models is very high for low return periods, since the quantiles of all scenarios are close to each other. This indicates that the uncertainty is low because similar or the same average maximum discharge values are associated for these return periods over the entire scenario range.

At return periods above 100 years, the quantiles of the individual scenarios begin to spread out. The uncertainty increases and the return periods can no longer be determined unambiguously with reference to all quantiles.

Differences can be detected in the quantiles with varying durations. In general, the spread of the quantiles is smaller with longer duration, which is why the uncertainties decrease with longer flood durations.

Looking at the spread of the quantiles for different stations and seasons at extreme return periods, one notices that the spread of the quantiles always has a relatively similar magnitude. However, one relationship can be observed. For Fréchet distributions the spread seems to be slightly larger than for Weibull or Gumbel distributions.

The winter quantiles of Schiffenen and Maigrauge are the only ones showing a different situation, because their spread is much more extreme than the quantiles of the remaining stations. The reason is that in winter, disproportionately large values can occur in some scenarios in contrast to the norm of the mean maximum discharge. Why these larger runoff values occur and why they only exist in winter is unclear. Since both stations have smaller catchments, marginal changes in precipitation or temperature can have large influences on the mean maximum discharge. The reason should therefore be found in the generation of the runoff, precipitation and temperature time series. Example reasons could be parameter changes in the HBV model or in the stochastic weather generator or by a process that has irreversibly removed a damping effect of the hydrographs in RS Minerve. It is fascinating however, that these scenarios tend to agree better with the observed quantiles and observed maximum mean discharges from the nearby gauging station than the remaining scenarios.

It is difficult to assess whether this type of uncertainty representation is more appropriate than that of confidence intervals. This methodology covers a much smaller range of possible return levels than confidence intervals. The spread of quantiles is relatively small and thus the totality of QdF curves may be overconfident, which means that the quantiles have too similar return levels for equal return

periods. The reason is that the quantiles of the QdF curves were all created using the same methodology and therefore adopt similar parameters and magnitudes. For example, if one quantile underestimates the return level of an extreme return period, there is a good chance that the 28 other quantiles will also underestimate the return level at that return period. The result is that this methodology does not represent the totality of possible return levels at extreme return periods and thus the total uncertainty of the QdF curves are possibly not represented.

Confidence intervals to represent uncertainty are therefore probably more appropriate, especially if the results are intended for non-expert users. The reason is that with confidence intervals the uncertainty is quantified whereas in this methodology the uncertainty cannot be clearly defined and thus for each station different sized uncertainty ranges can arise. Therefore, it would be most suitable to combine both methodologies.

5.6 Observations

Comparing the totality of observed and simulated mean maximum discharge, one notices that certain patterns are present. In winter, the observed mean maximum discharge values are in contrast to the simulated stations all considerably larger. The only exception is the Flumenthal station where the values are about the same. Thus, the simulations tend to underestimate the runoff in the winter months. In contrast, for almost all stations in spring, the observed values are smaller than in the simulated case. In spring, the simulations therefore tend to overestimate the maximum mean discharge. Noteworthy is the station Le Châlet, where the largest observed maximum mean discharge values are almost equal to the smallest simulated ones, especially because the Le Châlet and the measuring station are at the same location and thus the values should match well.

In autumn and summer the best agreements of simulated and observed data are recognizable. But also for these seasons some problems can be identified. These are mainly found at stations with large catchment areas (in the d3 and d6 groups). The observed values are smaller than the simulated values, so there is a tendency that the simulations tend to overestimate the maximum mean discharge. For the stations with small catchments, the discharge maxima of the observed and simulated stations agree well.

Over all stations, the simulated and observed quantiles show the worst agreement in winter, because in most of the cases different probability distributions are assumed. The quantiles for the remaining seasons agree relatively well. Exceptions are the stations Rossens, Maigrange and Schiffenen, where in spring the quantiles do not agree particularly well.

The reasons why the observed and simulated runoff maxima do not completely match are the uncertainties and errors that can arise and propagate in the complete model chain of the simulation. Such errors can occur in any part of the model chain, for example already at the beginning when the precipitation and temperature time series are generated by the stochastic weather generator or due to an inaccurate parameter choice in HBV. Of course, GEV also has some uncertainties, for example in the GEV parameter estimation or the fitting of the GEV distributions to the data.

Some issues can also occur in the observed datasets. For example measurement errors, changes in measurement methodology or measurement location can affect the data sets. Also the QdF curves strongly depend on the chosen plotting position and thus the length of the data set. Since the observed data sets are relatively short, inconsistencies and uncertainties can occur even for small return periods. Furthermore, one is never sure whether the mean maximum discharge values could already converge to the generalized extreme value distribution, especially concerning the length of

the observed datasets. Uncertainties also arise because the measurement stations and simulation stations are most of the times not at the same locations and oftentimes considerably far away. Overall, however, the observed and simulated data sets show relatively good agreement for many stations, so the simulations can be considered a success.

5.7 Precipitation distribution

The hypothesis that precipitation is concentrated around the respective station for flood events with return periods of 10'000 years is not evident from the precipitation distribution maps. The maps show patterns that for all stations, all durations, and all seasons the precipitation distributions look relatively similar. In summer, spring and autumn most of the precipitation is concentrated in a band that extends from the eastern to the southwestern part of the Aare basin. There always occurs a precipitation gradient from southeast to northwest, with higher precipitation values in the southeast. Only in winter the maps show a somewhat less pronounced structure in the precipitation distribution. But also in winter, the precipitation distributions between the stations show a very similar pattern. Maxima are mainly found in western, eastern and southern border catchments. In general, for flood events at all stations, precipitation values are very large in all catchments. Even for the station Le Châlet, which is located in the west and has a small catchment area, the precipitation distribution does not show a large change compared to other stations. This is despite the fact that the floods at Le Châlet can only be influenced by the precipitation falling in this small area. This leads to the conclusion that most flood events with 10'000 year return period happen simultaneously at all stations and for all durations. Thus, the precipitation is enormous over the whole area. Since the precipitation is focused in the south and east, it can be expected that during flood events with 10'000 year return period a large-scale front from the south (southwest) in northeast direction hits the Alps and discharges huge amounts of precipitation. Since all 29 flood events of a station are summarized in this work, individual floods may show different precipitation distributions, but in general it can be said that precipitation is mostly concentrated in the west and south of the Aare Basin during extreme flood events.

5.8 Snowmelt

In the temperature difference maps, an increase in temperature can be detected in almost all stations before the flood events. However, the spring runoff coefficient for the individual stations is most of the time lower than the coefficient of the remaining seasons. One example is the station Wichelsee, where an increase in temperature is identified and the spring coefficient has a large magnitude compared to the other seasons. At Wichelsee, therefore, snowmelt may have played a larger role for flood events with 10'000 years return period. But based on all the other stations, no correlation between the input of snowmelt and the flood events can be identified. Nevertheless, since an increase in temperature can be detected, a possible, but probably rather small influence of snowmelt can be assumed. Since all flood events of a station are summarized in this thesis, a larger influence of snowmelt on individual events cannot be excluded. In a larger context, however, it can be assumed that precipitation is mostly the driving factor. It can also be stated, that it is difficult to identify the correlation between extreme floods and snowmelt only on the basis of temperature, precipitation and runoff time series.

6. Conclusion

The devastating flood event in Switzerland in August 2005 raised questions about the likelihood of such floods and how to improve protection against them. Appropriate protection can only be ensured with precise planning of infrastructure and adequate preventive measures. This can only be accomplished if accurate flood characteristics in terms of return period and discharge magnitude are known. Extreme value theory can help to identify these characteristics. Extreme value theory is based on long and accurate time series. In reality however time series are oftentimes too short and inaccurate. In this thesis this problem was circumvented by using simulated time series with a combined length of 300'000 years for 18 stations in the Aare river basin.

The simulated time series were divided into the 4 seasons and the flood-duration-frequency method was applied. The resulting QdF curves were then used to infer the flood behavior in terms of seasonality, the differences between the individual stations, and the differences between the 4 flood durations. In addition, the converging QdF approach was used to determine the specific flood duration for each station.

It was found that floods show pronounced seasonal differences. Across all stations, the largest floods can be observed in summer, the smallest ones in winter. The magnitude of floods in spring and autumn are very similar, but considering the underlying probability distribution and the QdF curves of the observed stations, it can be concluded that in autumn the flood magnitude has a larger potential than in spring.

The different flood durations show similar characteristics in the QdF curves, since for the most part the same probability functions are assumed. Differences can only be seen in the magnitude of the mean maximum discharge values at same and larger return periods. There, the mean maximum discharge is larger for smaller flood durations, but the actual flood volume is smaller.

Flood characteristics between stations sometimes show large differences. However, the stations can be divided into homogeneous groups that are similar in terms of catchment size, mean maximum discharge for equal return periods, proximity and characteristic flood duration. Stations with larger catchments are more susceptible to smooth floods, whereas stations with small catchments are more prone to flash floods.

In a next step, the QdF curves were then validated using the rRMSE for each station, season, and different return periods. The conclusion is that the quantiles of the QdF curves can accurately describe the simulated mean maximum discharges up to a return period of 1'000 years. At return periods of 10'000 years sometimes larger errors can occur, but in general the goodness-of-fit of the GEV models is acceptable for these return periods as well.

The uncertainties of the simulated QdF curves were visualized by the simultaneous plotting of all quantiles of the 29 scenarios and the comparison with the QdF curves of the observed mean maximum discharges of the neighboring gauging stations. The conclusion is that for some stations and seasons the uncertainties can be partially large, but in general the simulations agree with the observations and therefore the simulations can be considered a success.

In the last step, extreme floods with a return period of 10,000 years were investigated with respect to the precipitation distribution and the influence of snowmelt. For this purpose, the QdF curves were used to identify such seasonal flood events and the corresponding precipitation amounts and the spring temperature differences before and during the floods were extracted. The flood events

were summarized to obtain the characteristics of all floods of a station at the same time. In addition, the runoff coefficient was calculated to improve the estimation of the influence of snowmelt.

It can be concluded that the precipitation distribution of the floods with 10'000 year return periods each show similar patterns between stations, seasons and different durations. The precipitation is predominantly found in a band extending from the east of the Aare basin to the southwest. Floods with a return period of 10,000 years therefore mostly occur at the same time for all stations, with high precipitation over the entire Aare basin and with similar precipitation patterns.

Although there is generally an increase in spring temperature prior to 10'000-year return period flood events, the influence of snowmelt is considered low because the spring runoff coefficient is always of similar magnitude than the coefficient of the remaining seasons.

The results of this thesis can now be used to improve and extend the risk assessment of the 18 stations and possibly lead to the modification of existing infrastructures to improve the protection against extreme floods. Further work could be done by regionalization methods to generate QdF curves for the whole Aare basin. Another way to improve the flood risk estimation for the 18 stations would be to include the non-stationarity of the climate change. This could be done in the simulation generation or in the parameter estimation with an extension in the the maximum likelihood method.

In conclusion, it can be boldly stated that this thesis has succeeded in producing QdF curves that are reliable and coherent.

7. References

- Andres, N., Badoux, A., Hegg, Ch. (Ed.) (2019), EXAR – Grundlagen Extremhochwasser Aare-Rhein, Hauptbericht Phase B, Eidg. Forschungsanstalt für Wald, Schnee und Landschaft WSL.
- Ashkar, F. (1980), Partial Duration Series Models for Flood Analysis, Ecole polytechnique de Montréal, Ph.D. Thesis, Montréal, QC.
- BAFU (2010), Topographische Einzugsgebiete Schweizer Gewässer: Teileinzugsgebiete 2 km², http://data.geo.admin.ch/ch.bafu.wasser-teileinzugsgebiete_2/
- BAFU (2014), Generalisierte Hintergrundkarte zur Darstellung hydrologischer Daten, <https://data.geo.admin.ch/ch.bafu.hydrologie-hintergrundkarte/>
- BAFU (n.d.), Gefahrengrundlagen für Extremhochwasser an Aare und Rhein (EXAR), accessed 15. January 2021, retrieved from <https://www.bafu.admin.ch/bafu/de/home/themen/naturgefahren/dossiers/grossprojekte-hochwasserschutz/gefahrengrundlagen-fuer-extremhochwasser-an-aare-und-rhein--exar.html>
- Balocki, J.B. and Burges, S.J. (1994), Relationships between n-Day Flood Volumes for Infrequent Large Floods, *Journal of Water Resources Planning and Management*, 120(6): 794-818.
- Bell, F.C. (1976), The Areal Reduction Factors in Rainfall Frequency Estimation, NERC Report 35, Institute of Hydrology, Wallingford, UK.
- Bergström, S. (1992) The HBV model: Its structure and applications, Swedish Meteorological and Hydrological Institute.
- Bezzola, G. R. and Hegg, C. (Ed.) (2007), Ereignisanalyse Hochwasser 2005, Teil 1 – Prozesse, Schäden und erste Einordnung. Bundesamt für Umwelt BAFU, Eidgenössische Forschungsanstalt WSL. Umwelt-Wissen Nr. 0707.
- Coles, S. (2001), *An Introduction to Statistical Modeling of Extreme Values*, London: Springer.
- ESRI (2011), *ArcGIS Desktop: Release 10*, Redlands, CA: Environmental Systems Research Institute.
- Evin, G., Favre, A.C. and Hingray, B. (2018), Stochastic generation of multi-site daily precipitation for the assessment of extreme floods in Switzerland, *Hydrology and Earth System Sciences*, 22, 655–672.
- Evin, G., Favre, A.C. and Hingray, B. (2019) Stochastic generators of multi-site daily temperature: comparison of performances in various applications, *Theor. App. Climatol.*, 135, 811–824, <https://doi.org/10.1007/s00704-018-2404-x>.
- Fisher, R. A., and Tippett, L.J.C. (1928) Limiting forms of the frequency distribution of the largest or smallest member of a sample, *Proceedings of the Cambridge Philosophical Society* 24, 180–190.
- Fukutome, S., Schindler, A., Capobianco, A. (2018), *MeteoSwiss extreme value analyses: User manual and documentation*, Technical Report MeteoSwiss, 255, 3rd Edition, 80 pp.
- Galéa, G. and Prudhomme, C. (1997), Notions de base et concepts utiles pour la compréhension de la modélisation synthétique des régimes de crue des bassins versants au sens des modèles QdF, *Revue des Sciences de l'Eau*, 10(1): 83-101.
- Galéa, G., Javelle, P. and Chaput, N. (2000), Un modèle débit-durée-fréquence pour caractériser le régime d'étiage d'un bassin versant, *Revue des Sciences de l'Eau*, 13(4): 421-440.

- García Hernández, J., Paredes Arquiola, J., Foehn, A. and Roquier, B. (2016). "RS MINERVE – Technical manual v2.3", RS MINERVE Group, Switzerland, 130p.
- Gilleland, E., Katz, R. and Young, G. (2009), extRemes: Extreme value toolkit. R package version 1.60. URL: <http://CRAN.R-project.org/package=extRemes>
- Gumbel, E. J. (1958), *Statistics of extremes*, Columbia University Press, New York.
- Hilker, N., Badoux, A. and Hegg, C. (2008), 'Unwetterschäden in der Schweiz im Jahre 2007'.
- Hosking, J.R.M, Wallis, J.R. (1997), *Regional flood frequency analysis: an approach based on L-moments*. Cambridge University Press, New York 224p
- Katz, R. W., Brush, G. S. and Parlange, M. B. (2005), 'Statistics of extremes: modeling ecological disturbances', *Ecology* 86(5), 1124–1134.
- Javelle, P., Grésillon, J.M. and Galéa, G. (1999), Discharge-Duration-Frequency Curves Modelling for Floods and Scale Invariance, *Comptes Rendus de l'Académie des Sciences, Sciences de la terre et des planets*, 329: 39-44.
- Javelle, P., Galéa, G. and Grésillon, J.M. (2000), L'approche debit-durée-fréquence historique et avancées, *Revue des Sciences de l'Eau*, 13(3): 303-321.
- Javelle, P. (2001), *Caractérisation du régime des cures: le modèle debit-durée-fréquence convergent. Approche locale et régionale*, PhD thesis, Cemagref-Lyon, Institut National Polytechnique de Grenoble, 268p.
- Javelle, P., Ouarda, T.B.M.J., Lang, M., Bobée, B., Galéa, G., Grésillon, J.M. (2002a), Development of regional flood-durationfrequency curves based on the index flood method. *Journal of Hydrology* 258 (1–4), 249–259.
- Javelle, P., Sauquet, E. and Grésillon, J. (2002b), Describing actual and future flood hydrological regimes., *Celt. Hydrol. Symp.*, d. 270-280.
- Javelle, P., Ouarda, T.B.M.J. and Bobée, B. (2003), Flood Regime Definition using the Flood-DurationFrequency Approach: Application to the Provinces of Quebec and Ontario, Canada, *Hydrological Processes*, 17(18): 3717-3736.
- Jenks, G. F. and Caspall, F.C. (1971), Error on choropleth maps: Definition, measurement, and reduction, *Annals of the Association of American Geographers*, 61 (2), 217–244.
- Makkonen L. (2006), Plotting positions in extreme value analysis, *J. Appl. Meteorol. Climatol.* 45: 334–340.
- Meunier, M. (2001), Regional Flow-DurationFrequency Model for Tropical Island of Martinique, *Journal of Hydrology*, 247, 31-53.
- Moreno, F. and Roldan, J. (1999), Regionalization of daily precipitation stochastic model parameters, Application to the Guadalquivir valley in Southern Spain, *Phys. Chem. Earth*, 24, 65-71.
- Musy, A., Hingray, B. and Picouet, C. (2005), *Hydrology: A Science for Engineers*, CRC Press.
- Musy, A. and Higy, C. (2011), *Hydrology A Science of Nature*, CRC Press, Science Publishers.
- NERC. (1975) Estimation of Flood Volumes over Different Durations, *Flood Studies Report, Vol. 1, Chapter 5*, 243-264.

- Ouarda, T.B.M.J., Haché, M., Bruneau, M., Bobée, P. (2000), Regional flood peak and volume estimation in a northern Canadian Basin, *Journal of Cold Regions Engineering*, American Society of Civil Engineering, (ASCE) 14 (4), 176-191.
- Pilgrim, D.H. (Ed.) (1987), *Australian Rainfall and Runoff: A Guide to Flood Estimation*, The Institution of Engineers Australia, Canberra, Australia.
- Papastathopoulos, I. and Tawn, A.J. (2013), Extended generalised Pareto models for tail estimation, *J. Stat. Plann. Inference*, 143, 131–143.
- R Development Core Team (2009), *R: A Language and Environment for Statistical Computing*, R Foundation for Statistical Computing, Vienna, Austria. ISBN 3-900051-07-0. URL: <http://www.R-project.org>
- Seibert, J. (1997) Estimation of parameter uncertainty in the HBV model, *Nordic Hydrology* 28, 247–262.
- Sherwood, J.M. (1994), Estimation of Volume-Duration-Frequency Relations of Ungauged Small Urban Streams in Ohio, *Water Resources Bulletin*, 30(2): 261-269.
- Sivapalan, M. and Blöschl, G. (1998), Transformation of Point Rainfall to Areal Rainfall: Intensity-Duration-Frequency Curves, *Journal of Hydrology*, 204: 150- 167.
- Smith, J.B. and Hulme, M. (1998), Climate change scenarios. In : *Handbook on Methods of Climate Change Impacts Assessment and Adaptation Strategies* [Feenstra, J., I. Burton, J.B. Smith, and R.S.J. Tol (eds.)], UNEP/IES, Version 2.0, October, Amsterdam, Chapter 3, 56-95.
- Wilks, D.S. and Wilby, R.L. (1999), The weather generation game: a review of stochastic weather models, *Progress in Physical Geography*, 23 (1999), 329-357.
- Zaidman, M.D., Keller, V., Young, A.R. and Cadman, D. (2003), Flow-Duration-Frequency Behaviour of British Rivers based on Annual Minima Data, *Journal of Hydrology*, 277: 195-213.

8. Appendices

8.1 Appendix A

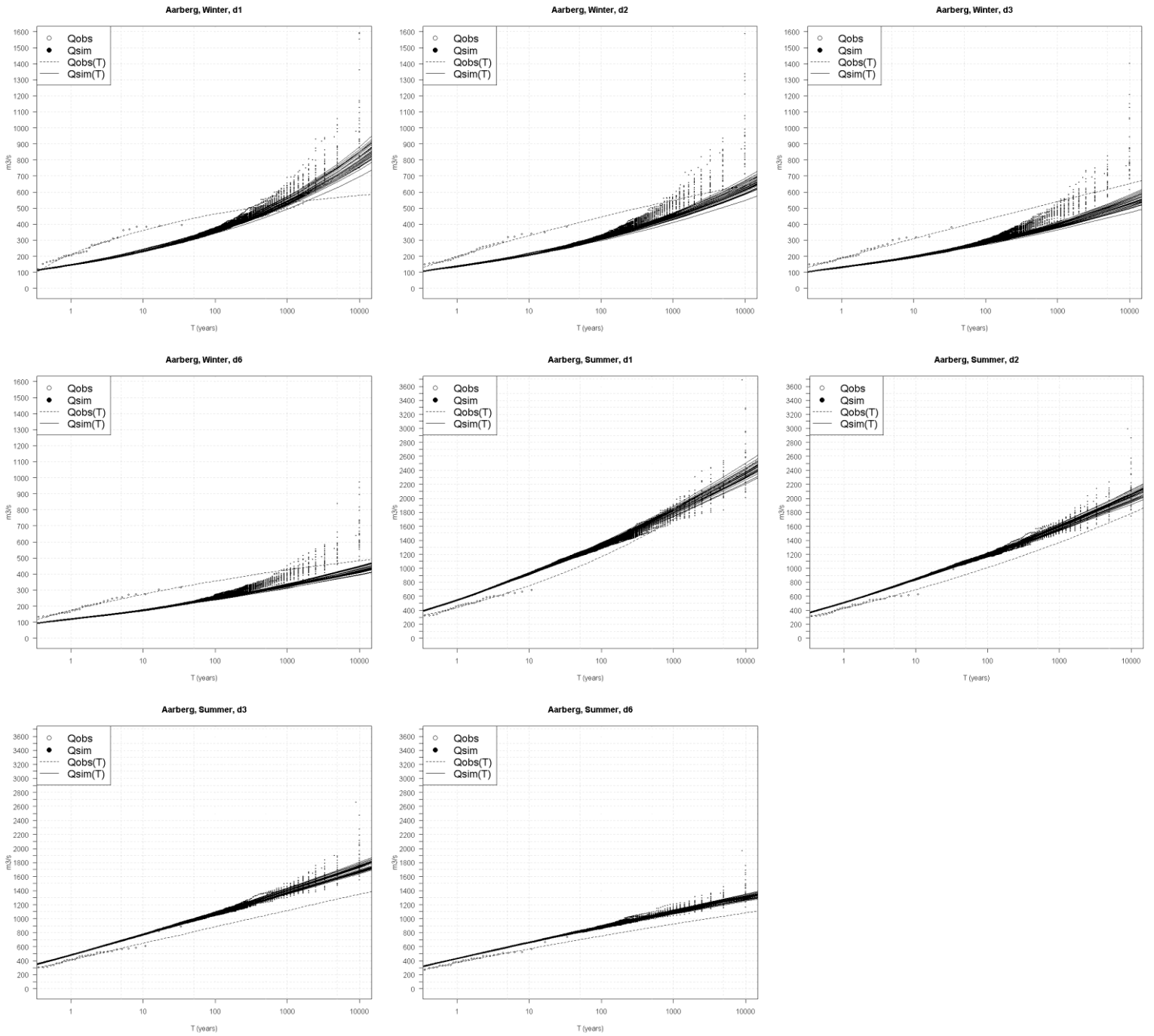


Figure 60: Winter and summer QdF curves for Aarberg and individual flood durations. From top left to bottom right: d1 winter, d2 winter, d3 winter, d6 winter, d1 summer, d2, summer, d3 summer, d6 summer.

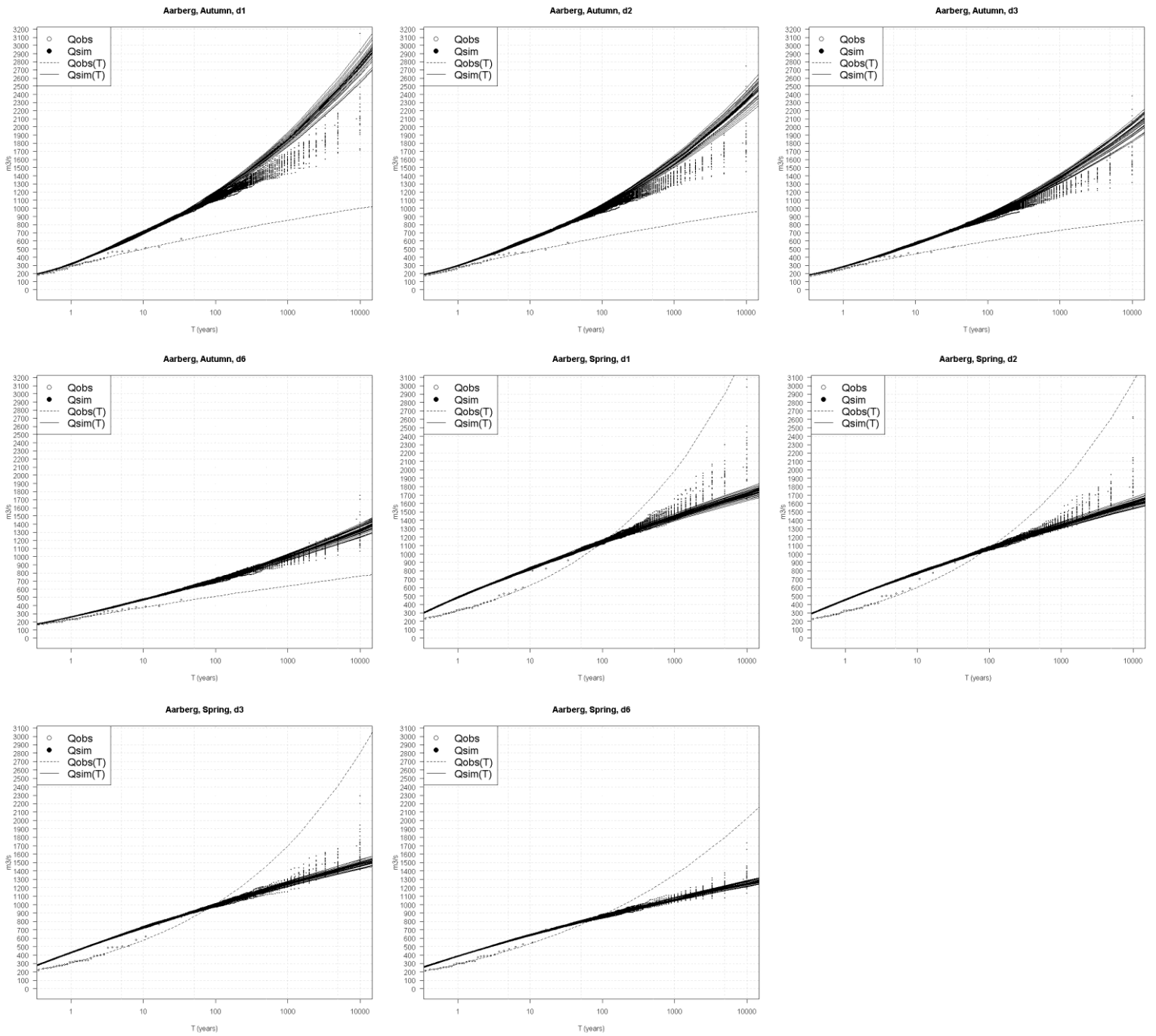


Figure 61: Autumn and spring QdF curves for Aarberg and individual flood durations. From top left to bottom right: d1 autumn, d2 autumn, d3 autumn, d6 autumn, d1 spring, d2, spring, d3 spring, d6 spring.

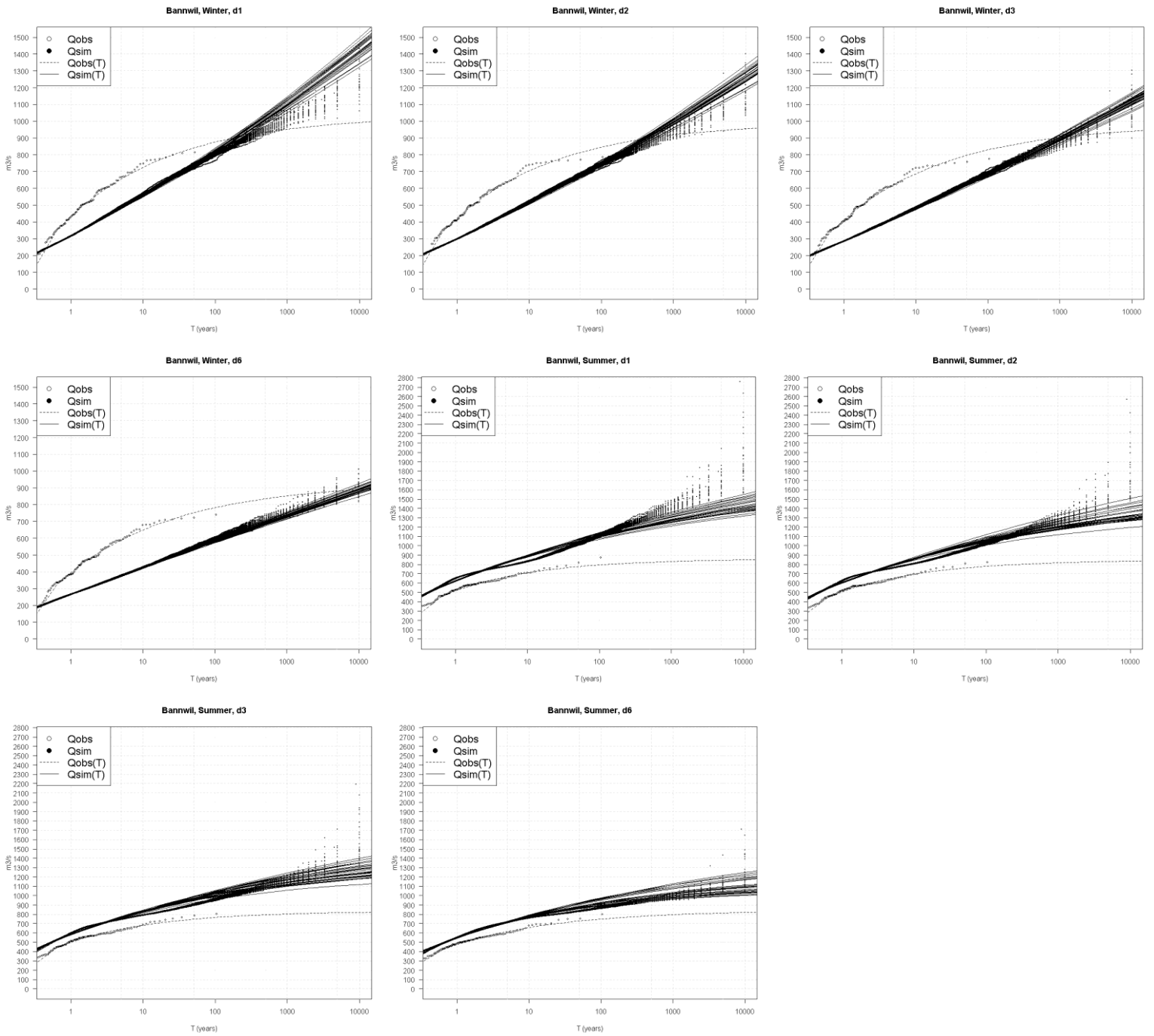


Figure 62: Winter and summer QdF curves for Bannwil and individual flood durations. From top left to bottom right: d1 winter, d2 winter, d3 winter, d6 winter, d1 summer, d2, summer, d3 summer, d6 summer.

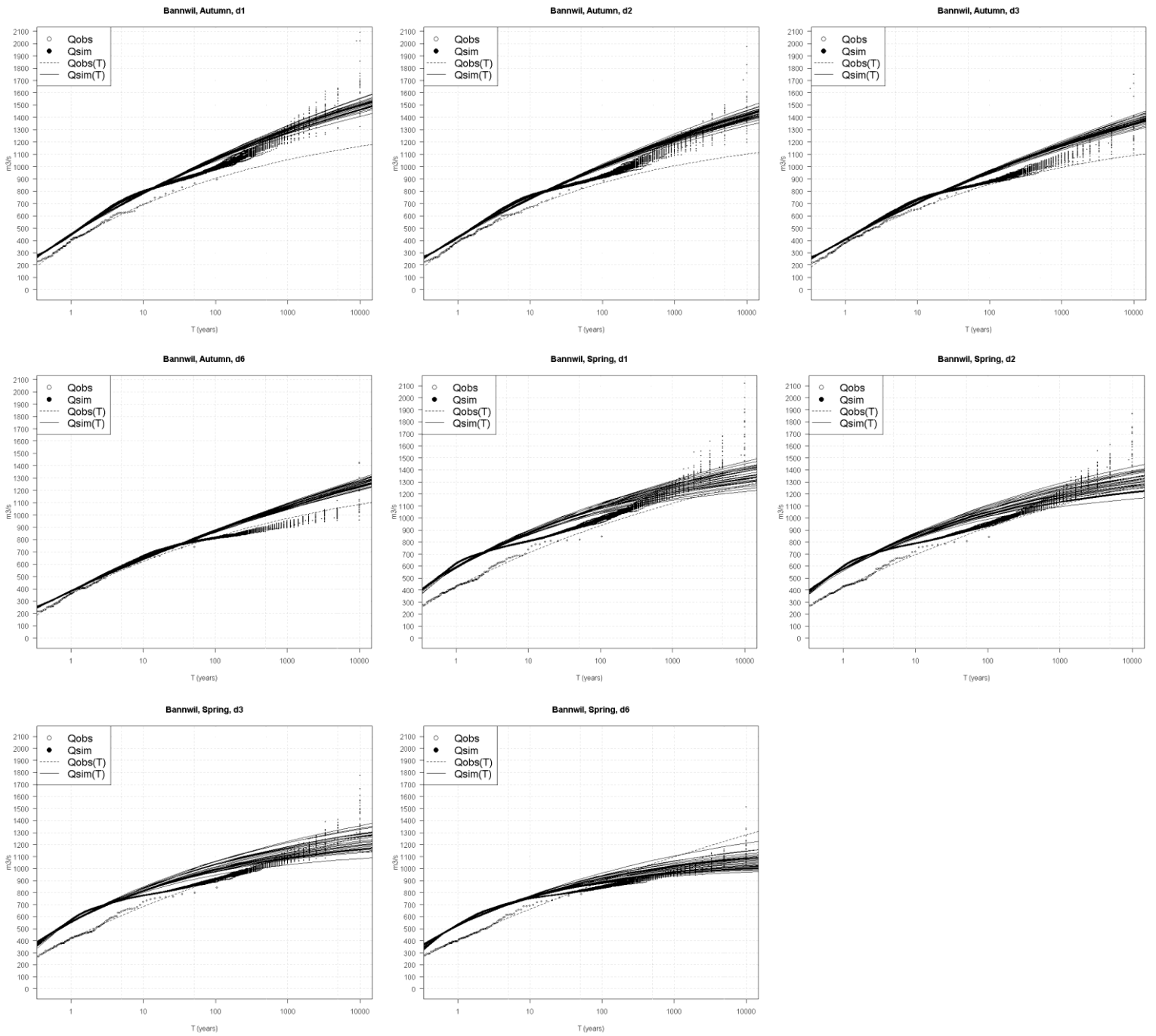


Figure 63: Autumn and spring QdF curves for Bannwil and individual flood durations. From top left to bottom right: d1 autumn, d2 autumn, d3 autumn, d6 autumn, d1 spring, d2, spring, d3 spring, d6 spring.

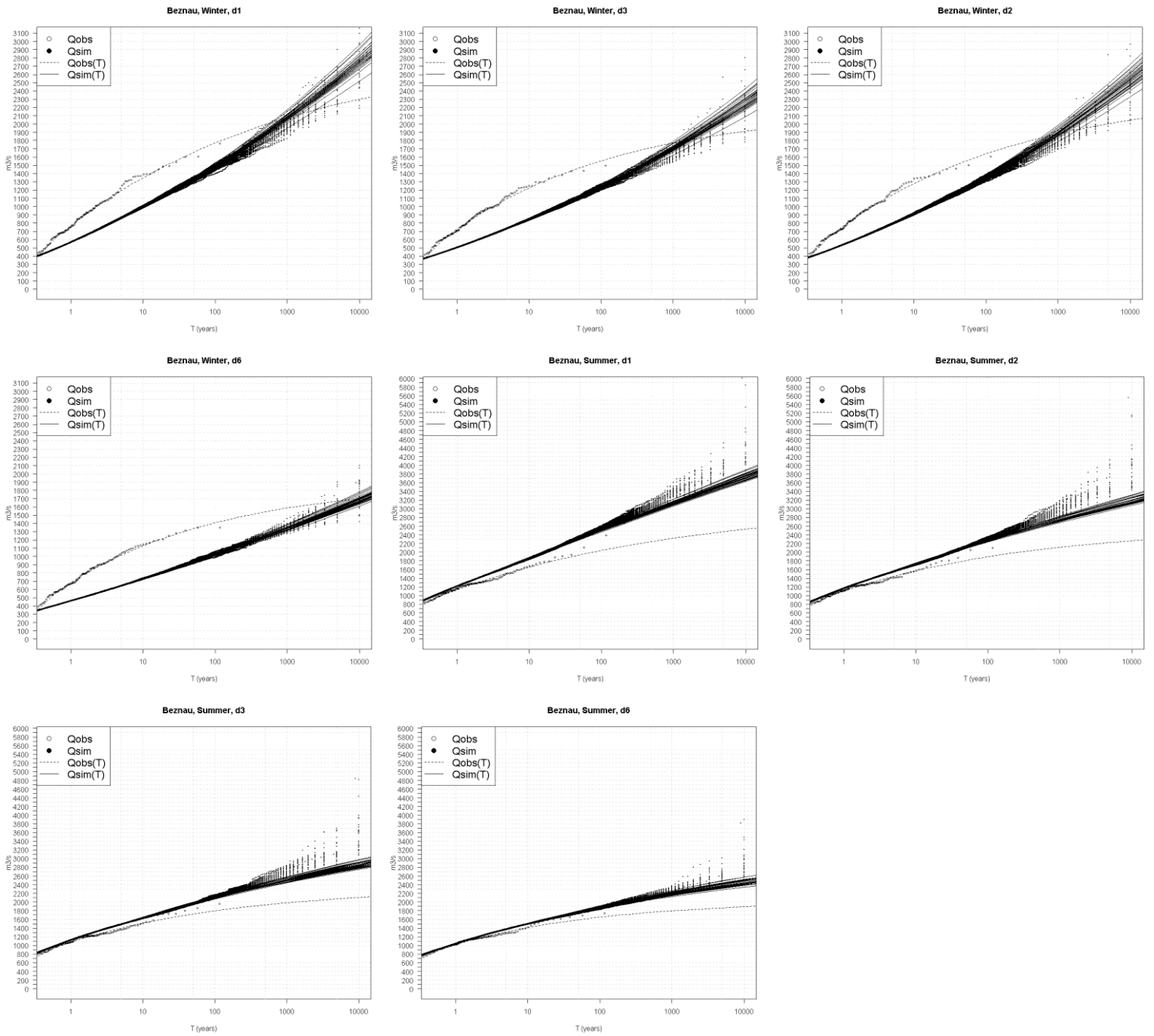


Figure 64: Winter and summer QdF curves for Beznau and individual flood durations. From top left to bottom right: d1 winter, d2 winter, d3 winter, d6 winter, d1 summer, d2, summer, d3 summer, d6 summer.

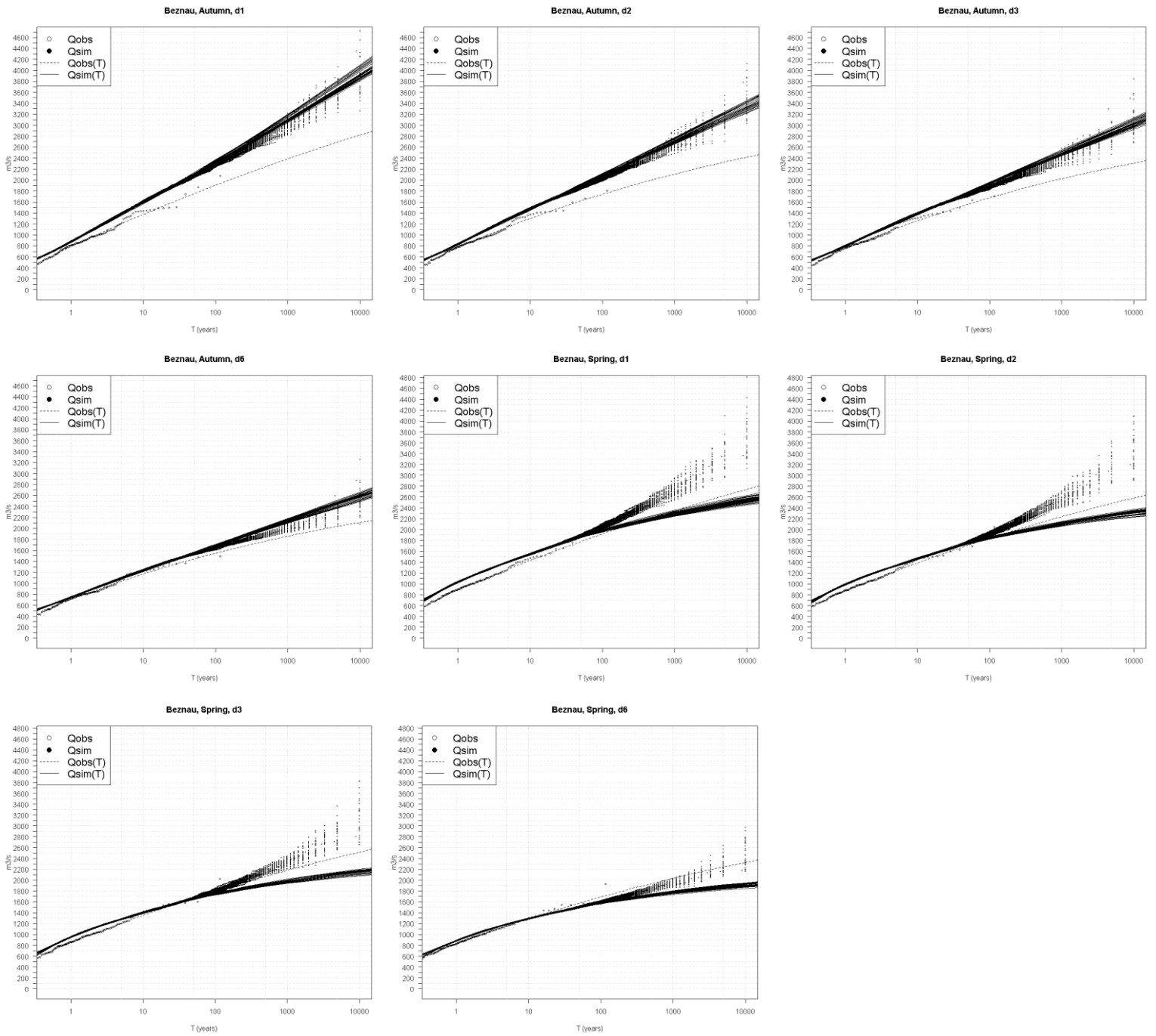


Figure 65: Autumn and spring QdF curves for Beznau and individual flood durations. From top left to bottom right: d1 autumn, d2 autumn, d3 autumn, d6 autumn, d1 spring, d2, spring, d3 spring, d6 spring.

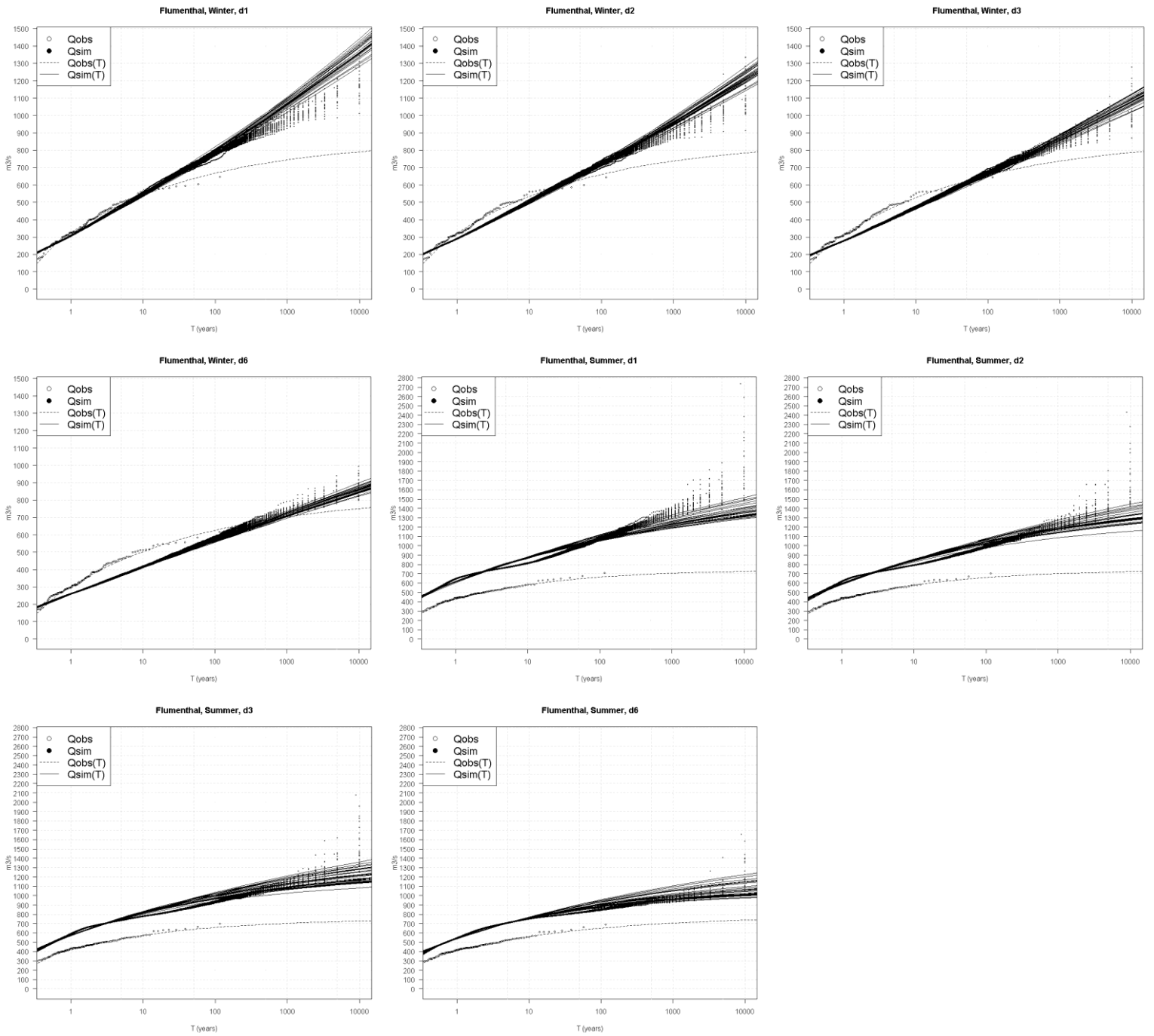


Figure 66: Winter and summer QdF curves for Flumenthal and individual flood durations. From top left to bottom right: d1 winter, d2 winter, d3 winter, d6 winter, d1 summer, d2, summer, d3 summer, d6 summer.

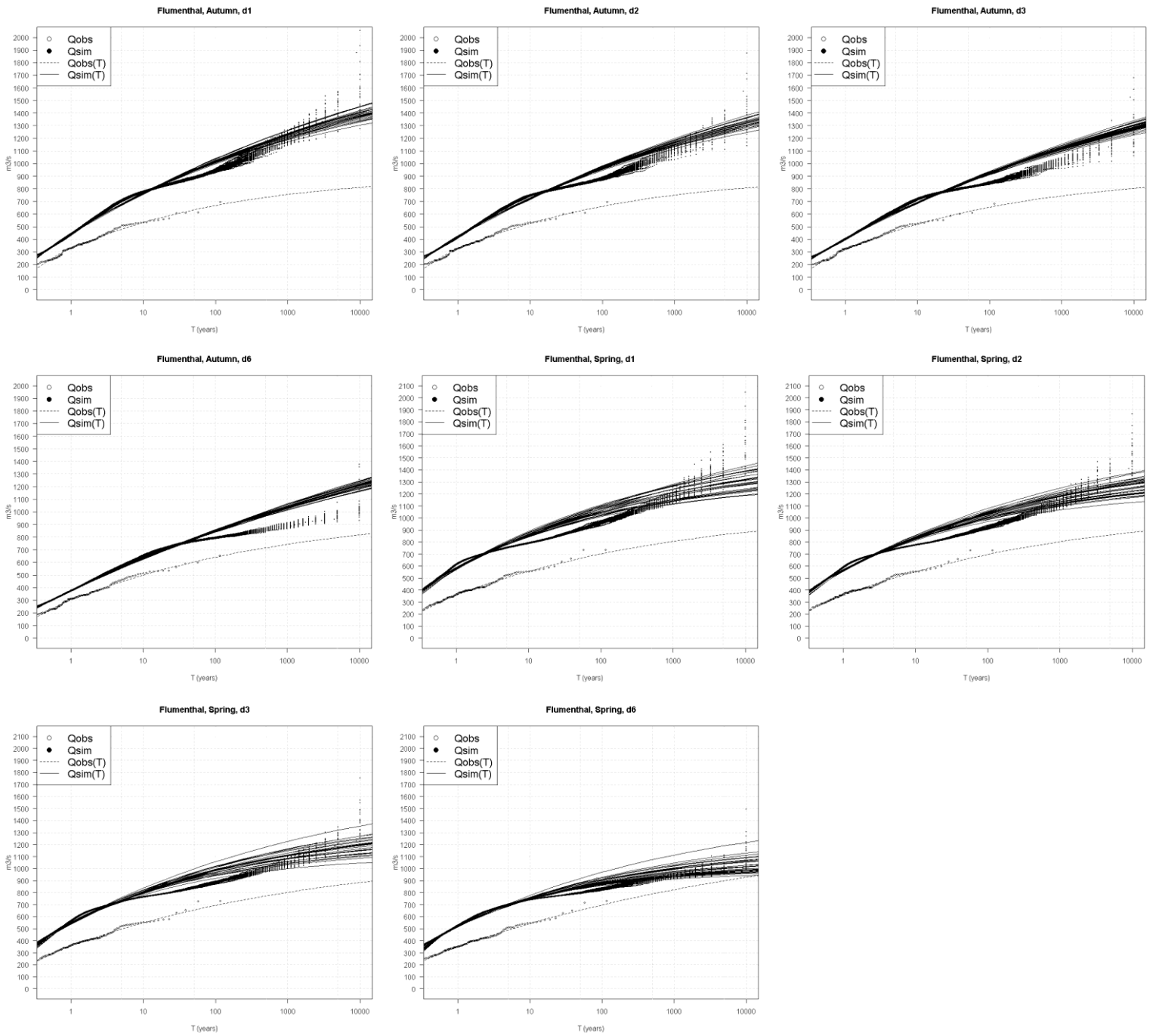


Figure 67: Autumn and spring QdF curves for Flumenthal and individual flood durations. From top left to bottom right: d1 autumn, d2 autumn, d3 autumn, d6 autumn, d1 spring, d2, spring, d3 spring, d6 spring.

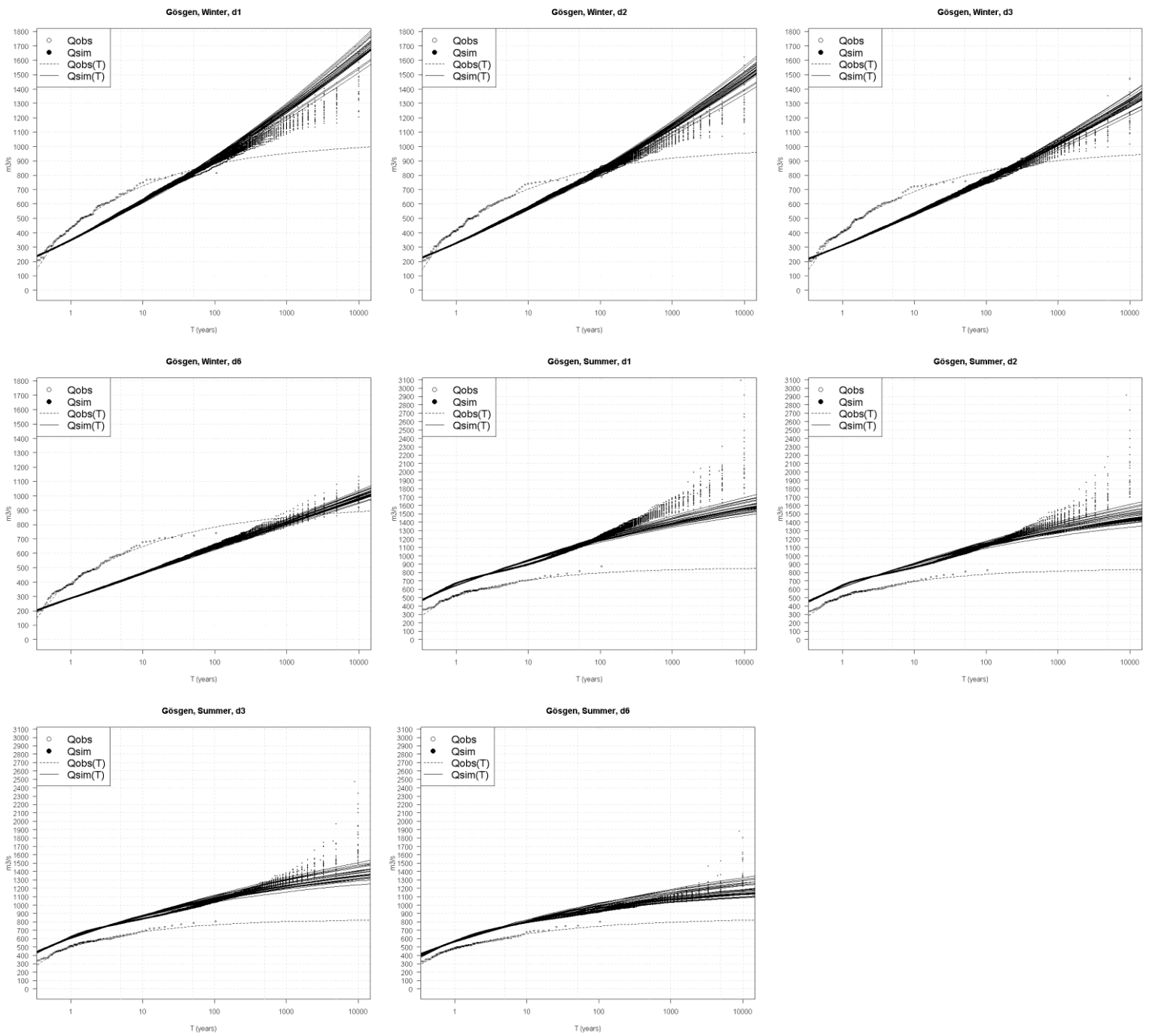


Figure 68: Winter and summer QdF curves for Gösgen and individual flood durations. From top left to bottom right: d1 winter, d2 winter, d3 winter, d6 winter, d1 summer, d2, summer, d3 summer, d6 summer.

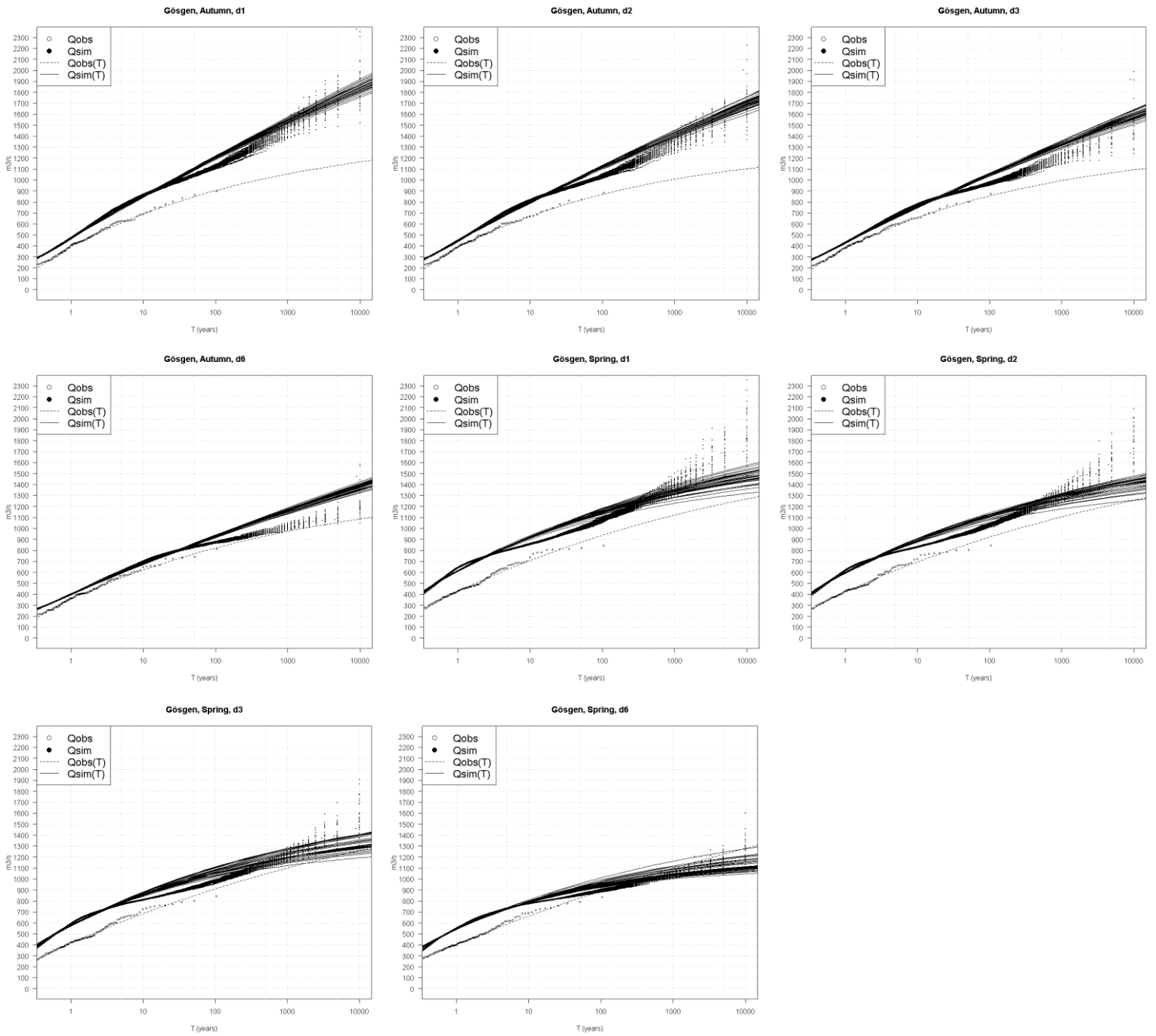


Figure 69: Autumn and spring QdF curves for Gösgen and individual flood durations. From top left to bottom right: d1 autumn, d2 autumn, d3 autumn, d6 autumn, d1 spring, d2, spring, d3 spring, d6 spring.

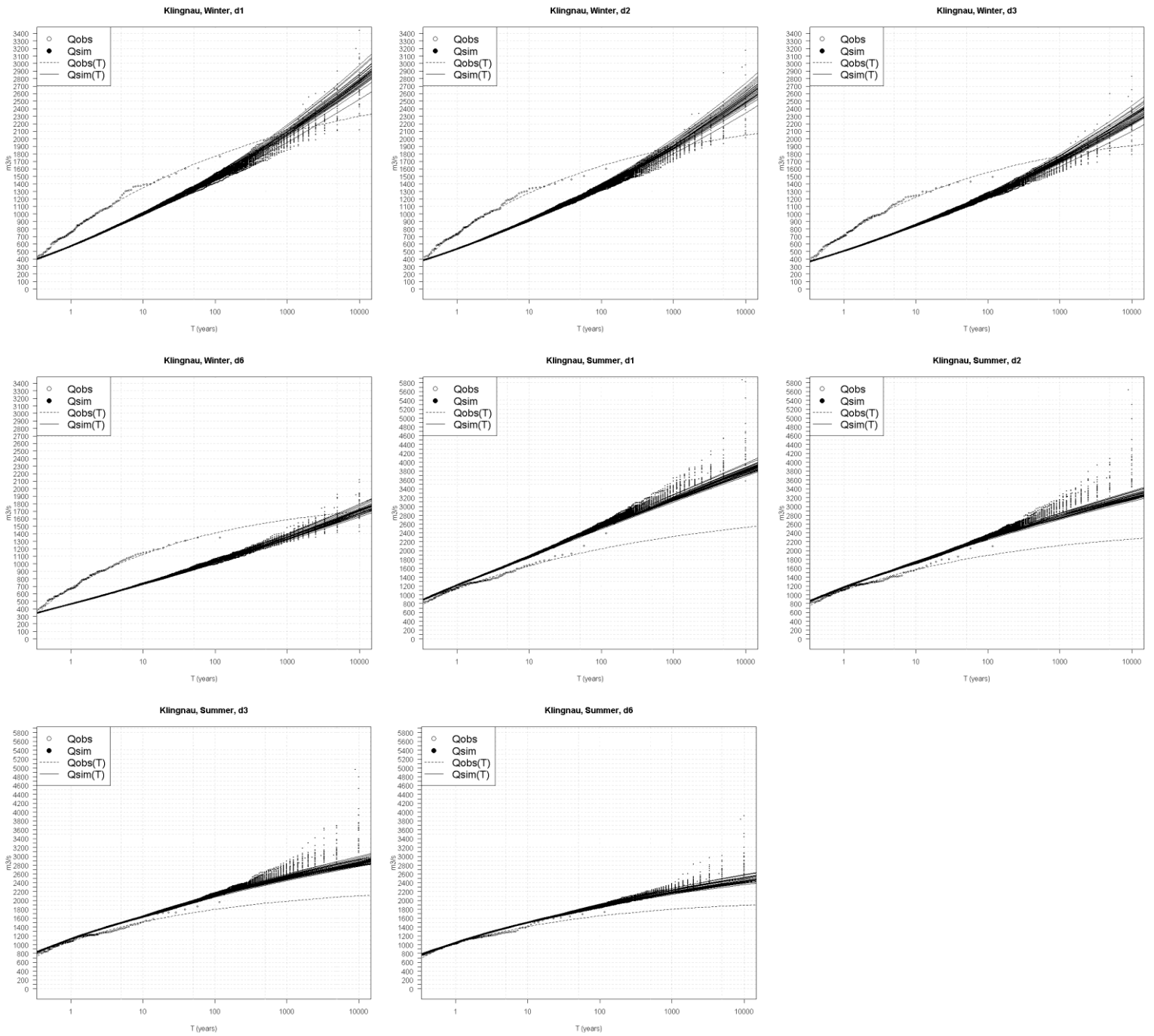


Figure 70: Winter and summer QdF curves for Klingnau and individual flood durations. From top left to bottom right: d1 winter, d2 winter, d3 winter, d6 winter, d1 summer, d2, summer, d3 summer, d6 summer.

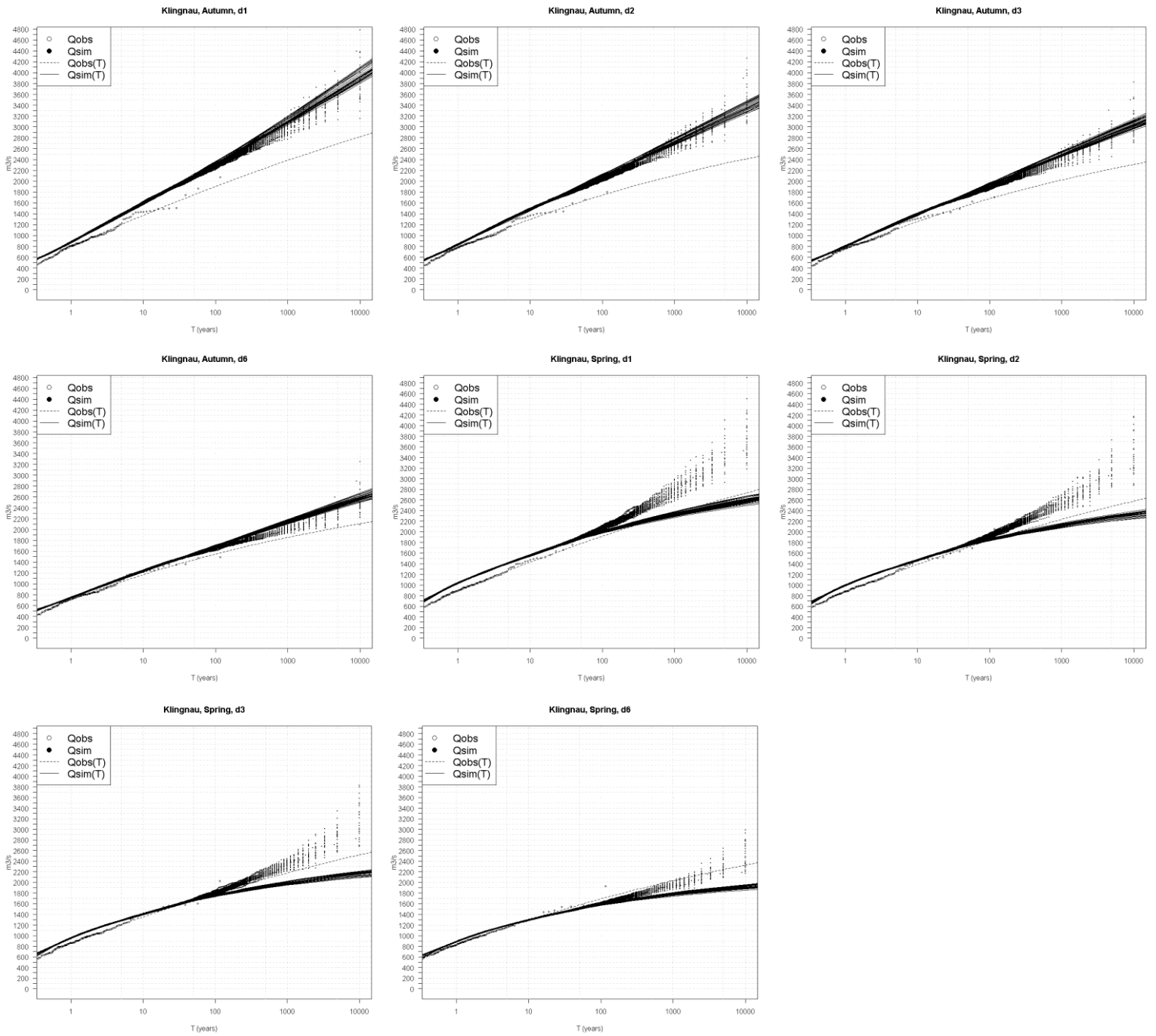


Figure 71: Autumn and spring QdF curves for Klingnau and individual flood durations. From top left to bottom right: d1 autumn, d2 autumn, d3 autumn, d6 autumn, d1 spring, d2, spring, d3 spring, d6 spring.

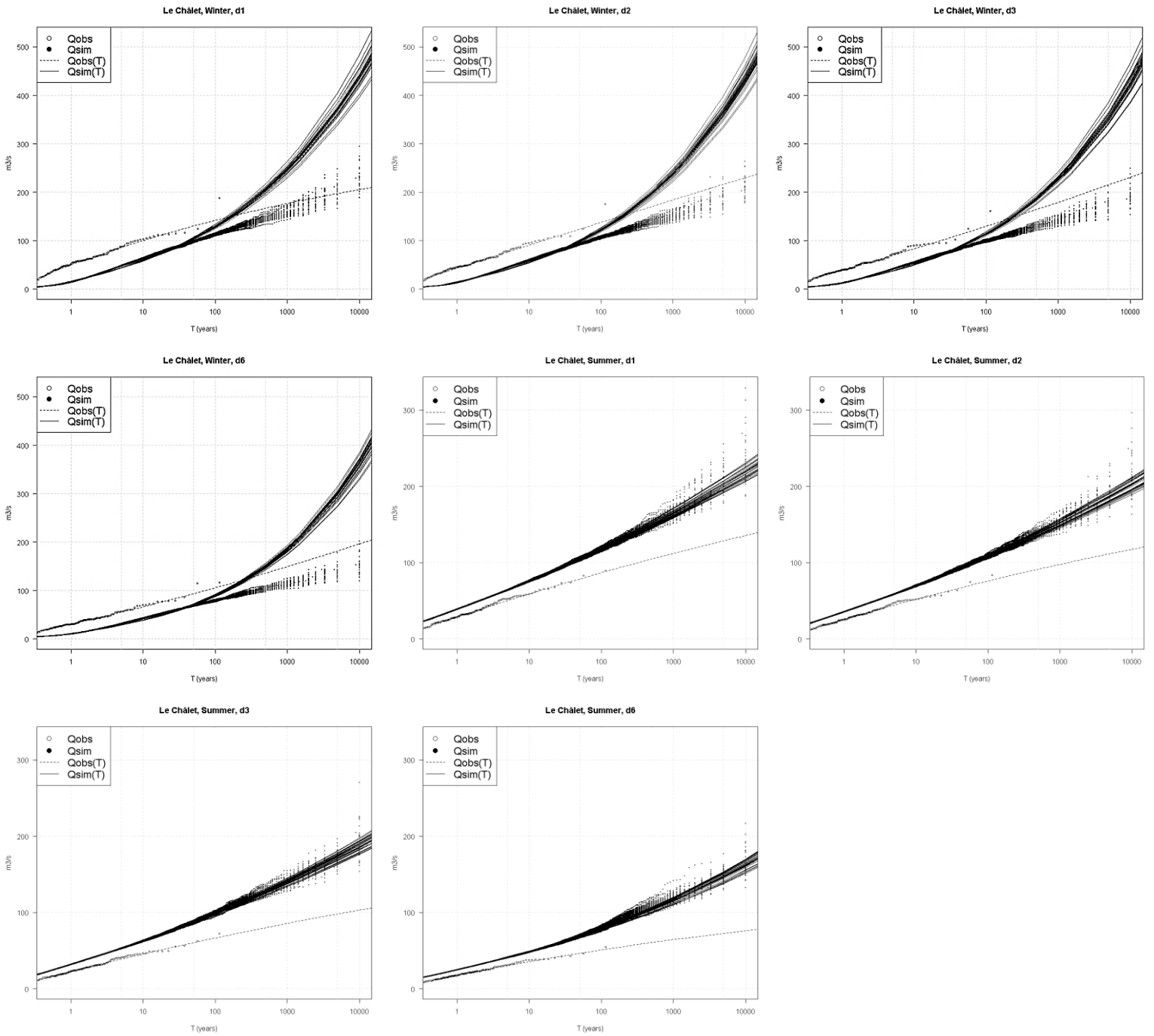


Figure 72: Winter and summer QdF curves for Le Châlet and individual flood durations. From top left to bottom right: d1 winter, d2 winter, d3 winter, d6 winter, d1 summer, d2, summer, d3 summer, d6 summer.

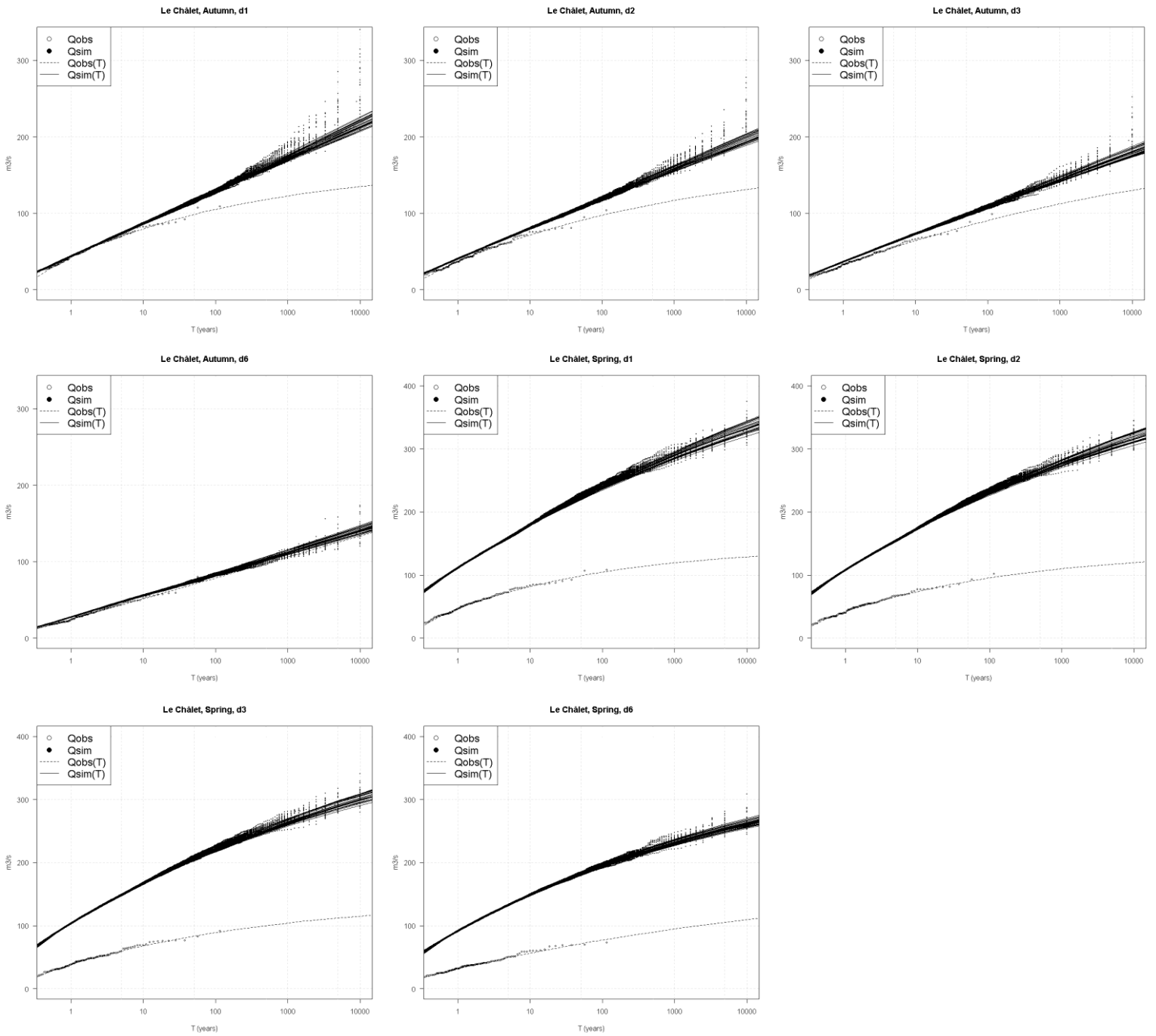


Figure 73: Autumn and spring QdF curves for Le Châlet and individual flood durations. From top left to bottom right: d1 autumn, d2 autumn, d3 autumn, d6 autumn, d1 spring, d2, spring, d3 spring, d6 spring.

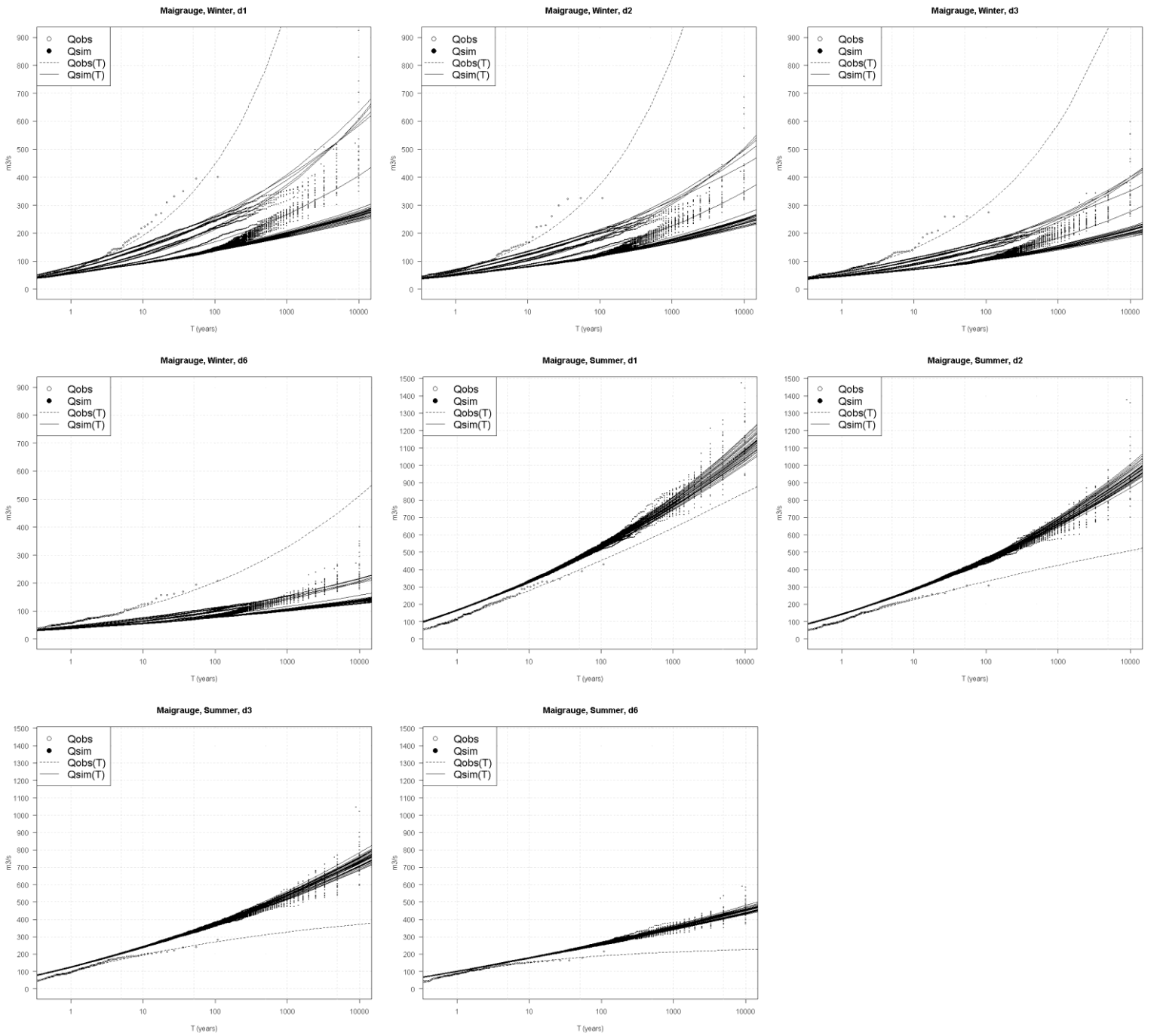


Figure 74: Winter and summer QdF curves for Maigrage and individual flood durations. From top left to bottom right: d1 winter, d2 winter, d3 winter, d6 winter, d1 summer, d2, summer, d3 summer, d6 summer.

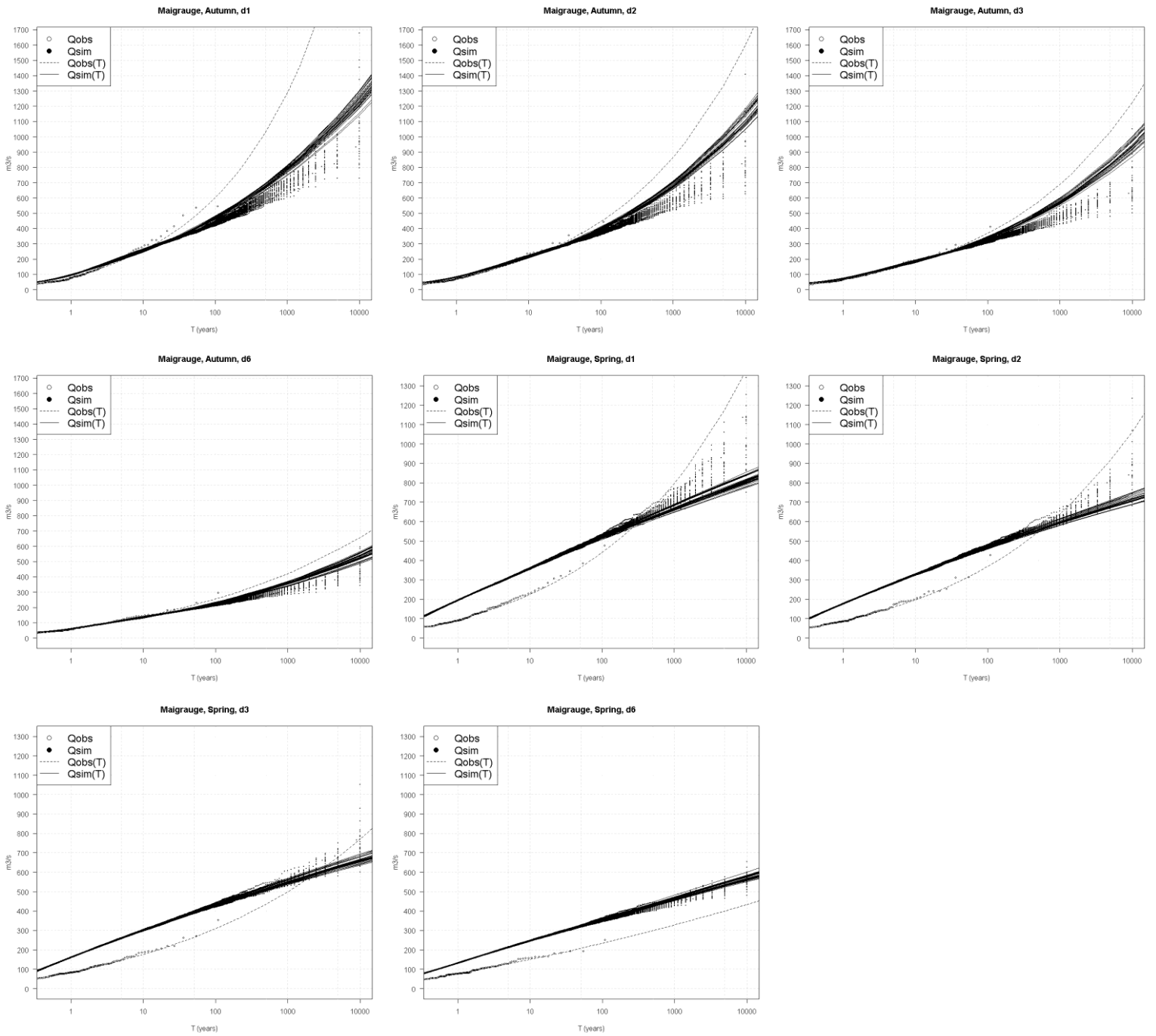


Figure 75: Autumn and spring QdF curves for Maigrage and individual flood durations. From top left to bottom right: d1 autumn, d2 autumn, d3 autumn, d6 autumn, d1 spring, d2, spring, d3 spring, d6 spring.

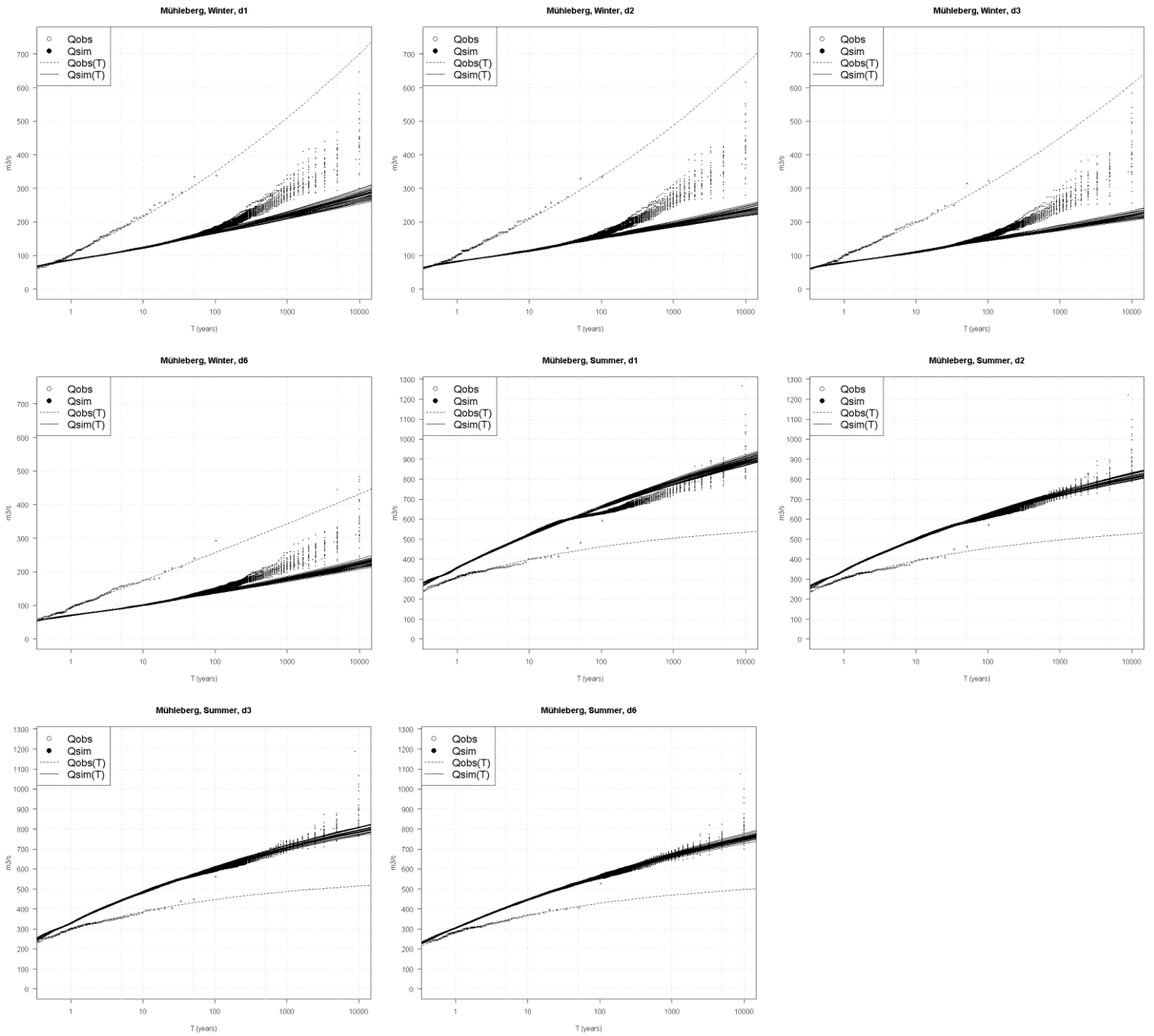


Figure 76: Winter and summer QdF curves for Mühleberg and individual flood durations. From top left to bottom right: d1 winter, d2 winter, d3 winter, d6 winter, d1 summer, d2, summer, d3 summer, d6 summer.

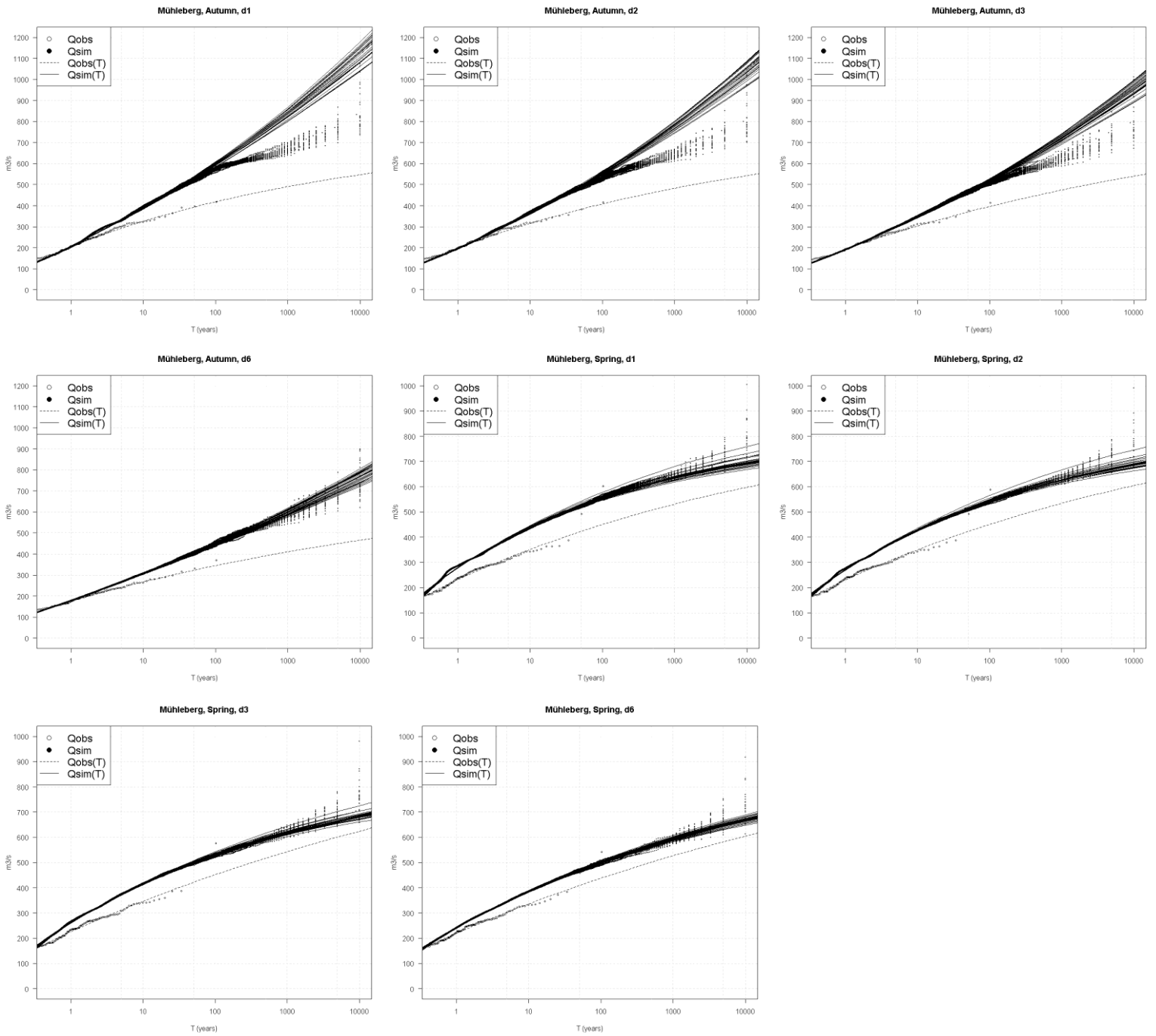


Figure 77: Autumn and spring QdF curves for Mühleberg and individual flood durations. From top left to bottom right: d1 autumn, d2 autumn, d3 autumn, d6 autumn, d1 spring, d2, spring, d3 spring, d6 spring.

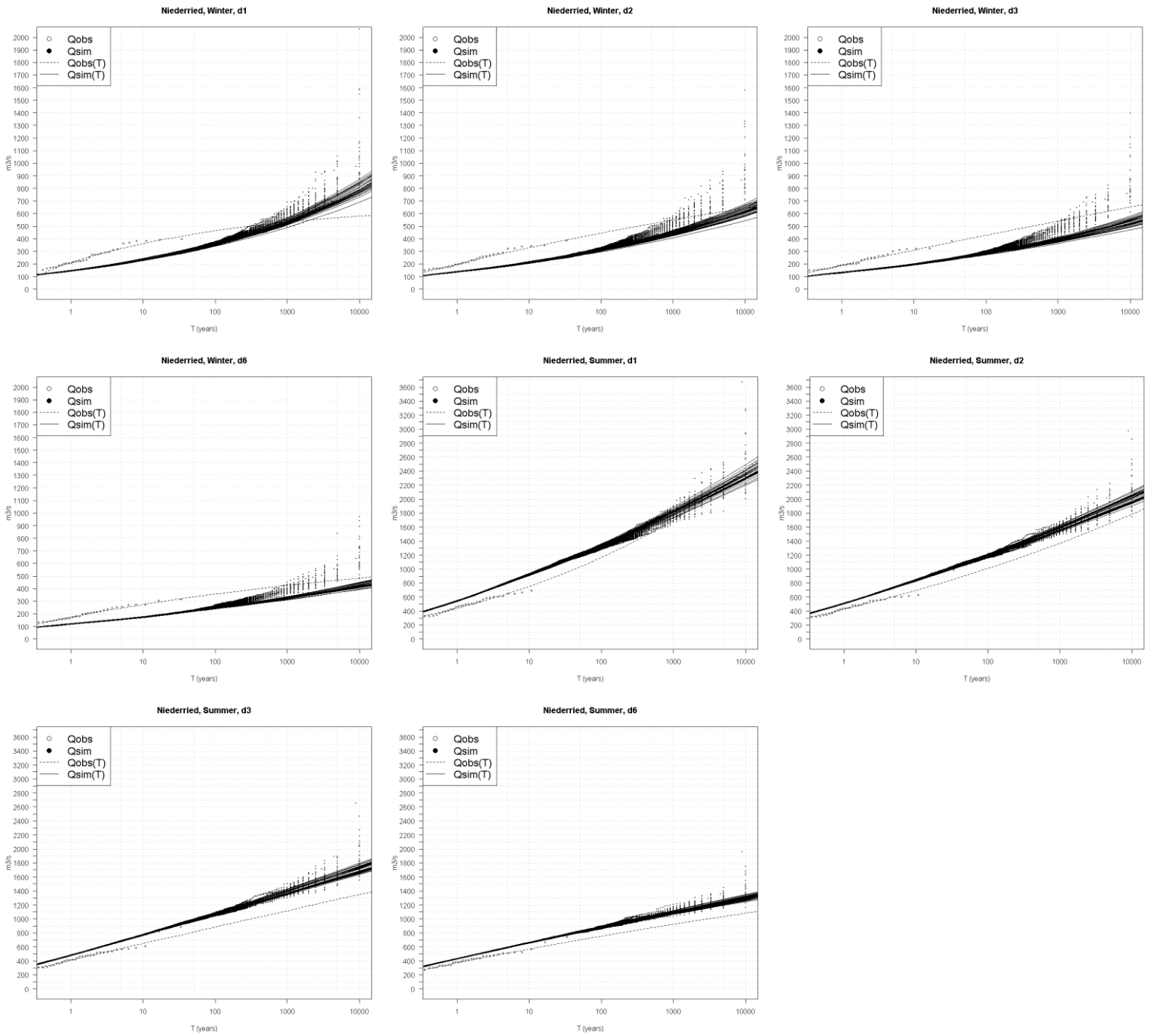


Figure 78: Winter and summer QdF curves for Niederried and individual flood durations. From top left to bottom right: d1 winter, d2 winter, d3 winter, d6 winter, d1 summer, d2, summer, d3 summer, d6 summer.

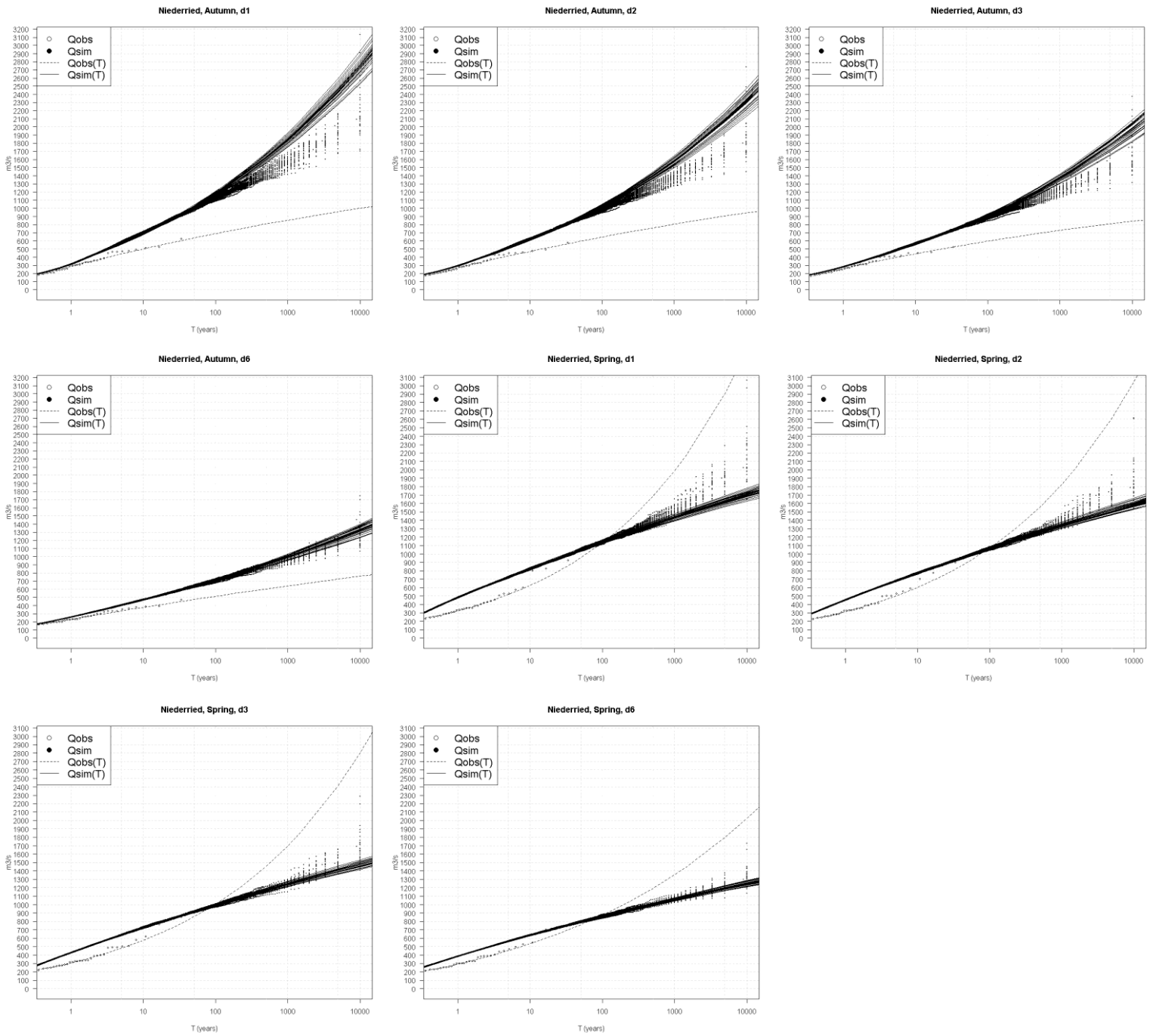


Figure 79: Autumn and spring QdF curves for Niederried and individual flood durations. From top left to bottom right: d1 autumn, d2 autumn, d3 autumn, d6 autumn, d1 spring, d2, spring, d3 spring, d6 spring.

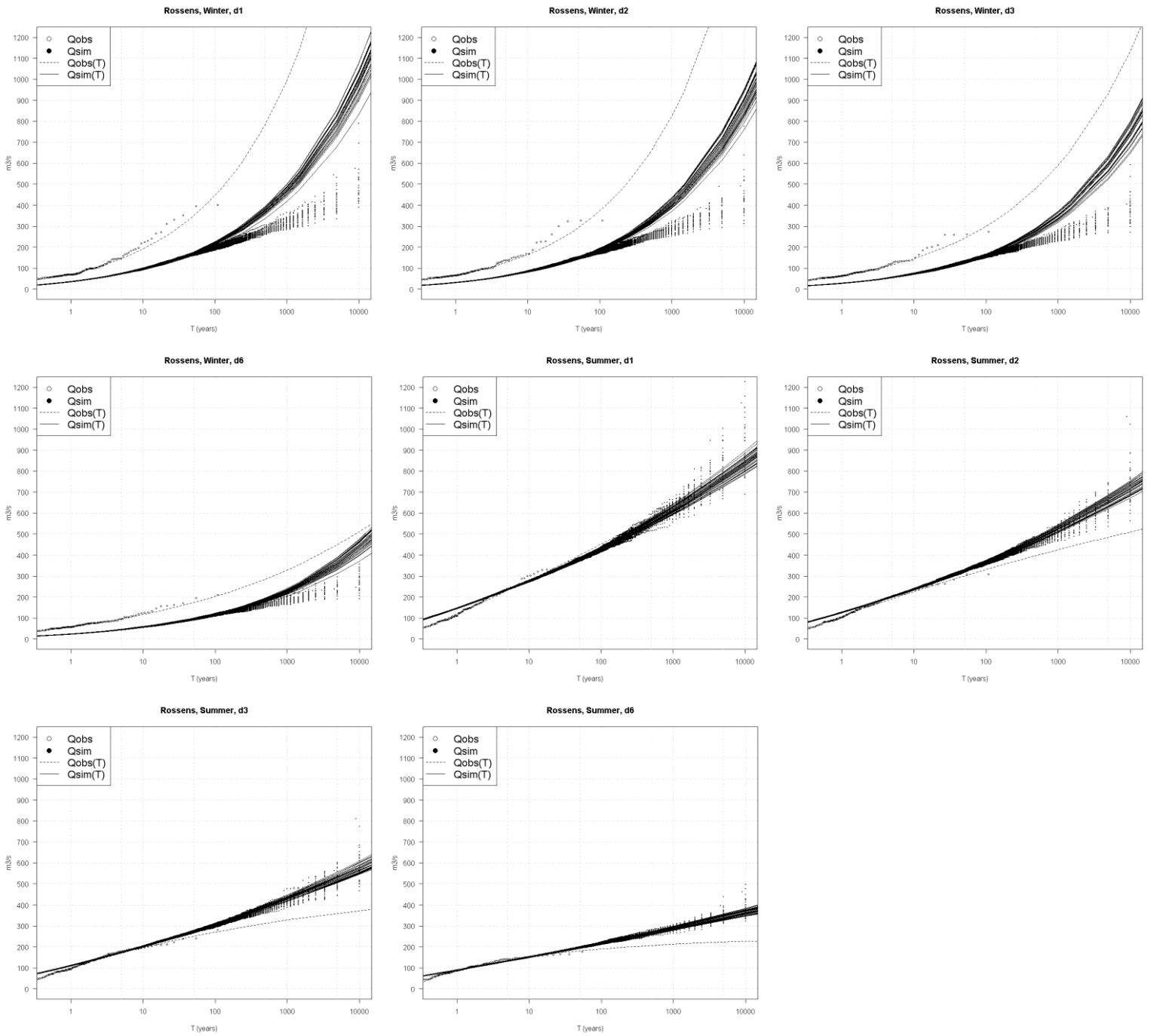


Figure 80: Winter and summer QdF curves for Rossens and individual flood durations. From top left to bottom right: d1 winter, d2 winter, d3 winter, d6 winter, d1 summer, d2, summer, d3 summer, d6 summer.

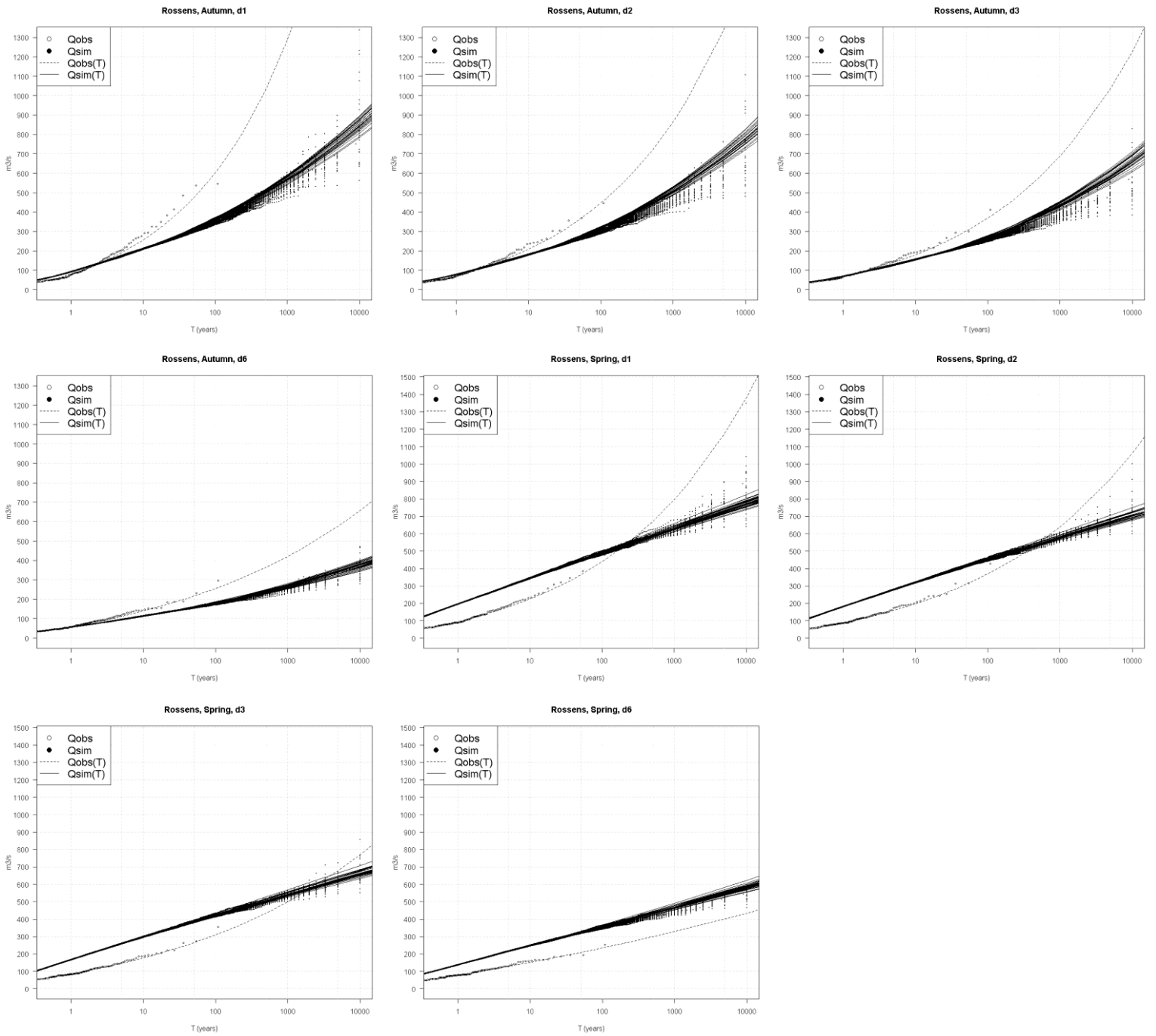


Figure 81: Autumn and spring QdF curves for Rossens and individual flood durations. From top left to bottom right: d1 autumn, d2 autumn, d3 autumn, d6 autumn, d1 spring, d2, spring, d3 spring, d6 spring.

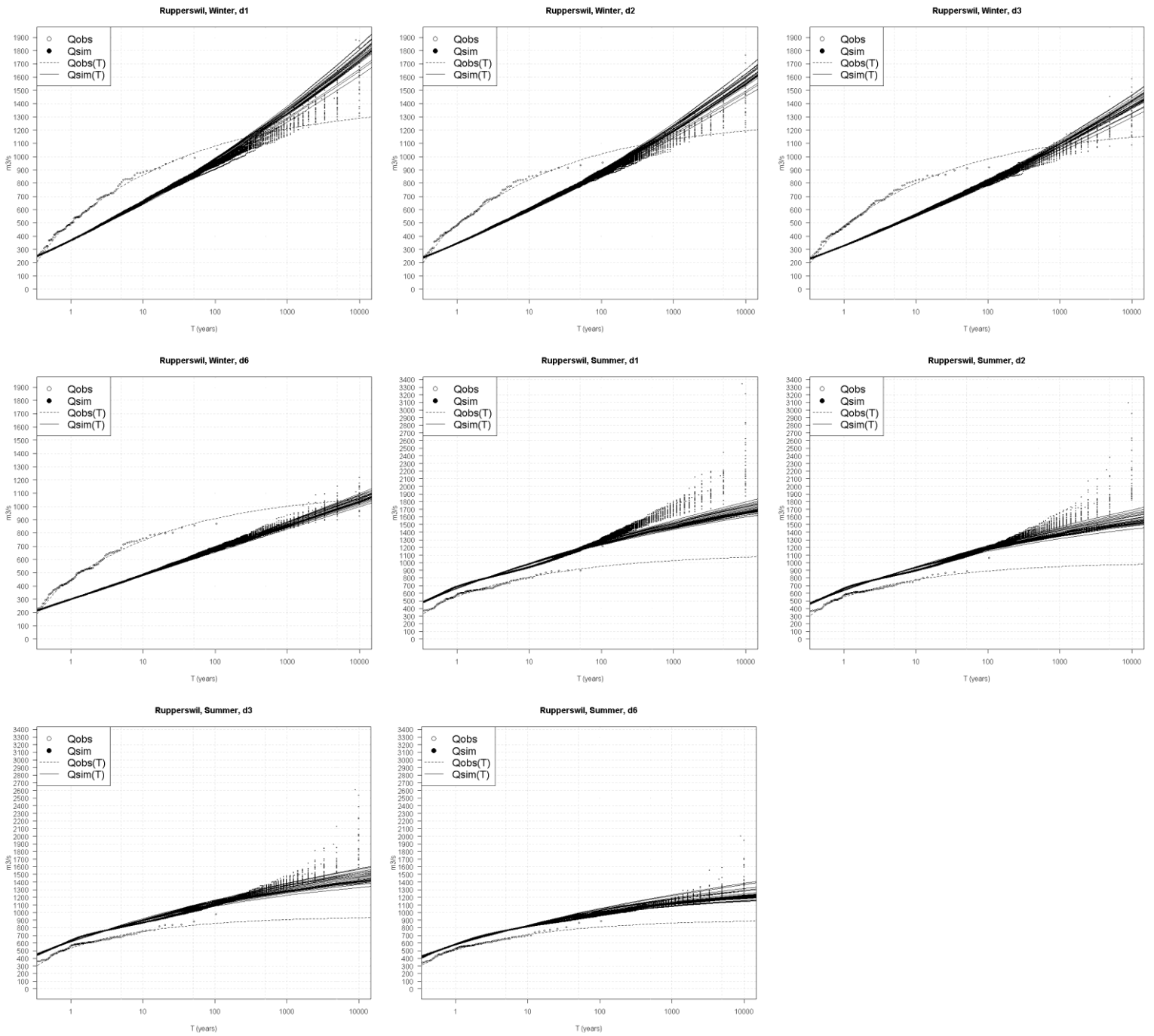


Figure 82: Winter and summer QdF curves for Ruppertswil and individual flood durations. From top left to bottom right: d1 winter, d2 winter, d3 winter, d6 winter, d1 summer, d2, summer, d3 summer, d6 summer.

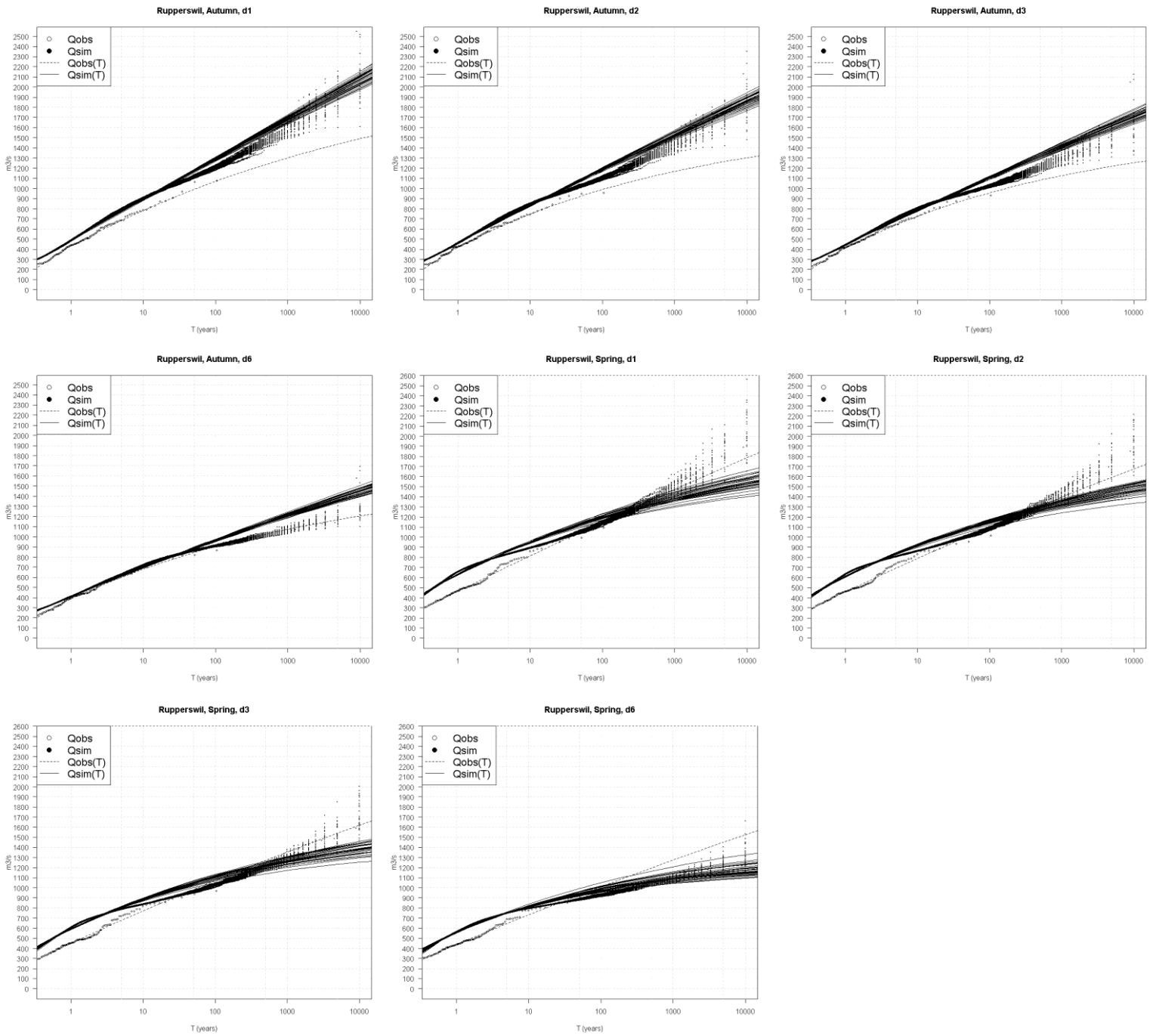


Figure 83: Autumn and spring QdF curves for Ruppertswil and individual flood durations. From top left to bottom right: d1 autumn, d2 autumn, d3 autumn, d6 autumn, d1 spring, d2, spring, d3 spring, d6 spring.

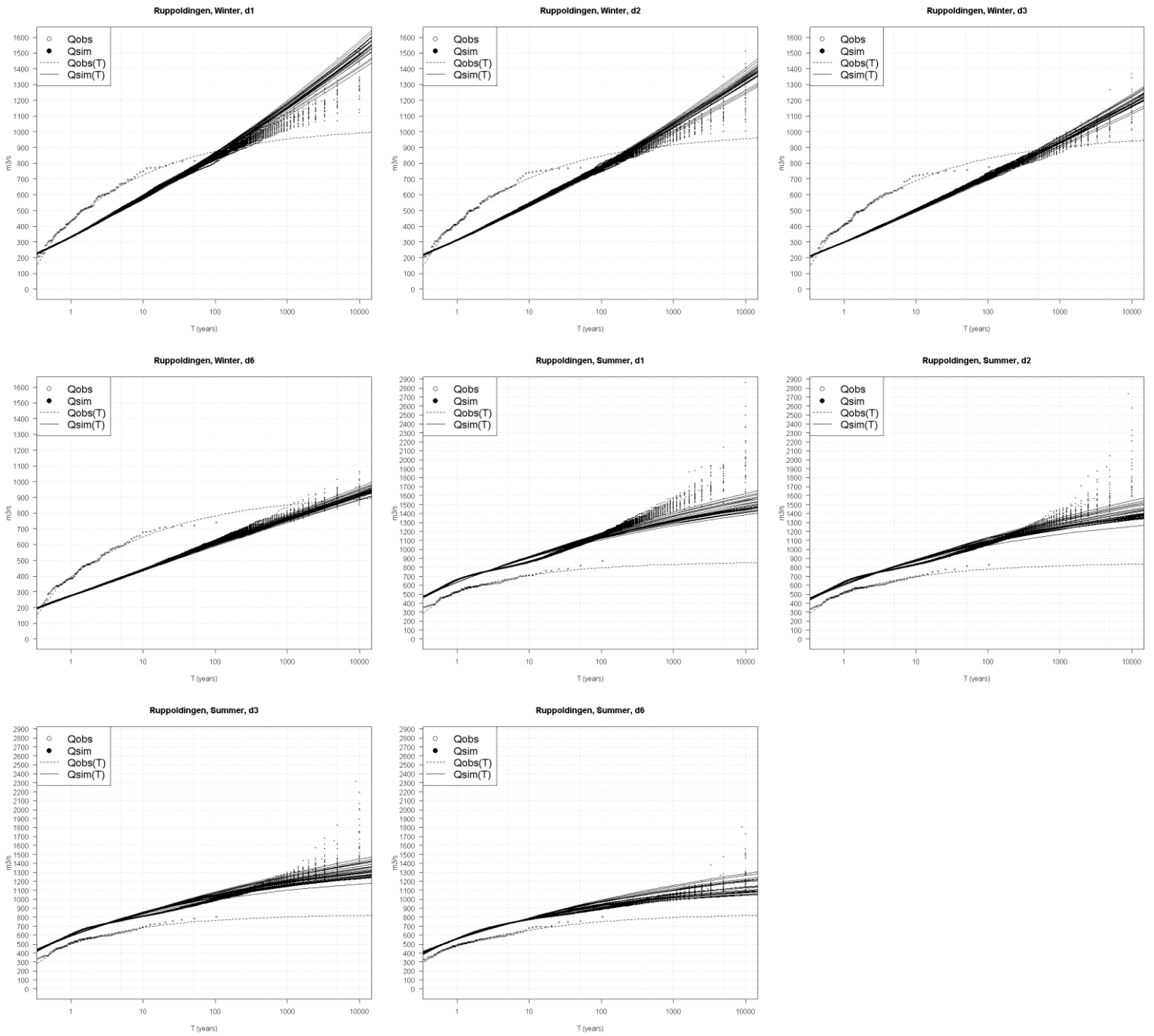


Figure 84: Winter and summer QdF curves for Ruppoldingen and individual flood durations. From top left to bottom right: d1 winter, d2 winter, d3 winter, d6 winter, d1 summer, d2, summer, d3 summer, d6 summer.

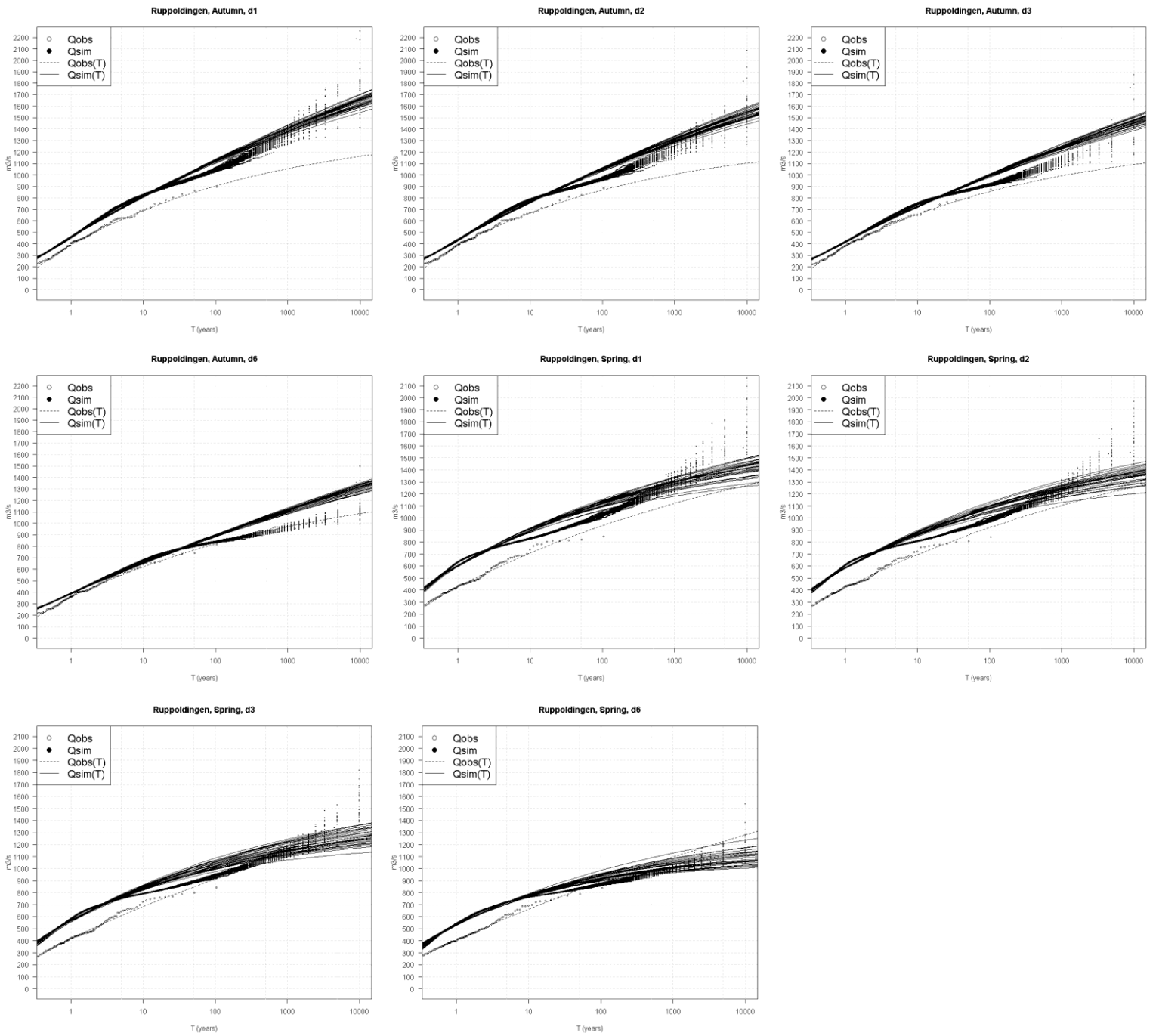


Figure 85: Autumn and spring QdF curves for Ruppoldingen and individual flood durations. From top left to bottom right: d1 autumn, d2 autumn, d3 autumn, d6 autumn, d1 spring, d2, spring, d3 spring, d6 spring.

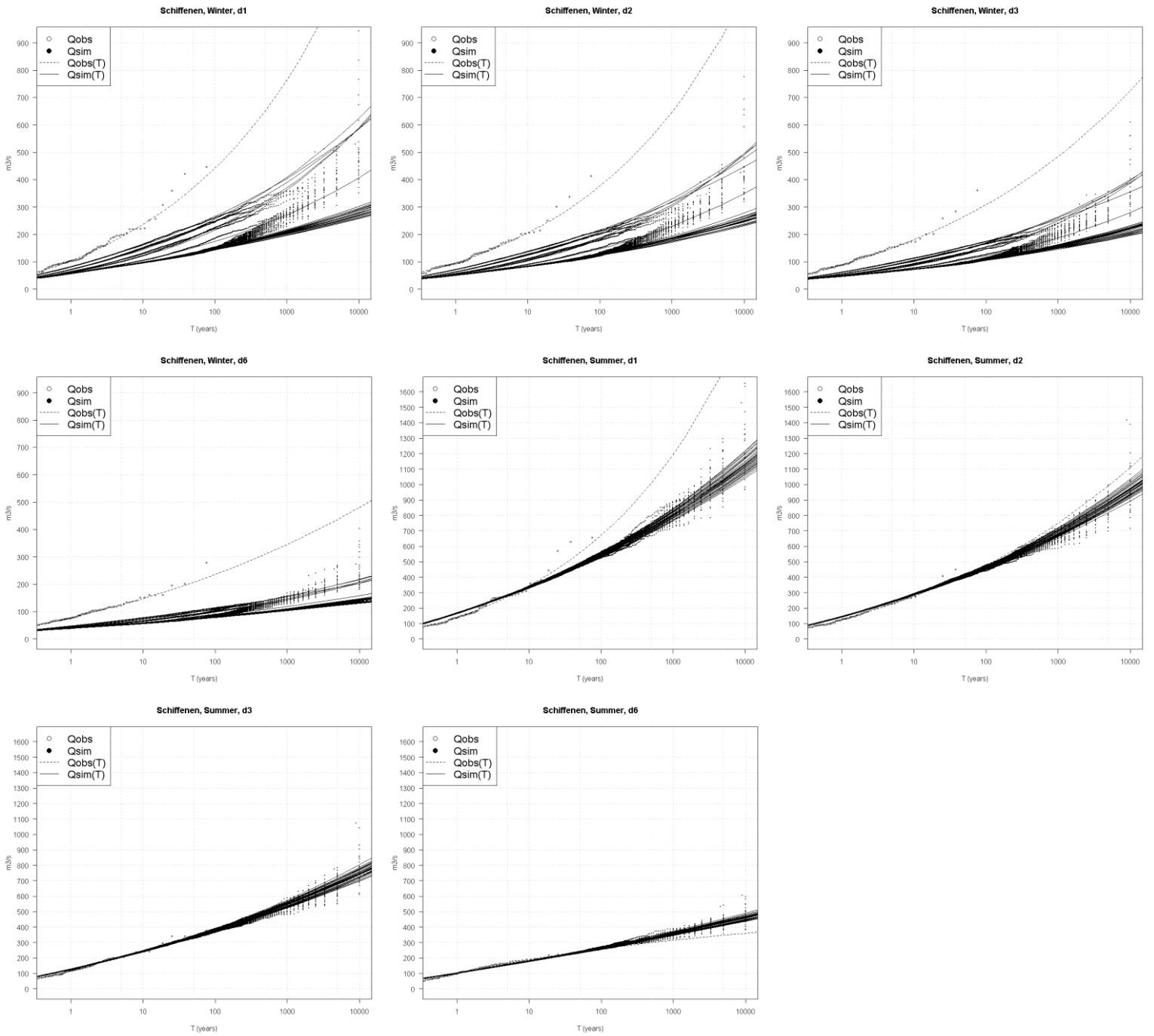


Figure 86: Winter and summer QdF curves for Schiffenen and individual flood durations. From top left to bottom right: d1 winter, d2 winter, d3 winter, d6 winter, d1 summer, d2, summer, d3 summer, d6 summer.

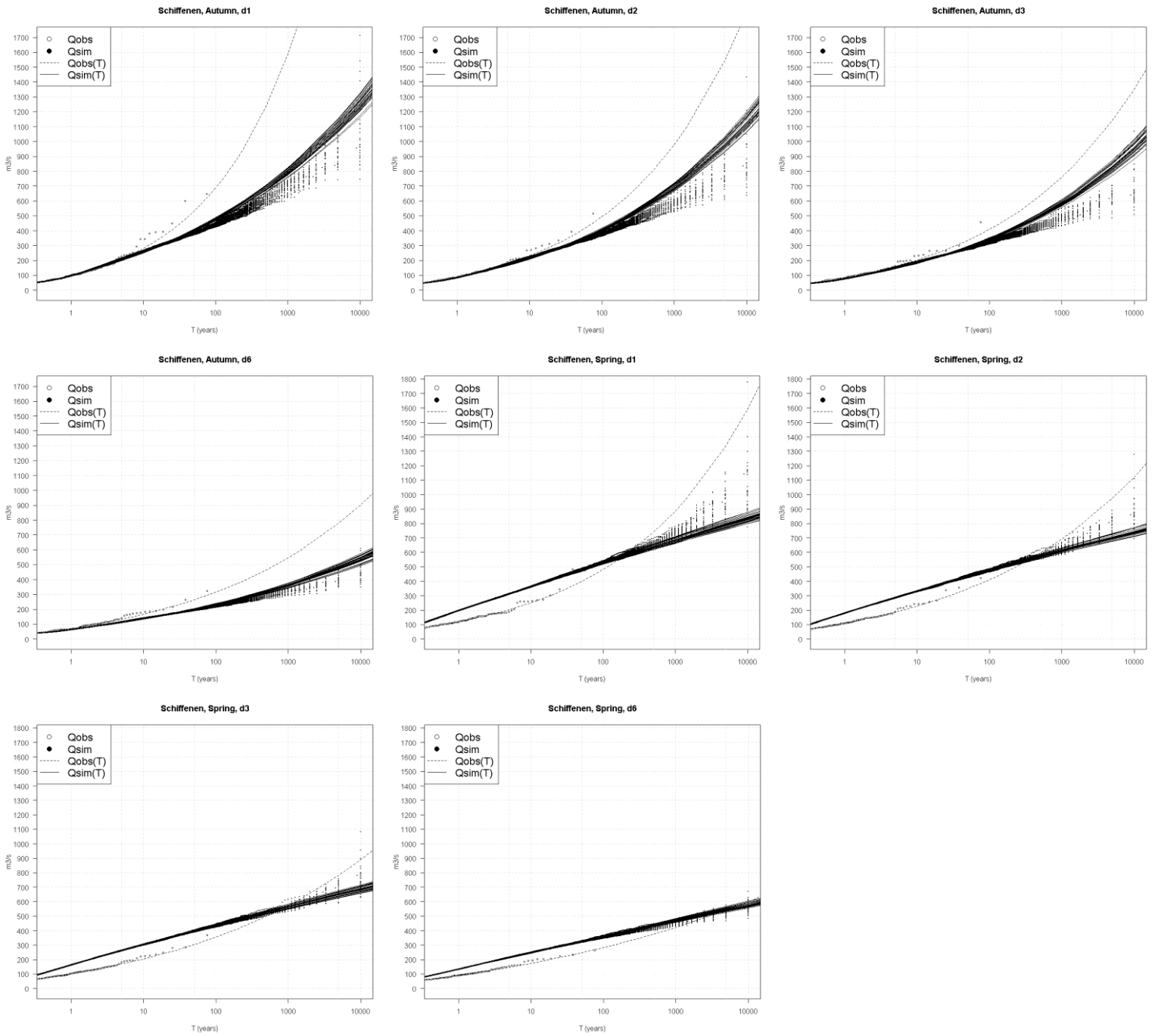


Figure 87: Autumn and spring QdF curves for Schiffenen and individual flood durations. From top left to bottom right: d1 autumn, d2 autumn, d3 autumn, d6 autumn, d1 spring, d2, spring, d3 spring, d6 spring.

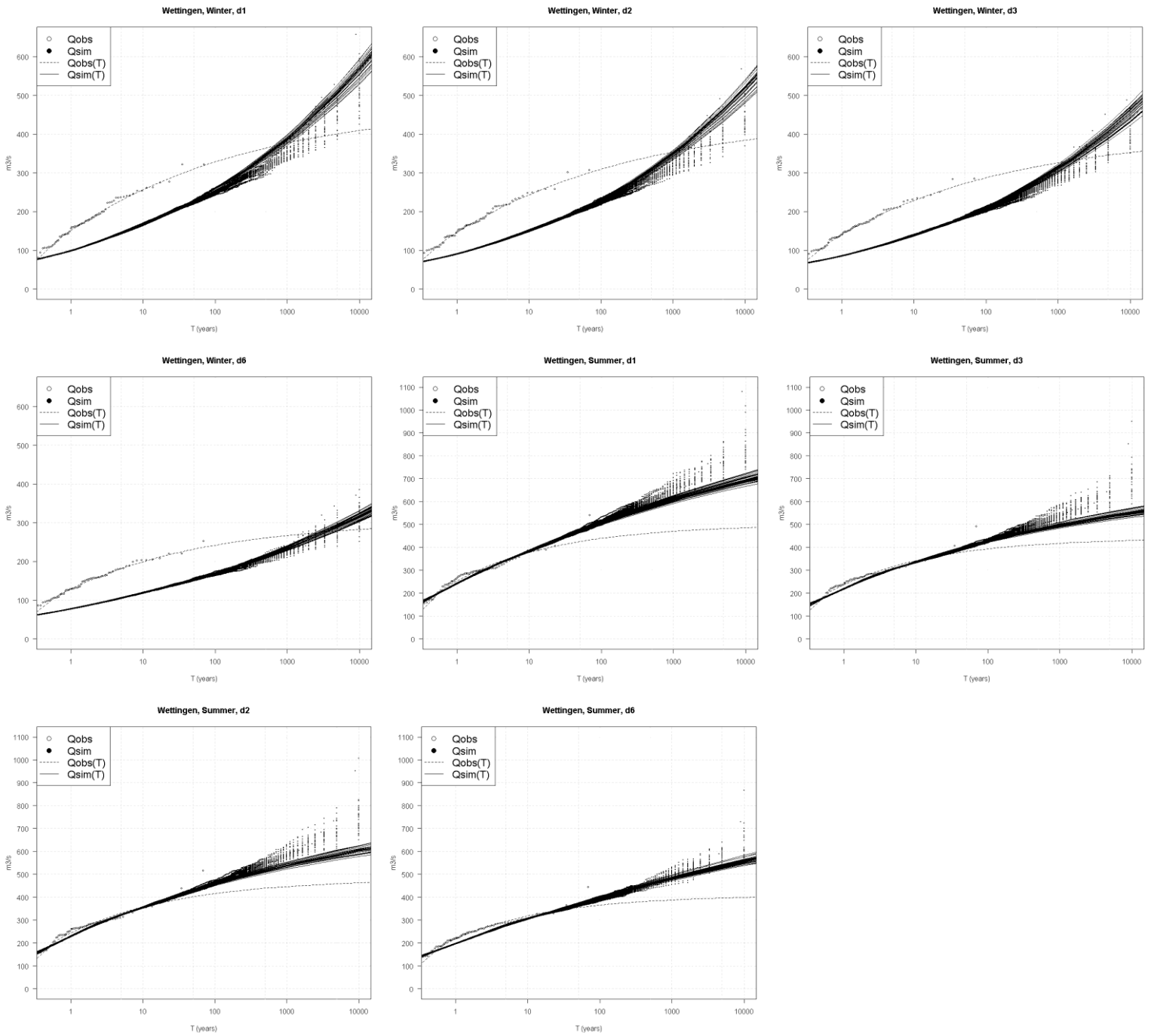


Figure 88: Winter and summer QdF curves for Wettingen and individual flood durations. From top left to bottom right: d1 winter, d2 winter, d3 winter, d6 winter, d1 summer, d2, summer, d3 summer, d6 summer.

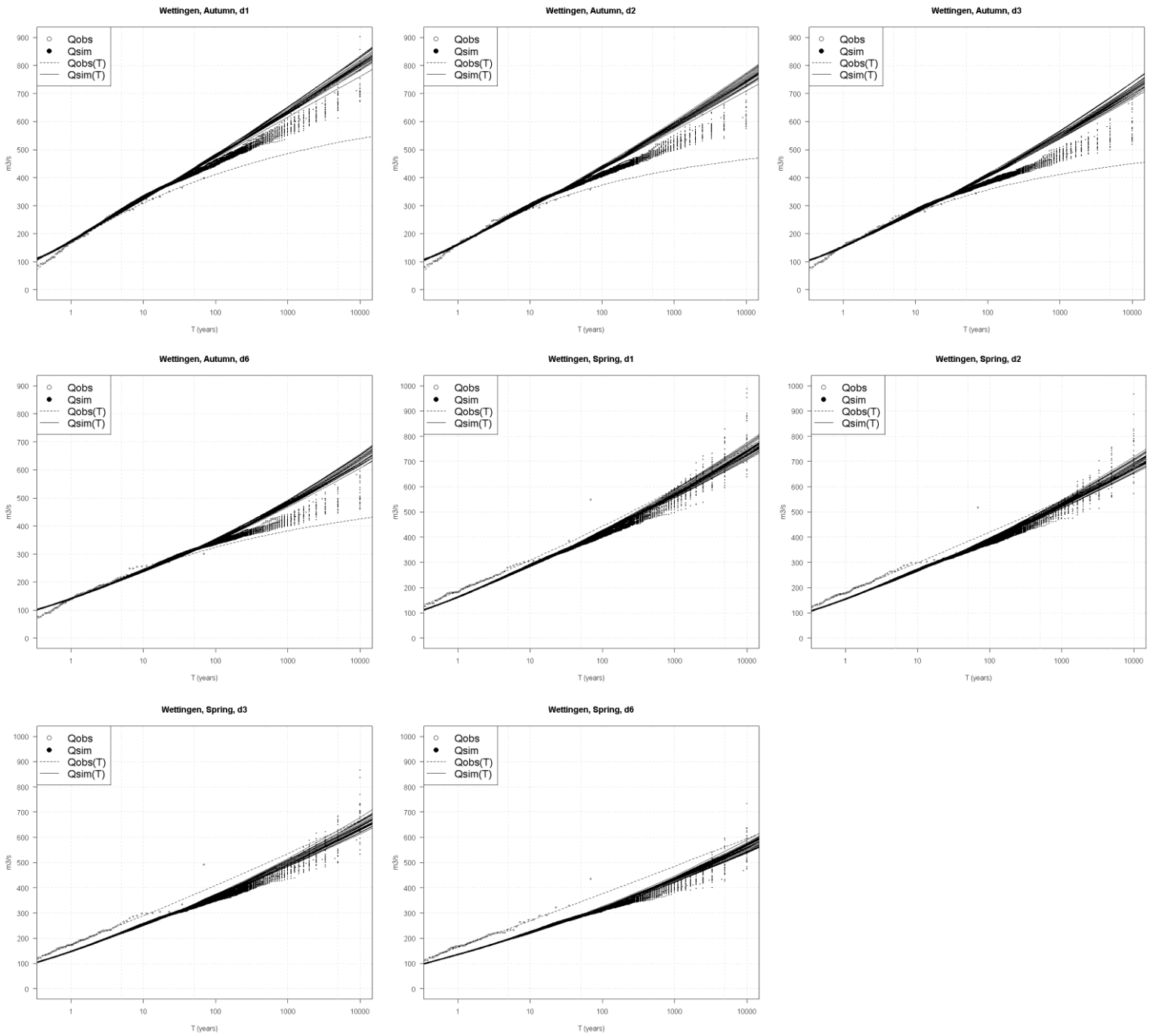


Figure 89: Autumn and spring QdF curves for Wettingen and individual flood durations. From top left to bottom right: d1 autumn, d2 autumn, d3 autumn, d6 autumn, d1 spring, d2, spring, d3 spring, d6 spring.

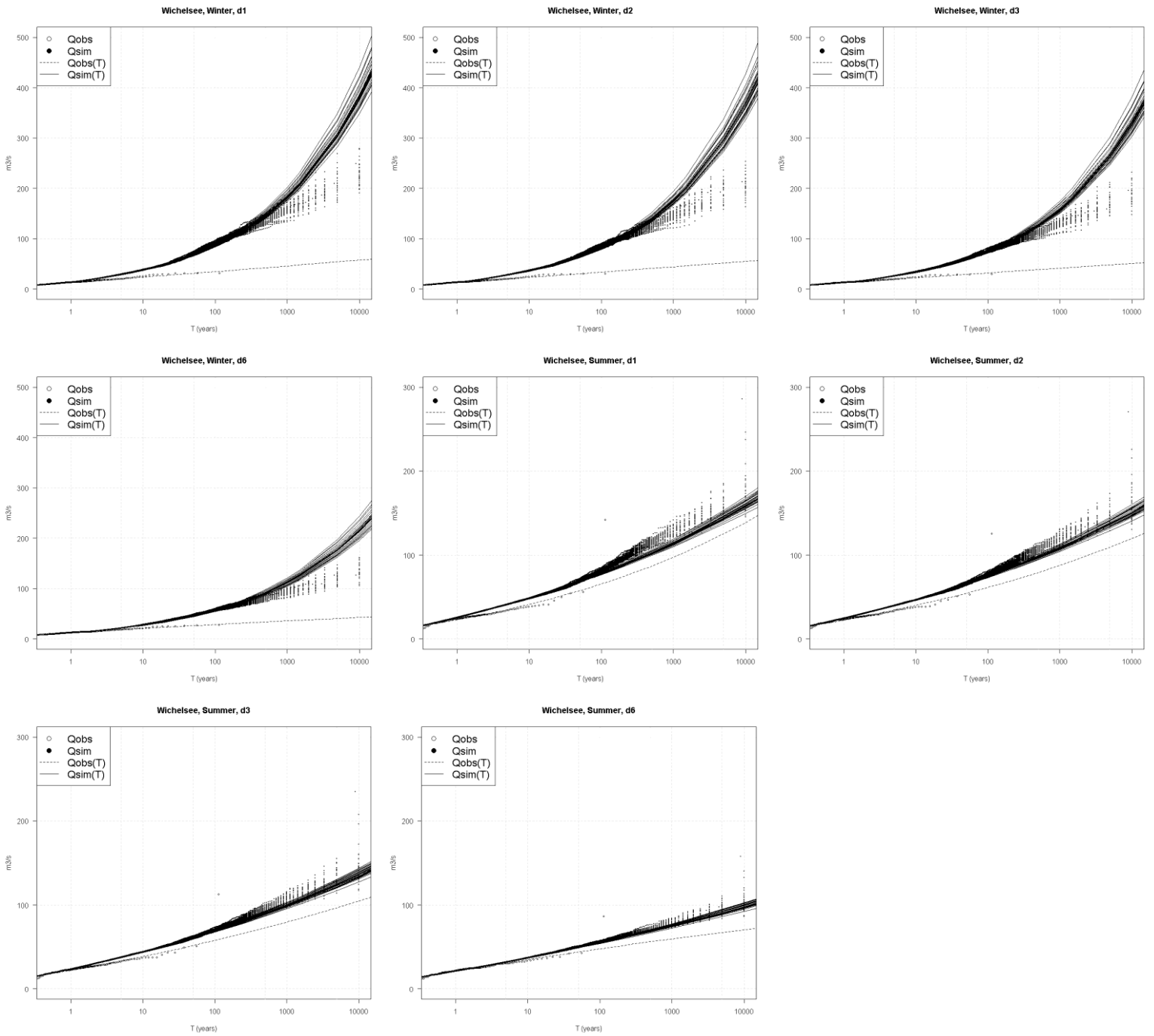


Figure 90: Winter and summer QdF curves for Wichelsee and individual flood durations. From top left to bottom right: d1 winter, d2 winter, d3 winter, d6 winter, d1 summer, d2, summer, d3 summer, d6 summer.

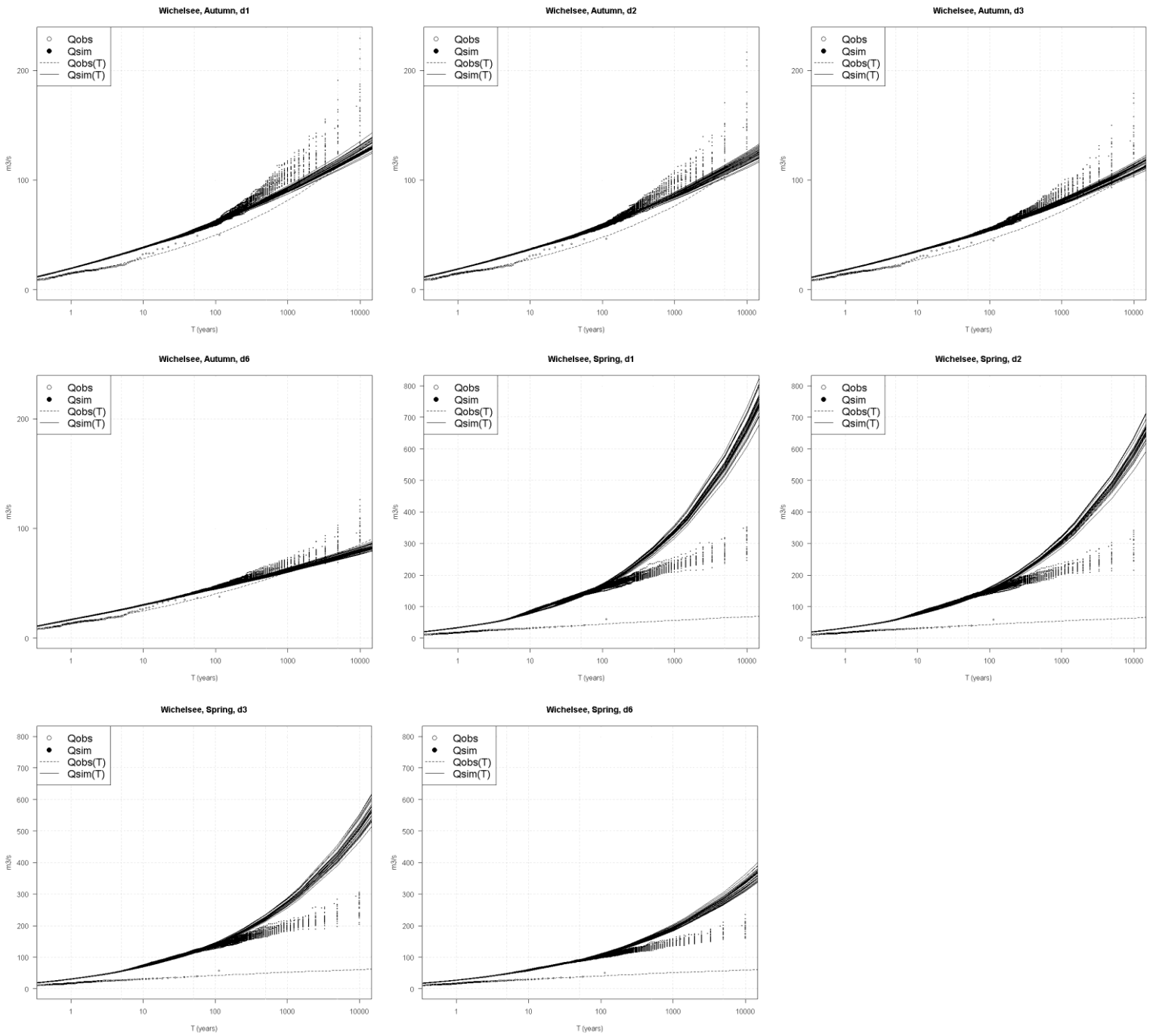


Figure 91: Autumn and spring QdF curves for Wichelsee and individual flood durations. From top left to bottom right: d1 autumn, d2 autumn, d3 autumn, d6 autumn, d1 spring, d2, spring, d3 spring, d6 spring.

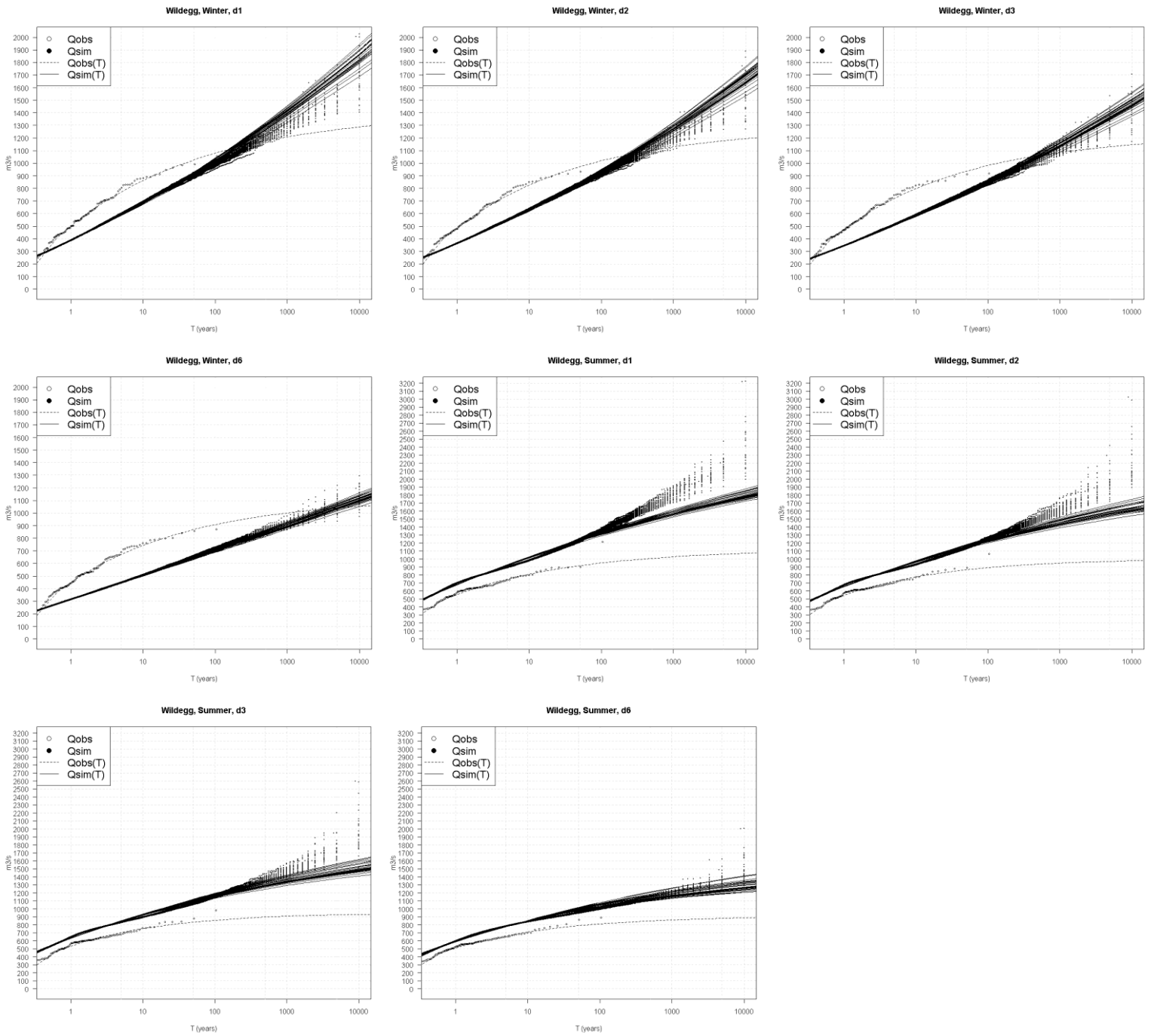


Figure 92: Winter and summer QdF curves for Wildegg and individual flood durations. From top left to bottom right: d1 winter, d2 winter, d3 winter, d6 winter, d1 summer, d2, summer, d3 summer, d6 summer.

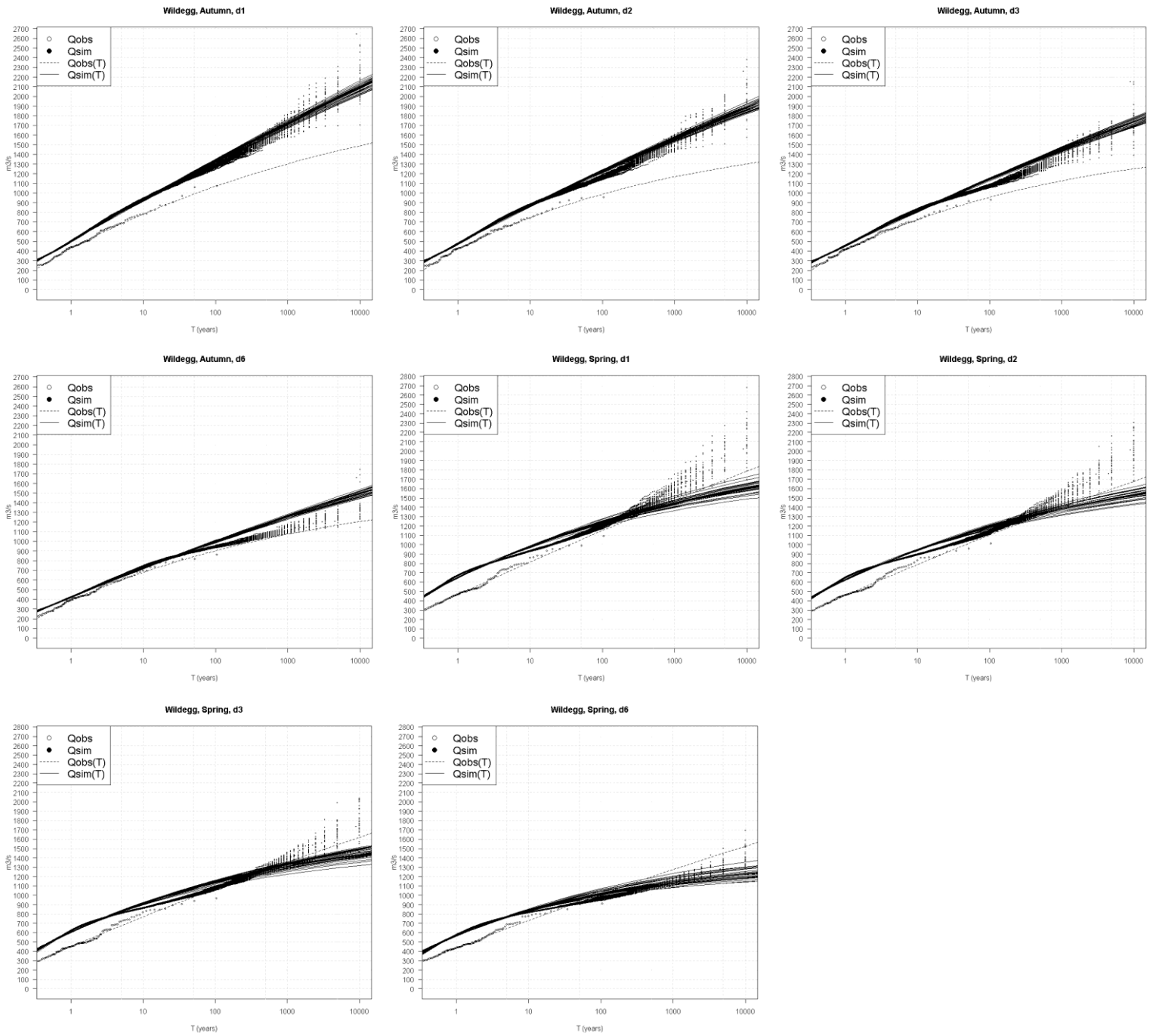


Figure 93: Autumn and spring QdF curves for Wildegg and individual flood durations. From top left to bottom right: d1 autumn, d2 autumn, d3 autumn, d6 autumn, d1 spring, d2, spring, d3 spring, d6 spring.

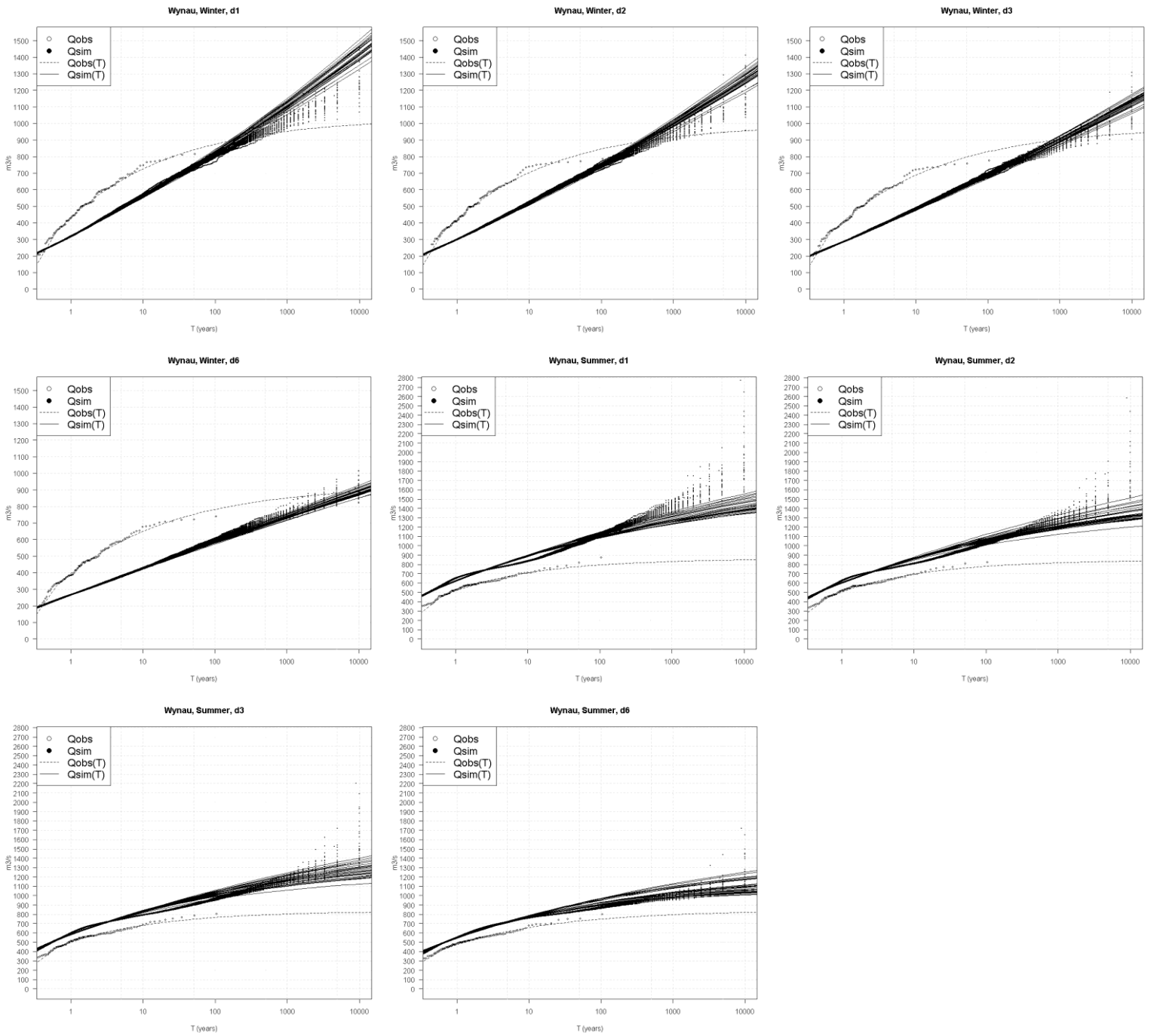


Figure 94: Winter and summer QdF curves for Wynau and individual flood durations. From top left to bottom right: d1 winter, d2 winter, d3 winter, d6 winter, d1 summer, d2, summer, d3 summer, d6 summer.

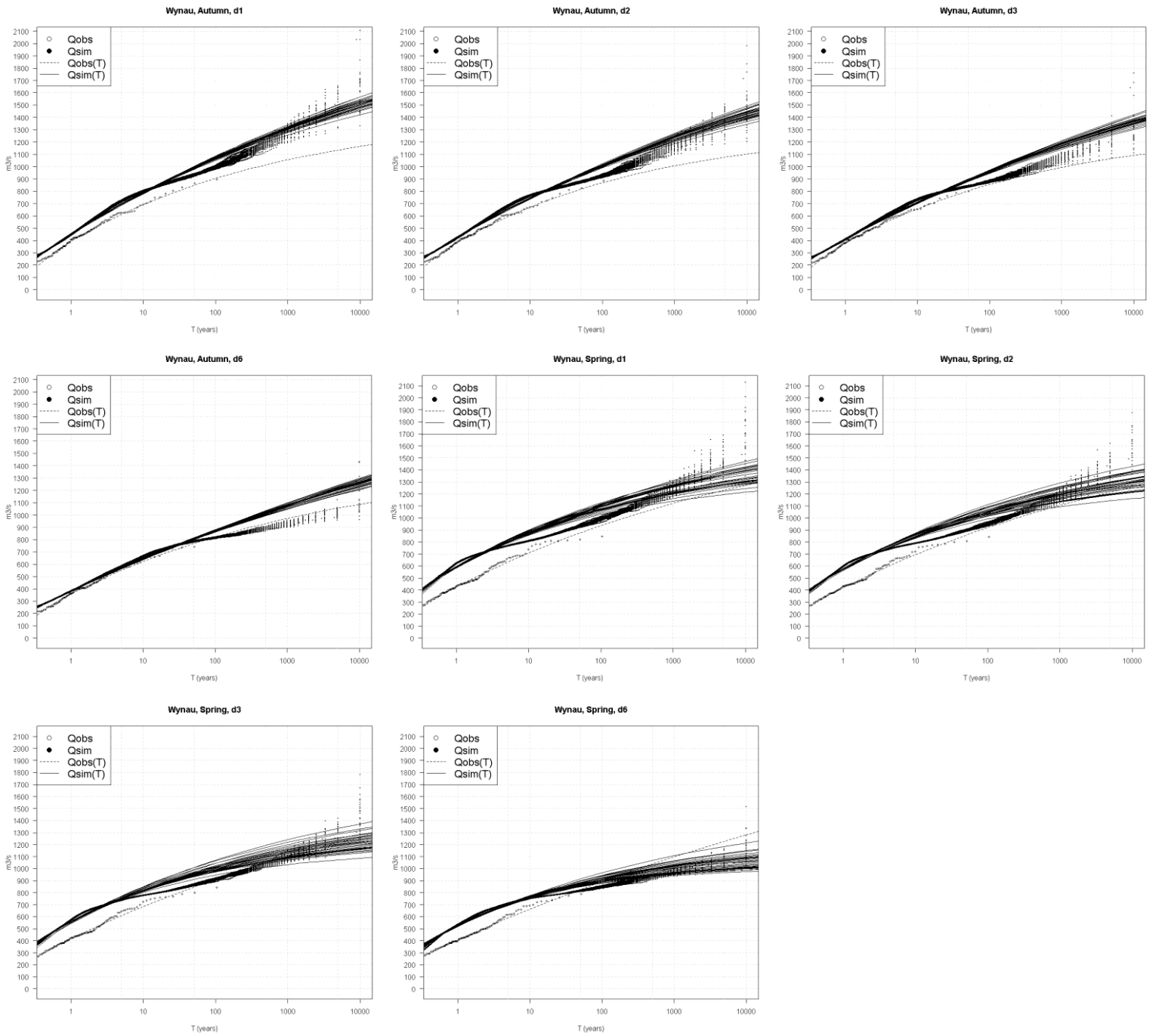


Figure 95: Autumn and spring QdF curves for Wynau and individual flood durations. From top left to bottom right: d1 autumn, d2 autumn, d3 autumn, d6 autumn, d1 spring, d2, spring, d3 spring, d6 spring.

8.2 Appendix B

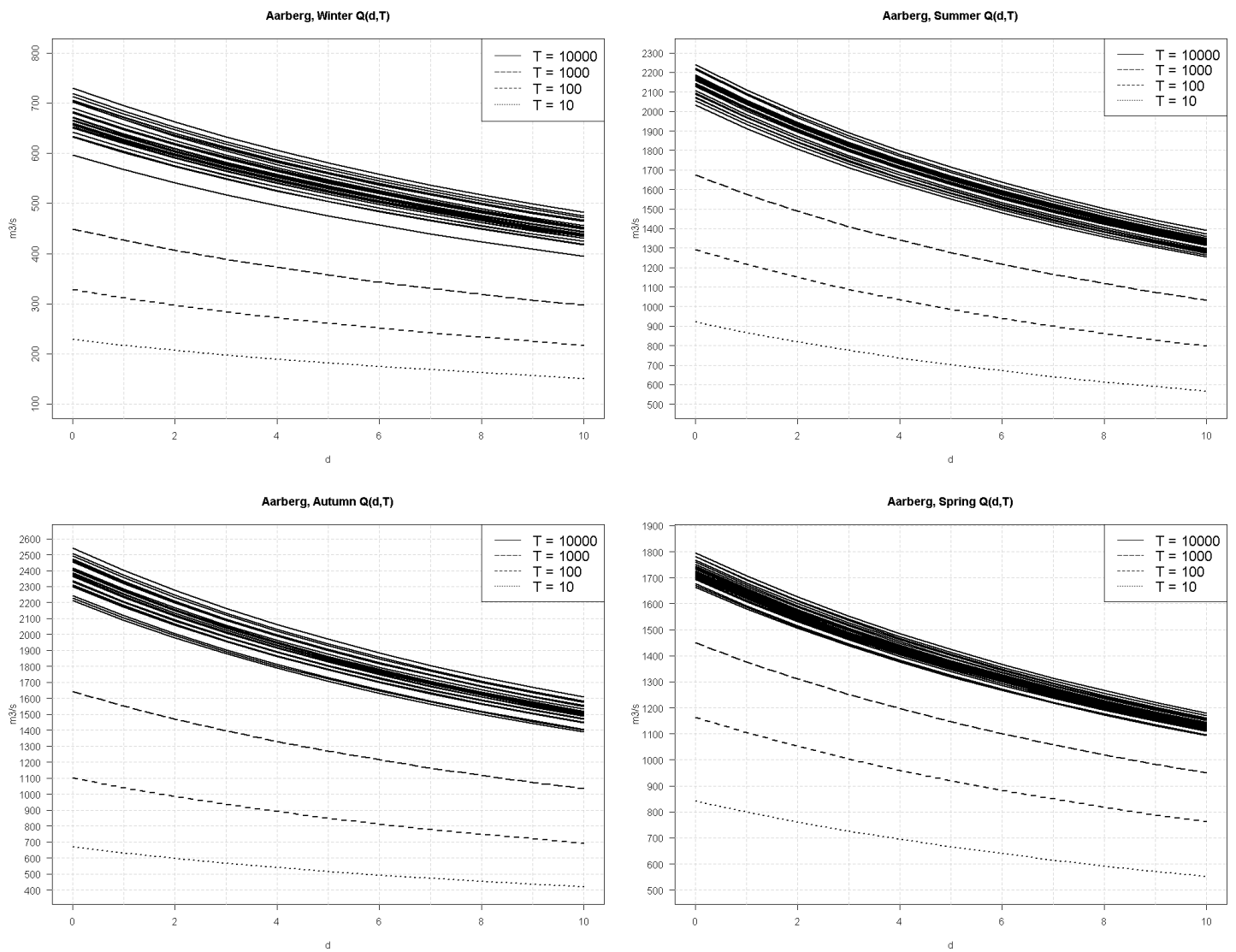


Figure 96: Seasonal converging QdF curves for Aarberg and return periods $T=10$, $T=100$, $T=1'000$ and $T=10'000$. For return periods $T=10$, $T=100$ and $T=1,000$, only 1 of the 29 quantiles is shown, otherwise the figure becomes too cluttered. From top left to bottom right: winter, summer, fall, spring.

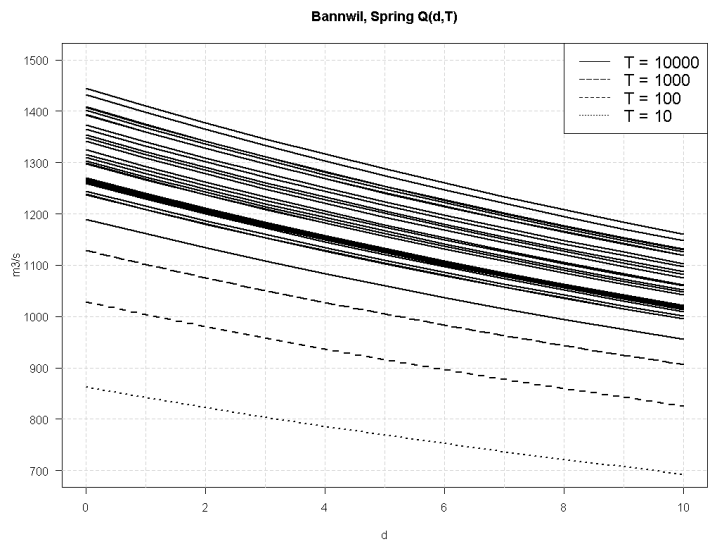
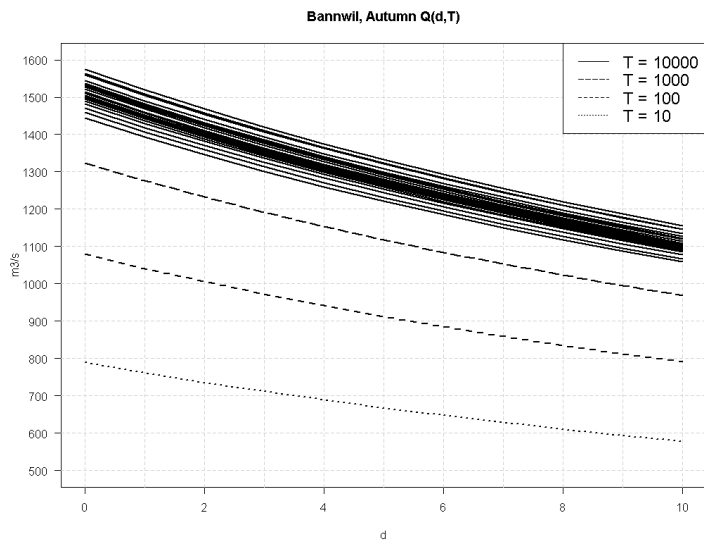
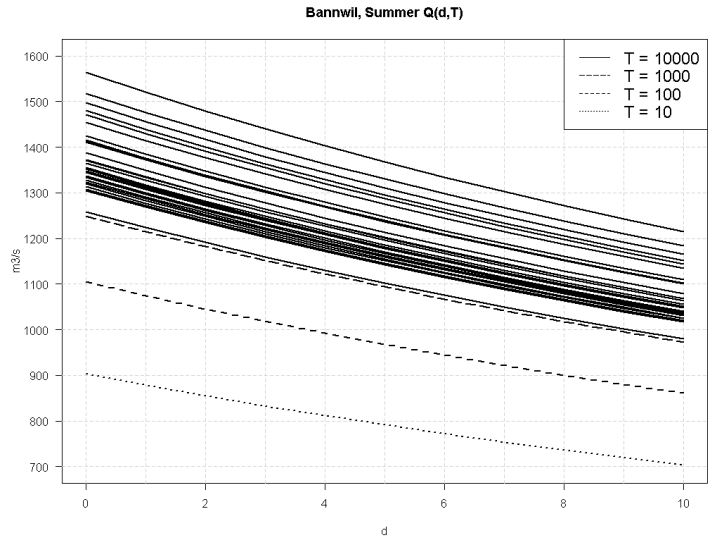
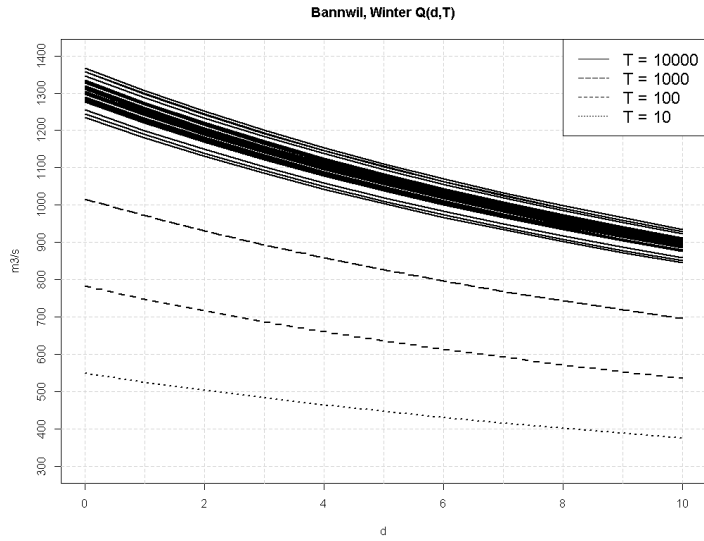


Figure 97: Seasonal converging QdF curves for Bannwil and return periods $T=10$, $T=100$, $T=1'000$ and $T=10'000$. For return periods $T=10$, $T=100$ and $T=1,000$, only 1 of the 29 quantiles is shown, otherwise the figure becomes too cluttered. From top left to bottom right: winter, summer, fall, spring.

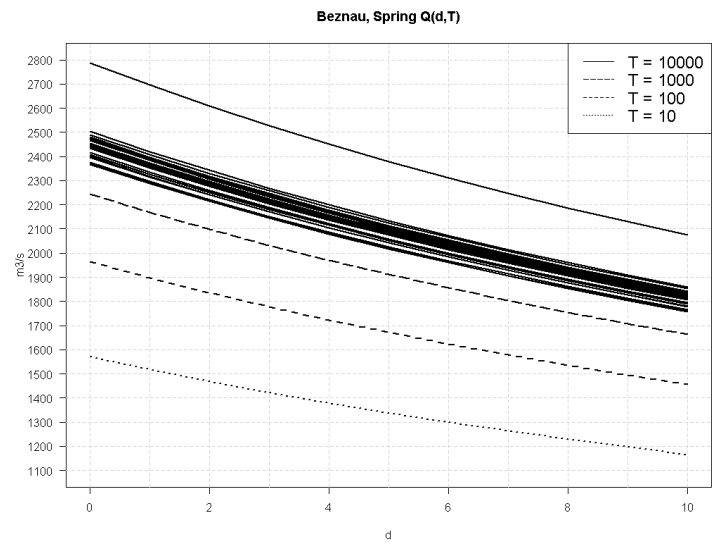
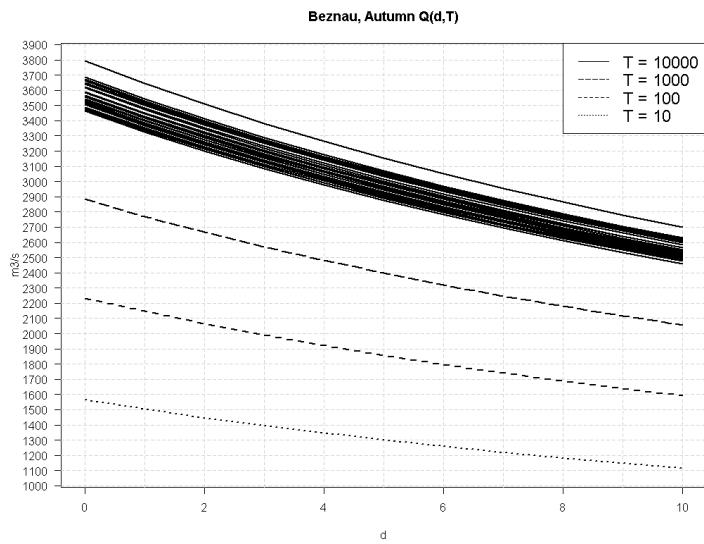
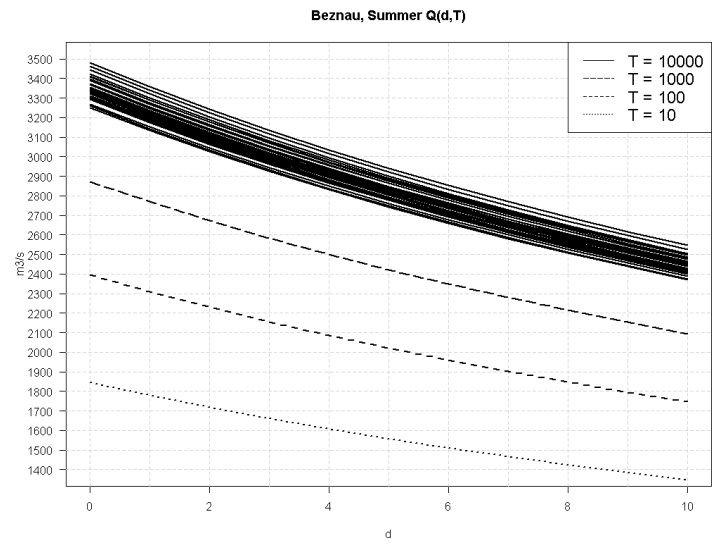
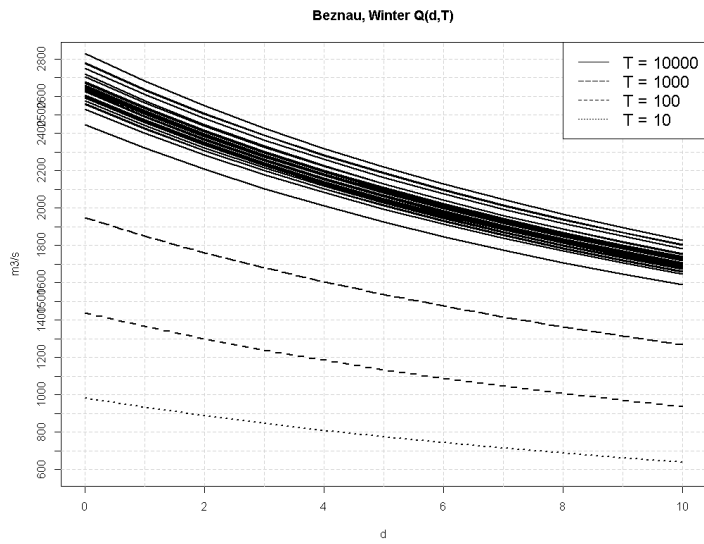


Figure 98: Seasonal converging QdF curves for Bezau and return periods $T=10$, $T=100$, $T=1'000$ and $T=10'000$. For return periods $T=10$, $T=100$ and $T=1,000$, only 1 of the 29 quantiles is shown, otherwise the figure becomes too cluttered. From top left to bottom right: winter, summer, fall, spring.

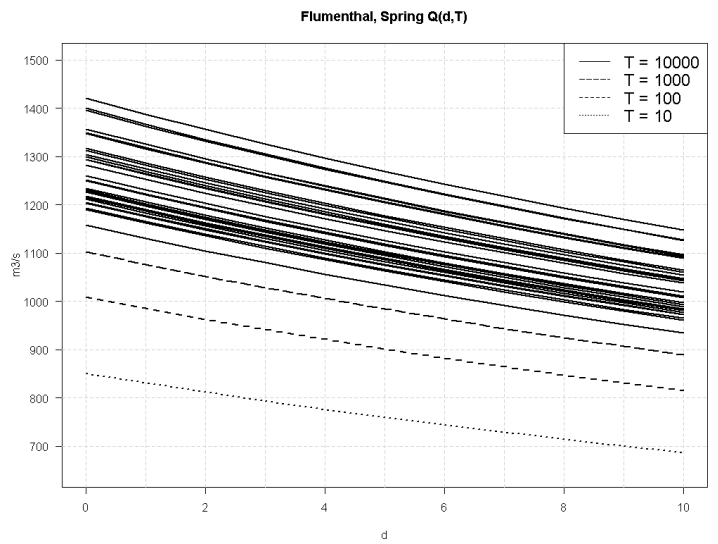
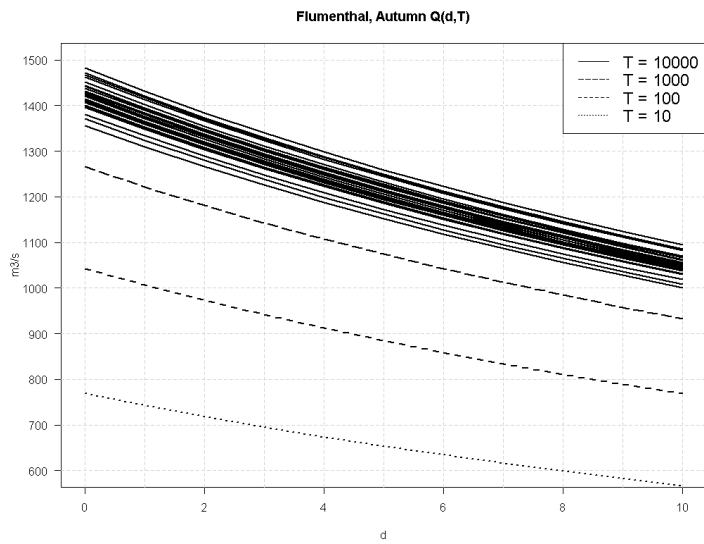
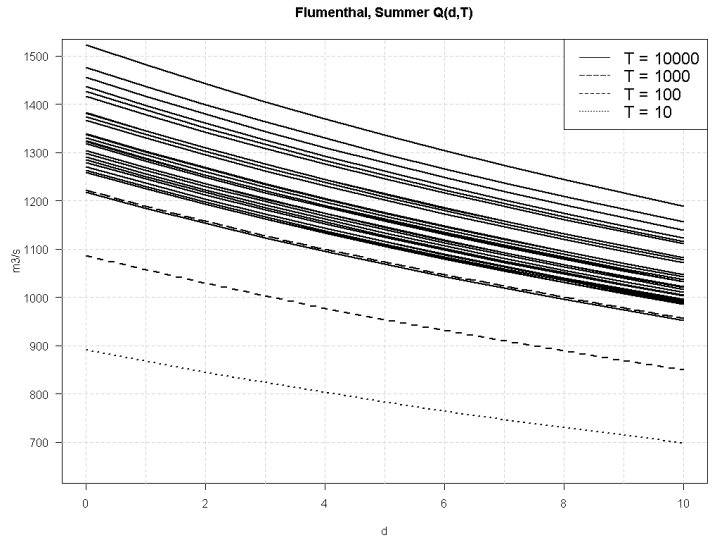
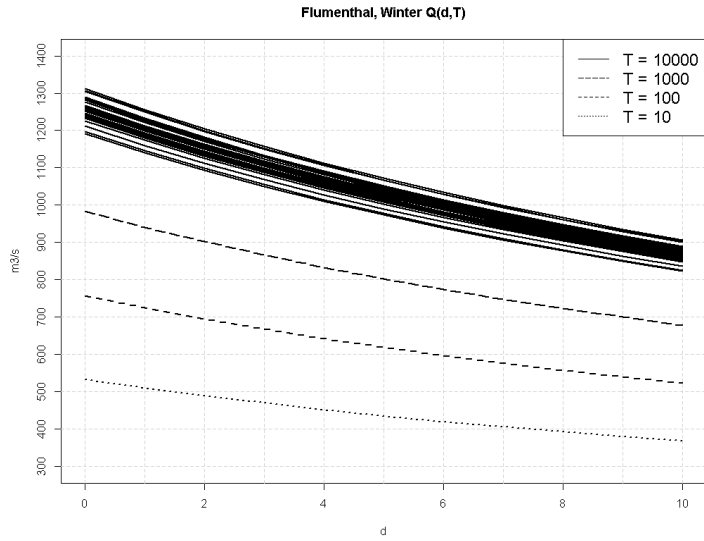


Figure 99: Seasonal converging QdF curves for Flumenthal and return periods $T=10$, $T=100$, $T=1'000$ and $T=10'000$. For return periods $T=10$, $T=100$ and $T=1,000$, only 1 of the 29 quantiles is shown, otherwise the figure becomes too cluttered. From top left to bottom right: winter, summer, fall, spring.

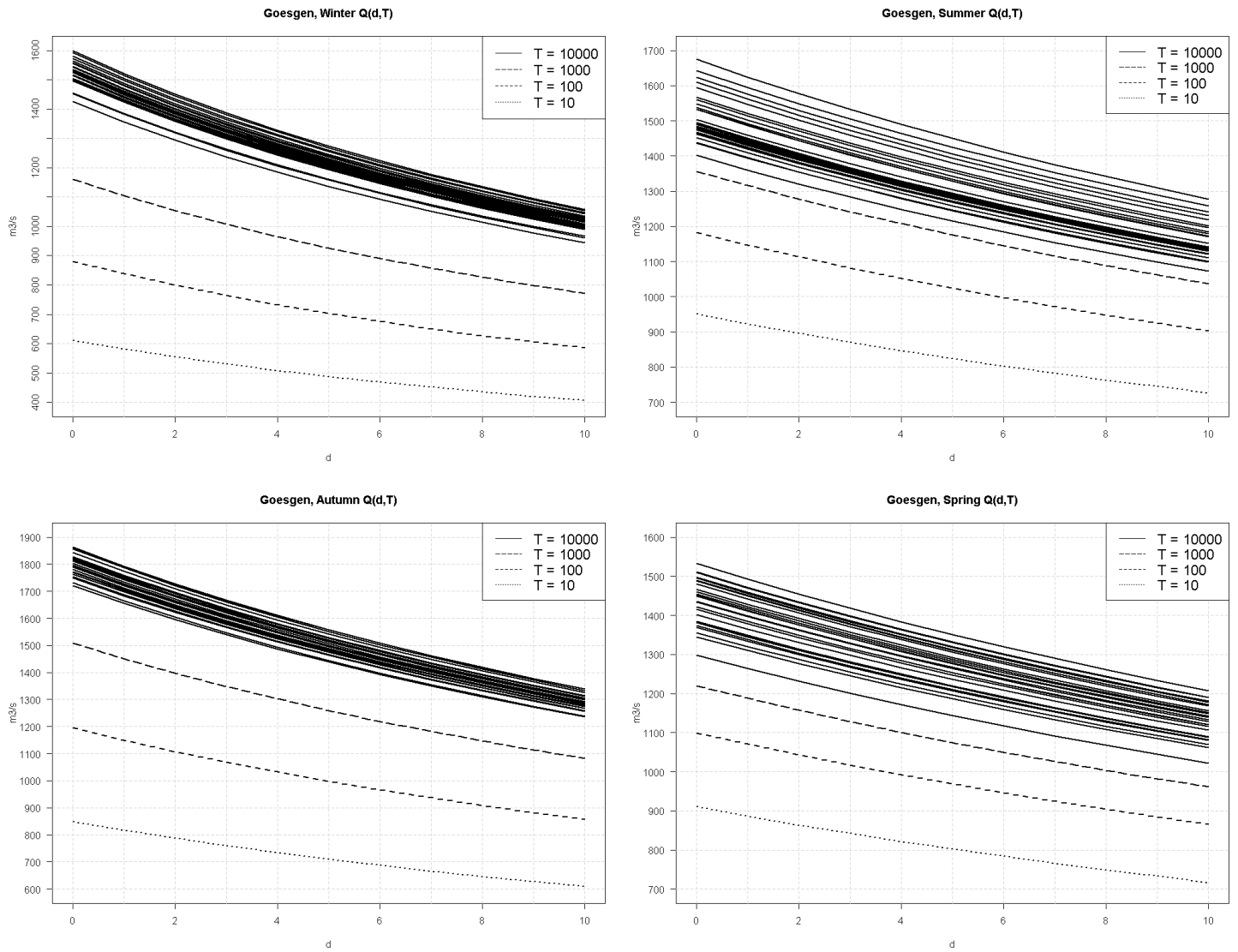


Figure 100: Seasonal converging QdF curves for Gösgen and return periods $T=10$, $T=100$, $T=1'000$ and $T=10'000$. For return periods $T=10$, $T=100$ and $T=1,000$, only 1 of the 29 quantiles is shown, otherwise the figure becomes too cluttered. From top left to bottom right: winter, summer, fall, spring.

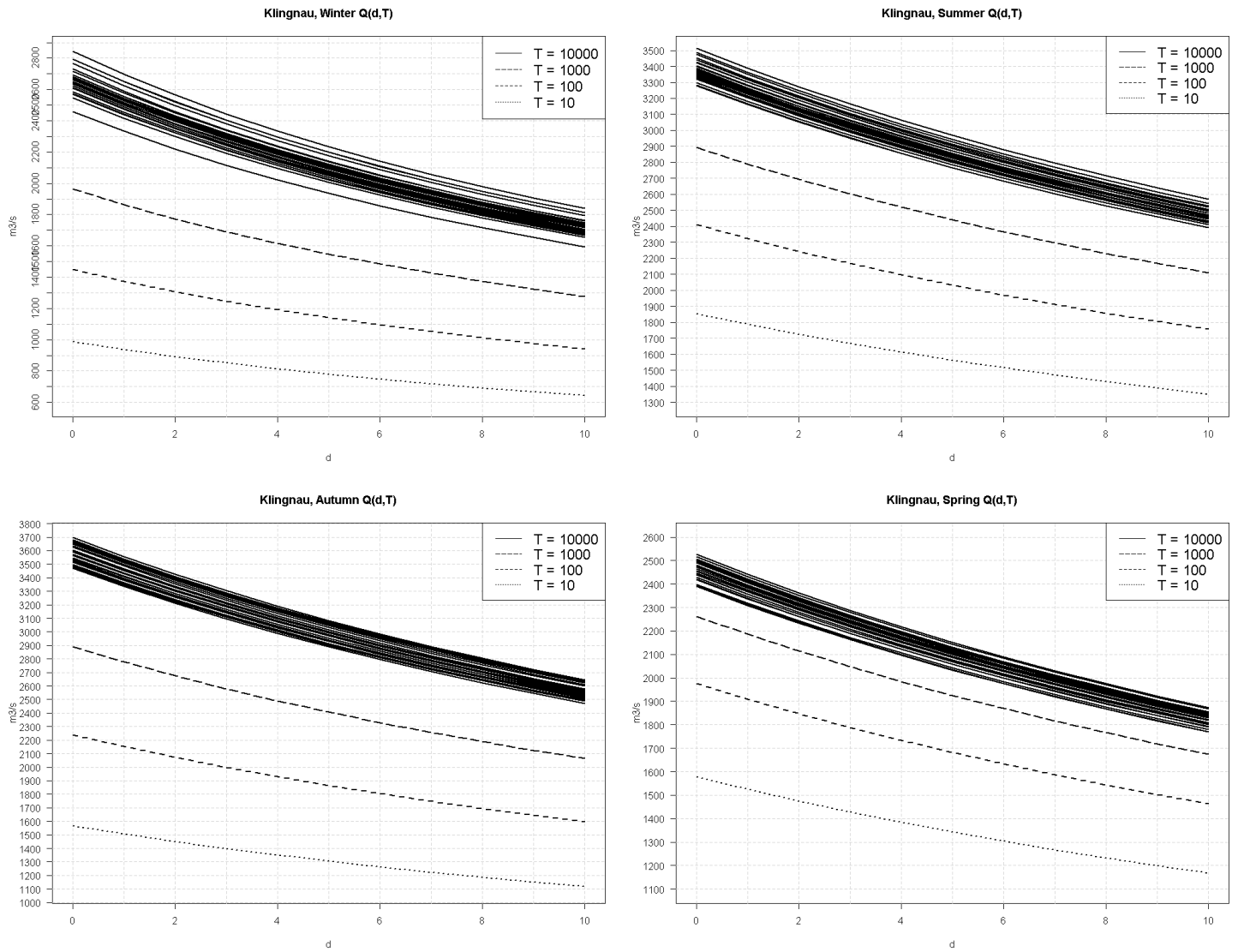


Figure 101: Seasonal converging QdF curves for Klingnau and return periods $T=10$, $T=100$, $T=1'000$ and $T=10'000$. For return periods $T=10$, $T=100$ and $T=1,000$, only 1 of the 29 quantiles is shown, otherwise the figure becomes too cluttered. From top left to bottom right: winter, summer, fall, spring.

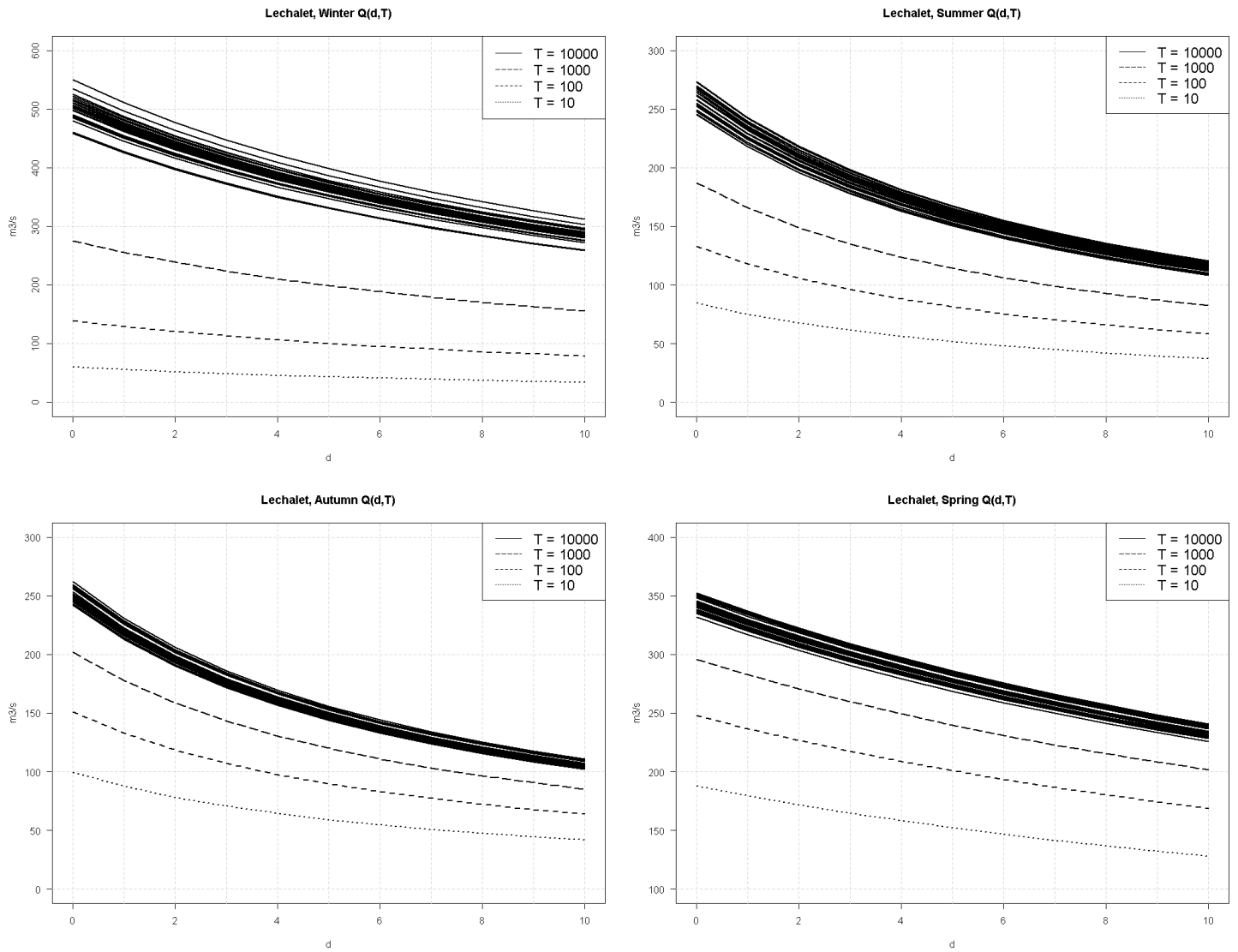


Figure 102: Seasonal converging QdF curves for Le Chalet and return periods $T=10$, $T=100$, $T=1'000$ and $T=10'000$. For return periods $T=10$, $T=100$ and $T=1,000$, only 1 of the 29 quantiles is shown, otherwise the figure becomes too cluttered. From top left to bottom right: winter, summer, fall, spring.

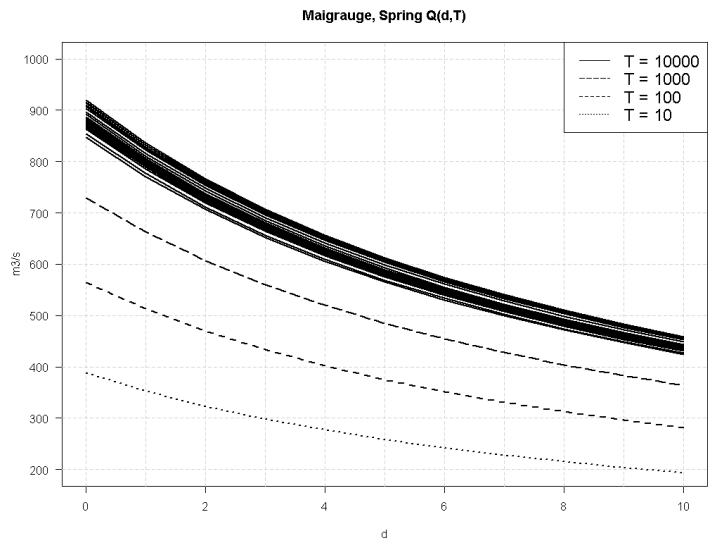
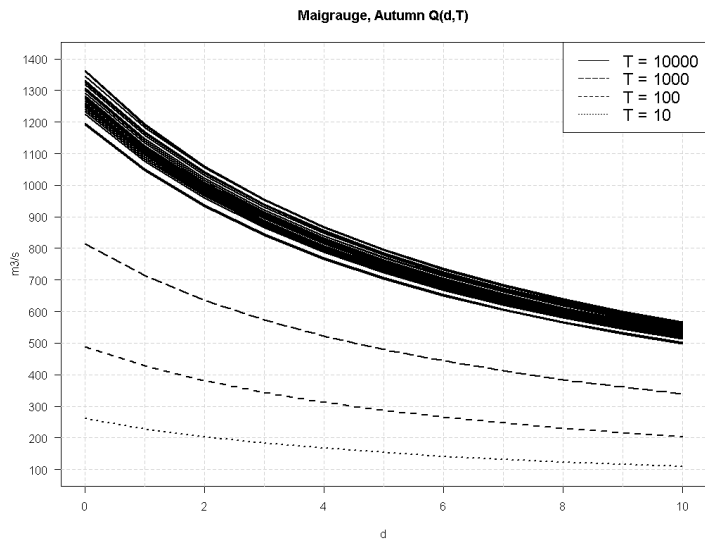
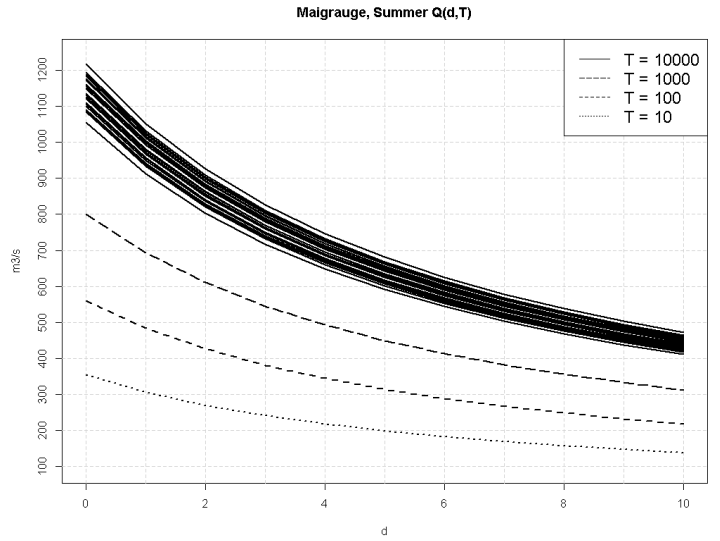
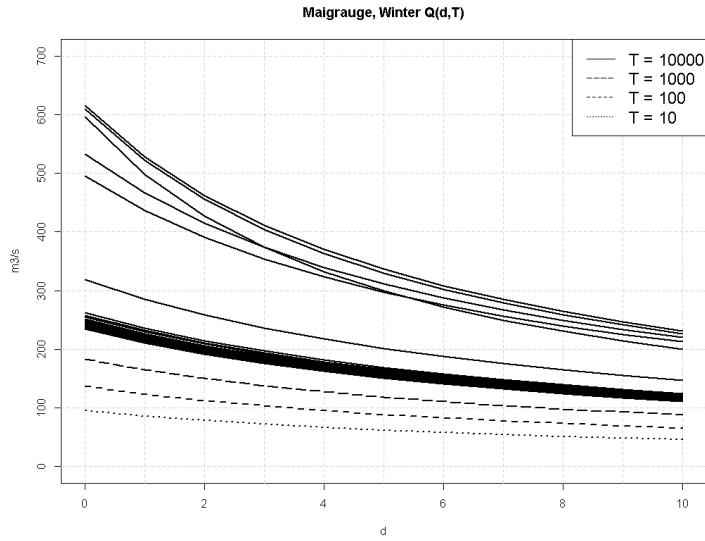


Figure 103: Seasonal converging QdF curves for Maigrauge and return periods $T=10$, $T=100$, $T=1'000$ and $T=10'000$. For return periods $T=10$, $T=100$ and $T=1,000$, only 1 of the 29 quantiles is shown, otherwise the figure becomes too cluttered. From top left to bottom right: winter, summer, fall, spring.

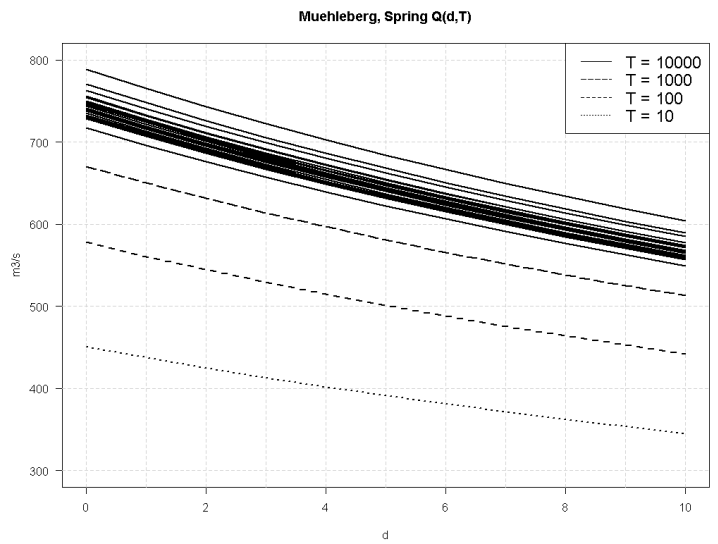
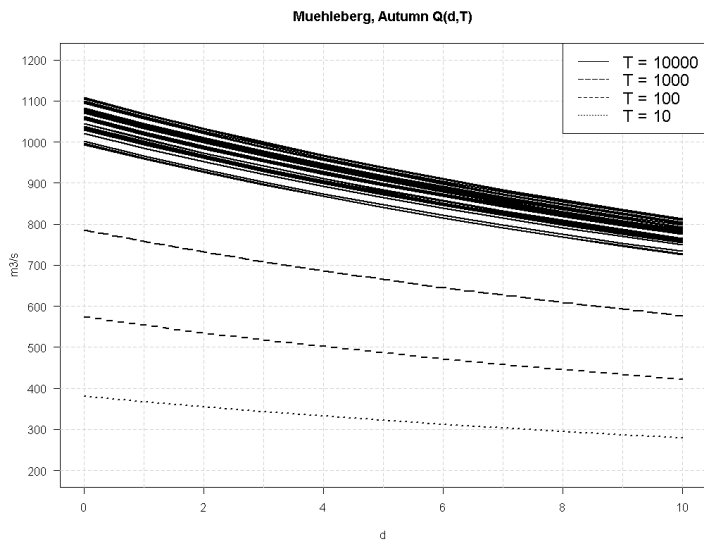
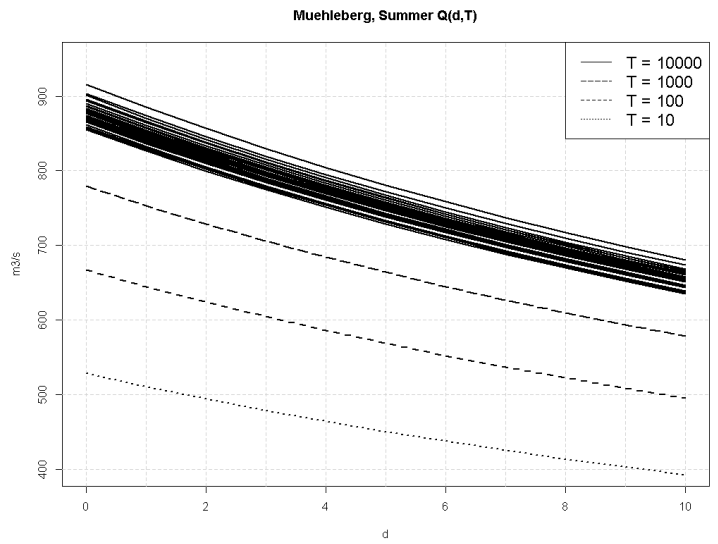
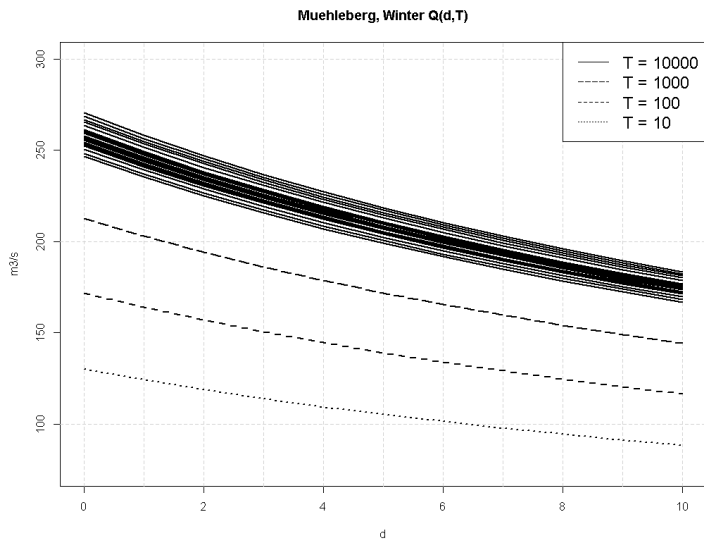


Figure 104: Seasonal converging QdF curves for Muehleberg and return periods $T=10$, $T=100$, $T=1'000$ and $T=10'000$. For return periods $T=10$, $T=100$ and $T=1,000$, only 1 of the 29 quantiles is shown, otherwise the figure becomes too cluttered. From top left to bottom right: winter, summer, fall, spring.

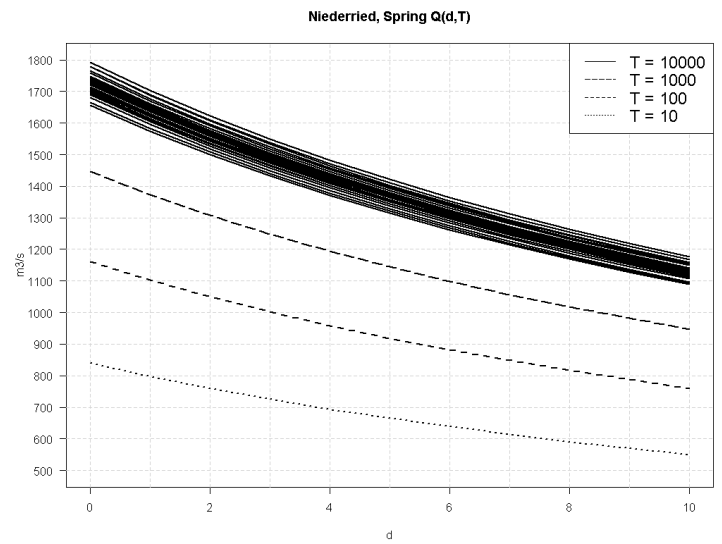
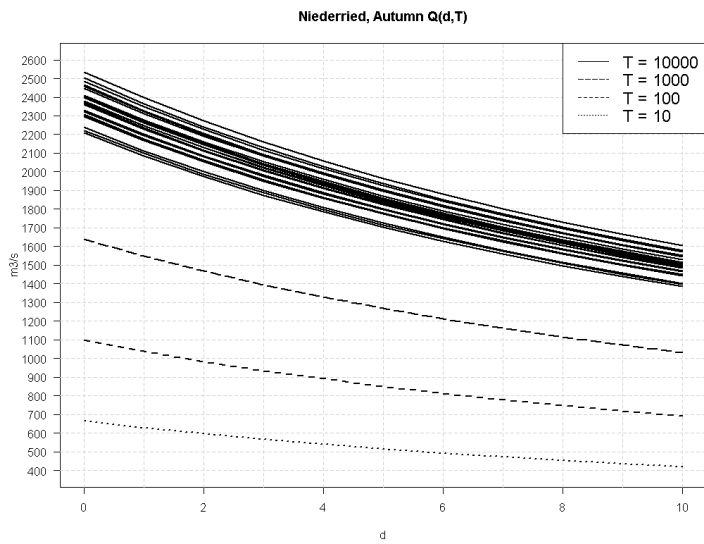
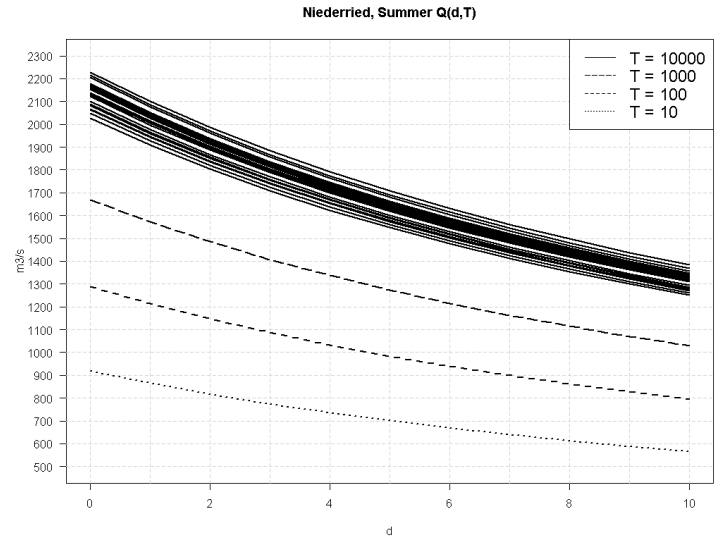
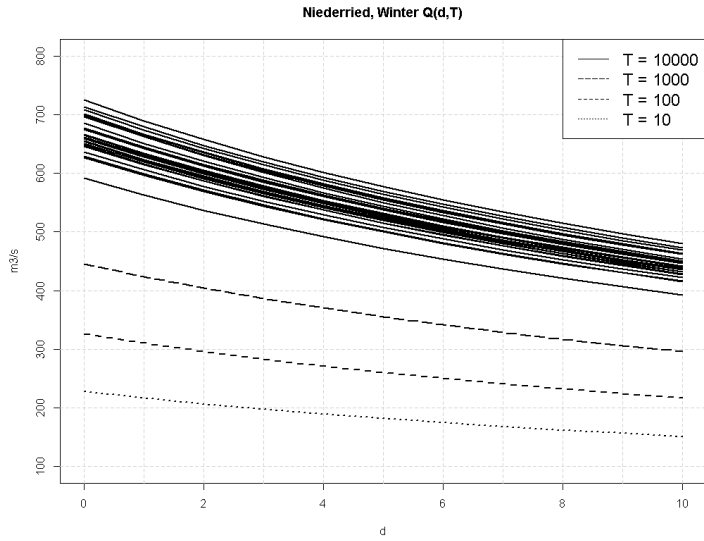


Figure 105: Seasonal converging QdF curves for Niederried and return periods $T=10$, $T=100$, $T=1'000$ and $T=10'000$. For return periods $T=10$, $T=100$ and $T=1,000$, only 1 of the 29 quantiles is shown, otherwise the figure becomes too cluttered. From top left to bottom right: winter, summer, fall, spring.

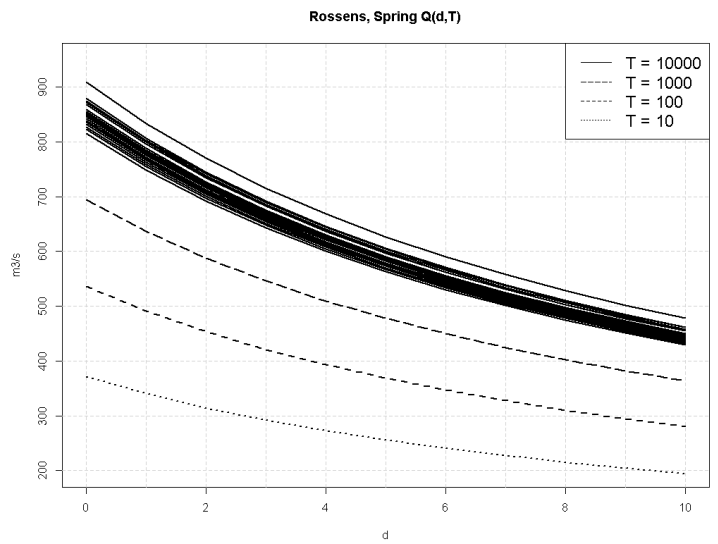
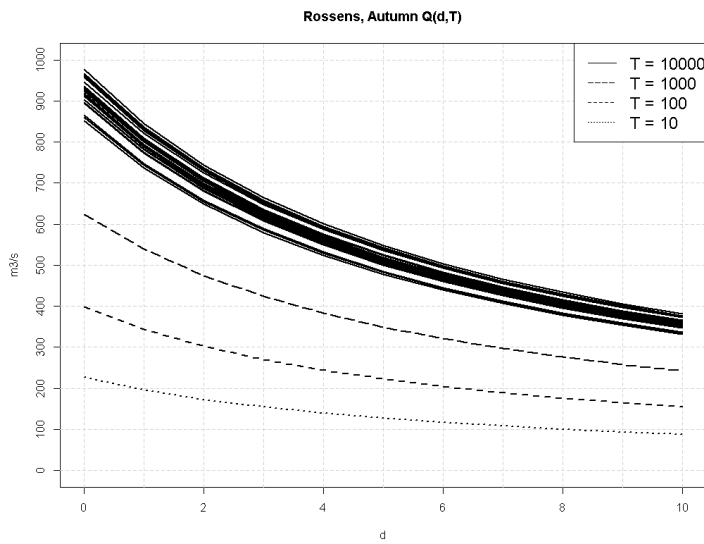
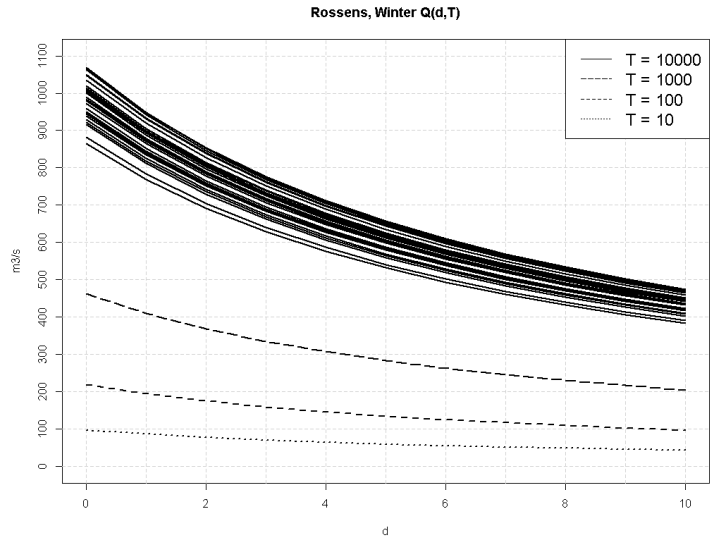
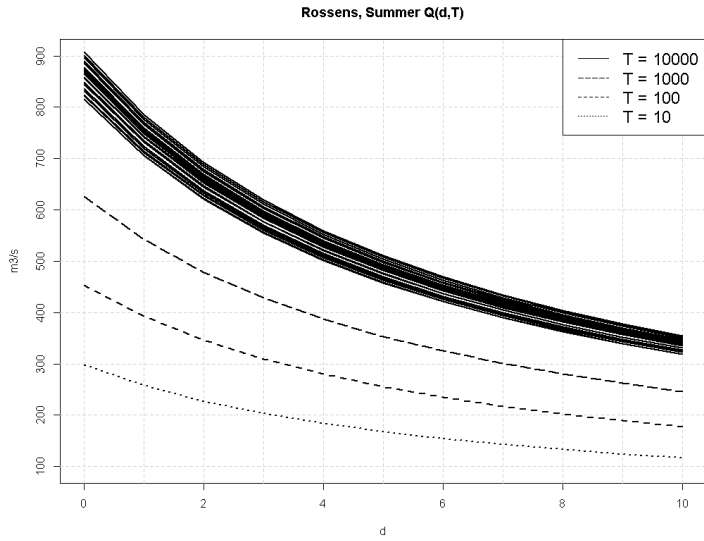


Figure 106: Seasonal converging QdF curves for Rossens and return periods $T=10$, $T=100$, $T=1'000$ and $T=10'000$. For return periods $T=10$, $T=100$ and $T=1,000$, only 1 of the 29 quantiles is shown, otherwise the figure becomes too cluttered. From top left to bottom right: winter, summer, fall, spring.

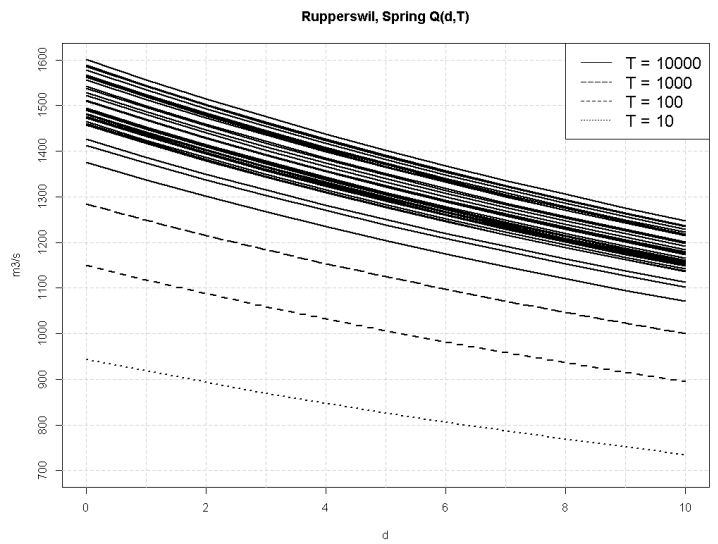
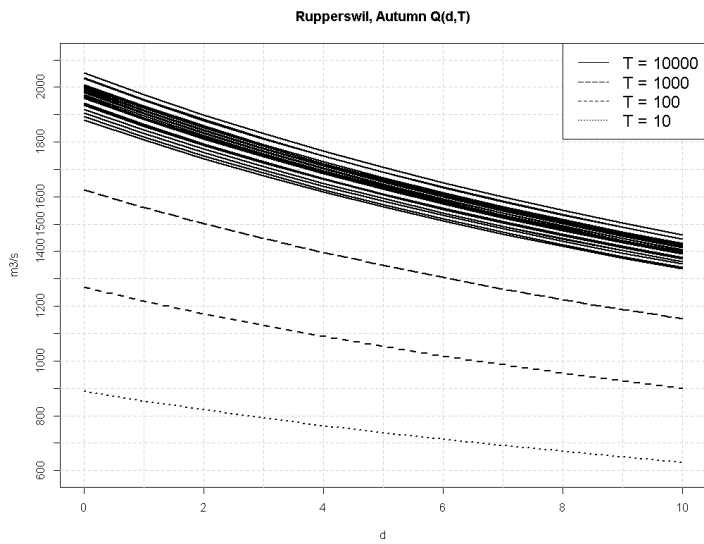
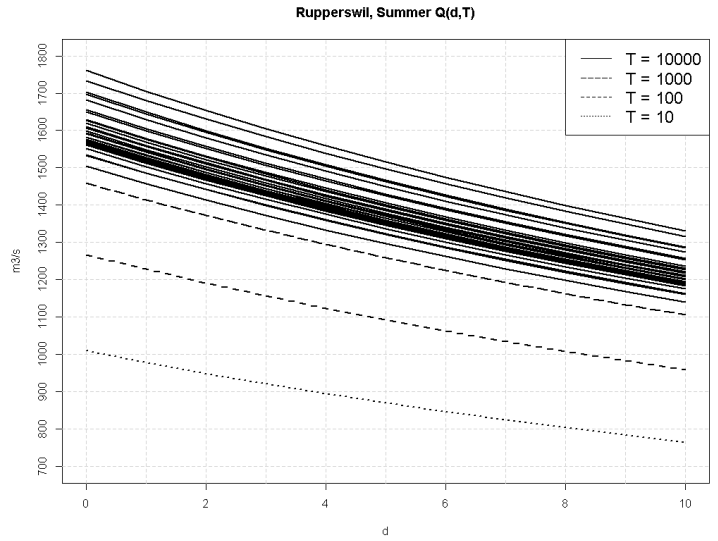
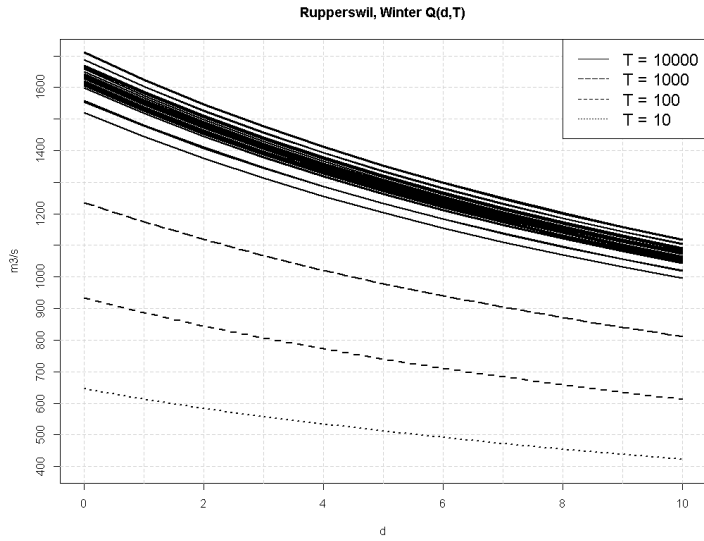


Figure 107: Seasonal converging QdF curves for Ruppertswil and return periods $T=10$, $T=100$, $T=1'000$ and $T=10'000$. For return periods $T=10$, $T=100$ and $T=1,000$, only 1 of the 29 quantiles is shown, otherwise the figure becomes too cluttered. From top left to bottom right: winter, summer, fall, spring.

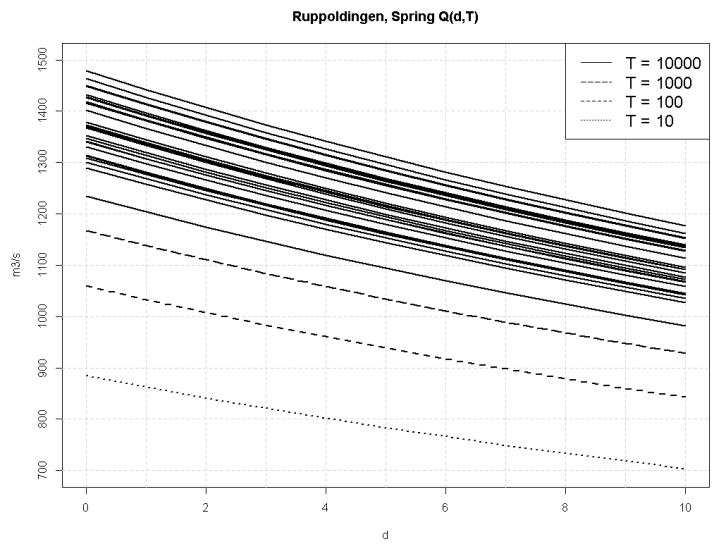
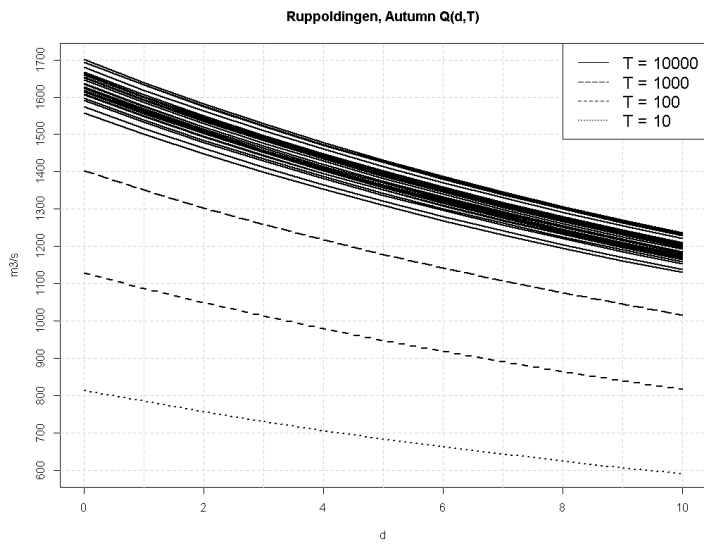
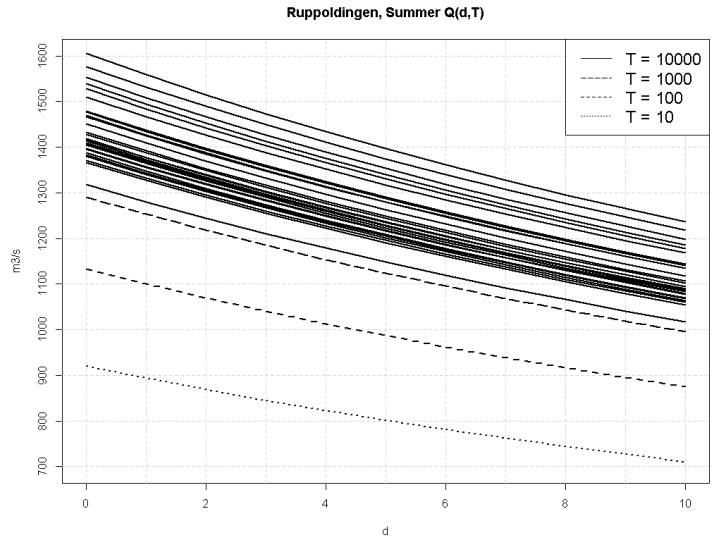
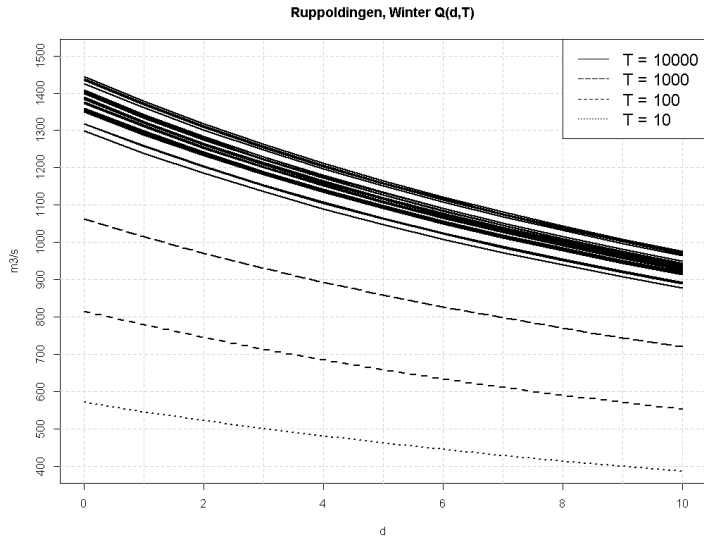


Figure 108: Seasonal converging QdF curves for Ruppoldingen and return periods $T=10$, $T=100$, $T=1'000$ and $T=10'000$. For return periods $T=10$, $T=100$ and $T=1,000$, only 1 of the 29 quantiles is shown, otherwise the figure becomes too cluttered. From top left to bottom right: winter, summer, fall, spring.

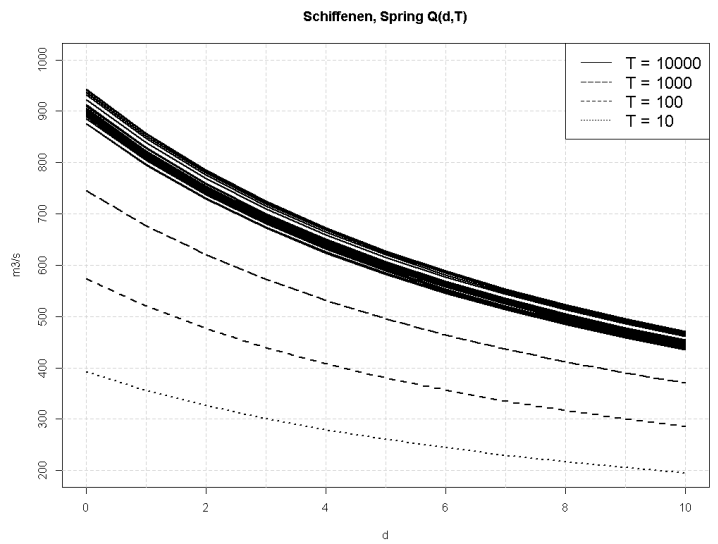
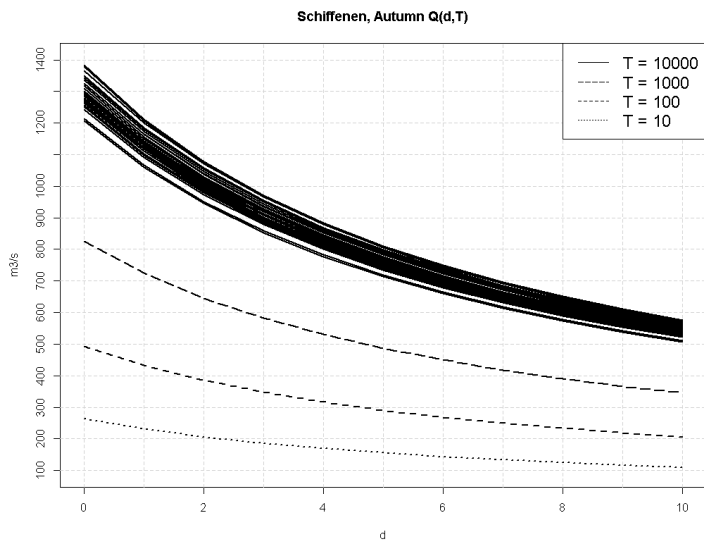
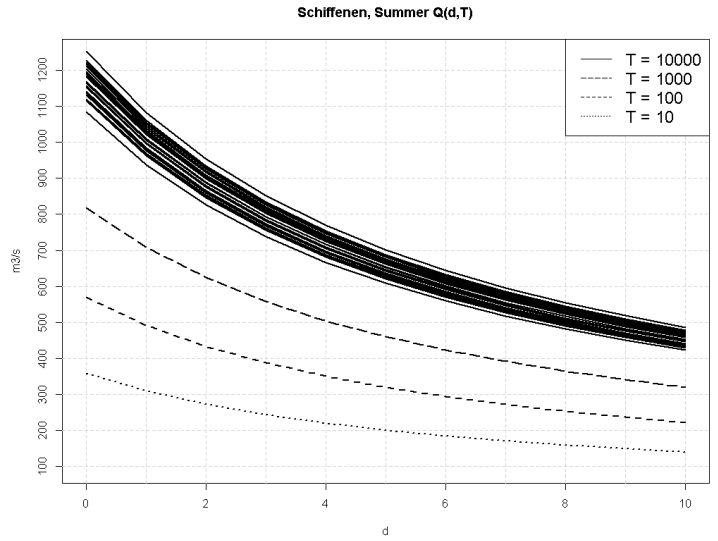
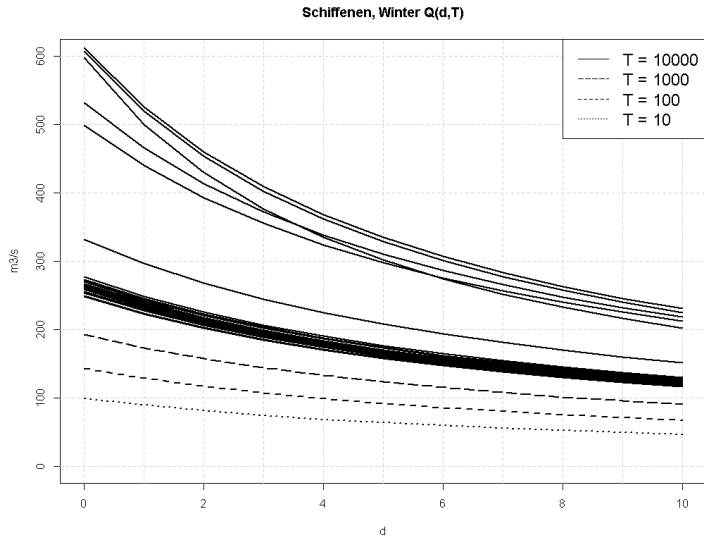


Figure 109: Seasonal converging QdF curves for Schiffenen and return periods $T=10$, $T=100$, $T=1'000$ and $T=10'000$. For return periods $T=10$, $T=100$ and $T=1,000$, only 1 of the 29 quantiles is shown, otherwise the figure becomes too cluttered. From top left to bottom right: winter, summer, fall, spring.

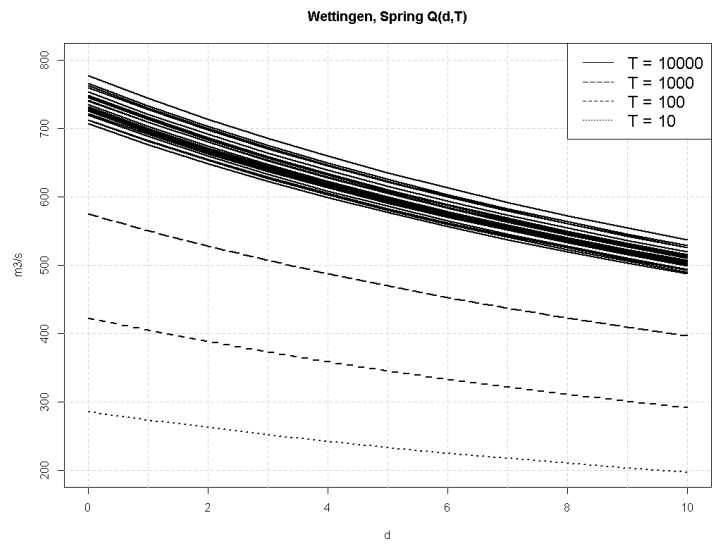
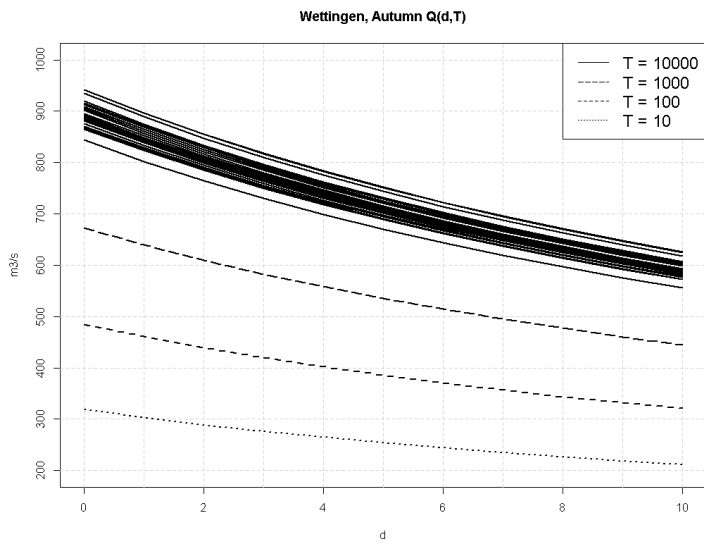
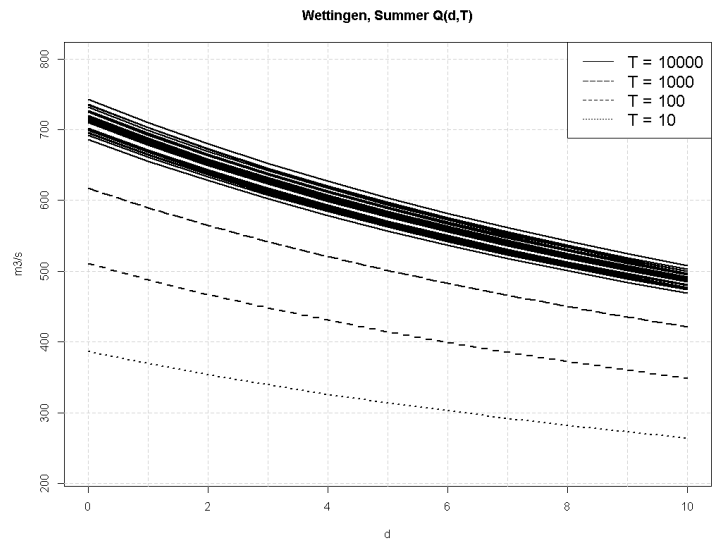
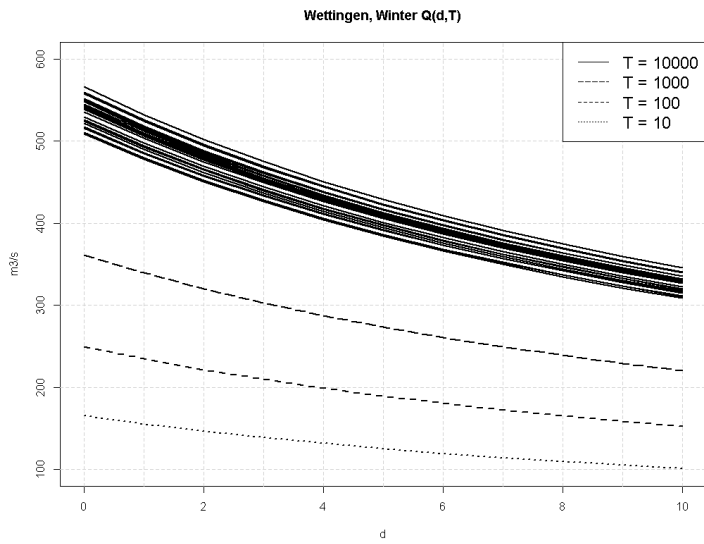


Figure 110: Seasonal converging QdF curves for Wettingen and return periods $T=10$, $T=100$, $T=1'000$ and $T=10'000$. For return periods $T=10$, $T=100$ and $T=1,000$, only 1 of the 29 quantiles is shown, otherwise the figure becomes too cluttered. From top left to bottom right: winter, summer, fall, spring.

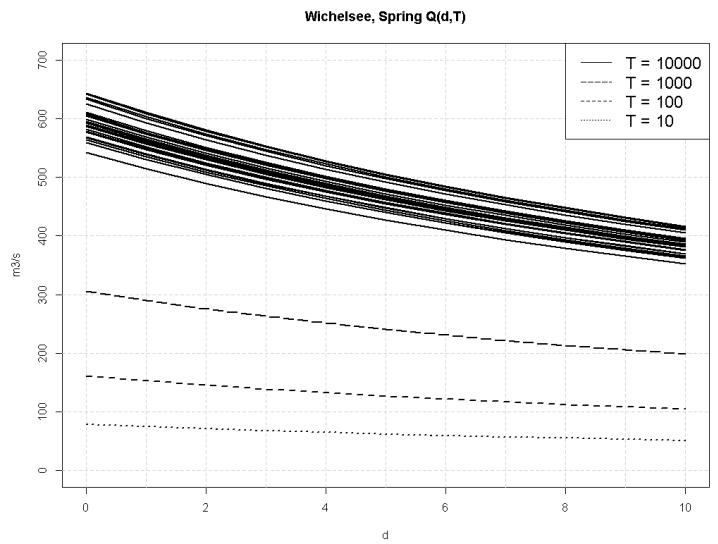
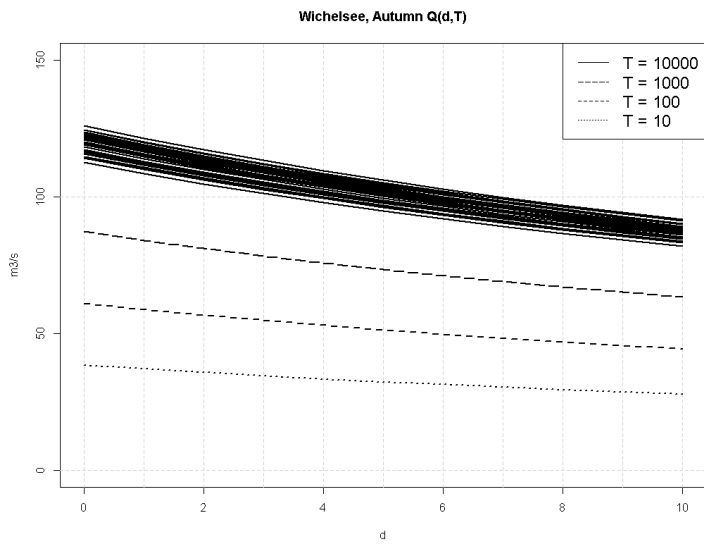
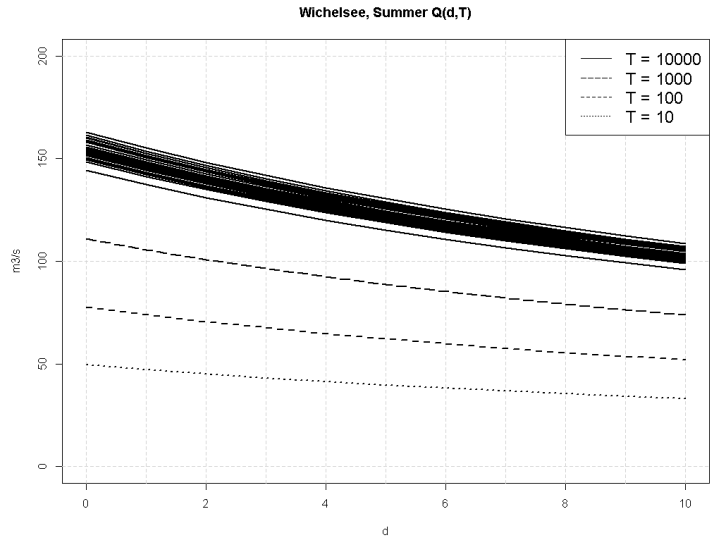
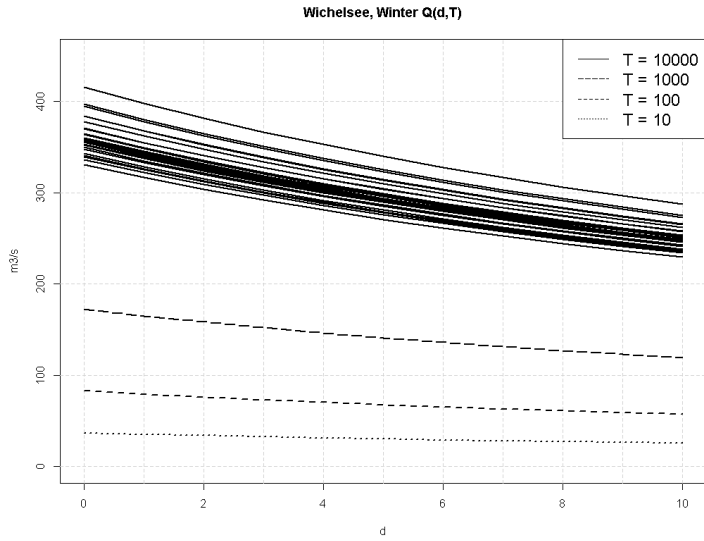


Figure 111: Seasonal converging QdF curves for Wichelsee and return periods $T=10$, $T=100$, $T=1'000$ and $T=10'000$. For return periods $T=10$, $T=100$ and $T=1,000$, only 1 of the 29 quantiles is shown, otherwise the figure becomes too cluttered. From top left to bottom right: winter, summer, fall, spring.

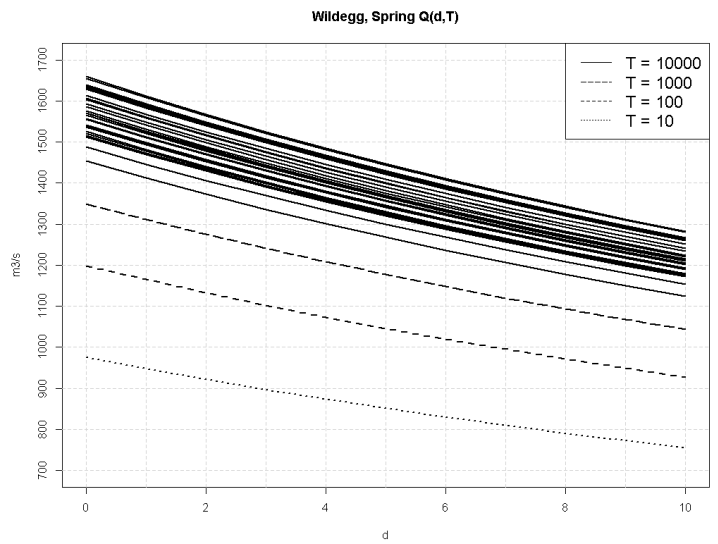
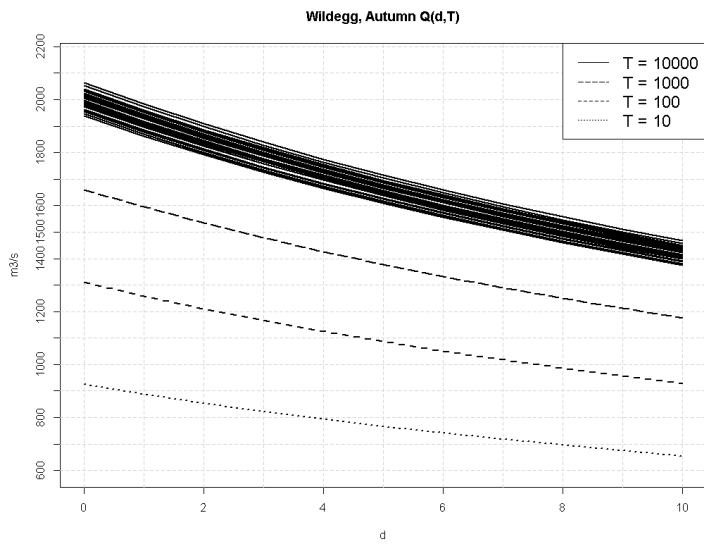
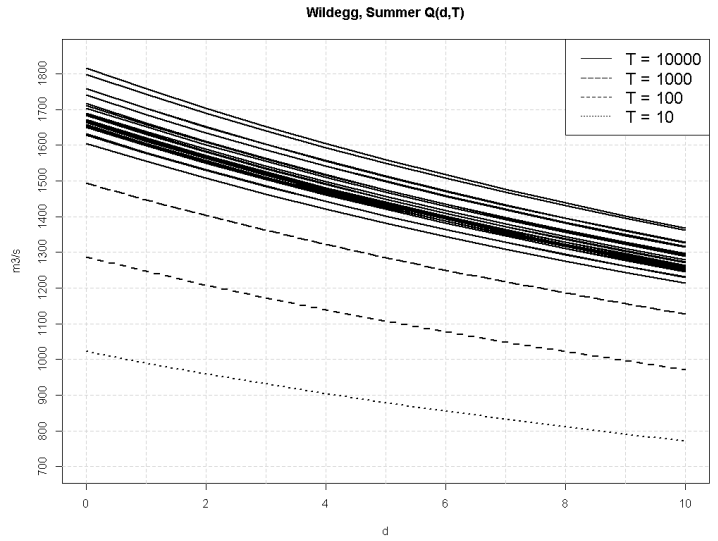
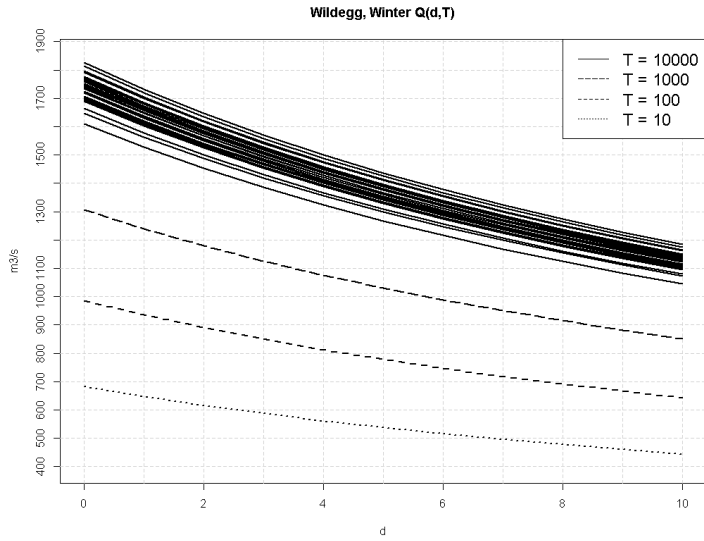


Figure 112: Seasonal converging QdF curves for Wildeg and return periods $T=10$, $T=100$, $T=1'000$ and $T=10'000$. For return periods $T=10$, $T=100$ and $T=1,000$, only 1 of the 29 quantiles is shown, otherwise the figure becomes too cluttered. From top left to bottom right: winter, summer, fall, spring.

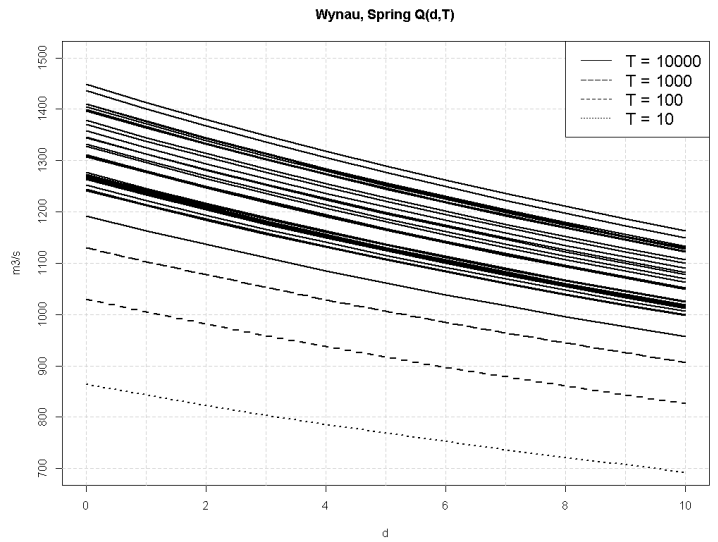
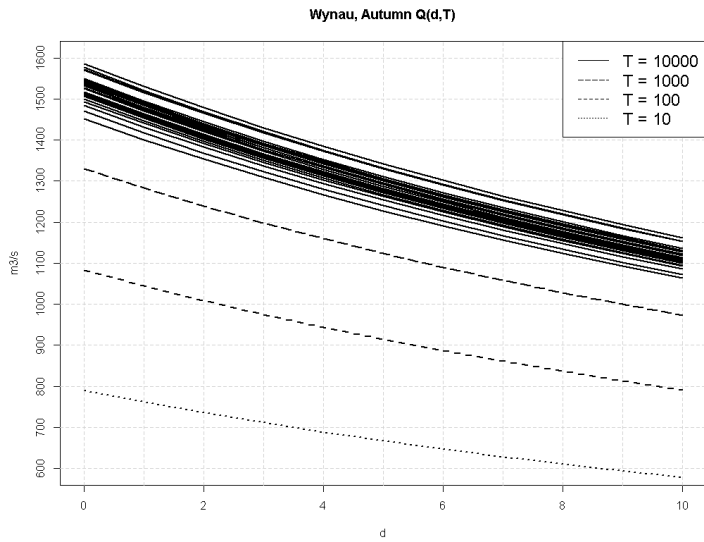
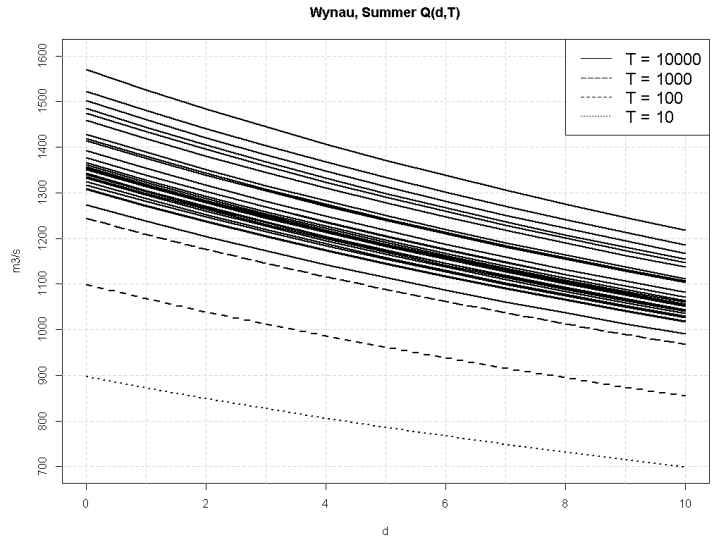
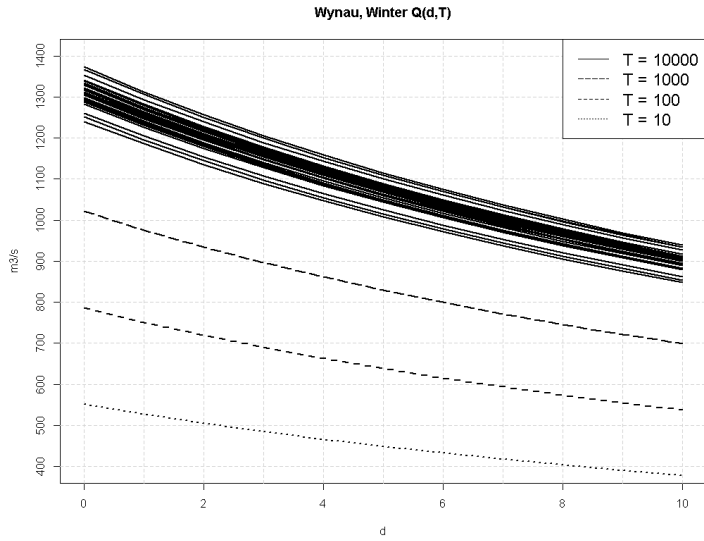
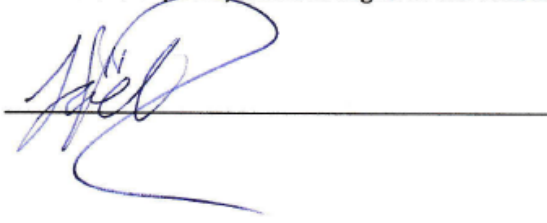


Figure 113: Seasonal converging QdF curves for Wynau and return periods $T=10$, $T=100$, $T=1'000$ and $T=10'000$. For return periods $T=10$, $T=100$ and $T=1,000$, only 1 of the 29 quantiles is shown, otherwise the figure becomes too cluttered. From top left to bottom right: winter, summer, fall, spring.

9. Personal declaration

I hereby declare that the submitted Thesis is the result of my own, independent work. All external sources are explicitly acknowledged in the Thesis.

A handwritten signature in blue ink is written over a horizontal black line. The signature is stylized and appears to be the initials 'H. B.' followed by a large, sweeping flourish that extends to the right and then loops back down.